Final Report

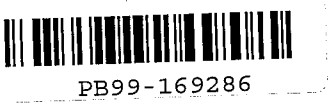

CENTRIFUGAL NUMERICAL EVALUATION OF PRELOADING ON POLK COUNTY PARKWAY

DR. MICHAEL C. M^{C} VAY PRINCIPAL INVESTIGATOR

ZAFAR AHMED GRADUATE STUDENT

WPI NO.: 0510752
STATE NO.: 99700-3333-119
CONTRACT NO.: B-9900
UF PROJECT NO.: 4910-4504-527-12

DEPARTMENT OF CIVIL ENGINEERING
UNIVERSITY OF FLORIDA
P.O. BOX 116580
GAINESVILLE, FLORIDA 32611-6580

SUBMITTED TO:

FLORIDA DEPARTMENT OF TRANSPORTATION

AUGUST 1999

DISCLAIMER

"The opinions, findings and conclusions expressed in this publication are those of the authors and not necessarily those of the Florida Department of Transportation or the U.S. Department of Transportation.

Prepared in cooperation with the State of Florida department of Transportation and the U.S. Department of Transportation."

SI* (MODERN METRIC) CONVERSION FACTORS

APPROXIMATE CONVERSIONS TO SI UNITS

Symbol	When You Know	Multiply By	To Find	Symbol
		LENGTH		
in	inches	25.4	millimeters	mm
ft	feet	0.305	meters	m
yd	yards	0.914	meters	m
mi	miles	1.61	kilometers	km
		AREA		
in^2	square inches	645.2	square millimeters	mm^2
ft^2	square feet	0.093	square meters	m^2
yd^2	square yards	0.836	square meters	m^2
ac	acres	0.405	hectares	ha
mi^2	square miles	2.59	square kilometres	km^2
		VOLUME		
fl oz	fluid ounces	29.57	milliliters	ml
gal	gallons	3.785	liters	l
ft^3	cubic feet	0.028	cubic meters	m^3
yd^3	cubic yards	0.765	cubic meters	m^3
NOTE: Volumes greater than 1000 l shall be shown in m^3.				
		MASS		
oz	ounces	28.35	grams	g
lb	pounds	0.454	kilograms	kg
T	short tons (2000 lb)	0.907	megagrams	Mg
		Temperature (exact)		
°F	Fahrenheit temperature	5(F-32)/9 or (F-32)/1.8	Celcius temperature	°C
		ILLUMINATION		
fc	foot-candles	10.76	lux	lx
fl	foot-Lamberts	3.426	candela/m^2	cd/m^2
		FORCE and PRESSURE or STRESS		
lbf	poundforce	4.45	newtons	N
psi	poundforce per square inch	6.89	kilopascals	kPa

APPROXIMATE CONVERSIONS FROM SI UNITS

Symbol	When You Know	Multiply By	To Find	Symbol
		LENGTH		
mm	millimeters	0.039	inches	in
m	meters	3.28	feet	ft
m	meters	1.09	yards	yd
km	kilometers	0.621	miles	mi
		AREA		
mm^2	square millimeters	0.0016	square inches	in^2
m^2	square meters	10.764	square feet	ft^2
m^2	square meters	1.195	square yards	yd^2
ha	hectares	2.47	acres	ac
km^2	square kilometers	0.386	square miles	mi^2
		VOLUME		
ml	milliliters	0.034	fluid ounces	fl oz
l	liters	0.264	gallons	gal
m^3	cubic meters	35.71	cubic feet	ft^3
m^3	cubic meters	1.307	cubic yards	yd^3
		MASS		
g	grams	0.035	ounces	oz
kg	kilograms	2.202	pounds	lb
Mg	megagrams	1.103	short tons (2000 lb)	T
		Temperature (exact)		
°C	Celcius temperature	1.8C + 32	Fahrenheit temperature	°F
		ILLUMINATION		
lx	lux	0.0929	foot-candles	fc
cd/m^2	candela/m^2	0.2919	foot-Lamberts	fl
		FORCE and PRESSURE or STRESS		
N	newtons	0.225	poundforce	lbf
kPa	kilopascals	0.145	poundforce per square inch	psi

* SI is the symbol for the International System of Units. Appropriate rounding should be made to comply with Section 4 of ASTM E380.

(Revised August 1992)

Technical Report Documentation Page

1. Report No.	2. Government Accession No.	3. Recipient's Catalog No.
WPI # 0510752		

4. Title and Subtitle	5. Report Date
Centrifugal Numerical Evaluation of Preloading on Polk County Parkway	June 1999
	6. Performing Organization Code
7. Author(s)	8. Performing Organization Report No.
M. C. M^{c} Vay, Principal Investigator; Zafar Ahmed, Graduate Assistant	4910-4504-527-12
9. Performing Organization Name and Address	10. Work Unit No. (TRAIS)
University of Florida Department of Civil Engineering 345 Weil Hall / P. O. Box 116580 Gainesville, FL 32611-6580	99700-3333-119
	11. Contract or Grant No.
	B-9900
12. Sponsoring Agency Name and Address	13. Type of Report and Period Covered
Florida Department of Transportation Research Management Center 605 Suwannee Street, MS 30 Tallahassee, FL 32399-0450	Draft Final Report 8/15/95 - 5/31/99
	14. Sponsoring Agency Code
	99700-3333-119

15. Supplementary Notes

Prepared in cooperation with the Federal Highway Administration

16. Abstract

A mathematical framework for large strain consolidation of fully saturated soil media is presented in this report. The algorithmic treatment of large strain response of the solid phase is based on multiplicative decomposition of deformation gradient and is coupled with the algorithm of fluid flow via the Kirchhoff pore water pressure. Balance laws are written for the soil-water mixture following the motion of the soil matrix alone.

Two different constitutive relations (elastoplastic and viscoplastic) based on modified Cam-Clay (MCC) model of critical state soil mechanics are formulated in this report to represent the nonlinear responses of the solid phase.

Proposed mathematical model is linearized to obtain consistent tangent operators and subsequently implemented in a displacement-based finite element code PlasFEM, developed by the Geotechnical Engineering group at the University of Florida. Numerical prediction of primary (consolidation and swell) and secondary (creep) consolidation settlement of phosphatic waste clay, found at the construction site Polk County Expressway, in the presence of vertical wick drains subject to surcharge loading, unloading and subsequent reloading (i.e. road construction) is conducted using PlasFEM. Simulation results showed a very good agreement with the field measurements.

17. Key Words	18. Distribution Statement
	No restrictions. This document is available to the public through the National Technical Information Service, Springfield, VA, 22161

19. Security Classif. (of this report)	20. Security Classif. (of this page)	21. No. of Pages	22. Price
Unclassified	Unclassified	188	

Form DOT F 1700.7 (8-72)

TABLE OF CONTENTS

LIST OF TABLES

LIST OF FIGURES

CHAPTER 1
INTRODUCTION

1.1 Introduction

Non-linear response of geotechnical structures typically results from plastic yielding and large deformation of the soil skeleton. There are many classical geotechnical applications where non-linear effects due to these two factors could critically influence the outcome of a numerical analysis. Two examples are large movement of slopes and tilting of a tower due to P-δ effect. The impact of large deformation and plastic response is most evident in soft clays. It is a well-known characteristic of clays that considerable time is required for the occurrence of the compression caused by a given increment of load. Two phenomena contribute to this large time lag. The first is due to time required for the escape of the pore water. It is called the hydrodynamic lag or consolidation, a phenomenon which involves transient interaction between the solid and fluid phases of a soil-water mixture. The second phenomenon is called plastic time lag or secondary compression. The slow continued compression that continues after the excess pore pressures have substantially dissipated is called secondary compression. Secondary compression occurs because the relationship between void ratio and effective stress is usually somewhat time-dependent: the longer the clay remains under a constant effective stress, the denser it becomes.

Various problems of coupled fluid flow and deformation in porous media arise frequently in the fields of geotechnical engineering, groundwater hydrology and plate tectonics, among others. Slope stability analysis, surcharge loading for consolidation drainage, embankment, excavation, settlement of bridge approach pavements etc. are a few examples of a wide spectrum of geotechnical applications that involves consolidation.

The behavior of soil during consolidation is governed by the differences between the total stresses acting on the soil mass and the pore pressure. In most practical field cases it is necessary to describe the *effective stress field* to characterize the strength and deformation properties of the soil. Although the no-flow (undrained) and the free-flow (drained) conditions can be analyzed using a single-phase continuum formulation, consideration of a two-phase soil-water relationship in a saturated soil medium is essential in characterizing the soil behavior during the transient period of excess pore pressure dissipation. The physics involved in consolidation phenomenon requires that appropriate numerical analysis address coupled response of solid and fluid phases.

1.2 Research Focus

The mathematical structure and numerical analysis of nonlinear consolidation at small strains are fairly well developed and adequately documented [1-10]. The general approach is to write the linear momentum and mass balance equations in terms of the solid displacement and fluid potential (or pore water pressure), and then solve them simultaneously via a two-fold mixed formulation. The small strain assumption simplifies the linear momentum balance equation since it produces an additive form of elastic and

plastic deformations. In the context of finite element analysis, the small strain assumption also simplifies the mass conservation equation since the volume change of the mixture becomes a linear function of the nodal solid displacements.

In spite of substantial development of computational methods for small strain consolidation, mathematical models capable of handling the problem of coupled fluid flow and large deformation of the soil matrix are not developed well enough to be useful for routine analysis of prototype geotechnical structures. Extensions of the small strain formulation of the classical consolidation equations to large deformation are based primarily on the use of rate-constitutive equations [8,9,12-14]. In addition to the restrictions of small elastic strains imposed by this hypoelastic formulation, it also obscures a proper definition of 'mean gradient' and 'average volume changes' necessary for imposing the mass conservation equation at finite increments. Consequently, second-order terms in the hypoelastic extension are ignored, particularly in the mass conservation equation, which leads to a degradation of accuracy when the load increment is large.

The present study adopts an alternative formulation for large strain elastoplasticity based on the multiplicative decomposition of the deformation gradient. This method completely circumvents the 'rate issue' in large deformation analysis [17,18], and allows for the development of large elastic strains. Multiplicative decomposition technique better represent the particulate nature of soil, much like for metals from its crystal microstructure. It provides a means for describing mathematically the relationships between the reference configuration, the current configuration, and the unloaded, stress-free intermediate configuration of a soil assembly subjected to large deformation in the microscopic sense. A more recent development [19,20] indicates that the multiplicative

decomposition technique can be exploited to such an extent that the resulting algorithms may inherit all the features of the classical model of small strain plasticity.

Proper characterization of fluid flow is another long-standing issue in large deformation consolidation analysis. Classical theory of mixtures [21-26] is employed in this study to describe coupled response of solid and fluid phases. Accordingly soil-water mixture is viewed as a two-phase continuum, appropriate balance principles that govern the interaction between the solid and fluid constituents are derived. In contrast to previous formulations of the mixture theories, however, this study focused on the motion of the solid phase alone and uses the constitutive flow theory in terms of relative motion of the fluid with that of the solid [27]. Spatial form of generalized Darcy's law is used to describe the constitutive relation of the fluid phase.

Due to its simplicity and practicality, modified Cam-Clay (MCC) model [28, 29] of critical state soil mechanics is adopted in this study to represent the nonlinear responses (plastic and viscoplastic) of the solid phase. Important features like hyperelasticity and bilogarithmic compressibility law are added to MCC model to better simulate the behavior of soft clay in large strain regime.

Finally the mathematical framework of non-linear large deformation consolidation analysis is implemented in a displacement-based finite element code PlasFEM, which is been developed by the Geotechnical Engineering group at the University of Florida over last few years. Numerical analysis is performed to study the consolidation behavior of a field case of low solid-content phosphatic waste clay.

1.3 Scope of Work

The dissertation is organized in twelve chapters. Chapter 2 presents literature review and historical development of the theory of mixtures for porous media based on balance laws, micromechanical approach for large strain based on the theory of multiplicative decomposition. In Chapter 3, general kinematics and balance laws for a non-interacting mixture of non-polar constituents are derived in the light of modern theory of mixtures. Balance equations, specific for a fully saturated soil media (two-phase), are further reduced from generalized equations. In Chapter 4, field equations or strong form of the boundary-value problem of consolidation phenomenon are established from balance equations, corresponding weak forms are derived for use in subsequent finite element formulation. Constitutive theories for solid and fluid phases, appropriate for large strain, are outlined. Constitutive models for phosphatic waste clay (low solid-content clay) are discussed in Chapters 5 and 6. Hyperelastic-plastic MCC (modified Cam-Clay) model, suitable for primary consolidation response, is presented in Chapter 5. Chapter 6 presents the development of a hyperelastic-viscoplastic MCC model, used for simulation of time-dependent secondary compression. Explicit expressions for the consistent tangent moduli of the constitutive models are derived in the framework of large deformation theory, based on multiplicative decomposition as mentioned before. In Chapter 7, corresponding variational equations for boundary value problems are developed and linearized for implementation into a finite element code. Chapter 8 presents the implementation issue of the governing equations, i.e., matrix formulation for finite element code. Descriptions of the centrifuge equipments and instrumentation, used for studying consolidation behavior of the phosphatice waste clay, are given in Chapter 9.

Chapter 9 also presents the aspects of centrifuge modeling and the results from the centrifuge tests. Chapter 10 presents numerical examples of one and two-dimensional hyperelastic consolidation. These examples demonstrate significance of large strain on consolidation responses compared to the same for small strain formulation. Chapter 11 presents a study of consolidation phenomena of phosphatic waste clay, deposited at the construction site of Polk County Expressway (a multi-lane expressway around Lakeland, Florida). Numerical simulations are run for cases of hyperelastic-plastic (primary) and hyperelastic-viscoplastic (secondary, i.e., creep settlement) consolidation. Field settlement and pore pressure data are compared with numerical predictions. Chapter 12 contains a summary of the work that has been presented, as well as conclusions and recommendations for future investigations.

CHAPTER 2
LITERATURE REVIEW

2.1 Consolidation

The first author to deal with the important problem of fluid-filled deformable porous solids was von Terzaghi. In a famous paper presented to the Academy of Sciences in Vienna in June 1923, von Terzaghi showed the derivation of his consolidation theory. This theory was later published in his book, which is now considered as the first substantial book [30] in soil mechanics.

In the early 40's Biot [1] generalized von Terzaghi's theory of consolidation by extending it to the three-dimensional case and by establishing equations valid for any arbitrary load varied with time. In the following years, Biot generalized his theory to include properties of anisotropy, variable permeability, linear viscoelasticity, and the propagation of elastic waves in a fluid saturated porous solid [2,31]. The main disadvantage of Biot's model, however, lies in the fact that the corresponding theory is not developed from the fundamental axioms and principles of mechanics and thermodynamics. Thus, some derivations are complicated and obscure. Finally, Biot [32] developed, within the framework of quasi-static and isothermal deformations, a theory of large deformations of porous media.

Since the beginning of the 1960's the study of porous media advanced with development of new continuum theory of mixtures. In 1960, Truesdell and Toupin [26] presented a treatise on the classical field theories where they developed in detail the

properties of motion and fundamental physical principle of balance. In 1965, Green and Naghdi [25] developed a dynamic theory for the relative flow of the two continua based on an energy equation and an entropy production inequality for the entire continuum.

With the advances in modern computational science and the development of rigorous numerical techniques, such as the finite element method, numerical implementations of the consolidation theory, Biot's equations and the mixture theories found wide applications. A variational formulation of the dynamics of fluid-saturated porous solids was the basis of a numerical method that Ghaboussi and Dikmen [33] developed for the purpose of discretizing the spatial media into finite elements. Sandhu and Wilson [34] first applied the finite element method to study fluid flow in saturated porous media. With the presence of finite element method as a sound numerical technique, it was possible to extend the mixture theory to encompass elasto-plastic non-linear constitutive models and obtain reliable solutions of the field displacements and pressures. A general analytical procedure that accounts for non-linear effects was presented by Prevost [8]. In his work, Prevost focused on the integration of the discretized field equations based on the mixture theories of Green and Naghdi [25]. Later he worked on several numerical applications to study the consolidation of inelastic porous media [35] and the non-linear transient phenomenon [36]. Due to the increasing necessity of nonlinear applications, Zienkiewicz and other researchers published a series of papers that elucidated various numerical solutions for pore-fluid interaction analysis. Zienkiewicz et al. [37] classified different method of analysis in a comprehensive paper on numerical solutions of the Biot formulation. A continuum theory of saturated porous

media that is applicable for soils exhibiting large strains was formulated later by Kiousis and Voyadjis [38]. Borja and Alarćon [39] recently proposed a framework for large strain consolidation based on continuum theory of mixtures.

The mathematical basis for balance principles presented in this study is derived from the general theory of mixtures [21-26]. This research is focussed on fully saturated porous media (two-phase continua). Field equations governing the interaction between soil skeleton and pore fluid are developed from balance laws.

2.2 Large Strain Multiplicative Plasticity

Up to the beginning of the 1980s computational methods for large strain elastoplasticity typically relied on hypoelastic extensions of the classical small strain models; see, e.g., the reviews of Needleman and Tvergvaard [40], hence remained restricted to small elastic strains. Computational approaches based on the multiplicative decomposition appear to have been first proposed by Argyris and Doltsinis [41] within the context of so-called natural formulation. Subsequently, however, these authors appear to favor hypoelastic rate models on the basis that multiplicative formulations '.... Lead in principle to non-symmetric relations between stress rates and strain rates' (see [21, p. 22]). Simo and Ortiz [43] and Simo [44] proposed a computational approach entirely based on multiplicative decomposition and pointed out the role of intermediate configuration in a definition of the trial state via mere function evaluation of hyper-elastic stress-strain relations. Extensions of classical volume/displacement mixed methods within the framework of the multiplicative decomposition, originally introduced for

plasticity problems in [45] are presented in [46]. In recent years, computational approaches based on multiplicative decomposition have received considerable attention in the literature. Simo [47] exploited a strain-space version of the principle of maximum dissipation to obtain the associative flow rule consistent with multiplicative decomposition, and used a (covariant) backward method to derive a large strain version of the return mapping algorithms. Subsequently, Weber and Anand [48] and Eterovich and Bathe [49] used the multiplicative decomposition in conjunction with the logarithmic stored energy function and an exponential approximation to the flow rule cast in terms of full plastic deformation gradient. The multiplicative decomposition along with a logarithmic stored energy function is used in [50]. More recently, Moran et al. [51] addressed a number of computational aspects of multiplicative plasticity and presented explicit/implicit integration algorithms. Methods of convex analysis, again in the context of the multiplicative decomposition, are discussed in [52]

The preceding survey, although by no means comprehensive, conveys the popularity gained in recent years by computational elasto-plasticity based on the multiplicative decomposition. Despite their success, these approaches involve modifications, and often a complete reformulation, of the standard closest-point algorithms of the small strain theory. From a practical stand-point the implication is that the implementation of classical models needs to be considered on a case-by-case basis in the large strain regime.

In a later study, Simo [20] proposed a state-of-the-art algorithm based on multiplicative decomposition of the deformation gradient, as suggested by Lee [53],

Mandel [15] and others. The appeal of his formulation is that: the closest-point projection algorithm of any classical simple-surface or multi-surface model of small strain plasticity carries over to the large deformation context without modification. In particular, the algorithmic tangent moduli of small strain theory remain unchanged while introducing a further simplification: the closest-point projection algorithm is now formulated in principal (Kirchhoff) stresses. For the static problem, the proposed algorithm preserves exactly plastic volume changes if the yield criterion is pressure insensitive. For dynamic problems, Simo [20] presented a class of time-stepping algorithms which inherits exactly the conservation laws of total linear and angular momentum. Simo's method is adopted with success in some recent works [39,54,55] for formulating nonlinear plasticity model in large deformation context.

Present study has followed the above-mentioned theory [20] of multiplicative decomposition to derive explicit expressions of consistent tangent moduli for the proposed elasto-plastic and viscoplastic constitutive models (see Chapters 5 and 6).

CHAPTER 3
THEORY OF MIXTURES

3.1 Basic Theory

The conceptual model of a multiphase continua is based on the phenomenological behavior of each phase rather than particulate nature and the microscopic origin of the phenomenon involved. In other words, each phase (or constituent) enters through its average properties obtained as if the particles were smeared out in space. In order to be able to derive multiphase field and constitutive equations for such a medium, a technique for obtaining local average quantities is therefore necessary. Furthermore the basic kinematics and balanced equations for each phase and for the mixture as a whole must be defined. In following sections (3.2 to 3.4) general kinematics and balance laws are derived for a multiphase (n-phase) continuum allowing for the selection of the constitutive relations to be defined according to the particular phases that composes the mixture. For simplicity, it is assumed that phases are non-interacting and non-polar.

3.2 Kinematics

A mixture can be viewed as a superposition of n single materials each of which may be regarded as a continuum. It is assumed that at any time t each place **x** of a mixture is occupied simultaneously by n different particles: X^1, X^2, …. , X^n. As in single-phase

theory, a fixed but otherwise arbitrary reference configuration and a motion are assigned to each phase [26] as

$$\mathbf{x} = \phi_t^{\alpha}(\mathbf{X}^{\alpha}) \qquad \forall\ \alpha = 1 \ldots n, \tag{3.1}$$

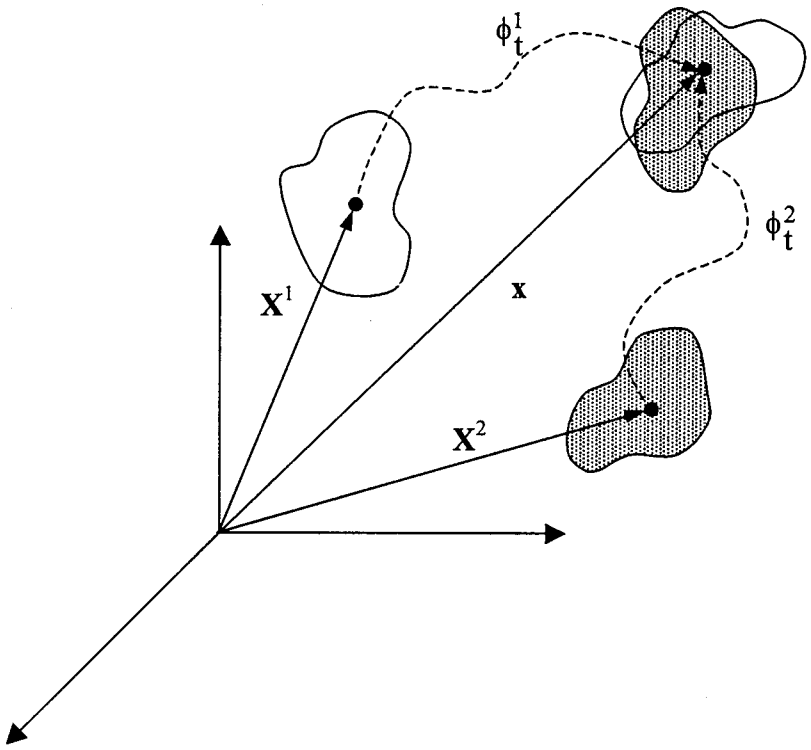

Figure 3.1 Geometric representation of kinematics for a two-phase mixture

where $\mathbf{X}^{\alpha}$ denotes the position of α phase in its reference configuration, and $\mathbf{x}$ is the spatial position occupied at the time t by the particle labeled $\mathbf{X}^{\alpha}$. The function ϕ_t^{α} in (3.1) is called the deformation function for α phase at time t. In classical continuum theory ϕ_t^{α} is assumed invertible, and thus

$$\mathbf{X}^{\alpha} = \left(\phi_t^{\alpha}\right)^{-1}(\mathbf{x}) \qquad \forall\ \alpha = 1 \ldots n. \tag{3.2}$$

The invertibility of the deformation function ensures that a particle at $\mathbf{X}^{\alpha}$ cannot occupy two spatial positions at a given time and that two particles of α phase with positions $\mathbf{X}_1^{\alpha}$ and $\mathbf{X}_2^{\alpha}$ cannot occupy the same spatial position. Figure 3.1 shows geometrical representation of (3.1) in Cartesian coordinate system $\in R^3$.

The velocity and acceleration of $\mathbf{X}^{\alpha}$ at time t are obtained from Equation (3.1) by time differentiation, viz.

$$\begin{aligned} \mathbf{v}^{\alpha} &= \mathbf{v}^{\alpha}(\mathbf{x}, t) = \frac{D^{\alpha}}{Dt}(\mathbf{x}) = \dot{\mathbf{x}}^{\alpha}; \\ \mathbf{a}^{\alpha} &= \mathbf{a}^{\alpha}(\mathbf{x}, t) = \frac{D^{\alpha}}{Dt}\left(\mathbf{v}^{\alpha}\right) = \ddot{\mathbf{x}}^{\alpha}, \end{aligned} \tag{3.3}$$

where a superimposed dot indicates differentiation with respect to time holding $\mathbf{X}^{\alpha}$ fixed (i.e., the material derivative following the motion of α phase). Material time derivative may be computed from spatial description using the following definition

$$\frac{D^{\alpha}}{Dt}(\bullet) = \frac{\partial}{\partial t}(\bullet) + \mathbf{v}^{\alpha} \cdot \operatorname{grad}(\bullet). \tag{3.4a}$$

Material time derivative of a volume integral can be expressed as

$$\frac{D^{\alpha}}{Dt}\int_{\Omega}(\bullet)^{\alpha}\, d\Omega = \frac{\partial}{\partial t}\int_{\Omega}(\bullet)^{\alpha}\, d\Omega + \int_{\Gamma}(\bullet)^{\alpha}\left(\mathbf{v}^{\alpha} \cdot \mathbf{n}\right) d\Gamma. \tag{3.4b}$$

See [56] for proof of the identities (3.4a), (3.4b). Here, and in the following, grad and GRAD are used to denote spatial and material derivatives, respectively. The deformation gradient for $\mathbf{X}^{\alpha}$ at time t is defined by

$$\mathbf{F}^{\alpha} = \mathbf{F}^{\alpha}(\mathbf{x},t) = \mathrm{GRAD}\,\mathbf{x} = \left[\frac{\partial x_a}{\partial X_A^{\alpha}}\right] = \left[\mathbf{F}_{aA}^{\alpha}\right], \tag{3.5}$$

and the velocity gradient is defined by

$$\mathbf{l}^{\alpha} = \mathbf{l}^{\alpha}(\mathbf{x},t) = \mathrm{grad}\,\mathbf{v}^{\alpha} = \dot{\mathbf{F}}^{\alpha} \cdot \left(\mathbf{F}^{\alpha}\right)^{-1}. \tag{3.6}$$

3.3 Average Quantities

An important assumption in the theory of mixtures is that the phases of a mixture are allowed to occupy common portions of a physical space. Then each spatial position **x** in a mixture is occupied by n elements, one from each phase (see Figure 3.1 for n = 2). To address this assumption one needs to define average quantities.

Average quantities are obtained by integrating microscopic quantities over an averaging volume or area. In the macroscopic field, the averaging volume represents a physical point, denoted by dV. Similarly, the averaging area dA, represents and characterizes a physical point on the surface of dV, and is an infinitesimal element of area in the macroscopic field. The part of dV occupied by the α phase is denoted by dV^{α}, and the volume fraction n^{α} of the α phase is the fraction of dV occupied by the α phase defined by

$$n^{\alpha} = n^{\alpha}(\mathbf{x},t) = \frac{dV^{\alpha}}{dV}, \tag{3.7}$$

where n^{α} is constrained by $\sum_{\alpha} n^{\alpha} = 1$ and $0 \le n^{\alpha} \le 1$. Similarly, the part of dA lying in the α phase is denoted by dA^{α}, and the areal fraction is defined by

$$\bar{n}^{\alpha} = \bar{n}^{\alpha}(\mathbf{x},t) = \frac{dA^{\alpha}}{dA}. \tag{3.8}$$

Again, $\sum_{\alpha} \bar{n}^{\alpha} = 1$ and $0 \le \bar{n}^{\alpha} \le 1$. It is assumed in the following that the identity $\bar{n}^{\alpha} = n^{\alpha}$ holds [57].

A macroscopic average mass density function, ρ^{α} is associated with each phase and is defined as the volume average of the microscopic density function, ρ_{α}.

$$\rho^{\alpha} = \frac{1}{dV} \int_{dV^{\alpha}} \rho_{\alpha} d\upsilon, \tag{3.9}$$

where $d\upsilon$ is the microscopic volume element. The intrinsic volume average mass density is defined as

$$\bar{\rho}^{\alpha} = \frac{1}{dV^{\alpha}} \int_{dV^{\alpha}} \rho_{\alpha} d\upsilon = \frac{1}{n^{\alpha}} \rho^{\alpha}. \tag{3.10}$$

If the mass density of the α phase is microscopically constant the intrinsic volume average mass density equals to the microscopic mass density, i.e., $\bar{\rho}^{\alpha} = \rho_{\alpha}$ and thus $\rho^{\alpha} = n^{\alpha}\rho_{\alpha}$.

The mass density ρ of the mixture is defined as

$$\rho = \rho(\mathbf{x},t) = \sum_{\alpha} \rho^{\alpha}, \tag{3.11}$$

and the volume-average velocity $\hat{\mathbf{v}}$ for the mixture is defined as

$$\hat{\mathbf{v}} = \hat{\mathbf{v}}(\mathbf{x},t) = \frac{1}{\rho} \sum_{\alpha} \rho^{\alpha} \mathbf{v}^{\alpha}. \tag{3.12}$$

Following the similar averaging approach, a macroscopic partial stress vector $\mathbf{t}^{\alpha}$ may be defined as

$$\mathbf{t}^{\alpha} = \frac{1}{d\Lambda} \int_{dA^{\alpha}} \mathbf{t}_{\alpha} da, \tag{3.13}$$

where da is microscopic area element. $\mathbf{t}_{\alpha}$ denotes the intrinsic stress vector of α phase, $\mathbf{t}^{\alpha} = n^{\alpha}\mathbf{t}_{\alpha}$.

3.4 Balance Laws

Once kinematics and local average quantities of a mixture are derived, one may postulate the laws of balance based on the theory of mixture [26] which must be satisfied irrespective of constitutive relations. Phases are understood to be material elements, which are open systems on a local state. Accordingly, local balance relations are derived for each individual phase. The equations are obtained in spatial configuration by applying the fundamental laws of mechanics: balance of mass, balance of linear momentum, balance of angular momentum, and the first and second laws of thermodynamics.

For consistency in notations, in the derivation of balance laws and in the following thereafter, spatial (deformed) configuration is represented by domain Ω, bounded by surface Γ while material (undeformed) configuration is represented by domain B, bounded by surface $\partial\mathsf{B}$.

3.4.1 Balance of Mass

The balance of mass can be expressed as "The time rate of mass in a fixed region in space Ω is equal to the time rate of mass flowing through the surface Γ that encloses Ω." In equation form

$$\int_{\Omega} \frac{\partial \rho}{\partial t} d\Omega = -\int_{\Gamma} \rho \mathbf{v} \cdot \mathbf{n} \, d\Gamma, \tag{3.14}$$

where $\mathbf{n}$ is the unit outward normal to the surface Γ, $\mathbf{v}$ is the flow velocity.

For illustration, mass flow through a control cube ($\delta x \times \delta y \times \delta z$) in Cartesian coordinate space $\in R^3$ is considered in Figure 3.2. Surface areas normal to the flow components along coordinate axes are $\Gamma_x = \delta y \delta z$, $\Gamma_y = \delta x \delta z$, $\Gamma_z = \delta x \delta y$.

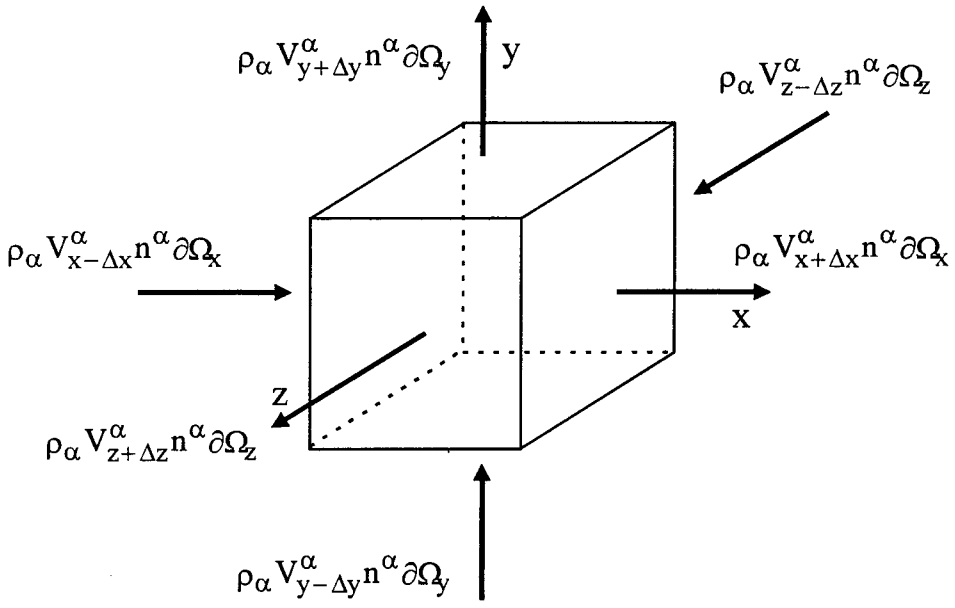

Figure 3.2 Balance of mass: flow through a control volume

For the cube (3.15) can be written as,

$$\Delta t\left\{\left[\rho_\alpha v^\alpha_{x+\Delta x} n^\alpha - \rho_\alpha v^\alpha_{x-\Delta x} n^\alpha\right]\delta y\delta z + \left[\rho_\alpha v^\alpha_{y+\Delta y} n^\alpha - \rho_\alpha v^\alpha_{y-\Delta y} n^\alpha\right]\delta x\delta z + \left[\rho_\alpha v^\alpha_{z+\Delta z} n^\alpha - \rho_\alpha v^\alpha_{z-\Delta z} n^\alpha\right]\right\}\delta x\delta y = \rho_\alpha dV^\alpha\Big|_{t+\Delta t} - \rho_\alpha dV^\alpha\Big|_t \tag{3.15}$$

Dividing by the volume $dV = \delta x\delta y\delta z$ and Δt, then upon rearrangement (3.16) can be written as

$$\mathrm{div}\left(n^\alpha \rho_\alpha \mathbf{v}^\alpha\right) + \frac{\partial}{\partial t}\left(n^\alpha \rho_\alpha\right) = 0. \tag{3.16}$$

(3.16) is the localized form of balance of mass for α phase.

3.4.2 Balance of Linear Momentum

In order to establish the balance of momentum laws for each α phase, one needs to consider the forces acting on the α phase within the region Ω such as drag forces, body forces or gravity forces, as well as, the effect on the α phase of the mixture outside the region Ω. This effect is accounted for by introducing partial stress vector $\mathbf{t}^\alpha$, defined in (3.13). Now, let σ^α be the Cauchy partial stress tensors [21-26] and $\mathbf{n}$ denotes the unit normal vector to the surface Γ. σ^α is related to $\mathbf{t}^\alpha$ by the relation $\mathbf{t}^\alpha = \sigma^\alpha \cdot \mathbf{n}$.

The first Euler equation postulates that "The rate of change of the total momentum of a given mass is equal to the vector sum of all the external forces acting on the mass." In equation form

$$\frac{D^\alpha}{Dt}\int_\Omega \rho^\alpha \mathbf{v}^\alpha d\Omega = \int_\Omega \hat{\mathbf{p}}^\alpha d\Omega + \int_\Gamma \sigma^\alpha \cdot \mathbf{n}\, d\Gamma + \int_\Omega \rho^\alpha \mathbf{g}\, d\Omega. \tag{3.17}$$

$\mathbf{g}$ is the vector of gravity acceleration, $\hat{\mathbf{p}}^{\alpha}$ is the momentum supply for the α phase from the rest of the mixture due to other interaction effects, e.g., relative motion of the phases. $\hat{\mathbf{p}}^{\alpha}$ is subject to $\sum_{\alpha} \hat{\mathbf{p}}^{\alpha} = \mathbf{0}$.

From divergence theorem

$$\int_{\Gamma} \sigma^{\alpha} \cdot \mathbf{n}\, d\Gamma = \int_{\Omega} \operatorname{div} \sigma^{\alpha}\, d\Omega. \tag{3.18}$$

Substitution of (3.18) in (3.17) results in

$$\frac{D^{\alpha}}{Dt} \int_{\Omega} \rho^{\alpha} \mathbf{v}^{\alpha}\, d\Omega = \int_{\Omega} \rho^{\alpha} \frac{D^{\alpha}}{Dt}\left(\mathbf{v}^{\alpha}\right) d\Omega = \int_{\Omega} \left[\operatorname{div} \sigma^{\alpha} + \hat{\mathbf{p}}^{\alpha} + \rho^{\alpha} \mathbf{g}\right] d\Omega, \tag{3.19}$$

which simplifies to the local version of the balance of linear momentum equations for individual phase as

$$\rho^{\alpha} \mathbf{a}^{\alpha} = \operatorname{div} \sigma^{\alpha} + \hat{\mathbf{p}}^{\alpha} + \rho^{\alpha} \mathbf{g}. \tag{3.20}$$

3.4.3 Balance of Angular Momentum

The principle of balance of moment of momentum states that the material rate of change of moment of momentum of a body about a fixed point $\mathbf{x}_0$, is equal to the resultant moment acting on the body around that point.

The moment of momentum for α phase is defined as

$$\mathrm{L}^{\alpha} = \int_{\Omega} \rho^{\alpha} \mathbf{r} \times \mathbf{v}^{\alpha}\, d\Omega. \tag{3.21}$$

$\mathbf{r}$ = vector of moment arm = $\mathbf{x} - \mathbf{x}_0$. Making use of (3.17) material derivative of (3.21) can be written in the form

$$\frac{D^{\alpha}}{Dt}L^{\alpha} = \frac{D^{\alpha}}{Dt}\int_{\Omega}\rho^{\alpha}\mathbf{r}\times\mathbf{v}^{\alpha}d\Omega$$
$$= \int_{\Omega}\mathbf{r}\times\left(\rho^{\alpha}\mathbf{g}+\hat{\mathbf{p}}^{\alpha}\right)d\Omega + \int_{\Gamma}\mathbf{r}\times\left(\sigma^{\alpha}\cdot\mathbf{n}\right)d\Gamma. \tag{3.22}$$

From divergence theorem

$$\int_{\Gamma}\mathbf{r}\times\left(\sigma^{\alpha}\cdot\mathbf{n}\right)d\Gamma = \int_{\Gamma}\mathbf{n}\cdot\left(\mathbf{r}\times\sigma^{\alpha}\right)d\Gamma = \int_{\Omega}\mathrm{div}\left(\mathbf{r}\times\sigma^{\alpha}\right)d\Omega. \tag{3.23}$$

Substitution of (3.23) in (3.22) yields

$$\frac{D^{\alpha}}{Dt}L^{\alpha} = \frac{\rho^{\alpha}D^{\alpha}}{Dt}\int_{\Omega}\mathbf{r}\times\mathbf{v}^{\alpha}d\Omega$$
$$= \int_{\Omega}\left\{\mathbf{r}\times\left(\rho^{\alpha}\mathbf{g}+\hat{\mathbf{p}}^{\alpha}\right)+\mathrm{div}\left(\mathbf{r}\times\sigma^{\alpha}\right)\right\}d\Omega. \tag{3.24}$$

Local form of (3.24) results

$$\rho^{\alpha}\frac{D^{\alpha}}{Dt}\left(\mathbf{r}\times\mathbf{v}^{\alpha}\right) = \mathbf{r}\times\left(\rho^{\alpha}\mathbf{g}+\hat{\mathbf{p}}^{\alpha}\right)+\mathrm{div}\left(\mathbf{r}\times\sigma^{\alpha}\right). \tag{3.25}$$

For cases of non-polar phases partial stress tenor, σ^{α} are symmetric since there is no supply of moment of momentum (i.e., antisymmetric part of σ^{α} is zero).

3.4.4 Balance of Energy

Principle of balance of energy or the first law of thermodynamics states that the material rate of change of internal energy in a body is equal to the resultant deformation power acting in the body plus the rate of heat added to the body.

The internal energy in the body for α phase may be defined as

$$U^{\alpha} = \int_{\Omega}\rho^{\alpha}e^{\alpha}\,d\Omega, \tag{3.26}$$

where e^{α} represents internal energy density for α phase. Assuming no supply of energy due to interaction, e.g., chemical interaction within the phases material rate of change of U^{α} can be decomposed into following components

$$\frac{D^{\alpha}U^{\alpha}}{Dt} = \frac{D^{\alpha}}{Dt}\left(P^{\alpha} + K^{\alpha} + Q^{\alpha}\right), \tag{3.27}$$

where P^{α} = Mechanical energy due to deformation of α phase

K^{α} = Kinetic energy of α phase

Q^{α} = Thermal energy of α phase due to heat generation within the domain Ω and heat flow across the boundary $d\Gamma$.

Material rates of energies for α phase can be expressed as follows:

$$\frac{D^{\alpha}P^{\alpha}}{Dt} = \int_{\Omega}\rho^{\alpha}\mathbf{g}\cdot\mathbf{v}^{\alpha}d\Omega + \int_{\Omega}\hat{\mathbf{p}}^{\alpha}\cdot\mathbf{v}^{\alpha}d\Omega + \int_{\Gamma}\sigma^{\alpha}:\mathbf{v}^{\alpha}\otimes\mathbf{n}\,d\Gamma, \tag{3.28a}$$

$$\begin{aligned}\frac{D^{\alpha}K^{\alpha}}{Dt} &= \frac{D^{\alpha}}{Dt}\int_{\Omega}\frac{1}{2}\rho^{\alpha}\mathbf{v}^{\alpha}\cdot\mathbf{v}^{\alpha}\,d\Omega \\ &= \frac{\partial}{\partial t}\int_{\Omega}\frac{1}{2}\rho^{\alpha}\mathbf{v}^{\alpha}\cdot\mathbf{v}^{\alpha}\,d\Omega + \int_{\Gamma}\left(\frac{1}{2}\rho^{\alpha}\mathbf{v}^{\alpha}\cdot\mathbf{v}^{\alpha}\right)\left(\mathbf{v}^{\alpha}\cdot\mathbf{n}\right)d\Gamma,\end{aligned} \tag{3.28b}$$

$$\frac{D^{\alpha}Q^{\alpha}}{Dt} = \int_{\Omega}\rho^{\alpha}H^{\alpha}\,d\Omega - \int_{\Gamma}\mathbf{q}^{\alpha}\cdot\mathbf{n}\,d\Gamma. \tag{3.28c}$$

H^{α} is the heat generation per unit mass for the α phase, and $\mathbf{q}^{\alpha}$ represents the heat flux vector associated with each phase. Substituting (3.28) in (3.27), one obtains for α phase the following expression

$$\frac{D^{\alpha}}{Dt}\int_{\Omega}\frac{1}{2}\rho^{\alpha}e^{\alpha}\,d\Omega = \int_{\Omega}\rho^{\alpha}\mathbf{g}\cdot\mathbf{v}^{\alpha}d\Omega + \int_{\Omega}\hat{\mathbf{p}}^{\alpha}\cdot\mathbf{v}^{\alpha}d\Omega + \int_{\Gamma}\sigma^{\alpha}:\mathbf{v}^{\alpha}\otimes\mathbf{n}\,d\Gamma$$
$$+\frac{\partial}{\partial t}\int_{\Omega}\frac{1}{2}\rho^{\alpha}\mathbf{v}^{\alpha}\cdot\mathbf{v}^{\alpha}\,d\Omega + \int_{\Gamma}\left(\frac{1}{2}\rho^{\alpha}\mathbf{v}^{\alpha}\cdot\mathbf{v}^{\alpha}\right)\left(\mathbf{v}^{\alpha}\cdot\mathbf{n}\right)d\Gamma \qquad (3.29)$$
$$+\int_{\Omega}\rho^{\alpha}H^{\alpha}\,d\Omega - \int_{\Gamma}\mathbf{q}^{\alpha}\cdot\mathbf{n}\,d\Gamma.$$

3.4.5 Entropy Inequality

Entropy inequality or the second law of thermodynamics puts limit on the direction of such processes where thermal phenomenon are involved, permitting energy transfer to occur spontaneously only in certain preferred directions. The limitation may be expressed mathematically as an inequality stating that the intrinsic entropy production of the entire mixture is always nonnegative and is positive for an irreversible process. In other words the material rate of change of the entropy increase is always higher or to that of the entropy due to heat transfer.

The entropy density for the entire mixture, η can be defined as

$$\eta = \sum_{\alpha}\rho^{\alpha}\eta^{\alpha}, \qquad (3.30)$$

η^{α} is the entropy density for α phase. Entropy increase for the entire mixture results

$$\int_{\Omega}\rho\eta\,d\Omega = \int_{\Omega}\sum_{\alpha}\rho^{\alpha}\eta^{\alpha}\,d\Omega. \qquad (3.31)$$

Assigning to each phase a temperature θ^{α}, given by a positive-valued function, the second law of thermodynamics may be expressed as

$$\sum_{\alpha}\frac{D^{\alpha}}{Dt}\int_{\Omega}\rho^{\alpha}\eta^{\alpha}\,d\Omega - \sum_{\alpha}\int_{\Omega}\frac{1}{\theta^{\alpha}}\rho^{\alpha}H^{\alpha}\,d\Omega + \sum_{\alpha}\int_{\Gamma}\frac{1}{\theta^{\alpha}}\mathbf{q}^{\alpha}\cdot\mathbf{n}\,d\Gamma \geq 0, \qquad (3.32)$$

H^α, $\mathbf{q}^\alpha$ are defined in (3.28c). Using (3.4b), divergence theorem and balance of mass (3.16), material time derivative of $\int_\Omega \rho^\alpha \eta^\alpha \, d\Omega$ can be derived as

$$\begin{aligned}\frac{D^\alpha}{Dt}\int_\Omega \rho^\alpha \eta^\alpha d\Omega &= \int_\Omega \left\{ \frac{\partial}{\partial t}\left(\rho^\alpha \eta^\alpha\right) + \operatorname{div}\left[\rho^\alpha \eta^\alpha \mathbf{v}^\alpha\right]\right\} d\Omega \\ &= \int_\Omega \left\{ \eta^\alpha \left[\frac{\partial}{\partial t}\rho^\alpha + \operatorname{div}\left(\rho^\alpha \mathbf{v}^\alpha\right)\right] + \rho^\alpha \left(\frac{\partial}{\partial t}\eta^\alpha + \operatorname{grad}\eta^\alpha \cdot \mathbf{v}^\alpha\right)\right\} d\Omega \\ &= \int_\Omega \rho^\alpha \frac{\partial \eta^\alpha}{\partial t} d\Omega.\end{aligned} \tag{3.33}$$

Substitution of (3.33) in (3.32) results

$$\sum_\alpha \int_\Omega \left(\rho^\alpha \frac{\partial \eta^\alpha}{\partial t} - \frac{1}{\theta^\alpha}\rho^\alpha {}_H{}^\alpha + \operatorname{div}\left[\frac{1}{\theta^\alpha}\mathbf{q}^\alpha\right]\right) d\Omega \geq 0 . \tag{3.34}$$

Localization of (3.34) yields

$$\rho^\alpha \frac{\partial \eta^\alpha}{\partial t} - \frac{1}{\theta^\alpha}\rho^\alpha {}_H{}^\alpha + \operatorname{div}\left[\frac{1}{\theta^\alpha}\mathbf{q}^\alpha\right] \geq 0. \tag{3.35}$$

Introducing the Helmholtz free energy function for α phase, ψ^α defined by

$$\psi^\alpha = e^\alpha - \theta^\alpha \eta^\alpha, \tag{3.36}$$

one can write

$$\rho^\alpha \frac{\partial \eta^\alpha}{\partial t} = \frac{\rho^\alpha}{\theta^\alpha}\left(\frac{\partial e^\alpha}{\partial t} - \frac{\partial \psi^\alpha}{\partial t} - \eta^\alpha \frac{\partial \theta^\alpha}{\partial t}\right). \tag{3.37}$$

Substituting (3.37) in (3.35), localized form of entropy inequality can be written as

$$\rho^\alpha \left(\frac{\partial e^\alpha}{\partial t} - \frac{\partial \psi^\alpha}{\partial t} - \eta^\alpha \frac{\partial \theta^\alpha}{\partial t}\right) - \rho^\alpha {}_H{}^\alpha + \theta^\alpha \operatorname{div}\left[\frac{1}{\theta^\alpha} q^\alpha\right] \geq 0. \tag{3.38}$$

3.5 Balance Laws for Saturated Soil

Balance laws of saturated soil medium are special case of generalized balance laws of n-phase continuum considering n = 2 (solid and fluid phases). Following the derivations in Section 3.4, necessary balance laws for soil-water mixture are deduced in this section. Motions of solid and fluid phases are considered separately.

3.5.1 Balance of Mass

Following (3.16), localized form of balance of mass for solid and fluid phases can be written, respectively, as

$$\operatorname{div}\left(n^{S}\rho_{S}\mathbf{v}^{S}\right)+\frac{\partial}{\partial t}\left(n^{S}\rho_{S}\right)=0, \tag{3.39a}$$

$$\operatorname{div}\left(n^{W}\rho_{W}\mathbf{v}^{W}\right)+\frac{\partial}{\partial t}\left(n^{W}\rho_{W}\right)=0. \tag{3.39b}$$

Adding (3.39a) and (3.39b) gives the conservation of mass for the soil-water mixture as

$$\frac{\partial\rho}{\partial t}+\operatorname{div}(\rho\hat{\mathbf{v}})=0, \tag{3.40}$$

where $\hat{\mathbf{v}}$ is the volume-average velocity, defined in (3.12).

3.5.2 Balance of Linear Momentum

In the absence of inertia forces balance laws of linear momentum for solid and fluid phases can be written from (3.17) as follows:

$$\int_{\Omega}\rho^{S}\mathbf{g}\,d\Omega+\int_{\Omega}\hat{\mathbf{p}}^{S}\,d\Omega+\int_{\Gamma}\sigma^{S}\cdot\mathbf{n}\,d\Gamma=\mathbf{0}, \tag{3.41a}$$

$$\int_{\Omega}\rho^{W}\mathbf{g}\,d\Omega+\int_{\Omega}\hat{\mathbf{p}}^{W}\,d\Omega+\int_{\Gamma}\sigma^{W}\cdot\mathbf{n}\,d\Gamma=\mathbf{0}. \tag{3.41b}$$

Since $\hat{\mathbf{p}}^S$ and $\hat{\mathbf{p}}^W$ are the internal forces which naturally will not affect the soil-water mixture as a whole, $\hat{\mathbf{p}}^S + \hat{\mathbf{p}}^W = \mathbf{0}$, i.e., the seepage force exerted by the fluid on the solid matrix is the negative of the reactive force exerted by the solid matrix on the fluid. Consequently, the sum of (3.41a) and (3.41b) results in

$$\int_\Omega \rho \mathbf{g}\, d\Omega + \int_\Gamma \tilde{\sigma} \cdot \mathbf{n}\, d\Gamma = \mathbf{0}. \tag{3.42}$$

$\tilde{\sigma}$ is the Cauchy total stress tensor, $\tilde{\sigma} = \sigma^S + \sigma^W$.

Now, let $\mathbf{P}^w$ and $\mathbf{P}^s$ be the (non-symmetric) first Piola-Kirchhoff partial stress tensors arising from the fluid and intergranular stresses, respectively. Also, let $\mathbf{N}$ denote the unit normal vector to the surface $\partial\mathsf{B}$ of the undeformed region B. The tensor $\mathbf{P}^w$ is defined such that $\mathbf{P}^w \cdot \mathbf{N}$ represents the resultant force exerted by the fluid per unit area of the solid matrix in the undeformed configuration. Similarly, the product $\mathbf{P}^s \cdot \mathbf{N}$ is the resultant net force exerted by the individual grains (which may include the partial effects of fluid pressures) over the same undeformed reference area. By the additive decomposition of the Cauchy total stress tensors, we obtain a similar expression for the first Piola-Kirchhoff total stress tensor $\tilde{\mathbf{P}}$

$$\tilde{\mathbf{P}} = J\tilde{\sigma} \cdot \mathbf{F}^{-t} = \mathbf{P}^s + \mathbf{P}^w, \tag{3.43}$$

where $\mathbf{P}^s = J\sigma^s \cdot \mathbf{F}^{-t}$ and $\mathbf{P}^s = J\sigma^s \cdot \mathbf{F}^{-t}$ are the first Piola-Kirchhoff partial stress tensors arising from the solid and fluid stresses, respectively, and

$$J = \det(\mathbf{F}); \quad \mathbf{F} = \frac{\partial \mathbf{x}}{\partial \mathbf{X}}; \quad \mathbf{x} = \mathbf{X} + \mathbf{u}. \tag{3.44}$$

In (3.44), J is the Jacobian, **F** is deformation gradient, **X** are the coordinates of a point X in undeformed configuration, **u** is the macroscopic displacement field of the solid phase, **x** are the spatial coordinates of point X.

$\widetilde{\mathbf{P}}$ can also be decomposed as

$$\widetilde{\mathbf{P}} = \mathbf{P} + \frac{\mathbf{P}^{w}}{n^{w}}, \tag{3.45}$$

where **P** is the first Piola-Kirchhoff effective stress tensor, and $(\mathbf{P}^{w}/n^{w})\cdot\mathbf{N}$ represents the resultant force exerted by the fluid per unit area of void in the undeformed configuration. **P** and $\mathbf{P}^{s}$ are related by the equation

$$\mathbf{P}^{S} = \mathbf{P} + \left(\frac{1}{n^{w}} - 1\right)\mathbf{P}^{w}. \tag{3.46}$$

An integral equation similar to (3.42) can be developed in terms of the tensor $\widetilde{\mathbf{P}}$. With reference to the undeformed configuration, (3.42) can be written in the form

$$\int_{B} \rho_0 \mathbf{g}\, dV + \int_{\partial B} \widetilde{\mathbf{P}}\cdot\mathbf{N}\, dA = \mathbf{0}, \tag{3.47}$$

$\rho_0 = J\rho$ is a pull-back mass density of the soil-water mixture and **g** is the vector of gravity accelerations.

It is very important to note that ρ_0 is not a constant quantity. Figure 3.3 would explain the scenario. In Figure 3.3, the fluid now occupying the void in a soil at a point $\phi_t(X)$ may not necessarily be the same fluid material that occupied the same void at a reference point X in the undeformed region B. Mathematically, $\phi_t(X) = \phi_t(Y)$, where $\phi_t(Y)$ is the spatial configuration of the fluid phase whose reference configuration is at Y.

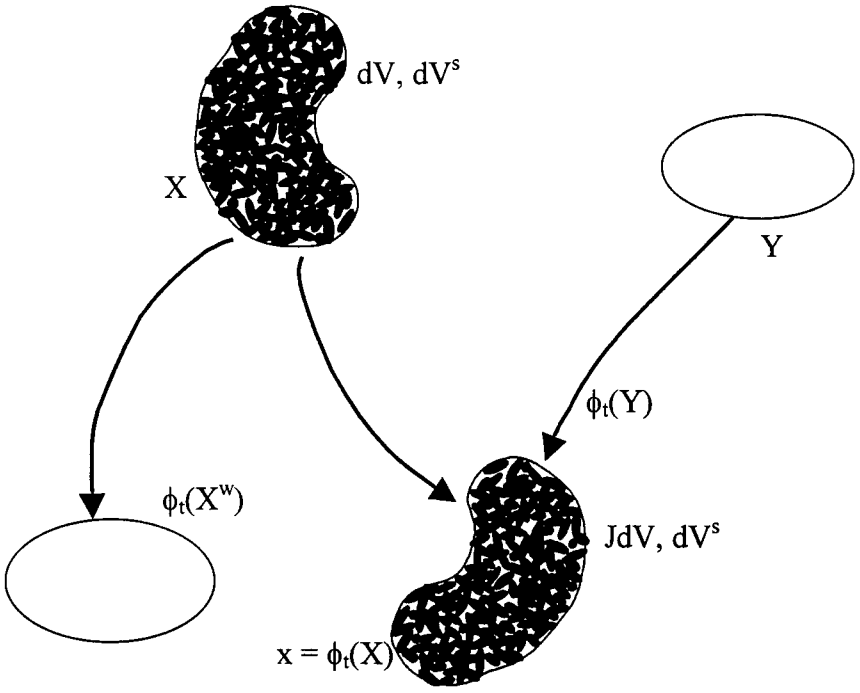

Figure 3.3 Balance of mass: total mass of material point X is not conserved in $\phi_t(X)$

Notice that Y does not necessarily have to be in B. Likewise, fluid phase of material point X, X^w might not necessarily be present in the spatial configuration $\phi_t(X)$. Hence, ρ_0 does not necessarily represents the true mass-density in B of the soil mass which now occupies the volume $\phi_t(B)$, since fluid can migrate into or out of the soil matrix during the motion. In other words, the total mass of the soil-water mixture in B is not necessarily conserved in $\phi_t(B)$.

A simple relationship analysis in the following would demonstrate the effects of diffusion on mass densities. Let $n_0^w(X, t = 0)$ be the initial porosity of the point X in B. Then, the initial volume of the voids in an elementary volume dV is $n_0^w dV$, while the

initial volume of the solid region is $\left(1-n_0^w\right)dV$. As the soil matrix deforms, its volume changes to dv = J dV. Now, assume the solid phase is incompressible. Since **u** is the displacement field of the solid phase, its volume is conserved at $\left(1-n_0^w\right)dV$ in dv, while the volume of the voids changes to $dv-\left(1-n_0^w\right)dV$. Consequently the porosity varies according to

$$n^w = \frac{J\,dV-\left(1-n_0^w\right)dV}{J\,dV} = 1-\left(1-n_0^w\right)J^{-1}. \tag{3.48}$$

Hence, the total mass density and the porosity of soil vary with deformation through the Jacobian J.

3.5.3 Balance of Energy

Ignoring kinetic energy and non-mechanical power, and assuming balance of momentum and balance of mass hold, (3.29) can be simplified for balance of energy of α phase as

$$\frac{D^\alpha}{Dt}\int_\Omega \rho^\alpha e^\alpha d\Omega = \int_\Omega \rho^\alpha \mathbf{g}\cdot\mathbf{v}^\alpha d\Omega + \int_\Omega \hat{\mathbf{p}}^\alpha\cdot\mathbf{v}^\alpha d\Omega + \int_\Gamma \sigma^\alpha : \mathbf{v}^\alpha \otimes \mathbf{n}\, d\Gamma. \tag{3.49}$$

The localized version of balance of energy can be derived in the following fashion. Consider the left-hand side of (3.49), for example. Following the derivation of (3.33), one can reduce

$$\frac{D^\alpha}{Dt}\int_\Omega \rho^\alpha e^\alpha d\Omega = \int_\Omega \rho^\alpha \dot{e}^\alpha\, d\Omega, \tag{3.50}$$

since grad $e^{\alpha} = \mathbf{0}$. Using divergence theorem and localized version of balance of linear momentum (3.20), one can reduce right-hand side of (3.49) as

$$\begin{aligned}
&\int_{\Omega}\left(\rho^{\alpha}\mathbf{g}+\hat{\mathbf{p}}^{\alpha}\right)\cdot\mathbf{v}^{\alpha}d\Omega+\int_{\Gamma}\sigma^{\alpha}:\mathbf{v}^{\alpha}\otimes\mathbf{n}\,d\Gamma \\
&=-\int_{\Omega}\operatorname{div}\sigma^{\alpha}\cdot\mathbf{v}^{\alpha}d\Omega+\int_{\Omega}\left[\operatorname{div}\sigma^{\alpha}\cdot\mathbf{v}^{\alpha}+\sigma^{\alpha}:\operatorname{grad}\mathbf{v}^{\alpha}\right]d\Omega \\
&=\int_{\Omega}\sigma^{\alpha}:\mathbf{l}^{\alpha}\,d\Omega=\int_{\Omega}\sigma^{\alpha}:\mathbf{d}^{\alpha}\,d\Omega.
\end{aligned} \tag{3.51}$$

$\mathbf{l}^{\alpha}$ is defined in (3.6), $\mathbf{d}^{\alpha} = \mathrm{Sym}(\mathbf{l}^{\alpha})$. Since σ^{α} is symmetric, $\sigma^{\alpha} : \mathbf{l}^{\alpha} = \sigma^{\alpha} : \mathbf{d}^{\alpha}$. Substituting (3.50) and (3.51) in (3.49), localized version of balance of energy for α phase can be written as

$$\rho^{\alpha}\dot{e}^{\alpha} = \sigma^{\alpha} : \mathbf{d}^{\alpha}, \tag{3.52}$$

Corresponding localization for the saturated soil media takes the form

$$\rho\dot{\bar{e}} = \sigma^{s} : \mathbf{d}^{s} + \sigma^{w} : \mathbf{d}^{w}, \tag{3.53}$$

where $\dot{\bar{e}}$ is the rate of internal energy for the soil-water mixture obtained from the volume average

$$\dot{\bar{e}} = \frac{\rho^{s}\dot{e}^{s} + \rho^{w}\dot{e}^{w}}{\rho}. \tag{3.54}$$

It is often convenient to describe the balance of energy in the material picture because the domain of integration of the functions remains fixed. To this end, one makes use of the following transformation. Let the right leg of the tensor $\tilde{\mathbf{P}}$ be pushed forward by the configuration ϕ_t. The result is the Kirchhoff total stress tensor $\tilde{\tau}$, which differs from the Cauchy total stress tensor $\tilde{\sigma}$ by the factor J, i.e.,

$$\tilde{\tau} = J\tilde{\sigma} = \tilde{\mathbf{P}}\cdot\mathbf{F}^{t}. \tag{3.55}$$

$\tilde{\tau}$ can be decomposed into solid and fluid counterparts in any of the following ways

$$\tilde{\tau} = \tau^{S} + \tau^{W} = \tau + \frac{\tau^{W}}{n^{W}} = \tau + \theta \mathbf{1}. \tag{3.56}$$

τ is Kirchhoff effective stress, θ is Kirchhoff pore water pressure (compression positive), $\mathbf{1}$ is the second order identity tensor. Now, pulling back the left leg of $\tilde{\mathbf{P}}$ by the inverse motion $(\phi_t)^{-1}$, one obtains symmetric $\tilde{\mathbf{S}}$, the second Piola-Kirchhoff total stress tensor such as

$$\tilde{\mathbf{S}} = \mathbf{F}^{-1} \cdot \tilde{\mathbf{P}} = \mathbf{F}^{-1} \cdot \tilde{\tau} \cdot \mathbf{F}^{-t} = J\mathbf{F}^{-1} \cdot \tilde{\sigma} \cdot \mathbf{F}^{-t}. \tag{3.57}$$

Following (3.56) and (3.57), additive decomposition of $\tilde{\mathbf{S}}$ can be written as

$$\tilde{\mathbf{S}} = \mathbf{S} + \theta \mathbf{C}^{-1}, \tag{3.58}$$

where $\mathbf{S}$ is the second Piola-Kirchhoff effective stress tensor and $\mathbf{C}$ is the right Cauchy-Green tensor given explicitly by

$$\mathbf{C} = \mathbf{F}^{t} \cdot \mathbf{F}. \tag{3.59}$$

$\mathbf{F}$ is defined in (3.44).

Let $\mathbf{x} = \phi(\mathbf{X}, t)$, $E^{\alpha}(\mathbf{X}, t) = e^{\alpha}(\mathbf{x}, t)$. If one multiplies the localized balance of energy (3.52) by J, and uses the porosity expression (3.48), one obtains the following expression for the balance of energy for the solid and fluid phases in localized material form

$$\begin{aligned} &\rho_S n_0^S \dot{E}^S = \tau^S : \mathbf{d}^S = \frac{1}{2}\mathbf{S}^S : \dot{\mathbf{C}}; \\ &\rho_W \left(J - n_0^S\right) \dot{E}^W = \tau^W : \mathbf{d}^W = \frac{1}{2}\mathbf{S}^W : \dot{\mathbf{C}}^W. \end{aligned} \tag{3.60}$$

Balance of energy for the soil-water mixture in the material picture is now given by

$$J\rho\dot{\bar{E}} = \tau^s : \mathbf{d}^s + \tau^w : \mathbf{d}^w = \frac{1}{2}\mathbf{S}^s : \dot{\mathbf{C}} + \frac{1}{2}\mathbf{S}^w : \dot{\mathbf{C}}^w, \tag{3.61}$$

Where $\dot{\bar{E}}$ is obtained from the volume average

$$\dot{\bar{E}} = \frac{\rho_s n_0^s \dot{E}^s + \rho_s \left(J - n_0^w\right)\dot{E}^w}{J\rho} = \dot{\bar{e}}. \tag{3.62}$$

The quantity $J\rho\,\dot{\bar{E}}$ is the mechanical power generated per unit reference volume of the soil-water mixture. (3.61) can be expressed in a more elegant form in terms of effective Kirchhoff stress and deformation of the solid phase as

$$J\rho\dot{\bar{E}} = \tau : \mathbf{d}^s, \tag{3.63}$$

i.e., the sum of the mechanical powers of the partial stresses is equal to the mechanical power of the effective stresses with respect to the deformation of the solid matrix computed from its own motion.

Proof of (3.63) is given in section A.2. (3.63) states that total mechanical power in soil-water mixture is absorbed by the energy rate $\tau : \mathbf{d}^s$, and that the pore pressure tensor τ^w / n^w in (3.56) performs no work. It is obvious from the fact that fluid is assumed incompressible and has no shear strength. By virtue of these assumptions, fluid cannot store volumetric nor deviatoric energy, i.e., it has no mechanical power.

3.5.4 Entropy Inequality

Ignoring non-mechanical power and kinetic energy production, the localized form of entropy inequality or the second law of thermodynamics (3.38) can be simplified as

$$\rho^{\alpha}\left(\dot{e}^{\alpha}-\dot{\psi}^{\alpha}\right)\geq 0. \tag{3.64}$$

In case of soil-water mixture (3.64) takes the form

$$\dot{e}-\dot{\bar{\psi}}\geq 0. \tag{3.65}$$

$\dot{e}$ is defined in (3.54). Similarly, $\dot{\bar{\psi}}$ is the rate of free energy for the soil-water mixture defined as

$$\dot{\bar{\psi}}=\frac{\rho^{s}\dot{\psi}^{s}+\rho^{w}\dot{\psi}^{w}}{\rho}. \tag{3.66}$$

Let $\mathbf{x}=\phi(\mathbf{X},t)$, $\Psi^{\alpha}(\mathbf{X},t)=\psi^{\alpha}(\mathbf{x},t)$. Similar to (3.62), volume average rate of free energy $\dot{\bar{\Psi}}$ can be expressed as

$$\dot{\bar{\Psi}}=\frac{\rho_{s}n_{0}^{s}\dot{\Psi}^{s}+\rho_{s}\left(J-n_{0}^{w}\right)\dot{\Psi}^{w}}{J\rho}=\dot{\bar{\psi}}. \tag{3.67}$$

From (3.62), (3.65), and (3.67) localized version of entropy inequality for soil-water mixture in undeformed configuration B can be written as

$$J\rho\dot{\bar{E}}-J\rho\dot{\bar{\Psi}}\geq 0. \tag{3.68}$$

$J\rho\dot{\bar{\Psi}}$ is the power generated from free energy. $J\rho\dot{\bar{\Psi}}=d\Psi/dt$; Ψ denotes the stored energy function, or free energy, per unit reference volume of soil matrix. Substituting (3.63), one can rewrite (3.68) as

$$\tau:\mathbf{d}^{s}-\frac{d\Psi}{dt}\geq 0. \tag{3.69}$$

CHAPTER 4
VARIATIONAL EQUATIONS, CONSTITUTIVE THEORIES

4.1 Boundary Value Problem

In order to formulate a well-defined boundary value problem for consolidation phenomenon, one needs to consider a problem domain with a set of suitable boundary conditions. Let $\mathsf{B} \subset R^{nsd}$ (nsd = no. of spatial dimensions) be an open set in material configuration (time t_0) with piecewise smooth boundary $\partial\mathsf{B}$. $\partial\mathsf{B}$ is assumed to admit the following decomposition

$$\begin{cases} \partial B^d \cup \partial B^t = \partial B, \\ \partial B^d \cap \partial B^t = \emptyset, \end{cases} \tag{4.1a}$$

$$\begin{cases} \partial B^\theta \cup \partial B^h = \partial B, \\ \partial B^\theta \cap \partial B^h = \emptyset. \end{cases} \tag{4.1b}$$

∂B^d, ∂B^t, ∂B^θ, ∂B^h are open sets in ∂B. ∂B^d and ∂B^t represent the portions of ∂B with prescribed displacement and tractions, respectively while ∂B^θ and ∂B^h represent portions with prescribed fluid potential and volumetric flow rate, respectively. $\emptyset$ is a null set.

In spatial description at any time $t \in [t_n, t_{n+1}]$, reference domain B will be mapped to the configuration $\Omega = \phi_t(B) \subset R^{nsd}$ with boundary $\Gamma = \phi_t(\partial B)$. Similar to (4.1), decomposition of boundary Γ will now take the following form

$$\begin{cases} \Gamma^d \cup \Gamma^t = \Gamma, \\ \Gamma^d \cap \Gamma^t = \emptyset, \end{cases} \tag{4.2a}$$

$$\begin{cases} \Gamma^{\theta} \cup \Gamma^{h} = \Gamma, \\ \Gamma^{\theta} \cap \Gamma^{h} = \emptyset. \end{cases} \tag{4.2b}$$

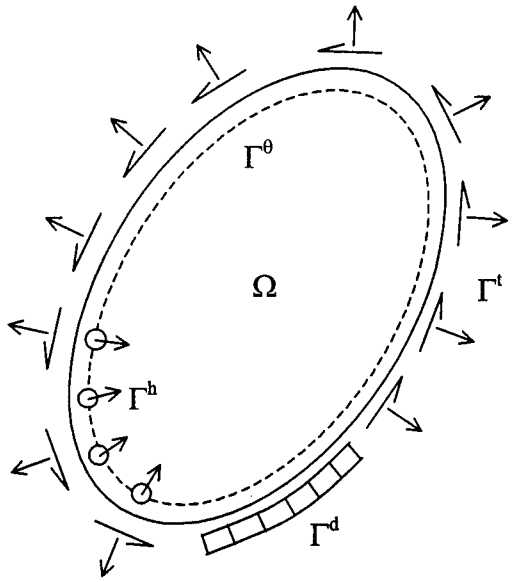

Figure 4.1 Prescribed boundary conditions of spatial domain Ω

In (4.2a) and (4.2b), $\Gamma^{d} = \phi_t(\partial B^{d})$, $\Gamma^{t} = \phi_t(\partial B^{t})$, $\Gamma^{\theta} = \phi_t(\partial B^{\theta})$, $\Gamma^{h} = \phi_t(\partial B^{h})$. Figure 4.1 shows decomposition of domain boundary in spatial configuration. Having outlined the domain boundary, one would require strong form of consolidation phenomenon with appropriate boundary conditions to define a well-posed mathematical problem.

4.2 Strong Form

Strong form or field equations of consolidation problem emanate from balance laws. Equation of equilibrium is derived from balance of linear momentum. Localization of (3.47) results in the following statement of stress equilibrium in material description

$$\mathrm{DIV}\,\tilde{\mathbf{P}} + \rho_0 \mathbf{g} = \mathbf{0}. \tag{4.3}$$

DIV is the material divergence operator. (4.3) is subject to the following boundary conditions: the motion ϕ is prescribed to be ϕ^d on $\partial B^d \subset \partial B$, and the traction $\tilde{\mathbf{P}} \cdot \mathbf{N} = \mathbf{t}$ is prescribed on the remainder ∂B^t; and subject further to the constraint imposed by the balance of mass. Push-forward of (4.3) in spatial configuration Ω can be obtained as

$$\mathrm{div}\,\tilde{\tau} + J\rho\mathbf{g} = \mathbf{0}, \tag{4.4}$$

since grad $J = \mathbf{0}$ (see Section A.1).

Equation of flow continuity is derived from the balance of mass. It is assumed in this study that both the fluid and solid phases are homogeneous and incompressible, i.e., $\partial(\rho^\alpha)/\partial t = 0$; grad $\rho_\alpha = \mathbf{0}$ (see Section A.1). Using these assumptions, ρ_α can be factored out and eliminated from (3.16), resulting an expression

$$\mathrm{div}\left(n^\alpha \mathbf{v}^\alpha\right) + \frac{\partial}{\partial t}\left(n^\alpha\right) = 0. \tag{4.5}$$

Adding (4.5) over the phases yields

$$\mathrm{div}\left[\left(1 - n^w\right)\mathbf{v}^s\right] + \mathrm{div}\left(n^w \mathbf{v}^w\right) = 0. \tag{4.6}$$

For future reference, it is useful to define a superficial, or Darcy, velocity as

$$\tilde{\mathbf{v}} = n^w\left(\mathbf{v}^w - \mathbf{v}^s\right). \tag{4.7}$$

The vector $\tilde{\mathbf{v}}$ represents the relative volumetric rate of flow of fluid per unit area of deforming soil mass in spatial configuration $\Omega = \phi_t(B)$. $\tilde{\mathbf{v}}$ is related to fluid potential Π by constitutive relationship. See Section 4.5 for discussion. For simplicity of notation, $\mathbf{v}$ will be used for solid phase velocity, $\mathbf{v}^s$ in subsequent discussion. Substituting (4.7) in (4.6), field equation of flow continuity can be obtained in the spatial reference as

$$\operatorname{div} \mathbf{v} + \operatorname{div} \tilde{\mathbf{v}} = 0. \tag{4.8}$$

(4.8) is subject to the following boundary conditions: fluid potential $\prod$ is prescribed to be $\prod^{\theta} \subset \phi_t(\partial B^{\theta})$, and the volumetric flow is $\tilde{\mathbf{v}} \cdot \mathbf{n} = -q$ on the remainder $\phi_t(\partial B^{h})$; and subject further to the constraint imposed by the conservation of momentum. Here $\mathbf{n}$ is the outward unit normal to the deformed surface $\phi_t(\partial B)$ and q is positive when fluid is being supplied to the system. In material description, (4.8) takes the following from

$$\operatorname{DIV} \mathbf{V} + \operatorname{DIV} \tilde{\mathbf{V}} = 0. \tag{4.9}$$

$\mathbf{V}, \tilde{\mathbf{V}}$ are pull-back velocities in undeformed, reference configuration B. $\mathbf{V}, \tilde{\mathbf{V}}$ can be obtained through Piola transform of $\mathbf{v}, \tilde{\mathbf{v}}$ such that, $\tilde{\mathbf{V}} = J\mathbf{F}^{-1} \cdot \tilde{\mathbf{v}}$, $\mathbf{V} = J\mathbf{F}^{-1} \cdot \mathbf{v}$. Let $\tilde{\mathbf{V}} \cdot \mathbf{N} = -Q$ be the prescribed volumetric rate of flow per unit undeformed area across the boundary ∂B^{h}, $\mathbf{N}$ being outward unit normal to the undeformed surface ∂B. Q maintains the same sense of direction as q.

4.3 Weak Form

In order to establish weak form of the boundary value problem, one needs to define following spaces in accordance with the standard arguments of variational principles. Let the space of admissible configurations be

$$C_{\phi} = \left\{ \phi : B \to R^{nsd} \,\middle|\, \phi_i \in H^1,\ \phi = \phi_d \text{ on } \partial B^{d} \right. \tag{4.10}$$

and the space of admissible variations be

$$V_{\phi} = \left\{ \eta : B \to R^{nsd} \,\middle|\, \eta_i \in H^1,\ \eta = \mathbf{0} \text{ on } \partial B^{d} \right\}, \tag{4.11}$$

where η is an admissible virtual displacement field, H^1 is the usual Sobolev space of functions of degree one. Further, let $G : C_\phi \times V_\phi \rightarrow R$ denote the weak form of equilibrium equation (4.8) in material description.

$$G(\phi,\Pi,\eta) = \int_B \left(\text{GRAD}\,\eta : \tilde{\mathbf{P}} - \rho_0 \eta \cdot \mathbf{g}\right) dV - \int_{\partial B} \eta \cdot \mathbf{t}\, dA. \tag{4.12}$$

The balance of linear momentum is given by the condition $G(\phi, \Pi, \eta) = 0$. The formal statement of (4.12) is: Find $\phi \in C_\phi$ such that $G(\phi, \Pi, \eta) = 0$ for all $\eta \in V_\phi$. Using (3.55) and (3.56), one can rewrite an equivalent expression of G of (4.12) in the same undeformed, material configuration with the integrands evaluated in spatial description as follows:

$$G(\phi,\Pi,\eta) = \int_B (\text{grad}\,\eta : \tau + \theta\, \text{div}\,\eta - \rho_0 \eta \cdot \mathbf{g}) dV - \int_{\partial B} \eta \cdot \mathbf{t}\, dA. \tag{4.13}$$

Now, let the space of potentials in spatial reference be

$$C_\theta = \left\{ \Pi : \phi_t(B) \rightarrow R^{nsd} \,\middle|\, \Pi \in H^1,\ \Pi = \Pi_\theta \text{ on } \Gamma^\theta \right. \tag{4.14}$$

and the corresponding space of variations be

$$V_\theta = \left\{ \psi : \phi_t(B) \rightarrow R^{nsd} \,\middle|\, \psi \in H^1,\ \psi = 0 \text{ on } \Gamma^\theta \right\}, \tag{4.15}$$

where ψ represents an arbitrary virtual pore pressure field. Further, let $H : C_\theta \times V_\theta \rightarrow R$ denotes the weak form of equation of continuity (4.8) in spatial description.

$$H(\phi,\Pi,\psi) = \int_\Omega (\psi\, \text{div}\mathbf{v} - \text{grad}\,\psi \cdot \tilde{\mathbf{v}}) d\Omega - \int_\Gamma \psi \cdot q\, d\Gamma. \tag{4.16}$$

One can show that the balance of mass is given by the condition $H(\phi, \Pi, \psi) = 0$. Formal statement of weak form (4.16) will translate as: Find $\Pi \in C_\theta$ such that $H(\phi, \Pi, \psi) = 0$ for all admissible $\psi \in V_\theta$.

The domain of integration of $H(\phi, \Pi, \psi)$ of (4.16) can be of evaluated quite easily in undeformed, material configuration by introducing the Jacobian J. In doing so, one would require the following identity

$$\dot{J} = J \operatorname{div} \mathbf{v}. \tag{4.17}$$

$\dot{J}$ is the time derivative of the J. See Section A.4 for proof of the identity (4.17). Substituting (4.17) in (4.16) yields

$$H(\phi, \Pi, \psi) = \int_B \left(\psi \dot{J} - \operatorname{grad} \psi \cdot J\tilde{\mathbf{v}}\right) dV - \int_{\partial B} \psi Q \, dA. \tag{4.18}$$

Relation of area transformation of flow rate, $q \, d\Gamma = Q \, dA$ (see Section A.4) is employed in deriving (4.18). $H(\phi, \Pi, \psi)$ in material description takes the form

$$H(\phi, \Pi, \psi) = \int_B \left(\psi \dot{J} - \operatorname{GRAD} \psi \cdot \tilde{\mathbf{V}}\right) dV - \int_{\partial B} \psi Q \, dA. \tag{4.19}$$

(4.18) and (4.19) are equivalent expressions since $\operatorname{GRAD} \psi \cdot \tilde{\mathbf{V}} = \operatorname{grad} \psi \cdot J\tilde{\mathbf{v}}$.

Presence of rate term $\dot{J}$ in the variational equation $H(\phi, \Pi, \psi)$ makes it mathematically awkward. One can eliminate rate terms altogether by semi-discretization in time domain, via finite difference, for example. Following is a brief discussion on time descretization scheme for consolidation problems.

4.4 Time Descretization Scheme

The ordinary differential equation associated with the problem of consolidation is generally stiff. A physical insight provides an explanation: points near drainage boundaries consolidate many times faster than do points at remote places. The spectrum of eigenvalues associated with the consolidation equation is therefore wide.

The general linear k-step method for approximating the solution of a system of ordinary differential equations of the first order,

$$\dot{\mathbf{d}} = \mathbf{f}(\mathbf{d}, t), \quad \mathbf{d}(0) = \mathbf{d}_0, \quad t \geq 0 \tag{4.20}$$

is

$$\sum_{m=0}^{k} (\alpha_m \mathbf{d}_{n+1-m} + \Delta t \beta_m \mathbf{f}_{n+1-m}) = \mathbf{0}, \tag{4.21}$$

where $\Delta t = t_{n+1} - t_n$ and α_m, β_m are unknown coefficients. A linear multistep (LMS) method is explicit if $\beta_0 = 0$, otherwise, it is implicit. Implicit method is preferred in this study because it has a larger region of stability than the explicit methods, and it is compatible with the stress point algorithms used in the development of constitutive models (see Chapters 5 and 6). As a result, $\beta_0 \neq 0$. (4.21) has $2k + 2$ unknown coefficients.

An effective technique for solving stiff differential equation is provided by so-called stiffly stable methods proposed by Gear [58-61]. These k-step methods of order k are based on backward differentiation formulas (BDF) derived by setting $\beta_0 \neq 0$, $\beta_1 = \beta_2 = \ldots \beta_k = 0$. The resulting BDF approximation is

$$\sum_{m=0}^{k} (\alpha_m \mathbf{d}_{n+1-m}) + \Delta t \beta_0 \mathbf{f}_{n+1} = \mathbf{0} \tag{4.22}$$

with $k + 1$ unknown coefficients which one can choose by forcing a k-step method to satisfy an accuracy of order k. There is an arbitrary normalizing factor so that one can set $\alpha_0 = -1.0$, leaving k unknowns. (4.22) then takes the form

$$\left(\mathbf{d}_{n+1} - \sum_{m=1}^{k} (\alpha_m \mathbf{d}_{n+1-m}) \right) - \Delta t \beta_0 \mathbf{f}_{n+1} = \mathbf{0}. \tag{4.23}$$

See [5] for determination of coefficients for BDF-k scheme. (4.23) can be made more generalized by introducing one-step recurrence relation for **f** such that

$$\left(\mathbf{d}_{n+1} - \sum_{m=1}^{k}(\alpha_m \mathbf{d}_{n+1-m})\right) - \Delta t\,\beta_0[\beta \mathbf{f}_{n+1} + (1-\beta)\mathbf{f}_n] = \mathbf{0}. \qquad (4.24)$$

$0 \le \beta \le 1$ is the parameter of generalized trapezoidal method. Some of the well-known families of β-methods are presented in the following.

Table 4.1 Generalized trapezoidal method

β	Method
0	Forward Euler
1/2	Crank-Nicolson
1	Backward Difference

Unconditional stability is achieved for any Δt if $\beta \ge 1/2$. In general, the nonlinear responses of interest are dominated by low-frequency component of the system, but high frequencies also enter into the solution because of the numerical approximation. It is known that the backward difference scheme ($\beta = 1.0$) can damp such high-frequency components but at the expense of accuracy. On the other hand, Crank-Nicholson scheme ($\beta = 1/2$) possesses a second order accuracy but lacks the numerical dissipation of the backward difference scheme. It was shown in [61] that the variable step size, variable order BDF methods are convergent and unconditionally stable for ordinary differential equations.

Following (4.24), one can obtain time-integrated variational forms of $H_{\Delta t}(\phi, \Pi, \psi)$ given as

$$H_{\Delta t}(\phi,\Pi,\psi) = \int_B \frac{\psi}{\Delta t}\left(J_{n+1} - \sum_{m=1}^{k} \alpha_m J_{n+1-m} \right) dV$$
$$- \beta_0 \int_B \left[\beta (\operatorname{grad}\psi \cdot J\tilde{\mathbf{v}})_{n+1} + (1-\beta)(\operatorname{grad}\psi \cdot J\tilde{\mathbf{v}})_n \right] dV \qquad (4.25)$$
$$- \beta_0 \int_{\partial B} \left[\beta Q_{n+1} + (1-\beta) Q_n \right] dA = 0,$$

$$H_{\Delta t}(\phi,\Pi,\psi) = \int_B \frac{\psi}{\Delta t}\left(J_{n+1} - \sum_{m=1}^{k} \alpha_m J_{n+1-m} \right) dV$$
$$- \beta_0 \int_B \left[\beta (\operatorname{GRAD}\psi \cdot \tilde{\mathbf{V}})_{n+1} + (1-\beta)(\operatorname{GRAD}\psi \cdot \tilde{\mathbf{V}})_n \right] dV \qquad (4.26)$$
$$- \beta_0 \int_{\partial B} \left[\beta Q_{n+1} + (1-\beta) Q_n \right] dA = 0.$$

(4.25) and (4.26) are obtained from (4.18) and (4.19), respectively.

4.5 Large Deformation Plasticity Model for Soil Skeleton

In this study, plasticity behavior of soil skeleton in large deformation is based on multiplicative decomposition of the deformation gradient, **F** [15, 16]. Let X be a macroscopic point containing a sufficient number of solid particles in the reference, undeformed configuration B, and x be the configuration of X at some time $t \geq 0$, i.e., $x = \phi_t(X)$. Recall from (3.44), $\mathbf{F} = \partial\mathbf{x}/\partial\mathbf{X}$. **x** and **X** are coordinates of x and X, respectively.

The motion of X produces both reversible as well as irreversible microstructural changes in the soil. Typical processes associated with reversible microstructural changes include elastic deformation and (for plate-like particles) elastic bending of the granules comprising the assembly. As x is unloaded, it moves to some intermediate, stress free configuration defined by the macroscopic point x^u. Assuming that this intermediate configuration exists, the chain rule can be used to express **F** in the product form

$$\mathbf{F} = \frac{\partial \mathbf{x}}{\partial \mathbf{x}^{u}} \cdot \frac{\partial \mathbf{x}^{u}}{\partial \mathbf{X}} \equiv \mathbf{F}^{e} \cdot \mathbf{F}^{p}. \tag{4.27}$$

$\mathbf{F}^e = \partial \mathbf{x}/\partial \mathbf{x}^u$, $\mathbf{F}^p = \partial \mathbf{x}^u/\partial \mathbf{X}$. Figure 4.2 presents the schematic of the multiplicative decomposition of $\mathbf{F}$.

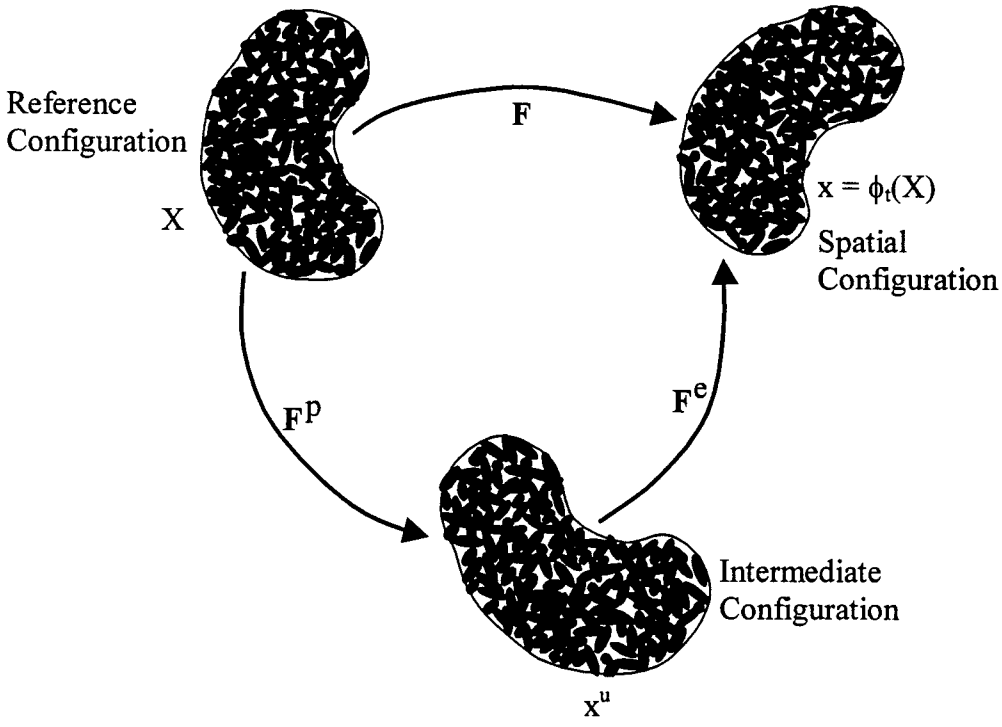

Figure 4.2 Illustration of multiplicative decomposition of the deformation gradient

Ignoring non-mechanical power and kinetic energy production, balance of energy and the use of the second law of thermodynamics lead to the following reduced dissipation inequality

$$D = \tau : \mathbf{d} - \frac{d\Psi}{dt} = \frac{1}{2}\mathbf{S} : \dot{\mathbf{C}} - \frac{d\Psi}{dt} \geq 0, \tag{4.28}$$

where $\mathbf{d} = \mathrm{Sym}(\mathbf{l})$ is the rate of deformation tensor, $\mathbf{l} = \dot{\mathbf{F}} \cdot \mathbf{F}^{-1}$ is the overall spatial velocity gradient, and ψ is the stored energy function. Clearly, $d\Psi/dt = J\rho\dot{\bar{E}}$ and $D = 0$ for an elastic material (see (3.63)).

The form of the stored energy function ψ determines the constitutive characteristics of the soil. For isothermal, elastic processes, ψ depends only on X and **C** if it is to satisfy the axiom of material and frame indifference. Equally well one can say that for isothermal, elastic processes ψ is a function of X and elastic left Cauchy-Green tensor, $\mathbf{b}^e$, provided that $\mathbf{b}^e$ satisfies an objective transformation.

An elasto-plastic process requires a yield function, a hardening rule, and the imposition of consistency condition. Let f be the yield function defined as $f(\tau, \chi) = 0$. $\chi \in R^m$ is a suitable vector of $m \geq 1$ (stress-like) internal variables characterizing the hardening response of the soil. $\xi \in R^m$ is a vector of internal plastic variable (strain-like) conjugate to χ in the sense that $\chi = -\partial\Psi/\partial\xi$. From the framework set in (4.27), ψ takes the form

$$\Psi = \Psi\left(X, \mathbf{b}^e, \xi\right); \qquad \mathbf{b}^e = \mathbf{F}^e \cdot \left(\mathbf{F}^e\right)^t. \tag{4.29}$$

Now, consider the following time-derivative of Ψ

$$\frac{d\Psi}{dt} = \frac{d\Psi}{d\mathbf{b}^e} : \dot{\mathbf{b}}^e = \frac{d\Psi}{d\mathbf{b}^e} : \left(\mathbf{l} \cdot \mathbf{b}^e + \mathbf{b}^e \cdot \mathbf{l}^t + \ell_{\upsilon}\mathbf{b}^e\right) + \frac{\partial\Psi}{\partial\xi} \cdot \dot{\xi}, \tag{4.30}$$

where $\ell_{\upsilon}\mathbf{b}^e$ is the Lie derivative of $\mathbf{b}^e$. Inserting (4.30) in (4.28) and assuming isotropy in the sense that $\mathbf{b}^e$ and $\partial\Psi/\partial\mathbf{b}^e$ commute, the dissipation inequality can be expressed as

$$D = \left(\tau - 2\frac{d\Psi}{d\mathbf{b}^e} \cdot \mathbf{b}^e\right) : \mathbf{d} + 2\frac{d\Psi}{d\mathbf{b}^e} \cdot \mathbf{b}^e : \left(-\frac{1}{2}\ell_{\upsilon}\mathbf{b}^e \cdot \mathbf{b}^{e^{-1}}\right) - \frac{\partial\Psi}{\partial\xi} \cdot \dot{\xi} \geq 0. \tag{4.31}$$

The first term of (4.31) yields the constitutive relationship

$$\tau = 2\frac{d\Psi}{d\mathbf{b}^e}\cdot\mathbf{b}^e, \tag{4.32}$$

while the other terms yield, following the requirement $f(\tau, \chi) = 0$ and the postulate of maximum dissipation,

$$-\frac{1}{2}\ell_{\upsilon}\mathbf{b}^e = \dot{\varphi}\frac{\partial f}{\partial \tau}\cdot\mathbf{b}^e, \qquad \dot{\xi} = \dot{\varphi}\frac{\partial f}{\partial \chi}. \tag{4.33}$$

$\dot{\varphi}$ and f satisfy the requirements of consistency conditions such that $\dot{\varphi} \geq 0$, $f \leq 0$, and $\dot{\varphi} f = 0$. Thus (4.33) defines the flow rule. (4.32) and (4.33) satisfy the reduced dissipation inequality of (4.28) even with the use of empirically derived hardening law. The flow rule (4.33) possesses a number of important properties. In particular, it gives the correct evolution of plastic volume changes as the following observations reveal:

(i) The total and elastic volume changes are given by $J = \det(\mathbf{F}) > 0$ and $J^e = (\det(\mathbf{b}^e))^{1/2} > 0$, respectively.

(ii) Let $J^p = \det(\mathbf{F}^p)$. The rate of plastic volume change predicted by the $(4.33)_1$ is given by the evolution equation

$$\frac{d}{dt}\left(\log J^p\right) = \dot{\varphi}\,\mathrm{tr}\left[\frac{\partial f}{\partial \tau}\right], \tag{4.34}$$

which implies exact conservation of plastic volume for pressure insensitive yield conditions; i.e., if $\mathrm{tr}[\partial f/\partial\tau] = 0$.

The left Cauchy-Green tensor $\mathbf{b}^e$ can be decomposed spectrally into

$$\mathbf{b}^e = \sum_{A=1}^{3}\left(\lambda_A^e\right)^2\mathbf{m}^{(A)}; \qquad \mathbf{m}^{(A)} = \mathbf{n}^{(A)}\otimes\mathbf{n}^{(A)}, \tag{4.35}$$

where λ_A^e is the elastic principle stretch corresponding to the principal direction $\mathbf{n}^{(A)}$. $\otimes$ is a vector operator defined as $(\mathbf{a}\otimes\mathbf{b})_{ij} = a_i b_j$ for any vectors **a** and **b**. Since τ and $\mathbf{b}^e$ commute, τ can be decomposed spectrally in the form

$$\tau = \sum_{A=1}^{3} \beta_A \mathbf{m}^{(A)}, \tag{4.36}$$

where β_A are the principal Kirchhoff effective stresses.

By the assumption of frame indifference and isotropy, the free energy function can be expressed as symmetric function of the elastic principal stretches, i.e.,

$$\Psi\left(X,\mathbf{b}^e\right) = \Psi\left(X,\varepsilon_1^e,\varepsilon_2^e,\varepsilon_3^e\right); \qquad \varepsilon_A^e = \ln\left(\lambda_A^e\right), \quad A = 1,2,3, \tag{4.37}$$

where ε_A^e's are principal elastic logarithmic stretches. Thus, the elastic constitutive equation (4.32) reduces to a scalar relationship between β_A and ε_A^e such that

$$\beta_A = \frac{\partial \Psi}{\partial \varepsilon_A^e}; \qquad A = 1,2,3, \tag{4.38}$$

In the elasto-plastic regime, the additional task of enforcing the consistency condition, $f(\tau, \chi) = 0$, is done incrementally. In the first step, plastic flow is frozen and an elastic assumption ignoring the constraints imposed by yield criterion leads to elastic a trial elastic state.

$$\dot{\mathbf{f}} = \mathbf{l}\cdot\mathbf{f}; \qquad \dot{\mathbf{b}}^e = 2\,\mathrm{Sym}\left(\mathbf{l}\cdot\mathbf{b}^e\right); \qquad \dot{\xi} = \mathbf{0}, \tag{4.39}$$

where $\mathbf{f} = \partial\mathbf{x}/\partial\mathbf{x}_n$ is the deformation gradient evaluated relative to the converged configuration $\phi_{t_n}(\mathrm{B})$. In the second step, trial state is held fixed and plastic relaxation is introduced. The algorithm is given explicitly

$$\dot{\mathbf{f}} = \mathbf{0}; \qquad \dot{\mathbf{b}}^{e} = -2\dot{\varphi}\frac{\partial f}{\partial \tau}\cdot \mathbf{b}^{e}; \qquad \dot{\xi} = \dot{\gamma}\frac{\partial f}{\partial \chi}, \tag{4.40}$$

subject to $\dot{\varphi} \geq 0$, $f \leq 0$, and $\dot{\varphi} f = 0$.

Incremental counterparts of the evolution equations (4.39) and (4.40) are obtained from the so called product formula algorithm [62]. From (4.39), trial elastic left Cauchy-Green tensor is obtained in incremental form by freezing plastic flow as

$$\mathbf{b}^{e,tr} = \mathbf{f}\cdot\mathbf{b}_{n}^{e}\cdot\mathbf{f}^{t}; \qquad \xi = \xi_{n}, \tag{4.41}$$

where $\mathbf{b}_{n}^{e}$ and ξ_{n} are the respective values of $\mathbf{b}^{e}$ and ξ at configuration $\phi_{t_n}(\mathrm{B})$. Similar to (4.27), $\mathbf{b}^{e,tr}$ can be decomposed spectrally in the form

$$\mathbf{b}^{e,tr} = \sum_{A=1}^{3}\left(\lambda_{A}^{e,tr}\right)^{2}\mathbf{m}^{tr(A)}; \qquad \mathbf{m}^{tr(A)} = \mathbf{n}^{tr(A)}\otimes\mathbf{n}^{tr(A)}. \tag{4.42}$$

Introducing the product formula algorithm into the plastic flow equation then yields

$$\mathbf{b}^{e} = \exp\left(-2\Delta\varphi\frac{\partial f}{\partial \tau}\right)\cdot\mathbf{b}^{e,tr}; \qquad \xi = \xi_{n} + \Delta\varphi\frac{\partial f}{\partial \chi}, \tag{4.43}$$

where $\Delta\varphi$ is an incremental consistency parameter that satisfies the conditions $\Delta\varphi \geq 0$, $f \leq 0$, and $\Delta\varphi f = 0$.

Now, by invoking isotropy one can conclude that there exists an equivalent function $f = f(\beta_1,\beta_2,\beta_3,\xi)$ such that

$$\frac{\partial f}{\partial \tau} = \sum_{A=1}^{3}\frac{\partial f}{\partial \beta_{A}}\mathbf{m}^{(A)}, \tag{4.44}$$

The function can then be used in (4.43), together with (4.35), to obtain

$$\mathbf{b}^{e,tr} = \sum_{A=1}^{3}\left[\left(\lambda_A^e\right)^2 \exp\left(2\Delta\varphi\frac{\partial f}{\partial \beta_A}\right)\right]\mathbf{m}^{(A)}. \tag{4.45}$$

Comparing spectral decomposition of $\mathbf{b}^{e,tr}$ in (4.42) and (4.45), one can conclude that

$$\mathbf{m}^{(A)} = \mathbf{m}^{tr(A)}; \quad \left(\lambda_A^e\right)^2 = \exp\left(-2\Delta\varphi\frac{\partial f}{\partial \beta_A}\right)\left(\lambda_A^{e,tr}\right)^2, \quad A = 1,2,3. \tag{4.46}$$

(4.46) states that the principle directions $\mathbf{n}^{(A)}$ coincide with the trial principle directions $\mathbf{n}^{tr(A)}$, and that the plastic relaxation equation takes place along the fixed axis defined by the trial elastic state.

Finally, an additive form of the plastic relaxation equation is obtained by taking the natural logarithms of both sides of $(4.46)_2$. The result reads

$$\varepsilon_{A,t}^e = \varepsilon_{A,t}^{e,tr} - \Delta\varphi\frac{\partial f}{\partial \beta_A}; \qquad A = 1,2,3. \tag{4.39}$$

(4.39) represents a linear return mapping algorithm in the strain space defined by the elastic logarithmic principal stretches. In Kirchhoff effective stress space, a linear return mapping algorithm similar to that presented in [63] can be derived if one assumes an elasticity operator α_{AB} from the equation

$$\beta_A = \frac{\partial \Psi}{\partial \varepsilon_A^e} = \sum_{B=1}^{3}\alpha_{AB}\varepsilon_B^e, \qquad A = 1,2,3. \tag{4.48}$$

The result reads

$$\beta_A = \beta_A^{tr} - \Delta\varphi\sum_{B=1}^{3}\alpha_{AB}\frac{\partial f}{\partial \beta_B}, \qquad A = 1,2,3. \tag{4.49}$$

Similarity in form between the standard linear return maps of the infinitesimal theory and (4.48), (4.49) allows the algorithms for the infinitesimal theory to be preserved and exploited for finite deformation analysis, with the added simplification that calculations now takes place in the fixed principal stretch directions.

4.6 Constitutive Law for Fluid Flow

Similar to solid phase one needs to describe appropriate constitutive law for fluid phase. In this study flow is assumed laminar and generalized Darcy's law is employed to describe the constitutive relation between relative volumetric flow $\tilde{\mathbf{v}}$ of (4.7) and fluid potential Π. Linear constitutive equation is given as

$$\tilde{\mathbf{v}} = -\mathbf{k} \cdot \operatorname{grad} \Pi, \tag{4.50}$$

where $\mathbf{k}$ is the second-order permeability tensor and Π is the fluid potential, defined in (4.14). The negative sign in (4.50) implies that fluid always flows in the direction of decreasing potential. Permeability $\mathbf{k}$ is an important soil parameter which depends on other material properties such as: particle size, void ratio, composition, fabric, degree of saturation [64]. For most practical purposes, $\mathbf{k}$ is assumed to be symmetric, positive-definite.

For incompressible flow the potential Π can be decomposed as

$$\Pi = \Pi^e + \Pi^\theta; \quad \Pi^\theta = \frac{\theta}{J\rho_w g}. \tag{4.51}$$

Π^θ and Π^e represent pressure and elevation counterparts, respectively. g is the gravity acceleration constant, θ is Kirchhoff pore pressure as defined in (3.56). Taking spatial gradient of $(4.51)_1$ and using (A.3), one obtains

$$\operatorname{grad}\Pi = \frac{\operatorname{grad}\theta}{J\rho_w g} + \frac{\mathbf{g}}{g}. \tag{4.52}$$

If Π^e is measured in the direction of gravity, $\mathbf{g}/g$ takes a convenient form of $\{0, 1, 0\}^T$ in Cartesian space $\in R^3$. Thus the variational equation (4.18) for the volume conservation may be written as

$$H(\phi,\Pi,\psi) = \int_B \psi \dot{J}\, dV + \int_B \operatorname{grad}\psi \cdot \mathbf{k} \cdot \left(\frac{\operatorname{grad}\theta}{\rho_w g} + J\frac{\mathbf{g}}{g} \right) dV - \int_{\partial B} \psi Q\, dA. \tag{4.53}$$

4.7 Definitions of Strains

Since both the small and large strain formulations of consolidation models are used for numerical analyses (see Chapters 10 and 11) it is important to define these two types of strains. Consider the case of one-dimensional compression loading as shown in Figure 4.3. Compression positive sign convention is used in the following definitions

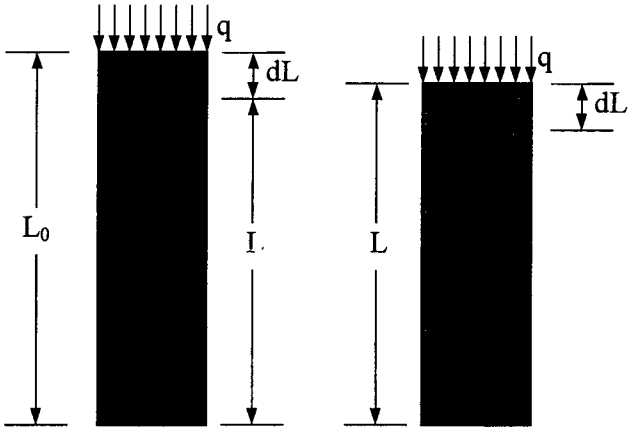

Figure 4.3 Small strain versus large strain

The small strain or the conventional strain e is defined as the change in length per unit initial length since the geometry is not updated in small strain formulation

$$de = \frac{dL}{L_0}; \quad e = \frac{1}{L_0}\int_L^{L_0} dL = \frac{L_0 - L}{L_0}. \tag{4.54}$$

In (4.54), de is the incremental small strain.

In large strain formulation geometry gets updated. As a result, the incremental large strain dε is defined as the change in length per unit contemporary length.

$$d\varepsilon = \frac{dL}{L}. \tag{4.55}$$

One can obtain an expression for large strain ε by integrating (4.55) for a finite amount of deformation as follows:

$$\varepsilon = \int_L^{L_0} \frac{dL}{L} = -\ln\left(\frac{L}{L_0}\right) = -\ln(1-e). \tag{4.56}$$

ε is also termed as logarithmic strain or natural strain.

CHAPTER 5
HYPERELASTIC-PLASTIC MCC MODEL

5.1 Introduction

Elasto-plastic models based on critical state formulations have been successful in describing many of the most important features of the mechanical behavior of soils such as hardening, softening and pressure sensitivity. The modified Cam-Clay (MCC) plasticity model of critical state soil mechanics [28] is one of the most widely used plasticity models because of its practicality and simplicity. As a result, MCC model is adopted in this study to simulate elasto-plastic response of phosphatic waste clay. Two important modifications are incorporated to the small strain version of MCC to take into account large deformation effects. These modifications are hyperelasticity and bilogarithmic compressibility.

Elasticity models are commonly incorporated into elasto-plastic constitutive models through a hypoelastic formulation. However, extension of a hypoelastic formulation to the case of nonlinear elastic soil response could result, in some cases, in conservative models [65]. In case of small strain formulation, the use of non-conservative elastic models consistent with critical state theory has been justified by the hypothesis of small deformation [66]. This argument is unacceptable in the large deformation regime particularly under conditions of cyclic loading where significant energy can either be extracted or dissipated from certain loading cycles. On the other hand, hyperelastic materials are those for which a stored energy function exists, and hence, are conservative.

Nonlinear hyperelasticity model with a constant elastic shear modulus is used for large deformation Cam-Clay model in [67]. Though energy conservative, use of constant shear modulus can be erroneous since experimental evidence suggests that for soil elastic shear modulus does vary with effective volumetric stress [60, 68]. Consequently, a class of two-invariant stored energy functions [68] is employed in this study which includes pressure-dependent as well as constant elastic shear modulus for special case. A variable elastic shear modulus leads to fully coupled volumetric and deviatoric elastic responses.

Another limitation in small strain formulation is the use of linear variation of the void ratio (or specific volume) with logarithm of effective volumetric stress to describe the hardening response of the soil [28]. This assumption can be justified for small volumetric strain, which does not hold for large deformation regime. In large strain, linear void ratio – logarithm of effective stress variation can result in a physically meaningless solution such as the prediction of negative specific volume even at realistically low values of stresses. In this study, this limitation is addressed by incorporating bilogarithmic compressibility law, i.e., linear relationship between the logarithm of specific volume and the logarithm of effective volumetric stress as proposed in [69-71]. Advantages and generality of bilogarithmic compressibility law are discussed in a following section.

5.2 Hyperelastic Model

The formation of hyperelasticity is based on the existence of a stored energy function $\Psi = \Psi(\varepsilon^e)$, where ε^e is the vector of elastic lograrithmic principal stretches. The

effective principal Kirchhoff stress vector β can be expressed in terms of Ψ (see (4.38)). Substituting (4.38), the elastic moduli $\mathbf{a}^e \in R^{3\times3}$ can be expressed in tensor notation as

$$a^e_{ij} = \frac{\partial \beta_i}{\partial \varepsilon^e_j} = \frac{\partial^2 \Psi}{\partial \varepsilon^e_i \partial \varepsilon^e_j}. \tag{5.1}$$

Assuming $\Psi\left(\varepsilon^e\right) = \Psi\left(\varepsilon^e_v, \varepsilon^e_s\right)$, one can use the chain rule to expand (4.38) as

$$\beta_i = \frac{\partial \Psi}{\partial \varepsilon^e_v}\frac{\partial \varepsilon^e_v}{\partial \varepsilon^e_i} + \frac{\partial \Psi}{\partial \varepsilon^e_s}\frac{\partial \varepsilon^e_s}{\partial \varepsilon^e_i}. \tag{5.2}$$

ε^e_v and ε^e_s are the volumetric and deviatoric invariants of ε^e, respectively.

$$\varepsilon^e_v = \varepsilon^e \cdot \delta; \qquad \varepsilon^e_s = \sqrt{\frac{2}{3}}\left\|\mathbf{e}^e\right\|; \qquad \mathbf{e}^e = \varepsilon^e - \frac{1}{3}\varepsilon^e_v \delta, \tag{5.3}$$

where $\delta = [1 \;\; 1 \;\; 1]^t$. Since

$$\frac{\partial \varepsilon^e_v}{\partial \varepsilon^e} = \delta; \qquad \frac{\partial \varepsilon^e_s}{\partial \varepsilon^e} = \sqrt{\frac{2}{3}}\hat{\mathbf{n}}, \tag{5.4}$$

where $\hat{\mathbf{n}} = \mathbf{e}^e \Big/ \left\|\mathbf{e}^e\right\|$, then (5.2) can be rewritten in the equivalent form

$$\beta = p\delta + \sqrt{\frac{2}{3}} q\hat{\mathbf{n}} = p\delta + \mathbf{s}, \tag{5.5}$$

where

$$p = \frac{\partial \Psi}{\partial \varepsilon^e_v} = \frac{1}{3}\beta \cdot \delta; \qquad q = \frac{\partial \Psi}{\partial \varepsilon^e_s} = \sqrt{\frac{3}{2}}\|\mathbf{s}\|; \qquad \mathbf{s} = \beta - p\delta. \tag{5.6}$$

p and q are the mean normal stress and the deviatoric invariant of β, respectively. **s** is the vector of deviatoric principal Kirchhoff stresses.

The elastic moduli tensor can be obtained by differentiating the stress equation (5.6) with respect to the corresponding strain components. In order to do that, one would need $\mathbf{D}^e = \nabla\nabla\Psi \in R^{2\times 2}$, Hessian matrix of Ψ.

$$\mathbf{D}^e = \begin{bmatrix} D_{11}^e & D_{12}^e \\ D_{21}^e & D_{22}^e \end{bmatrix} = \begin{bmatrix} \partial^2\Psi/\partial\varepsilon_v^e\partial\varepsilon_v^e & \partial^2\Psi/\partial\varepsilon_v^e\partial\varepsilon_s^e \\ \partial^2\Psi/\partial\varepsilon_s^e\partial\varepsilon_v^e & \partial^2\Psi/\partial\varepsilon_s^e\partial\varepsilon_s^e \end{bmatrix}. \tag{5.7}$$

The first time-variation of stress invariants now takes the form

$$\begin{Bmatrix} \dot{p} \\ \dot{q} \end{Bmatrix} = \mathbf{D}^e \begin{Bmatrix} \dot{\varepsilon}_v^e \\ \dot{\varepsilon}_s^e \end{Bmatrix}. \tag{5.8}$$

Note that $\mathbf{D}^e$ is symmetric provided that the function ψ exists. If $D_{12}^e \neq 0$, then the volumetric and deviatoric elastic responses couple, that is, an imposed volumetric strain produces a shearing stress response, and vice versa. The following section investigates the coupled elastic responses within the context of stored energy function developed specifically for cohesive soils.

Consider a class of stored energy function of the form [68]

$$\Psi\left(\varepsilon_v^e, \varepsilon_s^e\right) = p_0\kappa \exp\left(\frac{\varepsilon_v^e - \varepsilon_{v0}^e}{\kappa}\right) + \frac{3}{2}\mu\left(\varepsilon_s^e\right)^2, \tag{5.9}$$

where ε_{v0}^e = elastic volumetric strain corresponding to a mean normal stress of p_0; κ = elastic compressibility index; and μ = elastic shear modulus defined by the expression

$$\mu = \mu_0 + \alpha p_0 \exp\left(\frac{\varepsilon_v^e - \varepsilon_{v0}^e}{\kappa}\right). \tag{5.10}$$

μ contains a constant term μ_0 and a term that varies with ε_v^e through a constant coefficient α. If $\alpha = 0$ and $\mu_0 > 0$, then the elasticity model is defined by a variable elastic bulk modulus and a constant elastic shear modulus.

The following elastic constitutive equations can be derived from (5.7) and (5.9):

$$p = p_0 \beta \exp\left(\frac{\varepsilon_v^e - \varepsilon_{v0}^e}{\kappa}\right); \qquad q = 3\mu\varepsilon_s^e, \tag{5.11}$$

where $\beta = 1 + 3\alpha\left(\varepsilon_s^e\right)^2 / 2\kappa$.

$$D_{11}^e = K = \frac{p}{\kappa} = \frac{p_0}{\kappa}\beta \exp\left(\frac{\varepsilon_v^e - \varepsilon_{v0}^e}{\kappa}\right); \tag{5.12a}$$

$$D_{22}^e / 3 = \mu = \mu_0 + \left(\frac{\alpha}{\beta}\right)p = \mu_0 + \alpha p_0 \exp\left(\frac{\varepsilon_v^e - \varepsilon_{v0}^e}{\kappa}\right); \tag{5.12b}$$

$$D_{12}^e = D_{21}^e = \left(\frac{3\alpha\varepsilon_s^e}{\beta\kappa}\right)p = \frac{3\alpha p_0 \varepsilon_s^e}{\beta} \exp\left(\frac{\varepsilon_v^e - \varepsilon_{v0}^e}{\kappa}\right). \tag{5.12c}$$

An important feature of elastic soil behavior, presented in (5.12a), is that the elastic bulk modulus K is a linear function of p. With a suitable selection of parameters, elastic shear modulus μ can be made constant or a linear function of p (see (5.12b)). Since the coupling terms D_{12}^e and D_{21}^e can be nonzero for $\alpha \neq 0$, the elastic shear and volumetric responses are coupled for a general loading path. In extreme case, when $\mu_0 = 0$ and $\varepsilon_s^e = \sqrt{2\kappa / 3\alpha}$; $\det(\mathbf{D}^e) = 0$, i.e., $\mathbf{D}^e$ becomes singular. This situation arises when the stress ratio q/p reaches its maximum value of $\sqrt{3\alpha\kappa / 2}$ [68].

5.3 Plasticity Model

The essential ingredients of a plasticity model are a yield function, a flow rule and a hardening law. Two-invariant yield function of MCC model [28] is given by the ellipsoid

$$f = f(p,q,p_c) = \frac{q^2}{M^2} + p(p - p_c) = 0. \tag{5.13}$$

Here f is defined in the space of principal Kirchhoff stresses, β. Invariants p, q are given in (5.6), Kirchhoff preconsolidation pressure p_c is a plastic state variable that describes the size of f. M is the constant slope of the critical state cone in the p-q plane.

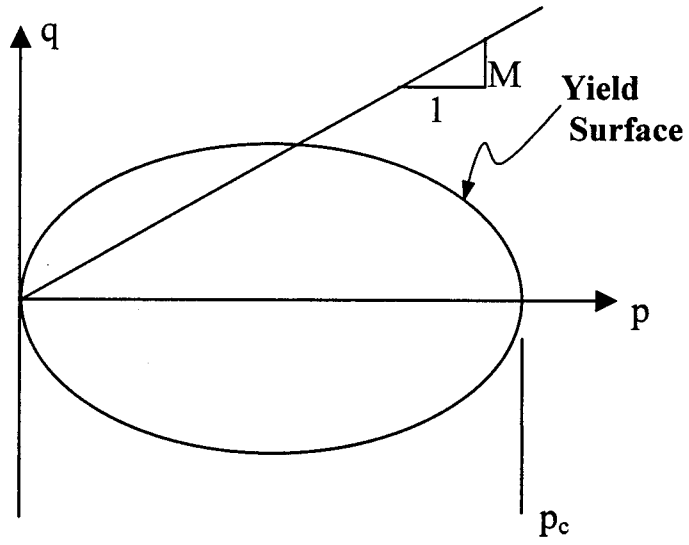

Figure 5.1 Yield surface of the MCC Model in p-q plane

Hardening law and flow rule of MCC, appropriate for large strain formulation, are presented in the following.

5.4 Hardening Law

In case of small strain, the growth of p_c is conventionally defined by a linear relationship between the void ratio e and the logarithm of p_c, or, equivalently, by a linear variation of the specific volume $\upsilon = 1 + e$ with the logarithm of p_c for virgin loading (see Fig. 5.2a). Corresponding hardening law takes the form

$$\frac{\dot{\upsilon}}{\upsilon_0} = -\tilde{\lambda}\frac{\dot{p}_c}{p_c}, \tag{5.14}$$

where υ_0 is the reference initial specific volume at a preconsolidation pressure p_{c0}, and $\tilde{\lambda}$ is a constant compressibility index of the soil. Upon integration, the hardening law (5.14) defines the following relationship between the specific volume υ and the logarithm of p_c

$$\frac{\upsilon}{\upsilon_0} = 1 - \tilde{\lambda}\ln\left(\frac{p_c}{p_{c0}}\right). \tag{5.15}$$

The limitations of this hardening law are generally well recognized, and include among others, that a negative void ratio can result even at realistically low values of preconsolidation pressure, and that the linear relationship is valid only over a narrow range of values of the effective volumetric stress.

An alternative hardening law for finite volume changes, which appears to have been first proposed by Hashiguchi and Ueno [69], and later studied more extensively by Butterfield [70] and Hashiguchi [71], is of the form

$$\frac{\dot{\upsilon}}{\upsilon} = -\lambda\frac{\dot{p}_c}{p_c}, \tag{5.16}$$

where λ is the appropriate compressibility soil index in the large deformation regime for virgin loading. A simple integration of (5.16) yields the relationship

$$\ln\left(\frac{\upsilon}{\upsilon_0}\right) = -\lambda \ln\left(\frac{p_c}{p_{c0}}\right) \tag{5.17}$$

which indicates a linear variation of ln υ with ln p_c (see Fig. 5.2b).

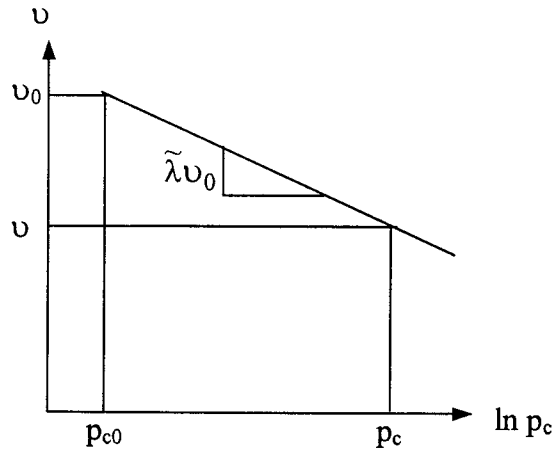

Figure 5.2a Unilogarithmic compressibility law

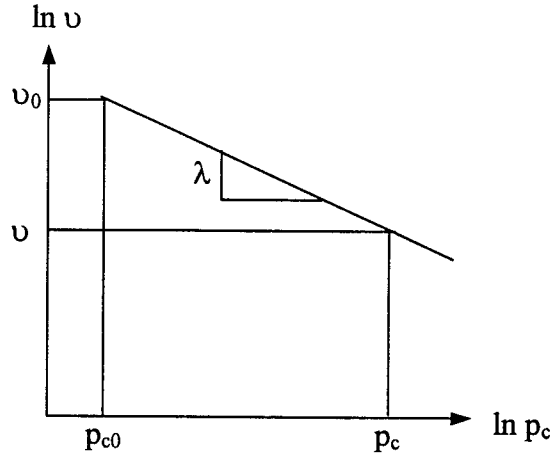

Figure 5.2b Bilogarithmic compressibility law

(5.17) can be also be written in the form

$$\frac{\upsilon}{\upsilon_0} = \left(\frac{p_{c0}}{p_c}\right)^{\lambda} \tag{5.18}$$

which implies that $\upsilon \to 0$ as $p_c \to \infty$. Since practically one cannot have $\upsilon < 1$ (or $e < 0$), the bilogarithmic compressibility law is not without limitation either. However, Butterfield [70] shows from compression test data on natural soils, specifically soft clays, that this law is more accurate than the unilogarithmic compressibility equation over a wide range of values of effective volumetric stress. Furthermore, the value of p_c below which $\upsilon \geq 1$ (or $e \geq 0$) is higher with the bilogarithmic compressibility law (see Fig. 5.3).

A simple inspection shows that in the limit of small strains, the natural volumetric strain $\ln(\upsilon/\upsilon_0) = \ln(1 - \Delta\upsilon/\upsilon_0)$, where $\Delta\upsilon = \upsilon_0 - \upsilon$, coincides with the natural volumetric strain $\Delta\upsilon/\upsilon_0$ of the infinitesimal theory. Thus, the bilogarithmic hardening law approaches the unilogarithmic law in the limit of small volumetric strains. However, large deformation analysis requires the use of natural, and not nominal, strains, and so (5.16) is more robust since it is useful both for small and large deformation analyses. In light of these desirable features, bilogarithmic law is adopted in the proposed model.

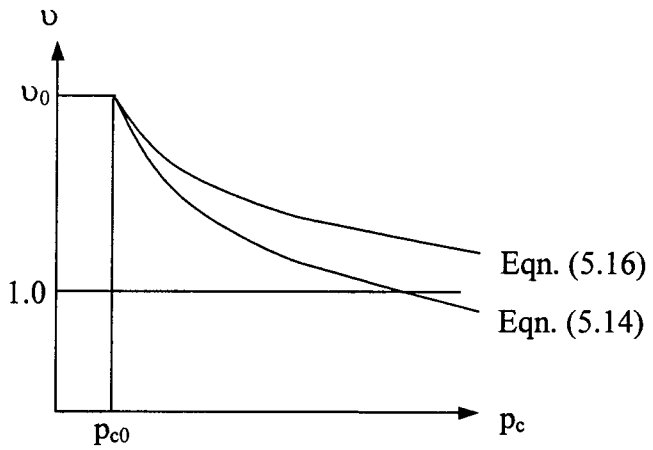

Figure 5.3 Limit of validity: comparison between unilogarithmic and bilogarithmic compressibility laws

In order to develop a hardening law appropriate for large strain plasticity model, one needs to exploit the properties of deformation gradient **F**. The product decomposition of the **F** given by (4.27) produces the identity

$$J = \det(\mathbf{F}) = J^e J^p, \tag{5.19}$$

where $J^e = \det(\mathbf{F}^e)$ and $J^e = \det(\mathbf{F}^p)$. In the space of principal logarithmic stretch, $\varepsilon_V = \ln J = \ln(\lambda_1\lambda_2\lambda_3) = \sum_{A=1}^{3}\varepsilon_A$; $\varepsilon_V^e = \ln J^e = \sum_{A=1}^{3}\varepsilon_A^e$ and $\varepsilon_V^p = \ln J^p = \sum_{A=1}^{3}\varepsilon_A^p$. Natural logarithm of (5.19) then yields

$$\ln J = \ln J^e + \ln J^p \qquad \Rightarrow \varepsilon_V = \varepsilon_V^e + \varepsilon_V^p. \tag{5.20}$$

In other words, the product decomposition of $\mathbf{F}$ is equivalent to the additive decomposition of the natural strains (see Section A.3). The rate form of (5.20) is

$$\frac{\dot{J}}{J} = \frac{\dot{J}^e}{J} + \frac{\dot{J}^p}{J} \qquad \Rightarrow \dot{\varepsilon}_V = \dot{\varepsilon}_V^e + \dot{\varepsilon}_V^p. \tag{5.21}$$

$\dot{J}/J = \dot{\upsilon}/\upsilon$ since $J = \upsilon/\upsilon_0$. υ is the specific volume with a reference value υ_0 in the undeformed configuration. Thus, the hardening law of (5.16) can also be written as

$$\frac{\dot{J}}{J} = \frac{\dot{\upsilon}}{\upsilon} = \dot{\varepsilon}_V^e + \dot{\varepsilon}_V^p = -\lambda\frac{\dot{p}_c}{p_c}. \tag{5.22}$$

Setting $\varepsilon_S^e = 0$, $q = 0$ and $p = p_c$ in (5.11) yields the following expressions for virgin isotropic loading:

$$p_c = p_0 \exp\left(\frac{\varepsilon_V^e - \varepsilon_{V0}^e}{\kappa}\right); \tag{5.23a}$$

$$\dot{p}_c = \frac{p_0}{\kappa}\exp\left(\frac{\varepsilon_V^e - \varepsilon_{V0}^e}{\kappa}\right)\dot{\varepsilon}_V^e = \frac{p_c}{\kappa}\dot{\varepsilon}_V^e. \tag{5.23b}$$

Substituting (5.23b) in (5.22) and simplifying, one can obtain the following hardening law expressed in terms of plastic component of the natural volumetric strain:

$$\frac{\dot{p}_c}{p_c} = \Theta \dot{\varepsilon}_v^p; \qquad \Theta = \frac{1}{\lambda - \kappa}. \tag{5.24}$$

Integration of $(5.24)_1$ produces

$$p_c = p_{c,n} \exp\left[\Theta\left(\varepsilon_v^p - \varepsilon_{v,n}^p\right)\right] = p_{c,n} \exp\left[\Theta\left(\varepsilon_v^{e,tr} - \varepsilon_v^e\right)\right], \tag{5.25}$$

where $p_{c,n}$ and $\varepsilon_{v,n}^p$ are the preconsolidation pressure and the plastic natural volumetric strain at time t_n, respectively. Thus, the hardening law given by (5.16) offers a further computational advantage in that the evolution equation p_c can now be integrated exactly over a finite load increment.

5.5 Flow Rule

Under the hypothesis of associative flow behavior, the integrated flow rule at any time t_{n+1} in the space of logarithmic principal stretches takes the form (cf. (4.47))

$$\varepsilon^e = \varepsilon^{e,tr} - \Delta\varphi \frac{\partial f}{\partial \beta}, \tag{5.26}$$

For simplicity of notations, in (5.26) and in the following subscript (n + 1) is omitted; it is assumed that the unsubscripted variables are all reckoned with respect to time station t_{n+1}. Volumetric and deviatoric components of (5.26) are as follows:

$$\varepsilon_v^e = \varepsilon_v^{e,tr} - \Delta\varphi \frac{\partial f}{\partial p}; \qquad \mathbf{e}^e = \mathbf{e}^{e,tr} - \Delta\varphi \sqrt{\frac{3}{2}} \frac{\partial f}{\partial q} \frac{\mathbf{s}}{\|\mathbf{s}\|}. \tag{5.27}$$

In terms of unit vectors $\hat{\mathbf{n}}, \hat{\mathbf{n}}^{tr}$ $(5.27)_2$ takes the form

$$\varepsilon_s^e \hat{\mathbf{n}} = \varepsilon_s^{e,tr} \hat{\mathbf{n}}^{tr} - \Delta\varphi \frac{\partial f}{\partial q} \hat{\mathbf{n}}, \tag{5.28}$$

where $\varepsilon_s^e = \sqrt{2/3}\|\mathbf{e}\|$, $\varepsilon_s^{e,tr} = \sqrt{2/3}\left\|\mathbf{e}^{tr}\right\|$, $\hat{\mathbf{n}}^{tr} = \mathbf{e}^{tr}/\left\|\mathbf{e}^{tr}\right\|$, $\hat{\mathbf{n}} = \mathbf{e}^e/\left\|\mathbf{e}^e\right\|$. Two useful identities, derived from the following assumptions, are: (i) from the assumption of associative flow rule, $\hat{\mathbf{n}} = \mathbf{e}^e/\left\|\mathbf{e}^e\right\| = \mathbf{s}/\|\mathbf{s}\|$. and (ii) from the assumption of convexity of the yield function, $\hat{\mathbf{n}} = \hat{\mathbf{n}}^{tr}$. Exploiting these identities (5.27) can be rewritten as

$$\varepsilon_v^e = \varepsilon_v^{e,tr} - \Delta\varphi\frac{\partial f}{\partial p}; \qquad \varepsilon_s^e = \varepsilon_s^{e,tr} - \Delta\varphi\frac{\partial f}{\partial q}, \tag{5.29}$$

subject to the conditions

$$f(p,q,p_c) \le 0; \quad \Delta\varphi \ge 0; \quad \Delta\varphi f(p,q,p_c) = 0. \tag{5.30}$$

In the elastic regime, $f(p^{tr},q^{tr},p_{c,n}) < 0$, $\Delta\varphi = 0$; $\varepsilon_v^e = \varepsilon_v^{e,tr}, \varepsilon_s^e = \varepsilon_s^{e,tr}$. Plastic regime is realized for the conditions: $f(p^{tr},q^{tr},p_{c,n}) > 0$, $\Delta\varphi > 0$. p^{tr} and q^{tr} are the predictor values defined from (5.6) as

$$p^{tr} = \frac{\partial\Psi\left(\varepsilon^{e,tr}\right)}{\partial\varepsilon_v^{e,tr}}; \qquad q^{tr} = \frac{\partial\Psi\left(\varepsilon^{e,tr}\right)}{\partial\varepsilon_s^{e,tr}}. \tag{5.31}$$

In the elasto-plastic regime, (5.29) and (5.30) can be viewed as a system of simultaneous nonlinear equations in the elastic strain invariants and the consistency parameter $\Delta\varphi$, represented by residual vector $\mathbf{r}$ and vector of unknowns $\mathbf{y}$, as follows:

$$\mathbf{r} = \begin{Bmatrix} \varepsilon_v^e - \varepsilon_v^{e,tr} + \Delta\varphi\,\partial f/\partial p \\ \varepsilon_s^e - \varepsilon_s^{e,tr} + \Delta\varphi\,\partial f/\partial q \\ f \end{Bmatrix}; \qquad \mathbf{y} = \begin{Bmatrix} \varepsilon_v^e \\ \varepsilon_s^e \\ \Delta\varphi \end{Bmatrix}. \tag{5.32}$$

In order to solve this system iteratively, one can employ Newton's method over the following loop:

$$\mathbf{y}^{k+1} = \mathbf{y}^k - \left(\mathbf{A}^k\right)^{-1}\mathbf{r}^k; \qquad \mathbf{A}^k = \frac{\partial \mathbf{r}^k}{\partial \mathbf{y}^k}. \tag{5.33}$$

k is the local iteration counter. $\mathbf{A}\in R^{3\times 3}$ is the consistent tangent operator. A closed form expression of **A** can be written in a compact form with the aid of the following matrices:

$$\mathbf{H} = \begin{bmatrix} H_{11} & H_{12} \\ H_{21} & H_{22} \end{bmatrix} = \begin{bmatrix} \partial^2 f/\partial p\partial p & \partial^2 f/\partial p\partial q \\ \partial^2 f/\partial q\partial p & \partial^2 f/\partial q\partial q \end{bmatrix};$$
$$\mathbf{G} = \mathbf{H}\mathbf{D}^e. \tag{5.34}$$

$\mathbf{H} = \nabla\nabla f\big|_{p_c} \in R^{2\times 2}$ is the Hessian matrix of yield function f with p_c held constant. The **A** matrix then takes the form

$$\mathbf{A} = \begin{bmatrix} 1+\Delta\varphi\left(G_{11}+K_p\partial^2 f/\partial p\partial p_c\right) & \Delta\varphi G_{12} & \partial f/\partial p \\ \Delta\varphi G_{21} & 1+\Delta\varphi G_{22} & \partial f/\partial q \\ D^e_{11}\partial f/\partial p + D^e_{21}\partial f/\partial q + K_p\partial f/\partial p_c & D^e_{12}\partial f/\partial p + D^e_{22}\partial f/\partial q & 0 \end{bmatrix} \tag{5.35}$$

where $K_p = \partial p_c/\partial\varepsilon^e_v = -\Theta p_c$ is the plastic hardening modulus. Using the yield function (5.13), one can have: $\partial f/\partial p = 2p - p_c$, $\partial f/\partial q = 2q/M^2$, $\partial f/\partial p_c = -p$, $\partial^2 f/\partial p\partial p_c = -1$; $H_{11} = 2, H_{22} = 2/M^2$, $H_{12} = H_{21} = 0$; $G_{11} = 2D^e_{11}, G_{12} = 2D^e_{12}$, $G_{21} = 2D^e_{21}/M^2, G_{22} = 2D^e_{22}/M^2$.

5.6 Consistent Tangent Moduli

Material tangent stiffness matrix $\mathbf{a}\in R^{3\times 3}$, defined in the spaces of β and ε, is expressed as

$$a_{ij} = \frac{\partial\beta_i}{\partial\varepsilon_j} = \frac{\partial\beta_i}{\partial\varepsilon^{e,tr}_j}. \tag{5.36}$$

For a fully elastic response with volumetric and deviatoric coupling, the matrix **a** takes the form

$$\mathbf{a}^{e} = \left(D_{11}^{e} - \frac{2q}{9\varepsilon_{s}^{e}} \right) \delta \otimes \delta + \sqrt{\frac{2}{3}} D_{12}^{e} (\delta \otimes \hat{\mathbf{n}} + \hat{\mathbf{n}} \otimes \delta) + \frac{2q}{3\varepsilon_{s}^{e}} (\mathbf{I} - \hat{\mathbf{n}} \otimes \hat{\mathbf{n}}) + \frac{2}{3} D_{22}^{e} \hat{\mathbf{n}} \otimes \hat{\mathbf{n}}, \quad (5.37)$$

where **I** is a 3×3 identity matrix, $\hat{\mathbf{n}}$ is a 3×1 vector obtained from the relations

$$\hat{\mathbf{n}} = \mathbf{e}^{e} \Big/ \left\| \mathbf{e}^{e} \right\| = \mathbf{e}^{e,tr} \Big/ \left\| \mathbf{e}^{e,tr} \right\| = \mathbf{s} / \|\mathbf{s}\|.$$

In case of isotropic, linear elasticity free energy function Ψ takes the form

$$\begin{aligned} \Psi &= \frac{1}{2}\lambda \left[\varepsilon_{1}^{e} + \varepsilon_{2}^{e} + \varepsilon_{3}^{e} \right]^{2} + \mu \left[\left(\varepsilon_{1}^{e} \right)^{2} + \left(\varepsilon_{2}^{e} \right)^{2} + \left(\varepsilon_{3}^{e} \right)^{2} \right] \\ &= \frac{1}{2} K \left(\varepsilon_{v}^{e} \right)^{2} + \frac{3}{2} \mu \left(\varepsilon_{s}^{e} \right)^{2}, \end{aligned} \quad (5.38)$$

where K and μ are constant elastic bulk and shear moduli, respectively. $K = \lambda + 2/3\mu$, λ is a Lamé's constant. Since $\mu = \mu_0 > 0$ (see (5.10)), $\alpha = 0$; elastic shear and volumetric responses uncouple, i.e., $D_{12}^{e} = D_{21}^{e} = 0$ (see (5.12c)). Now substituting $D_{11}^{e} = K$, $D_{22}^{e} = 3\mu$ (see (5.12a), (5.12b)), tangential elastic moduli of (5.37) degenerates to the familiar expression for linear elasticity as follows:

$$\mathbf{a}^{e} = K \delta \otimes \delta + 2\mu \left(\mathbf{I} - \frac{1}{3} \delta \otimes \delta \right). \quad (5.39)$$

In the elastoplastic regime, the tangential moduli matrix $\mathbf{a}^{ep}$ can be expressed using strain derivative of (5.5) as

$$\mathbf{a}^{ep} = \frac{\partial \beta}{\partial \varepsilon^{e,tr}} = \delta \otimes \frac{\partial p}{\partial \varepsilon^{e,tr}} + \sqrt{\frac{2}{3}} \hat{\mathbf{n}} \otimes \frac{\partial q}{\partial \varepsilon^{e,tr}} + \sqrt{\frac{2}{3}} q \frac{\partial \hat{\mathbf{n}}}{\partial \varepsilon^{e,tr}}, \quad (5.40)$$

where

$$\frac{\partial \hat{\mathbf{n}}}{\partial \varepsilon^{e,tr}} = \frac{\partial \left(\mathbf{e}^{e} / \left\| \mathbf{e}^{e} \right\| \right)}{\partial \varepsilon^{e,tr}} = \frac{\partial \left(\mathbf{e}^{e,tr} / \left\| \mathbf{e}^{e,tr} \right\| \right)}{\partial \varepsilon^{e,tr}} = \frac{1}{\left\| \mathbf{e}^{e,tr} \right\|} \left(\mathbf{I} - \frac{1}{3} \delta \otimes \delta - \hat{\mathbf{n}} \otimes \hat{\mathbf{n}} \right). \quad (5.41)$$

Substituting (5.41) in (5.40), and using the elements of the matrix $\mathbf{D}^e$ to enforce the chain rule, one can have

$$\begin{aligned} \mathbf{a}^{ep} = {} & \delta \otimes \left(D_{11}^{e} \frac{\partial \varepsilon_v^e}{\partial \varepsilon^{e,tr}} + D_{12}^{e} \frac{\partial \varepsilon_s^e}{\partial \varepsilon^{e,tr}} \right) + \sqrt{\frac{2}{3}} \hat{\mathbf{n}} \otimes \left(D_{21}^{e} \frac{\partial \varepsilon_v^e}{\partial \varepsilon^{e,tr}} + D_{22}^{e} \frac{\partial \varepsilon_s^e}{\partial \varepsilon^{e,tr}} \right) \\ & + \frac{2q}{3\varepsilon_s^{e,tr}} \left(\mathbf{I} - \frac{1}{3} \delta \otimes \delta - \hat{\mathbf{n}} \otimes \hat{\mathbf{n}} \right), \end{aligned} \quad (5.42)$$

Strain derivatives of the invariants ε_v^e and ε_s^e are obtained from (5.29) as

$$\frac{\partial \varepsilon_v^e}{\partial \varepsilon^{e,tr}} = \frac{\partial}{\partial \varepsilon^{e,tr}} \left(\varepsilon_v^{e,tr} - \Delta\varphi \frac{\partial f}{\partial p} \right); \qquad \frac{\partial \varepsilon_s^e}{\partial \varepsilon^{e,tr}} = \frac{\partial}{\partial \varepsilon^{e,tr}} \left(\varepsilon_s^{e,tr} - \Delta\varphi \frac{\partial f}{\partial q} \right). \quad (5.43)$$

In the expansion of (5.43), one will need the following strain derivative of p_c

$$\frac{\partial p_c}{\partial \varepsilon^{e,tr}} = K_p \frac{\partial \varepsilon_v^e}{\partial \varepsilon^{e,tr}} + K_p^{tr} \delta, \quad (5.44)$$

where $K_p = \partial p_c / \partial \varepsilon_v^e$ and $K_p^{tr} = \partial p_c / \partial \varepsilon_v^{e,tr}$. The expansion of $(5.43)_1$ and $(5.43)_2$ takes the following forms, respectively

$$b_{11} \frac{\partial \varepsilon_v^e}{\partial \varepsilon^{e,tr}} + b_{12} \frac{\partial \varepsilon_s^e}{\partial \varepsilon^{e,tr}} = c\delta - \frac{\partial f}{\partial p} \frac{\partial \Delta\varphi}{\partial \varepsilon^{e,tr}}, \quad (5.45a)$$

$$b_{21} \frac{\partial \varepsilon_v^e}{\partial \varepsilon^{e,tr}} + b_{22} \frac{\partial \varepsilon_s^e}{\partial \varepsilon^{e,tr}} = \sqrt{\frac{2}{3}} \hat{\mathbf{n}} - \frac{\partial f}{\partial q} \frac{\partial \Delta\varphi}{\partial \varepsilon^{e,tr}}, \quad (5.45b)$$

where

$$b_{11} = 1 + \Delta\varphi\left(G_{11} + K_p \frac{\partial^2 f}{\partial p \partial p_c} \right); \qquad b_{12} = \Delta\varphi G_{12};$$

$$b_{21} = \Delta\varphi\left(G_{21} + K_p \frac{\partial^2 f}{\partial q \partial p_c} \right); \qquad b_{22} = 1 + \Delta\varphi G_{22}; \tag{5.46}$$

$$c = 1 - \Delta\varphi K_p^{tr} \frac{\partial^2 f}{\partial p \partial p_c}.$$

Solving (5.45a) and (5.45b) simultaneously yields

$$\frac{\partial \varepsilon_v^e}{\partial \varepsilon^{e,tr}} = \frac{1}{\det(\mathbf{b})}\left[b_{22} c\delta - \sqrt{\frac{2}{3}} b_{12}\hat{\mathbf{n}} - \left(b_{22}\frac{\partial f}{\partial p} - b_{12}\frac{\partial f}{\partial q} \right)\frac{\partial \Delta\varphi}{\partial \varepsilon^{e,tr}} \right], \tag{5.47a}$$

$$\frac{\partial \varepsilon_s^e}{\partial \varepsilon^{e,tr}} = \frac{1}{\det(\mathbf{b})}\left[-b_{21} c\delta + \sqrt{\frac{2}{3}} b_{11}\hat{\mathbf{n}} - \left(b_{11}\frac{\partial f}{\partial q} - b_{21}\frac{\partial f}{\partial q} \right)\frac{\partial \Delta\varphi}{\partial \varepsilon^{e,tr}} \right], \tag{5.47b}$$

where $\det(\mathbf{b}) = b_{11}b_{22} - b_{21}b_{12}$.

The strain-gradient of $\Delta\varphi$ is obtained from the overall consistency condition

$$\frac{\partial f}{\partial \varepsilon^{e,tr}} = \frac{\partial f}{\partial p}\frac{\partial p}{\partial \varepsilon^{e,tr}} + \frac{\partial f}{\partial q}\frac{\partial q}{\partial \varepsilon^{e,tr}} + \frac{\partial f}{\partial p_c}\frac{\partial p_c}{\partial \varepsilon^{e,tr}} = \mathbf{0}. \tag{5.48}$$

Since p, q and p_c are functions of the strain invariants, one can expand (5.48) further by chain rule, and then use (5.47a) and (5.47b) to obtain the following result

$$\frac{\partial \Delta\varphi}{\partial \varepsilon^{e,tr}} = a_1\delta + a_2\hat{\mathbf{n}}, \tag{5.49}$$

where

$$a_1 = \frac{1}{e}\left[d_1 b_{22} c - d_2 b_{21} c + \det(\mathbf{b}) K_p^{tr}\frac{\partial f}{\partial p_c} \right], \quad a_2 = \frac{1}{e}\left[\sqrt{\frac{2}{3}}(d_2 b_{11} - d_1 b_{12}) \right],$$

$$e = d_1\left(b_{22}\frac{\partial f}{\partial p} - b_{12}\frac{\partial f}{\partial q} \right) + d_2\left(b_{11}\frac{\partial f}{\partial q} - b_{21}\frac{\partial f}{\partial p} \right), \tag{5.50}$$

$$d_1 = D_{11}^e\frac{\partial f}{\partial p} + D_{21}^e\frac{\partial f}{\partial q} + K_p\frac{\partial f}{\partial p_c}, \quad d_2 = D_{12}^e\frac{\partial f}{\partial p} + D_{22}^e\frac{\partial f}{\partial q}.$$

Plugging (5.49) in (5.47) yields

$$\frac{\partial \varepsilon_v^e}{\partial \varepsilon^{e,tr}} = D_{11}^p \delta + \sqrt{\frac{2}{3}} D_{12}^p \hat{\mathbf{n}}; \qquad \frac{\partial \varepsilon_s^e}{\partial \varepsilon^{e,tr}} = D_{21}^p \delta + \sqrt{\frac{2}{3}} D_{22}^p \hat{\mathbf{n}}, \tag{5.51}$$

$\mathbf{D}^p \in R^{2\times 2}$, consists of coefficients of base vectors δ and $\hat{\mathbf{n}}$ in (5.47a) and (5.47b), is defined as follows:

$$\begin{aligned}
D_{11}^p &= \frac{1}{\det(\mathbf{b})}\left[b_{22}\left(c - a_1 \frac{\partial f}{\partial p} \right) + b_{12} a_1 \frac{\partial f}{\partial q} \right]; \\
D_{12}^p &= \frac{1}{\det(\mathbf{b})}\left[b_{12}\left(-1 + \sqrt{\frac{3}{2}} a_2 \frac{\partial f}{\partial q} \right) - \sqrt{\frac{3}{2}} b_{22} a_2 \frac{\partial f}{\partial p} \right]; \\
D_{21}^p &= \frac{1}{\det(\mathbf{b})}\left[-b_{11} a_1 \frac{\partial f}{\partial q} - b_{21}\left(c - a_1 \frac{\partial f}{\partial p} \right) \right]; \\
D_{22}^p &= \frac{1}{\det(\mathbf{b})}\left[b_{11}\left(1 - \sqrt{\frac{3}{2}} a_2 \frac{\partial f}{\partial q} \right) + \sqrt{\frac{3}{2}} b_{21} a_2 \frac{\partial f}{\partial p} \right];
\end{aligned} \tag{5.52}$$

The strain gradients of the stress invariants then take the form

$$\frac{\partial p}{\partial \varepsilon^{e,tr}} = D_{11}^{ep} \delta + \sqrt{\frac{2}{3}} D_{12}^{ep} \hat{\mathbf{n}}; \qquad \frac{\partial q}{\partial \varepsilon^{e,tr}} = D_{21}^{ep} \delta + \sqrt{\frac{2}{3}} D_{22}^{ep} \hat{\mathbf{n}}, \tag{5.53}$$

where $\mathbf{D}^{ep} \in R^{2\times 2}$ is defined as

$$\mathbf{D}^{ep} = \mathbf{D}^e \mathbf{D}^p. \tag{5.54}$$

Substituting (5.53) in (5.40) then yields consistent elasto-plastic tangent moduli

$$\begin{aligned}
\mathbf{a}^{ep} &= \left(D_{11}^{ep} - \frac{2q}{9\varepsilon_s^e} \right) \delta \otimes \delta + \sqrt{\frac{2}{3}} D_{12}^{ep} \delta \otimes \hat{\mathbf{n}} + \sqrt{\frac{2}{3}} D_{12}^{ep} \hat{\mathbf{n}} \otimes \delta \\
&+ \frac{2q}{3\varepsilon_s^e} (\mathbf{I} - \hat{\mathbf{n}} \otimes \hat{\mathbf{n}}) + \frac{2}{3} D_{22}^{ep} \hat{\mathbf{n}} \otimes \hat{\mathbf{n}}.
\end{aligned} \tag{5.55}$$

For elastic loading, $\mathbf{D}^p = \mathbf{I}$, $\mathbf{D}^{ep} = \mathbf{D}^e$, and so (5.55) degenerates to (5.37). Thus (5.55) represents a generalized expression for both elastic and plastic loading. For elasto-plastic

loading $\mathbf{D}^p \neq \mathbf{I}$, and so $\mathbf{a}^{ep}$ loses its major symmetry due to the fact that $D_{12}^{ep} \neq D_{21}^{ep}$. Volumetric and deviatoric responses are coupled for elasto-plastic loading even if $\mathbf{D}^e$ is diagonal (in case of constant elastic shear modulus, i.e., $\mu_0 > 0$, $\alpha = 0$), since the matrix $\mathbf{D}^{ep}$ is generally full due to plastic volumetric and deviatoric coupling inherent in the Cam-Clay model.

CHAPTER 6
HYPERELASTIC-VISCOPLASTIC MCC MODEL

6.1 Introduction

Hyperelastic-plastic MCC model is further extended for viscoplasticity to model time-dependent secondary compression of phosphatic waste clay. Elasticity response is based on the stored energy function [68] of (5.9). Consequently, nonlinearity of elastic moduli and coupling of volumetric and deviatoric elastic responses follow the same constitutive relations as presented in Section 5.2. Yield function of MCC (see (5.13)) is coupled with a time rate flow rule to simulate viscid response.

Clay is a strain hardening, rate sensitive material that has remarkable characteristics such as rate sensitivity of strength, secondary compression, creep and stress relaxation. Various elasto-viscoplastic constitutive models have been proposed to describe the rheological behavior of clay. Most elasto-viscoplastic constitutive models can be classified as overstress models or non-stationary flow surface models. Overstress elasto-viscoplastic constitutive model was first introduced by Perzyna [72]. The Zienkiewicz et al. model [73], Adachi and Oka model [74], Dafalias model [75], Katona model [76], Baladi-Rohani model [77] belong to this category. The key assumption in these models is that viscous effects become pronounced only after the material undergoes yielding, and that viscous effects are not essential in the elastic domain. Overstress model is an outgrowth of classical plasticity where viscous response is introduced by a time rate flow rule with a plastic yield function. As opposed to

overstress model, in non-stationary flow surface model yield condition of a material changes with time as plastic straining occurs. Olszak and Perzyna [78] initiated this concept by introducing the time dependent yield condition. Later Sekiguchi [79], Dragon and Mroz [80], Nova [81], Matsui and Abe [82], among others, adopted this concept. Viscoplastic rate equations of the non-stationary flow surface model are characterized by the stress rate terms.

Overstress viscoplasticity model is adopted in this study to simulate secondary compression behavior of phosphatic waste clay. Motivations for selecting overstress model are: (1) the incorporation of MCC yield function is straightforward; (2) the generality of time-rate flow rule offers the capability of simulating time-dependent material behavior over a wide range of loading; (3) the formulation is amenable to finite element implementation.

6.2 Flow Rule

In viscoplasticity formulation, additive decomposition of $\dot{\varepsilon}$ takes the following form

$$\dot{\varepsilon} = \dot{\varepsilon}^{e} + \dot{\varepsilon}^{vp}, \tag{6.1}$$

where ε is the vector of principal logarithmic stretches. ε^{e} and ε^{vp} are the elastic and viscoplastic components of ε, respectively.

For an associative flow $\dot{\varepsilon}^{vp}$ is given by the relation

$$\dot{\varepsilon}^{vp} = \gamma\varphi(f)\frac{\partial f}{\partial \beta}, \tag{6.2}$$

where β is the vector of principal Kirchhoff stresses, γ is a material property called the fluidity parameter (units of inverse time) that establishes the relative rate of viscoplastic straining, $\varphi(f)$ is a scale function (dimensionless) of plastic yield function, f.

$$\varphi(f) = \begin{cases} \varphi(f), & f > 0 \\ 0, & f \le 0 \end{cases} \tag{6.3}$$

$\varphi(f)$ is called viscous flow function. Two commonly used forms of $\varphi(f)$ are:

$$\varphi(f) = \left(\frac{f}{f_0}\right)^N; \tag{6.4a}$$

$$\varphi(f) = \exp\left(\frac{f}{f_0}\right)^N - 1. \tag{6.4b}$$

N is an exponent; f_0 is a normalizing constant with the same unit as f so that $\varphi(f)$ is dimensionless. Although more elaborate functional forms of $\varphi(f)$ may be established, the forms given by (6.4) appear to suffice for many geologic materials [73].

(6.2) can be written in incremental form as

$$\Delta\varepsilon^{vp} = \gamma\Delta t\,\varphi(f)\frac{\partial f}{\partial \beta} = \Delta\gamma\varphi(f)\frac{\partial f}{\partial \beta}, \tag{6.5}$$

where $\Delta\gamma = \gamma\Delta t$. Substituting (6.5) in additive decomposition of natural strains, i.e., $\varepsilon = \varepsilon^e + \varepsilon^p = \varepsilon^{e,tr} + \varepsilon^p_n$, one can write the flow rule as

$$\varepsilon^e = \varepsilon^{e,tr} - \Delta\gamma\,\varphi(f)\frac{\partial f}{\partial \beta}. \tag{6.6}$$

Volumetric and deviatoric components of (6.6) are as follows:

$$\varepsilon^e_v = \varepsilon^{e,tr}_v - \Delta\gamma\,\varphi(f)\frac{\partial f}{\partial p}; \qquad \mathbf{e}^e = \mathbf{e}^{e,tr} - \Delta\gamma\,\varphi(f)\sqrt{\frac{3}{2}}\frac{\partial f}{\partial q}\frac{\mathbf{s}}{\|\mathbf{s}\|}. \tag{6.7}$$

In terms of unit vectors $\hat{\mathbf{n}}, \hat{\mathbf{n}}^{tr}$ $(6.7)_2$ takes the form

$$\varepsilon_S^e \hat{\mathbf{n}} = \varepsilon_S^{e,tr} \hat{\mathbf{n}}^{tr} - \Delta\gamma\, \varphi(f) \frac{\partial f}{\partial q} \hat{\mathbf{n}}, \tag{6.8}$$

where $\varepsilon_S^e = \sqrt{2/3}\,\|\mathbf{e}\|$, $\varepsilon_S^{e,tr} = \sqrt{2/3}\left\|\mathbf{e}^{tr}\right\|$, $\hat{\mathbf{n}}^{tr} = \mathbf{e}^{tr} \Big/ \left\|\mathbf{e}^{tr}\right\|$, $\hat{\mathbf{n}} = \mathbf{e}^{e} \Big/ \left\|\mathbf{e}^{e}\right\|$. Since $\hat{\mathbf{n}} = \hat{\mathbf{n}}^{tr}$ (see Section 5.5), (6.8) can be expressed in terms of scalar coefficients. Consequently, (6.7) can be rewritten as

$$\varepsilon_V^e = \varepsilon_V^{e,tr} - \Delta\gamma\, \varphi(f) \frac{\partial f}{\partial p}; \qquad \varepsilon_S^e = \varepsilon_S^{e,tr} - \Delta\gamma\, \varphi(f) \frac{\partial f}{\partial q}. \tag{6.9}$$

In the elastic regime, $f(p^{tr}, q^{tr}, p_{c,n}) < 0$, $\varphi(f) = 0$; $\varepsilon_V^e = \varepsilon_V^{e,tr}, \varepsilon_S^e = \varepsilon_S^{e,tr}$.

Viscoplastic regime is realized for the conditions: $f(p^{tr}, q^{tr}, p_{c,n}) > 0$, $\varphi(f) > 0$.

p^{tr} and q^{tr} are the predictor values as defined in (5.31). In the viscoplastic regime, (6.9) can be viewed as a system of simultaneous nonlinear equations in the elastic strain invariants, represented by residual vector $\mathbf{r}$ and vector of unknowns $\mathbf{y}$, as follows:

$$\mathbf{r} = \begin{Bmatrix} \varepsilon_V^e - \varepsilon_V^{e,tr} + \Delta\gamma\, \varphi(f) \partial f / \partial p \\ \varepsilon_S^e - \varepsilon_S^{e,tr} + \Delta\gamma\, \varphi(f) \partial f / \partial q \end{Bmatrix}; \qquad \mathbf{y} = \begin{Bmatrix} \varepsilon_V^e \\ \varepsilon_S^e \end{Bmatrix}. \tag{6.10}$$

One can employ Newton's method (cf. (5.33)) to solve this system iteratively while the tangent operator $\mathbf{A} \in R^{2\times 2}$ of (5.33) now takes the form

$$\mathbf{A} = \begin{bmatrix} A_{11} & A_{12} \\ A_{21} & A_{22} \end{bmatrix} = \begin{bmatrix} \partial r_1 / \partial \varepsilon_V^e & \partial r_1 / \partial \varepsilon_S^e \\ \partial r_2 / \partial \varepsilon_V^e & \partial r_2 / \partial \varepsilon_S^e \end{bmatrix}. \tag{6.11}$$

Individual components of $\mathbf{A}$ are derived as

$$
\begin{aligned}
A_{11} &= 1+\Delta\gamma\left[\varphi(f)\left(G_{11}+K_p\frac{\partial^2 f}{\partial p\partial p_c}\right)+\varphi'(f)\frac{\partial f}{\partial p}\left(D^e_{11}\frac{\partial f}{\partial p}+D^e_{21}\frac{\partial f}{\partial q}+K_p\frac{\partial f}{\partial p_c}\right)\right];\\
A_{12} &= \Delta\gamma\left[\varphi'(f)\frac{\partial f}{\partial p}\left(D^e_{12}\frac{\partial f}{\partial p}+D^e_{22}\frac{\partial f}{\partial q}\right)+\varphi(f)G_{12}\right];\\
A_{21} &= \Delta\gamma\left[\varphi'(f)\frac{\partial f}{\partial q}\left(D^e_{11}\frac{\partial f}{\partial p}+D^e_{21}\frac{\partial f}{\partial q}+K_p\frac{\partial f}{\partial p_c}\right)+\varphi(f)G_{21}\right];\\
A_{22} &= 1+\Delta\gamma\left[\varphi'(f)\frac{\partial f}{\partial q}\left(D^e_{12}\frac{\partial f}{\partial p}+D^e_{22}\frac{\partial f}{\partial q}\right)+\varphi(f)G_{22}\right].
\end{aligned}
\tag{6.12}
$$

$K_p = \partial p_c / \partial \varepsilon^e_v = -\Theta p_c$ (see (5.25)) is the plastic hardening modulus,

$\varphi'(f) = \partial\varphi(f)/\partial f$. Matrices $\mathbf{D}^e$, $\mathbf{G}$ are defined in Sections 5.2 and 5.5, respectively.

6.3 Consistent Tangent Moduli

Consistent tangent moduli matrix in elasto-viscoplastic regime $\mathbf{a}^{ep} \in R^{3\times3}$, defined in the spaces of β and ε, is expressed as

$$
a^{ep}_{ij} = \frac{\partial\beta_i}{\partial\varepsilon_j} = \frac{\partial\beta_i}{\partial\varepsilon^{e,tr}_j}. \tag{6.13}
$$

Following the developments of Section 5.6, one can obtain an expression of $\mathbf{a}^{ep}$, identical to (5.42), i.e.,

$$
\begin{aligned}
\mathbf{a}^{ep} = {} & \delta\otimes\left(D^e_{11}\frac{\partial\varepsilon^e_v}{\partial\varepsilon^{e,tr}}+D^e_{12}\frac{\partial\varepsilon^e_s}{\partial\varepsilon^{e,tr}}\right)+\sqrt{\frac{2}{3}}\,\hat{\mathbf{n}}\otimes\left(D^e_{21}\frac{\partial\varepsilon^e_v}{\partial\varepsilon^{e,tr}}+D^e_{22}\frac{\partial\varepsilon^e_s}{\partial\varepsilon^{e,tr}}\right)\\
& +\frac{2q}{3\varepsilon^{e,tr}_s}\left(\mathbf{I}-\frac{1}{3}\delta\otimes\delta-\hat{\mathbf{n}}\otimes\hat{\mathbf{n}}\right).
\end{aligned}
$$

Strain derivatives of the invariants ε^e_v and ε^e_s are obtained from (6.9) as

$$
\frac{\partial\varepsilon^e_v}{\partial\varepsilon^{e,tr}} = \frac{\partial}{\partial\varepsilon^{e,tr}}\left(\varepsilon^{e,tr}_v-\Delta\gamma\,\varphi(f)\frac{\partial f}{\partial p}\right);\quad \frac{\partial\varepsilon^e_s}{\partial\varepsilon^{e,tr}} = \frac{\partial}{\partial\varepsilon^{e,tr}}\left(\varepsilon^{e,tr}_s-\Delta\gamma\,\varphi(f)\frac{\partial f}{\partial q}\right). \tag{6.14}
$$

In order to expand (6.14) to the lowest order, one will need the following strain derivatives:

$$\frac{\partial f}{\partial \varepsilon^{e,tr}} = a_1\delta + a_2\frac{\partial \varepsilon_v^e}{\partial \varepsilon^{e,tr}} + a_3\frac{\partial \varepsilon_s^e}{\partial \varepsilon^{e,tr}}; \tag{6.15a}$$

$$\frac{\partial^2 f}{\partial p\partial \varepsilon^{e,tr}} = a_4\delta + a_5\frac{\partial \varepsilon_v^e}{\partial \varepsilon^{e,tr}} + G_{12}\frac{\partial \varepsilon_s^e}{\partial \varepsilon^{e,tr}}; \tag{6.15b}$$

$$\frac{\partial^2 f}{\partial q\partial \varepsilon^{e,tr}} = G_{21}\frac{\partial \varepsilon_v^e}{\partial \varepsilon^{e,tr}} + G_{22}\frac{\partial \varepsilon_s^e}{\partial \varepsilon^{e,tr}}. \tag{6.15c}$$

Coefficients of (6.15a) and (6.15b) are given as

$$\begin{aligned} &a_1 = K_p^{tr}\frac{\partial f}{\partial p_c}; \quad a_2 = D_{11}^e\frac{\partial f}{\partial p} + D_{21}^e\frac{\partial f}{\partial q} + K_p\frac{\partial f}{\partial p_c}; \quad a_3 = D_{12}^e\frac{\partial f}{\partial p} + D_{22}^e\frac{\partial f}{\partial q}; \\ &a_4 = K_p^{tr}\frac{\partial^2 f}{\partial p\partial p_c}; \quad a_5 = G_{11} + K_p\frac{\partial^2 f}{\partial p\partial p_c}. \end{aligned} \tag{6.16}$$

where $K_p = \partial p_c \big/ \partial \varepsilon_v^e = -\Theta p_c$ and $K_p^{tr} = \partial p_c \big/ \partial \varepsilon_v^{e,tr} = \Theta p_c$ (see (5.25)).

$$b_{11}\frac{\partial \varepsilon_v^e}{\partial \varepsilon^{e,tr}} + b_{12}\frac{\partial \varepsilon_s^e}{\partial \varepsilon^{e,tr}} = c_1\delta, \tag{6.17a}$$

$$b_{21}\frac{\partial \varepsilon_v^e}{\partial \varepsilon^{e,tr}} + b_{22}\frac{\partial \varepsilon_s^e}{\partial \varepsilon^{e,tr}} = -c_2\delta + \sqrt{\frac{2}{3}}\hat{\mathbf{n}}, \tag{6.17b}$$

where

$$\begin{aligned} &b_{11} = 1 + a_2\Delta\gamma\,\varphi'(f)\frac{\partial f}{\partial p} + \Delta\gamma\,\varphi(f)G_{21}; \quad b_{12} = a_3\Delta\gamma\,\varphi'(f)\frac{\partial f}{\partial p} + \Delta\gamma\,\varphi(f)G_{22}; \\ &b_{21} = a_2\Delta\gamma\,\varphi'(f)\frac{\partial f}{\partial q} + \Delta\gamma\,\varphi(f)G_{21}; \quad b_{22} = 1 + a_3\Delta\gamma\,\varphi'(f)\frac{\partial f}{\partial q} + \Delta\gamma\,\varphi(f)G_{22}; \\ &c_1 = 1 - a_1\Delta\gamma\,\varphi'(f)\frac{\partial f}{\partial p}; \quad c_2 = a_1\Delta\gamma\,\varphi'(f)\frac{\partial f}{\partial q}. \end{aligned} \tag{6.18}$$

Solving (6.17a) and (6.17b) simultaneously yields

$$\frac{\partial \varepsilon_v^e}{\partial \varepsilon^{e,tr}} = D_{11}^p \delta + \sqrt{\frac{2}{3}} D_{12}^p \hat{\mathbf{n}}; \qquad \frac{\partial \varepsilon_s^e}{\partial \varepsilon^{e,tr}} = D_{21}^p \delta + \sqrt{\frac{2}{3}} D_{22}^p \hat{\mathbf{n}}. \tag{6.19}$$

Coefficients of $\mathbf{D}^p \in R^{2\times 2}$ are given as

$$\begin{aligned} D_{11}^p &= \frac{1}{\det(\mathbf{b})}(b_{22}c_1 + b_{12}c_2); \quad & D_{12}^p &= \frac{-1}{\det(\mathbf{b})} b_{12}; \\ D_{21}^p &= \frac{1}{\det(\mathbf{b})}(-b_{21}c_1 - b_{11}c_2); \quad & D_{22}^p &= \frac{1}{\det(\mathbf{b})} b_{11}, \end{aligned} \tag{6.20}$$

where $\det(\mathbf{b}) = b_{11}b_{22} - b_{21}b_{12}$.

Substituting (6.19) in the expression of $\mathbf{a}^{ep}$ (cf. (5.42)) then yields consistent elasto-viscoplastic tangent moduli as follows:

$$\begin{aligned} \mathbf{a}^{ep} = &\left(D_{11}^{ep} - \frac{2q}{9\varepsilon_s^e} \right) \delta \otimes \delta + \sqrt{\frac{2}{3}} D_{12}^{ep} \delta \otimes \hat{\mathbf{n}} + \sqrt{\frac{2}{3}} D_{12}^{ep} \hat{\mathbf{n}} \otimes \delta \\ &+ \frac{2q}{3\varepsilon_s^e}(\mathbf{I} - \hat{\mathbf{n}} \otimes \hat{\mathbf{n}}) + \frac{2}{3} D_{22}^{ep} \hat{\mathbf{n}} \otimes \hat{\mathbf{n}}. \end{aligned} \tag{6.21}$$

$\mathbf{D}^{ep} = \mathbf{D}^e\mathbf{D}^p \in R^{2\times 2}$. Note that (6.21) and (5.55) have identical expressions. (6.21) represents a generalized expression for both elastic and plastic loading. For elastic loading, $\mathbf{D}^{ep} = \mathbf{D}^e$ since $\mathbf{D}^p = \mathbf{I}$ and so (6.21) degenerates to an expression of $\mathbf{a}^e$ identical to (5.37).

CHAPTER 7
LINEARIZATION

7.1 Preliminaries

Some useful formulas are summarized below. These will be helpful for linearization of strong and weak forms of coupled equations (see Chapter 4).

The first of these formulas is the Piola transformation, introduced first in Section 4.2. Let $\mathbf{y} \in R^{nsd}$ be a vector field in spatial configuration $\phi_t(\mathsf{B})$. Then, the Piola transform of $\mathbf{y}$ in reference configuration B is

$$\mathbf{Y} = J\mathbf{F}^{-1} \cdot \mathbf{y}, \tag{7.1}$$

provided that motion ϕ is regular in B. The following equation holds for $\mathbf{y}$, $\mathbf{Y}$.

$$\mathrm{DIV}\,\mathbf{Y} = J\,\mathrm{div}\,\mathbf{y}. \tag{7.2}$$

Proof of (7.2) is given in Section A.7. This identity may be extended to cases where $\mathbf{Y}$ and $\mathbf{y}$ are vectors derived from tensors of order greater than or equal to two by fixing all but one of the tensor's legs (for example, fixing one leg of the Kirchhoff stress tensor τ produces a vector of Kirchhoff stresses).

Following are linearization of some basic terms, one would need for subsequent development. Let $\delta\mathbf{u}$ be the variation of the displacement field; then the linearization of $\mathbf{F}$ and $\mathbf{F}^{-1}$ at any configuration $\phi_t(\mathsf{B})$ are given, respectively, by

$$L\mathbf{F} = \mathbf{F} + \mathrm{grad}\,\delta\mathbf{u} \cdot \mathbf{F} = \mathbf{F} + \mathrm{GRAD}\,\delta\mathbf{u}; \tag{7.3a}$$

$$L\mathbf{F}^{-1} = \mathbf{F}^{-1} - \mathbf{F}^{-1} \cdot \mathrm{grad}\,\delta\mathbf{u} = \mathbf{F}^{-1} - \mathbf{F}^{-1} \cdot \mathrm{GRAD}\,\delta\mathbf{u} \cdot \mathbf{F}^{-1}. \tag{7.3b}$$

Derivations of (7.3a) and (7.3b) are given in Section A.8. Linearization of the Jacobian and the rate of the Jacobian at spatial configuration $\phi_t(\mathsf{B})$ are given, respectively, by

$$\mathrm{L}J = J + J\,\mathrm{div}(\delta\mathbf{u}); \tag{7.4a}$$

$$\mathrm{L}\dot{J} = \dot{J} + J\Big[\,\mathrm{div}(\delta\mathbf{v}) - \mathrm{grad}\,\mathbf{v} : \mathrm{grad}^{\,t}(\delta\mathbf{u}) + \mathrm{div}(\delta\mathbf{u})\,\mathrm{div}\,\mathbf{v}\,\Big]. \tag{7.4b}$$

See Section A.9 for derivation of (7.4a) and (7.4b).

Linearization of the reference saturated mass density $\rho_0 = J\rho$ at the spatial configuration $\phi_t(\mathsf{B})$ is

$$\mathrm{L}\rho_0 = \rho_0 + \rho_w J\,\mathrm{div}(\delta\mathbf{u}). \tag{7.5}$$

Proof of (7.5) is given in Section A.10. Note that ρ_0 is not constant since, as pointed out previously (see Section 3.5.2), the total mass of the soil-water mixture in B is not necessarily conserved in $\phi_t(\mathsf{B})$. The variation of ρ_0 reflects the amount of fluid that enters into or escapes from the soil matrix due to the variation of the Jacobian.

7.2 Linearization of Strong Form

The results discussed in the previous section can be applied for the lineraization of strong form or the field equations of linear momentum and mass conservation. Since the field equations are mixed formulation involving finite deformation $\mathbf{u}$ and Kirchhoff pore pressure θ, linearizations are derived consistent with the imposed infinitesimal variations $\delta\mathbf{u}$ and $\delta\theta$.

7.2.1 Equation of Equilibrium

Let $E = DIV\,\tilde{\mathbf{P}} + \rho_0\mathbf{g}$ be the linear momentum equation (see (4.3)). Substituting (3.55) and (3.56), E can be rewritten as

$$E = DIV\left(\tilde{\mathbf{P}} + \theta\mathbf{F}^{-t}\right) + J\rho\mathbf{g}. \tag{7.6}$$

Taking the variation yields

$$\begin{aligned}\delta E &= DIV\left(\delta\mathbf{P} + \theta\,\delta\mathbf{F}^{-t} + \delta\theta\,\mathbf{F}^{-t}\right) + \delta(J\rho)\mathbf{g} \\ &= DIV\left(\mathbf{A} : \delta\mathbf{F} + \theta\,\delta\mathbf{F}^{-t} + \delta\theta\,\mathbf{F}^{-t}\right) + \delta(J\rho)\mathbf{g}.\end{aligned} \tag{7.7}$$

A is the first tangential elasticity tensor of order four. **A** has the structure $A_{ijkl} = \partial P_{ij}/\partial F_{kl}$.

One can write from (7.5)

$$\delta(J\rho)\mathbf{g} = \rho_W J\,div(\delta\mathbf{u})\mathbf{g}. \tag{7.8}$$

Now, using (7.1) and (7.2) one can express

$$J\,div(\delta\mathbf{u}) = DIV(\delta\mathbf{U}) = DIV\left(J\mathbf{F}^{-1}\cdot\delta\mathbf{u}\right), \tag{7.9}$$

where $\delta\mathbf{U}$ is the Piola transform of $\delta\mathbf{u}$. Substituting (7.9) in (7.8) results

$$\delta(J\rho)\mathbf{g} = \rho_W J\,div(\delta\mathbf{u})\mathbf{g} = \rho_W DIV\left(J\mathbf{F}^{-1}\cdot\delta\mathbf{u}\right)\mathbf{g}. \tag{7.10}$$

Substituting $\delta\mathbf{F}$, $\delta\mathbf{F}^{-1}$ from (7.3), $\delta(J\rho)$ from (7.10) in the expression of δE of (7.6), linearization of E may be written as

$$\begin{aligned}LE = E &+ DIV(\mathbf{A} : GRAD\,\delta\mathbf{u}) - DIV\left(\theta\mathbf{F}^{-t}\cdot GRAD^{t}\delta\mathbf{u}\cdot\mathbf{F}^{-t}\right) \\ &+ DIV\left(\delta\theta\,\mathbf{F}^{-t}\right) + \rho_W DIV\left(J\mathbf{F}^{-1}\cdot\delta\mathbf{u}\right)\mathbf{g}.\end{aligned} \tag{7.11}$$

A crucial step in the linearization of the linear momentum balance equation is the evaluation of the tangential elasticity tensors of the solid matrix. Four of them are introduced in this section: the tensors **A**, **D**, **a** and **d**. Each of these tensors can be derived

directly from others. For example, **A** can be obtained from **D** using the following expression

$$\mathbf{A} = 2\mathbf{F}\cdot\mathbf{D}\cdot\mathbf{F}^{t} + \mathbf{S}\oplus\mathbf{1}; \quad A_{ijkl} = 2F_{im}F_{kn}D_{mjnl} + S_{jl}\delta_{ik}. \tag{7.12}$$

See Section A.11 for derivation of (7.12). $\mathbf{D} = \partial\mathbf{S}/\partial\mathbf{C}$ (i.e., $D_{mjnl} = \partial S_{mj}/\partial C_{nl}$) is the second tangential elasticity tensor of order four. Constitutive relation (4.36) and pull backs of the Kirchhoff effective stress tensor τ yield the following expressions of the second Piola-Kirchhoff effective stress tensor **S** as

$$\mathbf{S} = \mathbf{F}^{-1}\cdot\tau\cdot\mathbf{F}^{-t} = \sum_{A=1}^{3}\beta_A\mathbf{M}^{(A)}; \quad \mathbf{M}^{(A)} = \mathbf{F}^{-1}\cdot\mathbf{m}^{(A)}\cdot\mathbf{F}^{-t}. \tag{7.13}$$

β_A's are the principal Kirchhoff effective stresses and $\mathbf{m}^{(A)}$'s are the dyads formed by juxtaposing the principal directions of the elastic stretches, as given explicitly by $(4.35)_2$. Using the chain rule, from $(7.13)_1$ one can obtain the following expression for the tensor **D** as

$$\mathbf{D} = \frac{\partial\mathbf{S}}{\partial\mathbf{C}} = \frac{1}{2}\sum_{A=1}^{3}\sum_{B=1}^{3}\frac{\partial\beta_A}{\partial\varepsilon_B}\mathbf{M}^{(A)}\otimes\mathbf{M}^{(B)} + \sum_{A=1}^{3}\beta_A\frac{\partial\mathbf{M}^{(A)}}{\partial\mathbf{C}}, \tag{7.14}$$

since $\partial\varepsilon_B/\partial\mathbf{C} = \mathbf{M}^{(B)}/2$ (see Section A.14).

By the symmetry of both **S** and **C**, and by the axiom of material frame indifference, the tensor **D** possesses both the major and minor symmetries such as $D_{ijkl} = D_{jikl} = D_{ijlk}$, $D_{ijkl} = D_{klij}$. Spatial tangential elasticity tensors **a** and **d** may be obtained from the push-forwards of **A** and **D** as

$$a_{ijkl} = F_{ja}F_{lb}A_{iakb}; \tag{7.15a}$$

$$d_{ijkl} = 2F_{ia}F_{jb}F_{kc}F_{ld}D_{abcd}. \tag{7.15b}$$

a and **d** have the symmetries [83]: $a_{ijkl} = a_{klij}$, $d_{ijkl} = d_{jikl} = d_{ijlk} = d_{klij}$. A push-forward of all the indices of **D** gives the following expression for the spatial tensor **d**

$$\mathbf{d} = \sum_{A=1}^{3}\sum_{B=1}^{3} \frac{\partial \beta_A}{\partial \varepsilon_B} \mathbf{m}^{(A)} \otimes \mathbf{m}^{(B)} + 2\sum_{A=1}^{3} \beta_A \mathbf{d}^{(A)}. \tag{7.16}$$

Here $\mathbf{d}^{(A)}$ is the push forward of $\partial \mathbf{M}^{(A)}/\partial \mathbf{C}$ as

$$d^{(A)}_{ijkl} = F_{ia} F_{jb} F_{kc} F_{ld} \frac{\partial M^{(A)}_{ab}}{\partial C_{cd}}. \tag{7.17}$$

For the general case of left Cauchy-Green tensor **b** having distinct eigenvalues λ_1^2, λ_2^2 and λ_3^2, $\mathbf{d}^{(A)}$ takes the form

$$\begin{aligned} \mathbf{d}^{(A)} = & \frac{1}{D_A}\left[\mathbf{I}_b - \mathbf{b}\otimes\mathbf{b} + I_3\lambda_A^{-2}(\mathbf{1}\otimes\mathbf{1} - \mathbf{I})\right] \\ & + \frac{1}{D_A}\left[\lambda_A^2\left(\mathbf{b}\otimes\mathbf{m}^{(A)} + \mathbf{m}^{(A)}\otimes\mathbf{b}\right) - \frac{1}{2}D'_A\lambda_A\mathbf{m}^{(A)}\otimes\mathbf{m}^{(A)}\right] \\ & - \frac{1}{D_A}\left[I_3\lambda_A^{-2}\left(\mathbf{1}\otimes\mathbf{m}^{(A)} + \mathbf{m}^{(A)}\otimes\mathbf{1}\right)\right], \end{aligned} \tag{7.18}$$

where $(\mathbf{I}_b)_{ijkl} = \frac{1}{2}\left[b_{ik}b_{jl} + b_{il}b_{jk}\right]$, $I_3 = \det(\mathbf{C})$, $\mathbf{I}_{ijkl} = \frac{1}{2}\left[\delta_{ik}\delta_{jl} + \delta_{il}\delta_{jk}\right]$, $D_A = \left(\lambda_A^2 - \lambda_B^2\right)\left(\lambda_A^2 - \lambda_C^2\right)$, $D'_A = 8\lambda_A^3 - 2I_1\lambda_A - 2I_3\lambda_A^{-3}$. {A,B,C} denotes an even permutation of the indices {1,2,3}. This expression is strictly valid only if the eigenvalues are different since $D_A = 0$ otherwise. Although it is possible to derive a similar result for the case of repeated eigenvalues [19], from a computational standpoint it is preferable to reduce this situation to the general case of distinct eigenvalues by introducing a perturbation of the repeated roots. For example, in case of repeated roots, a

small perturbation of $\pm 10^{-6}\times$ repeated eigenvalues is used in PlasFEM to obtain a general case of distinct eigenvalues.

The spatial counterpart of (7.11) may be derived directly from Piola transformation. Then, the linearization of E in the spatial picture takes the form

$$\mathrm{LE} = \mathrm{E} + \mathrm{div}(\mathbf{a} : \mathrm{grad}\,\delta\mathbf{u}) - \mathrm{div}\left(\theta\,\mathrm{grad}^{t}\delta\mathbf{u}\right) + \mathrm{grad}(\delta\theta) + J\rho_{W}\mathrm{div}(\delta\mathbf{u})\mathbf{g}. \quad (7.19)$$

An equivalent form to (7.19), using the spatial tangential elasticity tensor **d**, is

$$\mathrm{LE} = \mathrm{E} + \mathrm{div}[(\mathbf{d} + \tau \oplus \mathbf{1}) : \mathrm{grad}\,\delta\mathbf{u}] - \mathrm{div}\left(\theta\,\mathrm{grad}^{t}\delta\mathbf{u}\right) + \mathrm{grad}(\delta\theta) + J\rho_{W}\mathrm{div}(\delta\mathbf{u})\mathbf{g}, \quad (7.20)$$

since $\mathbf{a} = \mathbf{d} + \tau \oplus \mathbf{1}$ (see Section A.12). Here $(\tau \oplus \mathbf{1})_{ijkl} = \tau_{jl}\delta_{ik}$ represents the initial stress contribution to the spatial stiffness. Comparing term by term, equivalence between (7.11) and (7.19) can be established. Exploiting the Piola identity of (7.2), one can show that DIV(**A**:GRAD $\delta\mathbf{u}$) = div(**a**:grad $\delta\mathbf{u}$) since **A**:GRAD $\delta\mathbf{u}$ is the Piola transform of J^{-1} **a**:grad $\delta\mathbf{u}$ and grad J = **0** (see Section A.1). Similarly, second divergence terms can be shown equivalent noticing that $\theta\,\mathbf{F}^{-1}\cdot \mathrm{GRAD}^{t}\,\delta\mathbf{u}\cdot\mathbf{F}^{-t} = \theta\,\mathrm{grad}^{t}\,\delta\mathbf{u}\cdot\mathbf{F}^{-t}$ is Piola transform of $J^{-1}(\theta\,\mathrm{grad}^{t}\,\delta\mathbf{u})$. Expansion of the third divergence term of (7.11) yields $\mathrm{DIV}(\delta\theta\,\mathbf{F}^{-t}) = \mathrm{GRAD}\,\delta\theta\cdot\mathbf{F}^{-t} + \delta\theta\,\mathrm{DIV}(\mathbf{F}^{-t}) = \mathrm{grad}\,\delta\theta$ since $\mathrm{DIV}(\mathbf{F}^{-t}) = \mathbf{0}$. Equivalence between the last terms can be derived from (7.9).

7.2.2 Equation of Flow Continuity

Let $M = \mathrm{DIV}\,\mathbf{V} + \mathrm{DIV}\,\tilde{\mathbf{V}}$ be the equation of flow continuity for a saturated soil-water mixture in material reference (see (4.9)), where **V** and $\tilde{\mathbf{V}}$ are the Piola transform of

$\mathbf{v}$ and $\tilde{\mathbf{v}}$, respectively (see Section 4.2). Then, the linearization of M at any configuration $\phi_t(B)$ is

$$\mathrm{LM} = \mathrm{M} + \mathrm{DIV}\,\delta\mathbf{V} + \mathrm{DIV}\,\delta\tilde{\mathbf{V}}. \tag{7.21}$$

One needs expressions of $\delta\mathbf{V}$, $\delta\tilde{\mathbf{V}}$ for linearization of M. First consider variation of $\mathbf{V}$,

$$\delta\mathbf{V} = \delta\left(J\mathbf{F}^{-1}\cdot\mathbf{v}\right) = \delta J\,\mathbf{F}^{-1}\cdot\mathbf{v} + J\,\delta\mathbf{F}^{-1}\cdot\mathbf{v} + J\,\mathbf{F}^{-1}\cdot\delta\mathbf{v}. \tag{7.22}$$

From (7.4a), (7.9) and (7.3b), one can express

$$\begin{aligned} &\delta J\,\mathbf{F}^{-1}\cdot\mathbf{v} = \mathrm{DIV}\left(J\,\mathbf{F}^{-1}\cdot\delta\mathbf{u}\right)\mathbf{F}^{-1}\cdot\mathbf{v};\\ &J\,\delta\mathbf{F}^{-1}\cdot\mathbf{v} = -J\left\{\mathbf{F}^{-1}\cdot\mathrm{grad}\,\delta\mathbf{u}\right\}\cdot\mathbf{v} = -J\,\mathbf{F}^{-1}\cdot\mathrm{GRAD}\,\delta\mathbf{u}\cdot\mathbf{F}^{-1}\cdot\mathbf{v}. \end{aligned} \tag{7.23}$$

Substituting (7.23), one can rewrite (7.22) as

$$\delta\mathbf{V} = \delta\left(J\mathbf{F}^{-1}\cdot\mathbf{v}\right) = \mathrm{DIV}\left(J\mathbf{F}^{-1}\cdot\delta\mathbf{u}\right)\mathbf{F}^{-1}\cdot\mathbf{v} - J\,\mathbf{F}^{-1}\cdot\mathrm{GRAD}\,\delta\mathbf{u}\cdot\mathbf{F}^{-1} + J\,\mathbf{F}^{-1}\cdot\delta\mathbf{v}. \tag{7.24}$$

From (4.50) and (4.52), generalized Darcy's law can be written as

$$\tilde{\mathbf{v}} = -\mathbf{k}\cdot\left(\frac{\mathrm{grad}\,\theta}{J g\rho_W} + \frac{\mathbf{g}}{g}\right). \tag{7.25}$$

Piola transform of $\tilde{\mathbf{v}}$ yields

$$\tilde{\mathbf{V}} = J\mathbf{F}^{-1}\cdot\tilde{\mathbf{v}} = -\mathbf{K}\cdot\left(\frac{\mathrm{GRAD}\,\theta}{g\rho_W} + J\mathbf{F}^{t}\cdot\frac{\mathbf{g}}{g}\right), \tag{7.26}$$

where $\mathbf{K} = \mathbf{F}^{-1}\cdot\mathbf{k}\cdot\mathbf{F}^{-t}$ is the pull-back permeability tensor. $\mathbf{K}$ and $\mathbf{k}$ are assumed symmetric in following derivations. Using chain rule, one can expand $\delta\tilde{\mathbf{V}}$ as

$$\delta\tilde{\mathbf{V}} = -\delta\mathbf{K}\cdot\left(\frac{\mathrm{GRAD}\,\theta}{g\rho_W} + J\mathbf{F}^{t}\cdot\frac{\mathbf{g}}{g}\right) - \mathbf{K}\cdot\left(\frac{\mathrm{GRAD}\,\delta\theta}{g\rho_W} + \delta\left(J\mathbf{F}^{t}\right)\cdot\frac{\mathbf{g}}{g}\right). \tag{7.27}$$

Substituting δJ from $(7.23)_1$ and $\delta\mathbf{F}$ from (7.3a), one can write

$$\delta\left(\mathbf{J}\mathbf{F}^{t}\right)=\mathrm{DIV}\left(\mathbf{J}\mathbf{F}^{-1}\cdot\delta\mathbf{u}\right)\mathbf{F}^{t}+\mathbf{J}\,\mathrm{GRAD}^{t}\delta\mathbf{u}. \tag{7.28}$$

Substituting (7.28) and rearranging, (7.27) can be rewritten as

$$\begin{aligned}\delta\tilde{\mathbf{V}} = -\mathbf{K}\cdot\left\{\frac{\mathrm{GRAD}\,\delta\theta}{g\rho_{w}}+\left[\mathrm{DIV}\left(\mathbf{J}\mathbf{F}^{-1}\cdot\delta\mathbf{u}\right)\mathbf{F}^{t}+\mathbf{J}\,\mathrm{GRAD}^{t}\delta\mathbf{u}\right]\cdot\frac{\mathbf{g}}{g}\right\}\\ -\delta\mathbf{K}\cdot\left(\frac{\mathrm{GRAD}\,\theta}{g\rho_{w}}+\mathbf{J}\mathbf{F}^{t}\cdot\frac{\mathbf{g}}{g}\right),\end{aligned} \tag{7.29}$$

where

$$\delta\mathbf{K}=-\mathbf{F}^{-1}\cdot\left\{2\,\mathrm{Sym}\left(\mathrm{GRAD}\,\delta\mathbf{u}\cdot\mathbf{K}\cdot\mathbf{F}^{t}\right)-(1+e_{0})\,\mathrm{DIV}\left(\mathbf{J}\mathbf{F}^{-1}\cdot\delta\mathbf{u}\right)\frac{\partial\mathbf{k}}{\partial e}\right\}\cdot\mathbf{F}^{-t}. \tag{7.30}$$

If permeability tensor **k** is assumed to be varying with the deformation or void ratio of soil skeleton variation of **k** can be expressed as

$$\delta\mathbf{k}=(1+e_{0})\,J\,\mathrm{div}(\delta\mathbf{u})\frac{\partial\mathbf{k}}{\partial e}=(1+e_{0})\,\mathrm{DIV}\left(\mathbf{J}\mathbf{F}^{-1}\cdot\delta\mathbf{u}\right)\frac{\partial\mathbf{k}}{\partial e}, \tag{7.31}$$

where e_0 is void ratio of the soil-water mixture in reference configuration. See Section A.17 for derivations of (7.30) and (7.31).

Using (4.8) and (4.17), M can be written in spatial description as

$$\mathrm{M}=\mathrm{J}\,\mathrm{div}\,\mathbf{v}+\mathrm{J}\,\mathrm{div}\,\tilde{\mathbf{v}}=\dot{\mathrm{J}}+\mathrm{J}\,\mathrm{div}\,\tilde{\mathbf{v}}. \tag{7.32}$$

Corresponding lineraization takes the form

$$\begin{aligned}\mathrm{LM}&=\mathrm{M}+\delta\left(\dot{\mathrm{J}}+\mathrm{J}\,\mathrm{div}\,\tilde{\mathbf{v}}\right)\\ &=\mathrm{M}+\delta\dot{\mathrm{J}}+\delta\mathrm{J}\,\mathrm{div}\,\tilde{\mathbf{v}}+\mathrm{J}\,\delta\left(\mathrm{div}\,\tilde{\mathbf{v}}\right).\end{aligned} \tag{7.33}$$

Substituting (A.31), $\mathrm{J}\,\delta\left(\mathrm{div}\,\tilde{\mathbf{v}}\right)$ can be expressed as

$$\mathrm{J}\,\delta(\mathrm{div}\tilde{\mathbf{v}})=\mathrm{J}\,\mathrm{div}(\delta\tilde{\mathbf{v}})-\mathrm{grad}(\mathrm{J}\tilde{\mathbf{v}}):\mathrm{grad}^{t}\delta\mathbf{u}, \tag{7.34}$$

since $J \operatorname{grad} \tilde{\mathbf{v}} = \operatorname{grad}(J\tilde{\mathbf{v}})$ by knowing that grad J = **0**. Substituting (7.34) in (7.33) then yields

$$\mathrm{LM} = \mathrm{M} + \delta\dot{\mathrm{J}} + \operatorname{div}[\delta(J\tilde{\mathbf{v}})] - \operatorname{grad}(J\tilde{\mathbf{v}}) : \operatorname{grad}^{\mathrm{t}} \delta\mathbf{u}, \tag{7.35}$$

since

$$\begin{aligned} \operatorname{div}[\delta(J\tilde{\mathbf{v}})] &= \operatorname{div}(\delta J\,\tilde{\mathbf{v}}) + \operatorname{div}(J\,\delta\tilde{\mathbf{v}}) \\ &= \operatorname{grad}\delta J \cdot \tilde{\mathbf{v}} + \delta J \operatorname{div}\tilde{\mathbf{v}} + \operatorname{grad} J \cdot \delta\tilde{\mathbf{v}} + J \operatorname{div}(\delta\tilde{\mathbf{v}}) \\ &= \left(\mathrm{GRAD}\,\delta J \cdot \mathbf{F}^{-1}\right) \cdot \tilde{\mathbf{v}} + \delta J \operatorname{div}\tilde{\mathbf{v}} + J \operatorname{div}(\delta\tilde{\mathbf{v}}) \\ &= \delta(\mathrm{GRAD}\,J) \cdot \mathbf{F}^{-1} \cdot \tilde{\mathbf{v}} + \delta J \operatorname{div}\tilde{\mathbf{v}} + J \operatorname{div}(\delta\tilde{\mathbf{v}}) \\ &= \delta J \operatorname{div}\tilde{\mathbf{v}} + J \operatorname{div}(\delta\tilde{\mathbf{v}}). \end{aligned} \tag{7.36}$$

Component terms of (7.35) are given as

$$\delta\dot{J} = J\left[\operatorname{div}(\delta\mathbf{v}) - \operatorname{grad}\mathbf{v} : \operatorname{grad}^{\mathrm{t}}(\delta\mathbf{u}) + \operatorname{div}(\delta\mathbf{u}) \operatorname{div}\mathbf{v}\right]; \tag{7.37a}$$

$$J\tilde{\mathbf{v}} = -\mathbf{k} \cdot \left(\frac{\operatorname{grad}\theta}{g\rho_w} + J\frac{\mathbf{g}}{g}\right); \tag{7.37b}$$

$$\begin{aligned} \delta(J\tilde{\mathbf{v}}) = -\mathbf{k} \cdot &\left[\frac{\operatorname{grad}(\delta\theta) - \operatorname{grad}\theta \cdot \operatorname{grad}\delta\mathbf{u}}{g\rho_w} + J \operatorname{div}(\delta\mathbf{u})\frac{\mathbf{g}}{g}\right] \\ &- (1 + e_0) J \operatorname{div}(\delta\mathbf{u}) \frac{\partial\mathbf{k}}{\partial e} \cdot \left[\frac{\operatorname{grad}\theta}{\rho_w g} + J\frac{\mathbf{g}}{g}\right]. \end{aligned} \tag{7.37c}$$

(7.37a) and (7.37b) are obtained directly from (7.4b) and (7.25), respectively. Derivation of (7.37c) is given in Section A.19.

7.3 Linearization of Weak Form

Linearization of weak form $G(\phi, \Pi, \eta)$ of (4.13) takes the form

$$LG = G + \int_B \operatorname{grad}\eta : (\mathbf{d} + \tau \oplus \mathbf{1}) : \operatorname{grad}\delta\mathbf{u}\, dV + \int_B \left(\delta\theta \operatorname{div}\eta - \theta \operatorname{grad}^t\eta : \operatorname{grad}\delta\mathbf{u}\right) dV$$
$$- \int_B \rho_W J \operatorname{div}(\delta\mathbf{u})\eta : \mathbf{g}\, dV - \int_{\partial B} \eta \cdot \delta t\, dA. \tag{7.38}$$

where $\delta\mathbf{u}$, $\delta\theta$ and δt are the variations of the displacement vector, Kirchhoff pore pressure, and traction vector, respectively.

First integral term of (7.38) is derived from the variation of grad η: τ (see Section A.20). The variation $\delta(\theta \operatorname{div}\eta) = \delta\theta \operatorname{div}\eta + \theta\delta(\operatorname{div}\eta)$ produces the second integral term upon substitution of the identity $\delta(\operatorname{div}\eta) = \operatorname{div}\delta\eta - \operatorname{grad}^t\eta : \operatorname{grad}\delta\mathbf{u} = -\operatorname{grad}^t\eta : \operatorname{grad}\delta\mathbf{u}$ following (A.31) (note that $\delta\eta = \mathbf{0}$ since η is a vector of arbitrary virtual displacements). The third integral term emanates from the linearization of ρ_0 (see (7.5)). The last integral term is derived from a straight-forward linearization of the traction vector $\mathbf{t}$.

Upon substitution of (3.55) and (3.56), linearization of weak form $G(\phi, \Pi, \eta)$ in material description (see (4.12)) can be expressed as

$$\begin{aligned} LG &= G + \int_B \delta\left(\operatorname{GRAD}\eta : \tilde{\mathbf{P}} - \rho_0\eta \cdot \mathbf{g}\right)dV - \int_{\partial B} \delta(\eta \cdot \mathbf{t})dA \\ &= G + \int_B \delta(\operatorname{GRAD}\eta : \mathbf{P})dV + \int_B \delta\left(\operatorname{GRAD}\eta : \left(\theta\mathbf{F}^{-t}\right)\right)dV \\ &\quad - \int_B \delta(\rho_0\eta \cdot \mathbf{g})dV - \int_{\partial B} \delta(\eta \cdot \mathbf{t})dA. \end{aligned} \tag{7.39}$$

Variation of the first integrand is given as $\delta(\operatorname{GRAD}\eta : \mathbf{P}) = \operatorname{GRAD}\eta : \mathbf{A} : \operatorname{GRAD}\delta\mathbf{u}$ (see Section A.21).Variation of the second integrand in material description may take the form

$$\delta\left(\mathrm{GRAD}\,\eta : \left(\theta \mathbf{F}^{-t}\right)\right) = \delta\theta\ \mathrm{GRAD}\,\eta : \mathbf{F}^{-t} - \theta\ \mathrm{GRAD}\,\eta : \left(\mathbf{F}^{-t} \cdot \mathrm{GRAD}^{t}\delta\mathbf{u} \cdot \mathbf{F}^{-t}\right).$$

Upon substitution of (7.10), variation of the third integrand yields

$$\delta(\rho_0 \eta \cdot \mathbf{g}) = \rho_W \mathrm{DIV}\left(\mathrm{JF}^{-1} \cdot \delta\mathbf{u}\right)\eta : \mathbf{g}.$$

Substituting all these identities in (7.39), one can obtain linearization of G in material description as

$$\begin{aligned} \mathrm{LG} = \mathrm{G} &+ \int_B \mathrm{GRAD}\,\eta : \mathbf{A} : \mathrm{GRAD}\,\delta\mathbf{u}\ \mathrm{dV} + \int_B \delta\theta\,\mathrm{GRAD}\,\eta : \mathbf{F}^{-t}\ \mathrm{dV} \\ &- \int_B \theta\,\mathrm{GRAD}\,\eta : \left(\mathbf{F}^{-t} \cdot \mathrm{GRAD}^{t}\delta\mathbf{u} \cdot \mathbf{F}^{-t}\right)\mathrm{dV} \\ &- \int_B \rho_W \mathrm{DIV}\left(\mathrm{JF}^{-1} \cdot \delta\mathbf{u}\right)\eta : \mathbf{g}\,\mathrm{dV} - \int_{\partial B} \eta \cdot \delta\mathbf{t}\ \mathrm{dA}. \end{aligned} \tag{7.40}$$

(7.39) and (7.40) are equivalent expressions.

Linearization of weak form $\mathrm{H}_{\Delta t}(\phi, \Pi, \psi)$ of (4.25) is given as

$$\begin{aligned} \mathrm{LH}_{\Delta t} = \mathrm{H}_{\Delta t} &+ \int_B \frac{\psi}{\Delta t} \mathrm{J}\,\mathrm{div}(\delta\mathbf{u})\mathrm{dV} + \beta\beta_0 \int_B \mathrm{grad}\,\psi \cdot \frac{\mathbf{k}}{g\rho_W} \cdot \mathrm{grad}\,\delta\theta\ \mathrm{dV} \\ &- 2\beta\beta_0 \int_B \mathrm{grad}\,\psi \cdot \mathrm{Sym}\left(\frac{\mathbf{k}}{g\rho_W} \cdot \mathrm{grad}^{t}\delta\mathbf{u}\right) \cdot \mathrm{grad}\,\theta\ \mathrm{dV} \\ &- \beta\beta_0 \int_B \mathrm{grad}\,\psi \cdot [\mathrm{grad}\,\delta\mathbf{u} - (\mathrm{div}\ \delta\mathbf{u})\mathbf{1}] \cdot \mathbf{k} \cdot \frac{\mathbf{g}}{g} \mathrm{J}\ \mathrm{dV} \\ &+ \beta\beta_0 (1 + e_0) \int_B \mathrm{grad}\,\psi \cdot (\mathrm{div}\ \delta\mathbf{u})\mathbf{1} \cdot \frac{\partial \mathbf{k}}{\partial e} \cdot \left\{\frac{\mathrm{grad}\,\theta}{\rho_W g} + \mathrm{J}\frac{\mathbf{g}}{g}\right\} \mathrm{J}\,\mathrm{dV} \\ &- \beta\beta_0 \int_{\partial B} \psi\delta\mathrm{Q}\ \mathrm{dA}. \end{aligned} \tag{7.41}$$

The first integral term of (7.41) results from the variation of J (see (7.4a)). The second, third, fourth and fifth integral terms result from the variation of $\mathrm{grad}\,\psi \cdot \mathrm{J}\tilde{\mathbf{v}}$ (see Section A.22). The last term results from the variation of Q.

Linearization of weak form $\mathrm{H}_{\Delta t}(\phi, \Pi, \psi)$ of material description (see (4.26)) is given as

$$
\begin{aligned}
{}^{L}H_{\Delta t} = {} & H_{\Delta t} + \int_B \frac{\psi}{\Delta t} \mathrm{DIV}\left(\mathbf{J}\mathbf{F}^{-1}\cdot\delta\mathbf{u}\right)\mathrm{dV} + \beta\beta_0 \int_B \mathrm{GRAD}\,\psi \cdot \frac{\mathbf{K}}{g\rho_w}\cdot \mathrm{GRAD}\,\delta\theta\,\mathrm{dV} \\
& - 2\beta\beta_0 \int_B \mathrm{GRAD}\,\psi\cdot\mathbf{F}^{-1}\cdot\mathrm{Sym}\left(\mathrm{GRAD}\,\delta\mathbf{u}\cdot\frac{\mathbf{K}}{g\rho_w}\cdot\mathbf{F}^{t}\right)\cdot\mathbf{F}^{-t}\cdot\mathrm{GRAD}\,\theta\,\mathrm{dV} \\
& - \beta\beta_0 \int_B \mathrm{GRAD}\,\psi\cdot\mathbf{F}^{-1}\cdot\mathrm{GRAD}\,\delta\mathbf{u}\cdot\mathbf{K}\cdot\mathbf{F}^{t}\cdot J\frac{\underline{\mathbf{g}}}{g}\,\mathrm{dV} \\
& + \beta\beta_0 \int_B \mathrm{GRAD}\,\psi\cdot\mathbf{K}\cdot\mathrm{DIV}\left(\mathbf{J}\mathbf{F}^{-1}\cdot\delta\mathbf{u}\right)\mathbf{F}^{t}\cdot\frac{\underline{\mathbf{g}}}{g}\,\mathrm{dV} \\
& + \beta\beta_0(1+e_0)\int_B \mathrm{GRAD}\,\psi\cdot\mathbf{F}^{-1}\cdot\mathrm{DIV}\left(\mathbf{J}\mathbf{F}^{-1}\cdot\delta\mathbf{u}\right)\frac{\partial\mathbf{k}}{\partial e}\cdot\mathbf{F}^{-t}\cdot\left\{\frac{\mathrm{GRAD}\,\theta}{\rho_w g} + J\mathbf{F}^{t}\cdot\frac{\underline{\mathbf{g}}}{g}\right\}\mathrm{dV} \\
& - \beta\beta_0 \int_{\partial B} \psi\delta Q\,\mathrm{dA}.
\end{aligned}
\tag{7.42}
$$

The first integral term of (7.42) results from the variation of J (see (7.4a) and (7.9)). The second, third, fourth and fifth integral terms result from the variation of $\mathrm{GRAD}\,\psi\cdot\tilde{\mathbf{V}}$ (see Section A.23). The last term results from the variation of Q.

Considering term by term, one can show that (7.41) and (7.42) are equivalent expressions. Equivalence between first integral terms can be obtained from (7.9). Equivalence between second integral terms can be drawn from the relations: $\mathrm{grad}\,\psi = \mathrm{GRAD}\,\psi\cdot\mathbf{F}^{-1}$, $\mathrm{grad}\,\delta\theta = \mathrm{GRAD}\,\delta\theta\cdot\mathbf{F}^{-1}$, and $\mathbf{K} = \mathbf{F}^{-1}\cdot\mathbf{k}\cdot\mathbf{F}^{-t}$. Similarly, the third integral terms can be proved equivalent since

$$
\mathrm{Sym}\left(\mathrm{GRAD}\,\delta\mathbf{u}\cdot\frac{\mathbf{K}}{g\rho_w}\cdot\mathbf{F}^{t}\right) = \mathrm{Sym}\left(\mathrm{grad}\,\delta\mathbf{u}\cdot\frac{\mathbf{k}}{g\rho_w}\right) = \mathrm{Sym}\left(\frac{\mathbf{k}}{g\rho_w}\cdot\mathrm{grad}^{t}\,\delta\mathbf{u}\right).
$$

By contracting and rearranging the remaining volume integral terms of (7.42) into equivalent spatial descriptions, one can obtain identical expressions for the fourth and fifth integral terms of (7.41).

CHAPTER 8
FINITE ELEMENT FORMULATION

8.1 Finite Element Framework

System of equations for consolidation problem can take a general form

$$\mathbf{K}_{n+1}^{k}\,\delta\mathbf{d}_{n+1}^{k} = \mathbf{f}_{n+1}^{k} \tag{8.1}$$

at any iteration k of time step t_{n+1}. **K** is the global stiffness matrix or consistent tangent operator, $\delta\mathbf{d}$ is the vector of incremental generalized displacement defined as

$$\delta\mathbf{d}_{n+1}^{k+1} = \mathbf{d}_{n+1}^{k+1} - \mathbf{d}_{n+1}^{k}. \tag{8.2}$$

For large strain consolidation, **d** consists of solid-phase displacement vector **u** and Kirchhoff pore pressure vector θ. **f** is the vector of residual out-of-balance forces defined as

$$\mathbf{f}_{n+1}^{k} = (\mathbf{F}_{EXT})_{n+1} - (\mathbf{F}_{INT})_{n+1}^{k} \tag{8.3}$$

$\mathbf{F}_{EXT}$ is the vector of externally applied forces, e.g., gravity forces, prescribed surface tractions, fluid potential, flow rate etc. It is assumed that $\mathbf{F}_{EXT}$ is constant for a given time step t_{n+1}. $\mathbf{F}_{INT}$ is the vector of internal nodal forces. **f** is formed from the coupled equations of weak form $G(\phi, \Pi, \eta)$ and $H(\phi, \Pi, \psi)$ (see Chapter 4), integrated over the problem domain.

Finite element formulation solves the system of equations ieteratively using some standard methods (e.g., Newton-Raphson method) so that **f**, at some configuration, is

minimized within a tolerance (e.g., 1.0×10^{-4}). $\mathbf{F}_{INT}$ is function of the generalized displacement vector **d**, and can be approximated by Taylor series expansion

$$(\mathbf{F}_{INT})_{n+1} = \mathbf{F}_{INT}\left(\mathbf{d}_{n+1}^{k+1}\right) = \mathbf{F}_{INT}\left(\mathbf{d}_{n+1}^{k}\right) + \left(\frac{\partial \mathbf{F}_{INT}}{\partial \mathbf{d}}\right)_{n+1}^{k}\left(\mathbf{d}_{n+1}^{k+1} - \mathbf{d}_{n+1}^{k}\right) + O(h). \qquad (8.4)$$

Neglecting the higher order terms $O(h)$, the exact solution is approximated by

$$\mathbf{d}_{n+1} \approx \mathbf{d}_{n+1}^{k+1} = \mathbf{d}_{n+1}^{k} + \left(\frac{\partial \mathbf{F}_{INT}}{\partial \mathbf{d}}\right)^{-1}\left[(\mathbf{F}_{EXT})_{n+1} - \mathbf{F}_{INT}\left(\mathbf{d}_{n+1}^{k}\right)\right]. \qquad (8.5)$$

The Jacobian matrix $\partial\mathbf{F}_{INT}/\partial\mathbf{d}$ is equal to the tangent operator **K** of (8.1). It is evaluated at each iteration due to material and geometric nonlinearities so that

$$\left(\frac{\partial \mathbf{F}_{INT}}{\partial \mathbf{d}}\right)_{n+1}^{k} = \mathbf{K}_{n+1}^{k}. \qquad (8.6)$$

Substituting (8.6), (8.4) and (8.5) can be reduced to (8.1)

At the end of each iteration, displacement vector **d**, i.e., the configuration is updated according to (8.5). If equilibrium is achieved within a prescribed tolerance, the solution is started for next time step. Otherwise, a new iteration is performed.

8.2 Matrix Equations

This section discusses derivation of matrix forms of the weak form equations and their variations (see Sections 4.3 and 7.3), amenable for finite element formulation, for D9P4 axisymmetric element (see Section 9.1). Because of the simplicity of the linearization of the integrands in spatial description, (7.38) and (7.41) are implemented in finite element code.

According to the standard procedure, one needs interpolation function or shape function matrices for approximating the solid phase motion ϕ and pore pressure field θ. Let $\mathbf{N}^{\phi}(\mathbf{x})$ and $\mathbf{N}^{\theta}(\mathbf{x})$ be two distinct matrices of spatial interpolation functions representing ϕ and θ, respectively. Let $\mathbf{u}^h(\mathbf{x}) \in R^{nsd}$ represents spatial displacement field describing ϕ, nsd being the number of spatial dimensions. In matrix form

$$\mathbf{u}^h(\mathbf{x}) = \mathbf{N}^{\phi}(\mathbf{x})\{\mathbf{u} + \mathbf{u}_g\}, \tag{8.7}$$

where $\mathbf{u}$, $\mathbf{u}_g \in R^{nq}$ are the vectors of unknown and prescribed nodal displacements, respectively, nq is the number of displacement components for an element (= number of displacement degrees of freedom per node × number of nodes).

Similarly,

$$\theta^h(\mathbf{x}) = \mathbf{N}^{\theta}(\mathbf{x})\{\theta + \theta_r\}, \tag{8.8}$$

where $\theta^h \in R^1$ represents spatial Kirchhoff pore pressure field θ. θ, $\theta_r \in R^{np}$ are the vectors of unknown and prescribed nodal Kirchhoff pore pressures, respectively. Now, arbitrary weighting functions $\eta$and ψ may be interpolated in a similar fashion in terms of their nodal values $\tilde{\eta}$ and $\tilde{\psi}$ as follows:

$$\eta^h(\mathbf{x}) = \mathbf{N}^{\phi}(\mathbf{x})\tilde{\eta}; \quad \psi^h(\mathbf{x}) = \mathbf{N}^{\theta}(\mathbf{x})\tilde{\psi}, \tag{8.9}$$

where $\tilde{\eta} \in R^{nq}$ and $\tilde{\psi} \in R^{np}$. For D9P4 elements nsd = 2, nd = 9, np = 4, nq =18. $\mathbf{N}^{\phi}$ and $\mathbf{N}^{\theta}$ matrices for D9P4 element are given in Appendix B.

Employing these preliminaries of (8.7) to (8.9), one can formulate the necessary finite element equations. Let the weighting function η be approximated by arbitrary nodal

values $\tilde{\eta} \in R^{nq}$ via (8.9), then the finite element equation for weak form of the balance of linear momentum, $G(\phi, \Pi, \eta)$ (see (4.13)) may be written as

$$G^h(\phi, \Pi, \tilde{\eta}) = \tilde{\eta}^t \left[\mathbf{N}^S(\mathbf{u}) + \mathbf{N}^W(\theta) - \mathbf{F}_{EXT} \right. \tag{8.10}$$

where

$$\mathbf{N}^S(\mathbf{u}) = \int_B \mathbf{B}^t \{\tau\} \, dV \tag{8.11a}$$

$$\mathbf{N}^W(\theta) = \int_B \mathbf{b}^t \mathbf{N}^\theta \{\theta + \theta_r\} \, dV = \int_B \mathbf{b}^t \theta^h \, dV \tag{8.11b}$$

$$\mathbf{F}_{EXT} = \int_B \rho_0 \mathbf{N}^{\phi t} \mathbf{g} \, dV + \int_{\partial B} \mathbf{N}^{\phi t} \mathbf{t} \, dA \tag{8.11c}$$

For axisymmetric element, Kirchhoff stress vector $\{\tau\}$ is defined as $\{\tau_{11}, \tau_{22}, \tau_{33}, \tau_{12}, \tau_{21}\}^t$; subscripts 1,2,3 denote radial, axial and circumferential directions, respectively. $\mathbf{B}$ is the spatial strain-displacement transformation matrix, $\mathbf{b} = \{1\}^t \mathbf{B}$. See Appendix B for the structures of $\mathbf{B}$ and $\mathbf{b}$. By expanding terms, one can have $\tilde{\eta}^t \mathbf{B}^t \{\tau\} = \text{grad}\,\eta : \tau$. Thus, (8.11a) produces the first integral term of (4.13). (8.11b) represents the second integral term of (4.13) following the identity $\mathbf{b}\tilde{\eta} = \tilde{\eta}^t \mathbf{b}^t = \text{div}\,\eta$. Third and fourth integral terms of (4.13) can be obtained from (8.11c) using the identity $\eta = \tilde{\eta}^t \mathbf{N}^{\phi t}$. It is important to note that ρ_0 is reference mass density. So, it is a non-constant term. Following (7.5), ρ_0 is updated at each iteration as $(\rho_0)^{i+1}_{n+1} = (\rho_0)^{i}_{n+1} + \left\{ J \, \text{div}\left(\delta \mathbf{u}^h \right) \right\}^{i}_{n+1}$; in equivalent matrix form $(\rho_0)^{i+1}_{n+1} = (\rho_0)^{i}_{n+1} + \{ J \mathbf{b} \delta \mathbf{u} \}^{i}_{n+1}$.

Next, finite element equation of weak form for the balance of mass, $H_{\Delta t}(\phi, \Pi, \psi)$ (see (4.25)) may be written as

$$\Delta t\, H^{h}_{\Delta t}(\phi,\Pi,\tilde{\psi}) = \tilde{\psi}[\mathbf{J}(\mathbf{u}) - \beta_0 \Delta t\, \Phi(\theta) - \beta_0 \Delta t\, \mathbf{H}_{EXT}] = 0, \tag{8.12}$$

where

$$\mathbf{J}(\mathbf{u}) = \int_B \mathbf{N}^{\theta t}\left(J_{n+1} - \sum_{m=1}^{k} \alpha_m J_{n+1-m} \right) dV \tag{8.13a}$$

$$\Phi(\theta) = \beta \int_B \mathbf{E}^{t} (J\tilde{v})_{n+1}\, dV + (1-\beta) \int_B \mathbf{E}_n^{t} (J\tilde{v})_n\, dV \tag{8.13b}$$

$$\mathbf{H}_{EXT} = \int_B \mathbf{N}^{\theta t} [\beta Q_{n+1} + (1-\beta) Q_n]\, dA \tag{8.13c}$$

From $(8.9)_2$, one can have $\mathbf{N}^{\theta}\tilde{\psi} = \tilde{\psi}^{t}\mathbf{N}^{\theta t} = \psi^{h}$, and so (8.13a) and (8.13c) produce the first and third integral term in (7.42), respectively. $\mathbf{E}$, $\mathbf{E}_n$ in (8.13b) are the gradient-pressure transformation matrices (see (B.8)) computed with respect to coordinates $\mathbf{x}$ and $\mathbf{x}_n$, respectively. Since, $\psi^{t}\mathbf{E}^{t} = \text{grad}\,\psi$ and $\psi^{t}\mathbf{E}_n^{t} = (\text{grad}\,\psi)_n$, one can obtain second integral in (7.42) from (8.13b). $J\tilde{v}$ is computed from (7.36b) using the relation grad $\theta = \mathbf{E}\theta$.

Finite element equation for the first variation of the weak form $G(\phi, \Pi, \eta)$ (see (7.38)) may be written as

$$\delta G^{h}(\phi,\Pi,\tilde{\eta}) = \tilde{\eta}^{t}\left[\mathbf{K}_{\phi\phi}\, \delta\mathbf{u} + \mathbf{K}_{\phi\theta}\, \delta\theta\right] \tag{8.14}$$

where

$$\mathbf{K}_{\phi\phi} = \int_B \left(\mathbf{B}^{t}(\tilde{\mathbf{D}} + \mathbf{T} + \mathbf{I}_{\theta})\mathbf{B} - \rho_w J \mathbf{N}^{\phi t}\mathbf{g}\mathbf{b} \right) dV \tag{8.15a}$$

$$\mathbf{K}_{\phi\theta} = -\int_B \mathbf{b}^{t}\mathbf{N}^{\theta} dV \tag{8.15b}$$

$\delta\mathbf{u}$ and $\delta\theta$ are the first variations of $\mathbf{u}$ and θ, respectively.

$\tilde{\mathbf{D}}$ is a rank-two material stiffness matrix. Terms of rank-four tensor **d** in (7.38) is arranged in $\tilde{\mathbf{D}}$ (see (B.9)) in such a way that scalar product term $\tilde{\eta}^t\mathbf{B}^t\tilde{\mathbf{D}}\mathbf{B}\,\delta\mathbf{u}$ yields an equivalent expressions for grad η^h :**d**: grad $\delta\mathbf{u}^h$. Initial stress matrix **T** (see (B.10)) is assembled from fourth-order tensor $(\tau \oplus \mathbf{1})_{ijkl} = \tau_{jl}\,\delta_{ik}$ such that $\tilde{\eta}^t\mathbf{B}^t\tilde{\mathbf{D}}\mathbf{B}\,\delta\mathbf{u}$ = grad η^h :**c**: grad $\delta\mathbf{u}^h$. Similarly, $\tilde{\eta}^t\mathbf{B}^t\mathbf{I}_\theta\mathbf{B}\,\delta\mathbf{u}$ produces an equivalent expression for the scalar product term θ^h grad^t η^h : grad $\delta\mathbf{u}^h$. $\mathbf{I}_\theta$ is defined in (B.11). The remaining terms in (7.38) can be proved using the identities **b** $\delta\mathbf{u}$ = div $(\delta\mathbf{u}^h)$ and $\mathbf{b}\tilde{\eta}$ = div$\left(\eta^h\right)$.

Finite element equation for the first variation of weak form $\mathbf{H}^h_{\Delta t}(\phi,\Pi,\psi)$ (see (7.41)) may be written as

$$-\Delta t\,\delta H^h_{\Delta t}(\phi,\Pi,\tilde{\psi}) = \tilde{\psi}^t\left[\mathbf{K}_{\theta\phi}\delta\mathbf{u} + \mathbf{K}_{\theta\theta}\,\delta\theta\right] \tag{8.16}$$

where

$$\mathbf{K}_{\theta\phi} = -\int_B J\mathbf{N}^{\theta t}\mathbf{b}\,dV + \beta\beta_0\Delta t\int_B\left(\frac{1}{\rho_w g}\mathbf{E}^t\Xi\mathbf{B} + J\mathbf{E}^t\Theta_1\mathbf{B} - J(1+e_0)\mathbf{E}^t\Theta_2\mathbf{B}\right)dV \tag{8.17a}$$

$$\mathbf{K}_{\theta\theta} = -\frac{\beta\beta_0\Delta t}{\rho_w g}\int_B\mathbf{E}^t\mathbf{k}\mathbf{E}\,dV \tag{8.17b}$$

Matrix forms for the first two integrals in (7.41) are trivial. With respect to the third integral in (7.41), which arises from geometric nonlinearity, the following identity can be obtained by direct expansion:

$$2\,\mathrm{grad}\,\psi^h\cdot\mathrm{Sym}\left[\mathbf{k}\cdot\mathrm{grad}^t\left(\delta\mathbf{u}^h\right)\right]\cdot\mathrm{grad}\,\theta = \tilde{\psi}^t\,\mathbf{E}^t\Xi\mathbf{B}\,\delta\mathbf{u}, \tag{8.18}$$

where

$$\Xi = \Xi_1 + \Xi_2\,. \tag{8.19}$$

For D9P4 axisymmetric element

$$\Xi_1 = \begin{bmatrix} k_{11}\theta_{,1} & k_{12}\theta_{,2} & 0 & k_{12}\theta_{,1} & k_{11}\theta_{,2} \\ k_{21}\theta_{,1} & k_{22}\theta_{,2} & 0 & k_{22}\theta_{,1} & k_{21}\theta_{,2} \end{bmatrix}, \tag{8.20a}$$

$$\Xi_2 = \begin{bmatrix} k_{1j}\theta_{,j} & 0 & 0 & k_{2j}\theta_{,j} & 0 \\ 0 & k_{2j}\theta_{,j} & 0 & 0 & k_{1j}\theta_{,j} \end{bmatrix} \quad (\text{sum on } j = 1,2). \tag{8.20b}$$

with respect to the fourth integral in (7.41), which also arises from geometric nonlinearity, the following identity can be obtained from direct expansion:

$$\operatorname{grad}\psi^h \cdot \left[\operatorname{grad}\left(\delta\mathbf{u}^h\right) - \operatorname{div}\left(\delta\mathbf{u}^h\right)\mathbf{1}\right] \cdot \mathbf{k} \cdot \frac{\mathbf{g}}{g} = \tilde{\psi}^t \, \mathbf{E}^t \Theta_1 \, \mathbf{B}\,\delta\mathbf{u}, \tag{8.21}$$

where

$$\Theta_1 = \frac{1}{g}\begin{bmatrix} 0 & -k_{12}g & -k_{12}g & k_{22}g & 0 \\ -k_{22}g & 0 & -k_{22}g & 0 & k_{12}g \end{bmatrix} \tag{8.22}$$

for D9P4 axisymmetric element. Matrix from of the fifth integral term in (7.41), representing the variation of permeability with Jacobian, is obtained from the following identity

$$\operatorname{grad}\psi^h \cdot \operatorname{div}\left(\delta\mathbf{u}^h\right)\mathbf{1} \cdot \frac{\partial \mathbf{k}}{\partial e} \cdot \left\{\frac{\operatorname{grad}\theta}{\rho_w g} + J\frac{\mathbf{g}}{g}\right\} = \tilde{\psi}^t \, \mathbf{E}^t \Theta_2 \, \mathbf{B}\,\delta\mathbf{u}. \tag{8.23}$$

For D9P4 axisymmetric element

$$\Theta_2 = \begin{bmatrix} \dfrac{\partial k_{1j}}{\partial e}\upsilon_{,j} & \dfrac{\partial k_{1j}}{\partial e}\upsilon_{,j} & \dfrac{\partial k_{1j}}{\partial e}\upsilon_{,j} & 0 & 0 \\ \dfrac{\partial k_{2j}}{\partial e}\upsilon_{,j} & \dfrac{\partial k_{2j}}{\partial e}\upsilon_{,j} & \dfrac{\partial k_{2j}}{\partial e}\upsilon_{,j} & 0 & 0 \end{bmatrix} \quad (\text{sum on } j = 1,2). \tag{8.24}$$

where $\upsilon = \dfrac{\operatorname{grad}\theta}{\rho_w g} + J\dfrac{\mathbf{g}}{g}$.

Since $\tilde{\eta}$ and $\tilde{\psi}$ are both arbitrary, the conditions stated in (8.10) and (8.12) can be satisfied by the following coupled vector equations:

Balance of linear momentum:

$$\mathbf{r}_\phi(\mathbf{u},\theta) = \mathbf{F}_{EXT} - \left\{\mathbf{N}^S(\mathbf{u}) + \mathbf{N}^W(\theta)\right\} = \mathbf{0}. \tag{8.25}$$

Balance of mass:

$$\mathbf{r}_\theta(\mathbf{u},\theta) = \beta_0 \Delta t\, \mathbf{H}_{EXT} - \{\mathbf{J}(\mathbf{u}) - \beta_0 \Delta t\, \Phi(\theta)\} = \mathbf{0}. \tag{8.26}$$

For numerical analysis, the problem boils down to determining the configurations defined by the nodal values $\mathbf{u}$ and θ at which (8.25) and (8.26) are simultaneously satisfied.

Residual force vector and displacement vector of an element, $\mathbf{f}_e$ and $\delta\mathbf{d}_e$, respectively, are given as

$$\mathbf{f}_e = \begin{Bmatrix} \mathbf{r}_\phi(\mathbf{u},\theta) \\ \mathbf{r}_\theta(\mathbf{u},\theta) \end{Bmatrix}, \qquad \delta\mathbf{d}_e = \begin{Bmatrix} \delta\mathbf{u} \\ \delta\theta \end{Bmatrix}. \tag{8.27}$$

Consistent tangent operator discretized at element level, $\mathbf{K}_e$ is assembled from coefficient matrices (8.14) and (8.16) as

$$\mathbf{K}_e = \begin{bmatrix} \mathbf{K}_{\phi\phi} & \mathbf{K}_{\phi\theta} \\ \mathbf{K}_{\theta\phi} & \mathbf{K}_{\theta\theta} \end{bmatrix} \tag{8.28}$$

Global matrices $\mathbf{K}$, $\mathbf{f}$ and $\delta\mathbf{d}$ of (8.1) are assembled from $\mathbf{K}_e$, $\mathbf{f}_e$, and $\delta\mathbf{d}_e$, respectively, according to the node numbering scheme of the problem domain. In PlasFEM, incremental displacements $\delta\mathbf{u}$ and pore pressures $\delta\theta$ are actually grouped on a nodal basis in order to preserve bandedness of the global stiffness matrix which costs less CPU time for matrix inversion.

In general, matrix $\mathbf{K}_e$ is nonsymmetric and indefinite. The lack of symmetry of $\mathbf{K}_e$ is a consequence of solving a non-symmetric consolidation problem. However, there are conditions which results in a symmetric $\mathbf{K}_e$ even if the problem of consolidation is inherently non-symmetric. Obviously, $\mathbf{K}_e$ being symmetric requires that $\mathbf{K}_{\theta\theta} = \mathbf{K}_{\theta\theta}^t$, which is true if and only if the permeability tensor $\mathbf{k}$ is symmetric. Furthermore, for small strain analysis the Jacobian J is identically equal to unity, while the second integral in (8.17a) vanishes identically since it originates from geometric nonlinearity. Thus, for this condition, $\mathbf{K}_{\theta\phi} = \mathbf{K}_{\phi\theta}^t$. Under the same setting imposed by the assumption of small strains, the last term in the integral of (8.15a) also vanishes, since this term is simply the linearization of the constant Jacobian. Thus, under the assumption of small strains, $\mathbf{K}_{\phi\phi} = \mathbf{K}_{\phi\phi}^t$ provided that material stiffness matrix $\tilde{\mathbf{D}}$ is symmetric.

CHAPTER 9
CENTRIFUGE MODELING

9.1 University of Florida Centrifuge Equipment

The University of Florida currently has two fully operative geotechnical centrifuges. The University of Florida geotechnical centrifuge used in this research was originally designed and built in 1957 for the Sperry Rand Corporation, by the Rucker Company. It was initially designed for the purpose of testing vacuum tubes for the National Aeronautics and Space Administration (NASA). In the early 1970's it was donated to the Department of Mechanical Engineering and installed at the Weil Hall Annex basement. A large variety of geotechnical engineering investigations has since been conducted with this centrifuge such as, the study of flexible retaining walls in granular soils, the study of pile friction freeze, the study of bearing capacity of shallow foundations on sands, etc. Sink hole collapse potential and consolidation/sedimentation processes in phosphatic clays also have been investigated in the past.

A schematic drawing of the uninstrumented centrifuge is shown in Figure 9.1. It has two rotating arms, each with a length of approximately one meter and each with a platform where the testing container and counterweight can be mounted. The choice of several sizes of containers can be made by the researcher to model the problem at hand. A protective metal housing encloses the entire centrifuge and access to the centrifuge is possible through two swinging doors and one hinged top panel.

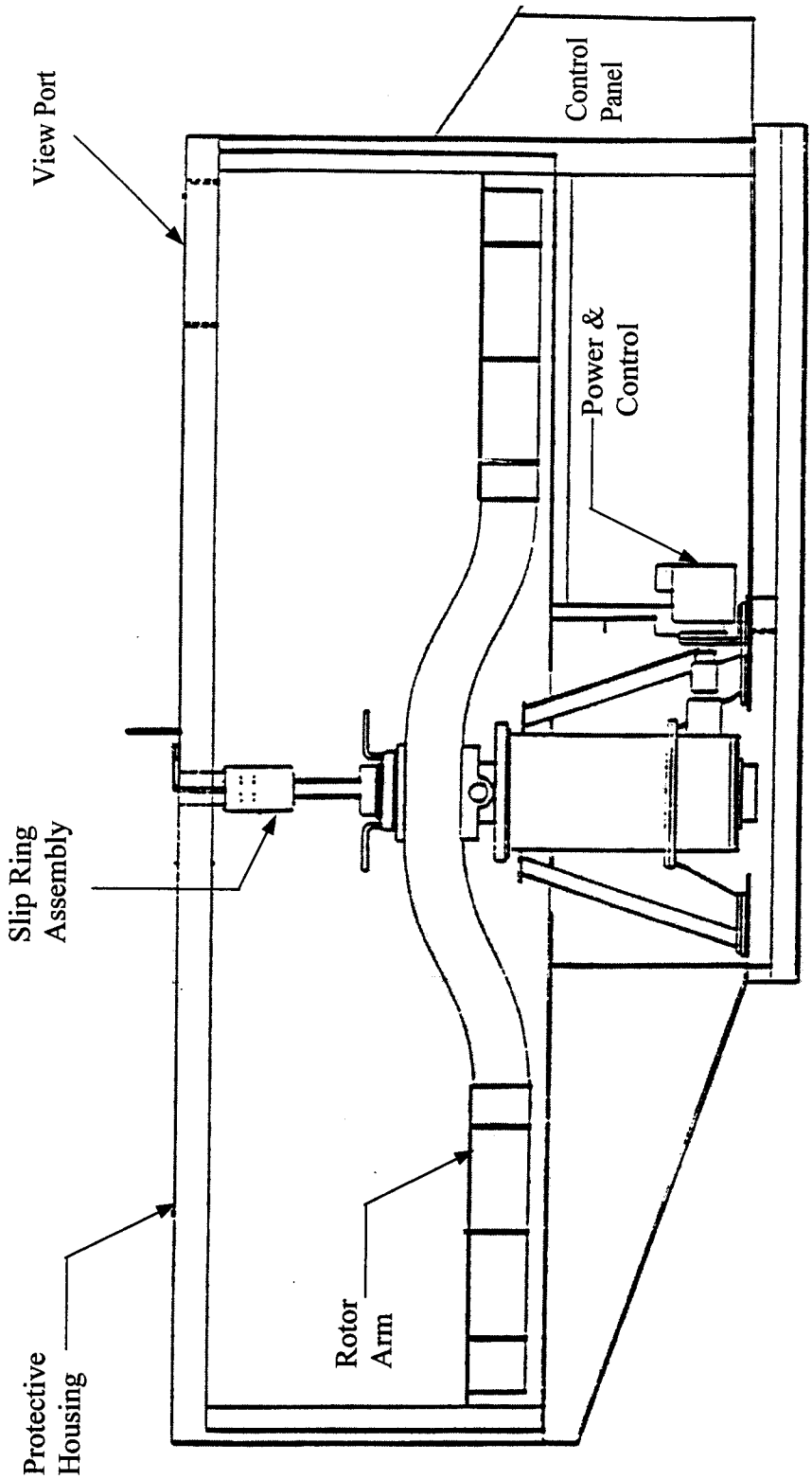

Figure 9.1 Schematic of Centrifuge

The centrifuge is powered by a 5 HP electric motor and is controlled by a Parajust electronic direct-current (DC) motor controller, both installed in 1989. This size of motor allows long flights at significant g-levels. Electrical and hydraulic connections to instrumentation inside the centrifuge is achieved through a 40 channel slip ring unit. The slip ring unit is fixed to the top cover and remains motionless while the center shaft is spinning. It has a series of metal brushes that maintain electrical contact with the shaft. Any instrumentation of the model is connected to an electrical panel existing on the centrifuge arm. From here the signals pass through the slip rings, via electronic wiring, into the data acquisition system.

The experiment can be monitored in motion via a camera mounted on the center shaft, rotating with the same speed as the container. The camera used in this investigation is a Panasonic closed-circuit TV camera. This camera originally had a stationary lens installed but to achieve a more precise monitoring, a zoom lens was purchased and installed.

The container used is a cylindrical aluminum container with a height of 25.6 cm and a diameter of 16.2 cm. Inside of this container a plexi-glas bucket can be placed and this is the actual container for the soil sample. The height of this plexi-glas bucket is 16.5 cm and the diameter is 13.9 cm. The aluminum bucket rotates around hinges fixed to a bucket housing (see Figure 9.2).

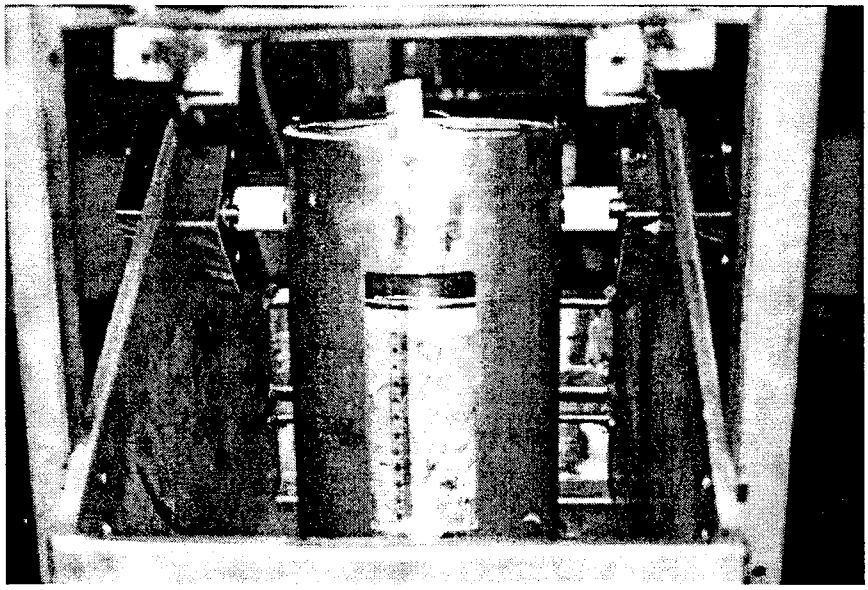

Figure 9.2 Soil sample in container

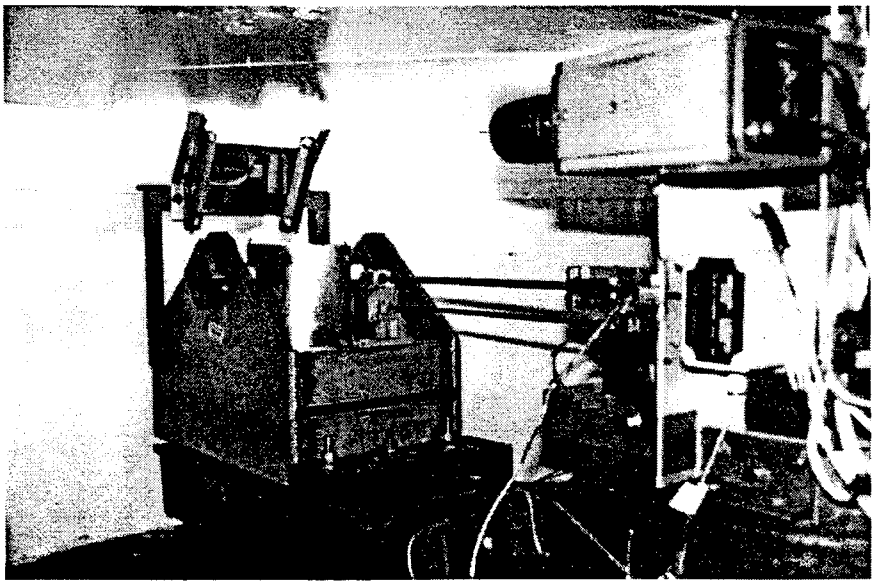

Figure 9.3 Test monitoring in centrifuge

There is a slot cut in the aluminum container that allows the soil sample to be monitored through the plexi-glas. A mirror was installed above the container (on the bucket housing) such that, when the container was accelerated up into a horizontal position, the sample could be monitored laterally by the camera via the mirror. The whole setup is shown in Figure 9.3. A ruler was fixed to the plexi-glas bucket which allowed settlements to be monitored with a precision of 0.25 mm.

Table 9.1 Centrifuge Specifications

Manufacturer	Parametrics
Model	6051 (modified !)
Driving System	5 HP electric motor
Capacity	appr. 2.4 g-ton
Radius (Center-Container Hinge)	93 cm
Radius (Center-Container Floor)	109 cm
Dimensions of soil container (Area/height)	151.8 cm^2 / 16.5 cm
Electrical Pick-Ups	40 slip rings
Fluid Transmission	2 hydraulic slip rings
Test Recording	Closed Circuit TV, Panasonic Camera (WV-1410), zoom lens (M6Z 1212)

9.2 Centrifuge Testing

The purpose of centrifuge testing was to study the rate and magnitude of settlement of a prototype soil deposit of phosphatic waste clay. Other purposes included

determining the appropriate time scaling exponent (by performing modeling of models), monitoring the clogging phenomena of wick drains. Approximately 20 successful centrifuge tests were conducted in this research, some of which duplicate each other in order to ascertain the validity of the results.

Different methods and combinations of tests were used throughout the centrifuge testing program. Testing was performed at two different g-levels, with and without wick drains, with and without surcharges, and with different widths of wick drain. In the following the tests and their results are presented.

9.3 Modeling of Models

Tests for modeling of models were performed in order to determine the exponent for scaling times from centrifuge consolidation tests to prototypes. Modeling of models involved performing a series of centrifuge tests at a minimum of two different acceleration levels and comparing times for equivalent solid contents or heights of interface.

The basic equation used in the modeling of models theory is expressed as

$$t_p = t_{m1}\, n_1^x = t_{m2}\, n_2^x, \tag{9.1}$$

where

t_p is the prototype time,
t_{m1} is the time in model 1,
t_{m2} is the time in model 2,
n_1 is the 'g'-acceleration in model 1,
n_2 is the 'g'-acceleration in model 2, and
x is the time scaling exponent.

(9.1) expresses the relationship between two centrifuge models and the same prototype with a given solids content. Hence, this equation does not only relate prototype to model, but also relates model to model. From (9.1) one can obtain the following expression for x as

$$x = \frac{\log\left(\frac{t_{m1}}{t_{m2}}\right)}{\log\left(\frac{n_2}{n_1}\right)}. \qquad (9.2)$$

An experimental study presented by Bloomquist [84] concerning Kingsford waste clay, found that the time scaling exponent varied from 1.6 to 2 depending on the solid content of the clay being tested. Bloomquist [84] also found that any increase in solid content above 22% was found to be in the consolidation phase, and a time scaling factor of 2 was appropriate.

In this study, two models were used to perform the modeling of models. The first model had an initial height of 12 cm (~ 4.7"), corresponding to a prototype height of 8.4 m (~ 27.6') when exposed to a 'g'-acceleration of 70 (n = 70). The second model had an initial height of 7.6 cm (~3") which corresponds to the same prototype height as the first model when exposed to a 'g'-acceleration of 110 (n = 110). Four tests were conducted in the modeling of models: Two tests at 70 g (with and without wick drain) and two tests at 110g (with and without wick drain). All four tests had a surcharge applied, corresponding to a prototype surcharge height of approximately 6 m sand (~ 20 feet). A comparison of the settlements from the 2 tests with wick drains can be seen on Figure 9.4.

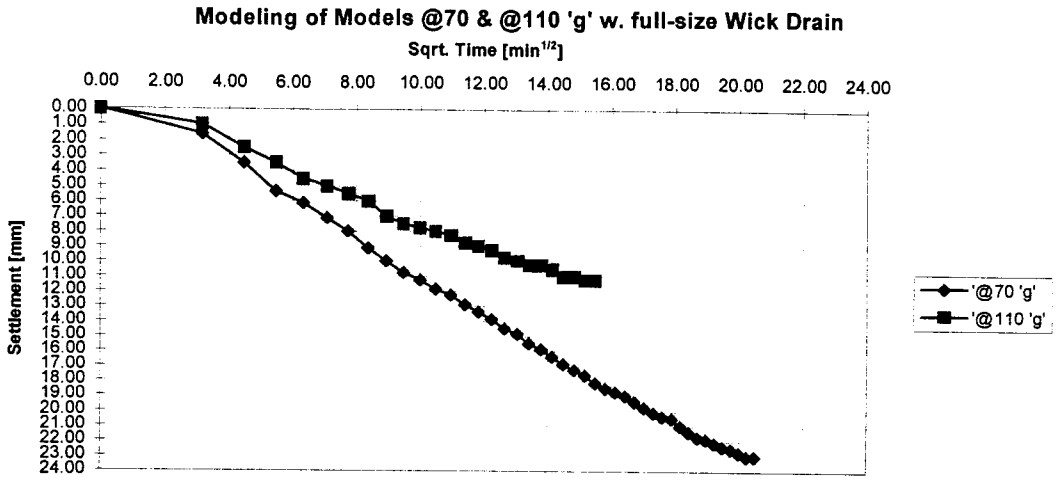

Figure 9.4 Settlements from 70 g and 110 g tests

Bloomquist [84] derived the following equation relating the change in height during consolidation to the change in solid content.

$$S_i = \frac{S_0}{1-\left(\frac{H_t - H_i}{H_t}\right)\left(1-S_0\left(\frac{G_s - 1}{G_s}\right)\right)}, \tag{9.3}$$

where

S_i is the solids content at time (i),

S_0 is the initial solids content,

H_t is the initial height,

H_i is the height of the sample at time (i), and

G_s is the specific gravity.

Table 9.2 in the following is produced from (9.2) and (9.3).

Table 9.2 Modeling of models results

Samples at 110g with Wick Drain and Surcharge Initial heights: 120 and 76mm Initial solids contents: 32.75 and 32.78%		
Settlement [mm]	Time Scaling Exponent	Solids Content [%]
5.00	1.34	34.59
8.00	1.35	35.77
10.00	1.68	36.60
11.00	1.83	37.03
11.50	1.94	37.25

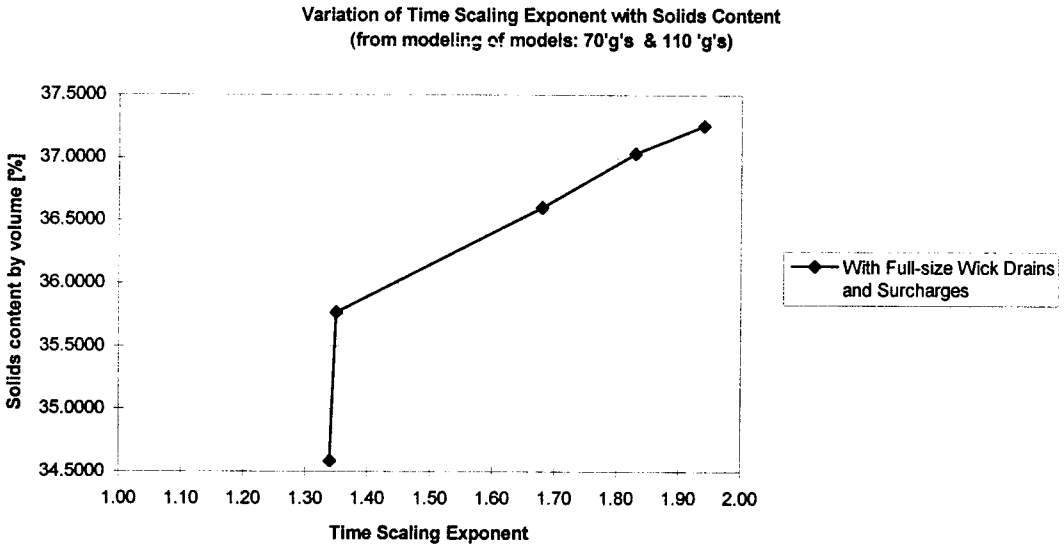

Figure 9.5 Variation of time scaling exponent with solid content

In Figure 9.5 the variation of the solid contents with the time scaling factor as the consolidation advances can be seen. Notice that there is a significant "jump" in the curve at a time scaling factor of approximately 1.35. This was also found by Townsend and Israel [85], however, with a much lower solid content (15%). Plots of the solid content versus time should produce essentially parallel curves and this is evident in Figure 9.6.

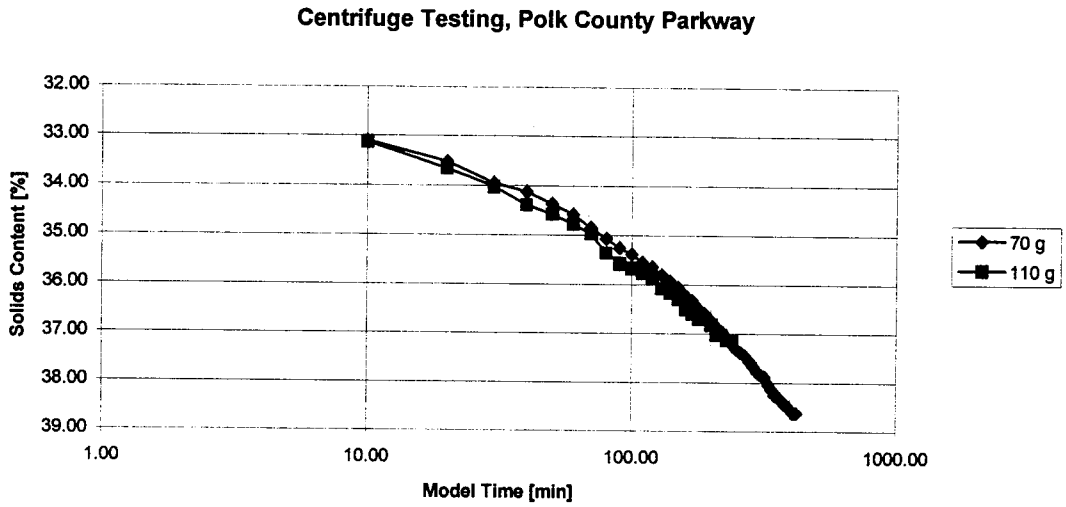

Figure 9.6 Solid content versus model time

The curves on Figure 9.6 also have approximately equal final solid contents as expected (at the point where the test at 110 g is terminated).

The theoretical limit for the time scaling exponent is 2.0 and once consolidation is reached the exponent should reach this maximum value. The results from this modeling of models study indicate that the time scaling factor approaches the value of 2.0 when consolidation is progressing, however, in the final stages of the tests. Thus, from these considerations it is apparent that scaling up the centrifugal model to prototype times is an incremental procedure and the appropriate time scaling exponent must be used.

Accordingly, a semi-logarithmic plot the percent of total settlement U versus elapsed time (in log scale) is plotted for the two tests (70 g and 110 g), and a table of the time scaling exponent for different percentage of total consolidation is established as shown in the following.

The percent of total settlement U at time t_i can be determined by:

$$U = \frac{H_0 - H_i}{H_0 - H_f} \cdot 100\% \tag{9.4}$$

where:

H_o is the initial sample height,

H_f is the final sample height, and

H_i is the height of the sample at time t_i.

The time scaling exponent x for different values of U can be determined from the following equation:

$$x = \frac{\log\left(\frac{t_{70}}{t_{110}}\right)}{\log\left(\frac{110}{70}\right)} = 5.0944 \log\left(\frac{t_{70}}{t_{110}}\right), \tag{9.5}$$

where

t_{70} is the time to reach a given value of U at 70 g's,

t_{110} is the time to reach a given value of U at 110 g's.

In order to determine the elapsed model time for different percentage of consolidation the wick drains were reduced to a quarter of their original width (i.e., new width = 2.5cm) so that they do not act as reinforcement and thus hinder the consolidation process. Elapsed model time versus the percentage of total consolidation is shown on

Figure 9.7. The trendlines are third-order polynomials with reasonable R^2-values. The equations for the trendlines and Equation 9.5 are used to produce Table 9.3 which shows the time scaling exponent for different percentages of consolidation for the two tests at 70 g and 110 g.

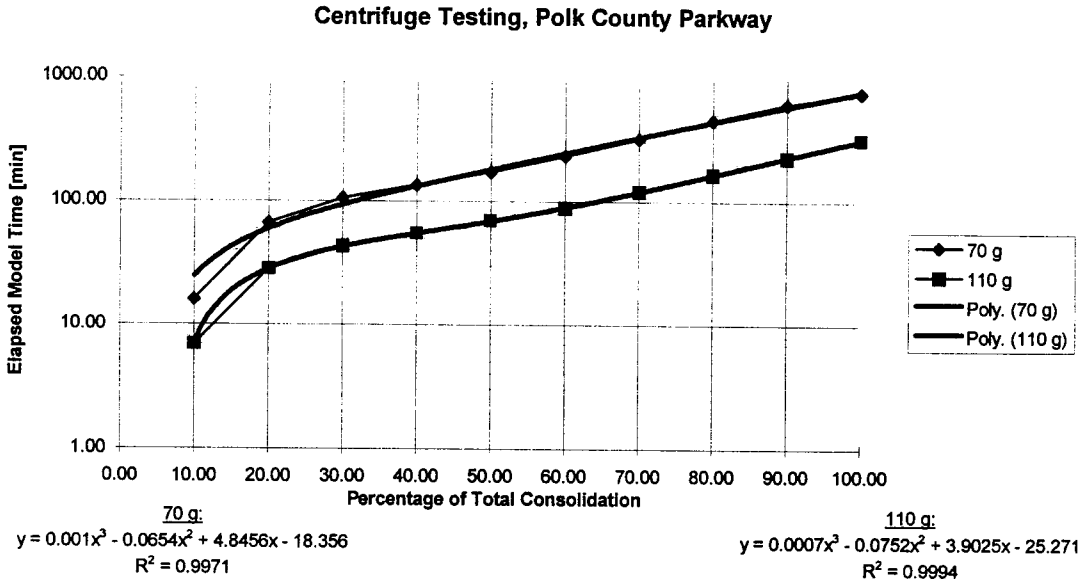

Figure 9.7 Trendlines for model time versus percent of total consolidation

Table 9.3 Time scaling exponents x for different percentages of settlement

U [%]	t_{70} [min]	t_{110} [min]	x
10.00	15.98	6.93	1.85
20.00	67.04	28.30	1.91
30.00	105.47	43.02	1.98
40.00	135.00	55.31	1.97
50.00	172.34	69.35	2.01
60.00	230.14	89.36	2.09
70.00	317.28	119.52	2.16
80.00	449.53	164.05	2.23
90.00	608.42	227.13	2.18
100.00	751.21	312.98	1.94

Table 9.3 shows that the modeling of models produced sensible time scaling exponents, with an average value of 2.03 as shown on Figure 9.8

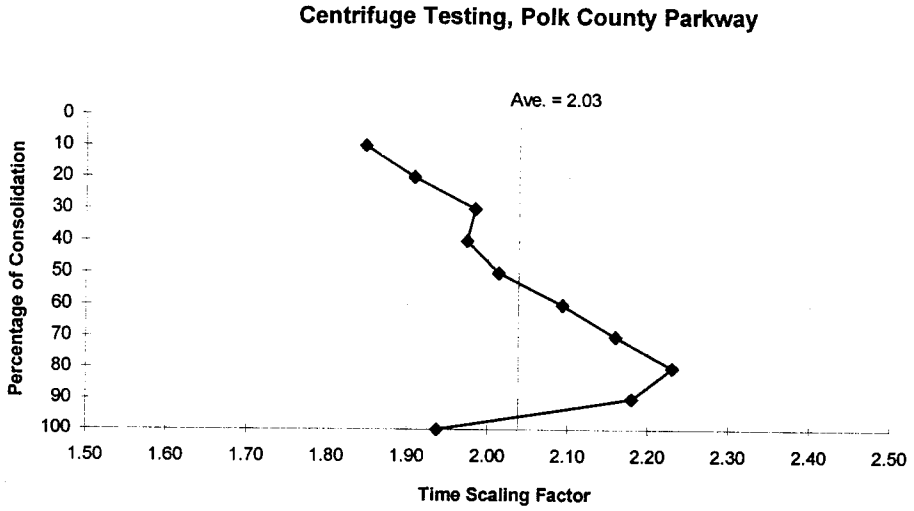

Figure 9.8 Variation of time scaling exponent with percentage of consoliadtion

It is concluded from the two conducted modeling of model analyses that the time scaling exponent is close to 2 with reduced size wick drains and less than 2 for the tests with full size wick drains and this is kept in mind during the finite element analyses.

9.4 Centrifuge Test Results

The testing program started with 4 tests of the slime with wick drains (no surcharge), and at both 70 g and 110 g. These tests took very long time and there were hardly any settlement. The next step was the tests at 70 g, and 4 tests were performed at this g-level. Two with wick drains and two without wick drains. The results from these tests can be seen in Figures 9.9 and 9.10.

Figure 9.9 presents the prototype settlements for these four tests. The total settlements for the samples without wick drains were between between 0.67m and 0.70m and the total settlements for the samples with wick drains were between 1.58m and 1.61m.

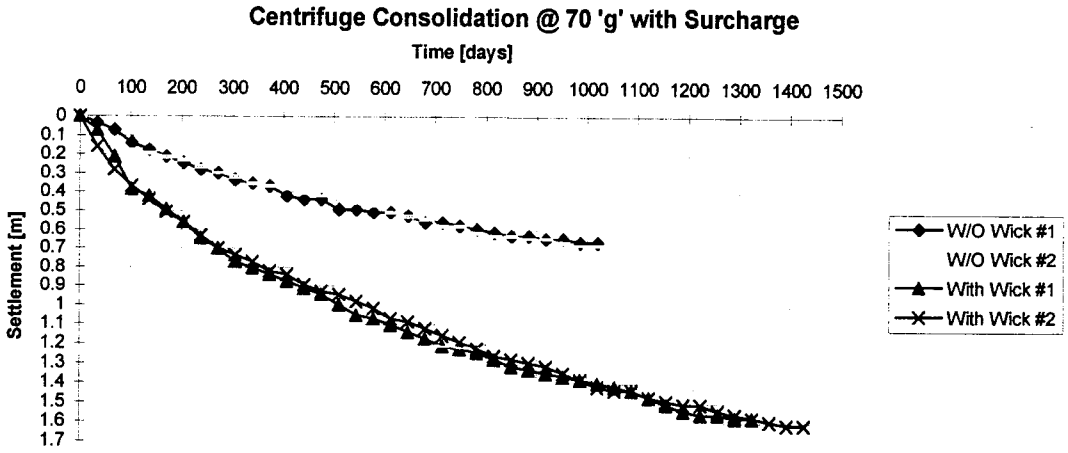

Figure 9.9 Prototype results from 70 g tests

The total improvement in settlement, due to the implementation of wick drains, was 0.91m and for the time of termination of the two tests without wick drains, the two tests with wick drains had settled approximately twice as much. The normalized prototype results are shown on Figure 9.10. It can be seen that 90% of the total settlement is reached after approximately 800 days (2.19 years) for the samples without wick drains and 1050 days (2.88 years) for the samples with wick drains.

The tests performed at an acceleration of 110 g were the major portion of the performed tests. The prototype settlements from 6 tests with and without wick drains are shown on Figure 9.11.

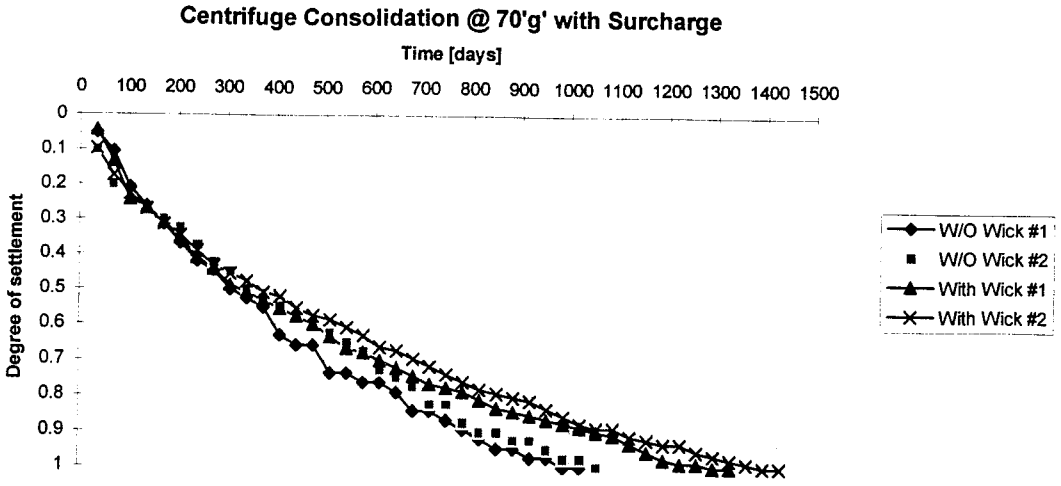

Figure 9.10 Normalized prototype results from 70 g tests

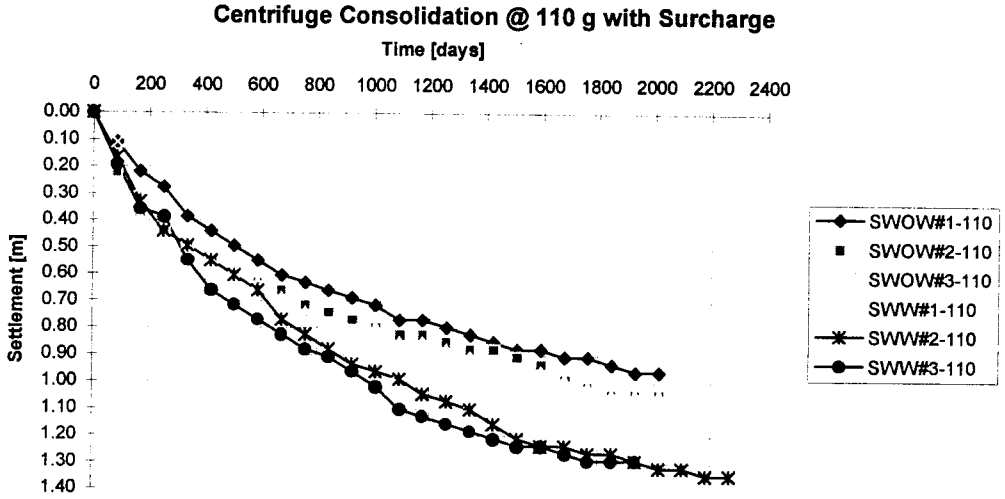

Figure 9.11 Prototype results from 110 g tests

The difference in settlement between the two groups of samples in Figure 9.11 is not as well-defined as the tests at 70 g but still recognizable. The group without wick drains settles to a level of approximately 1m, while the group with wick drains reaches a level of settlement of approximately 1.3m. These results are normalized on Figure 9.12,

and it can be seen that 90 % of the total settlement is reached after approximately 1250 days (low) to 1600 days (high). This corresponds to 3.4 years and 4.4 years, respectively.

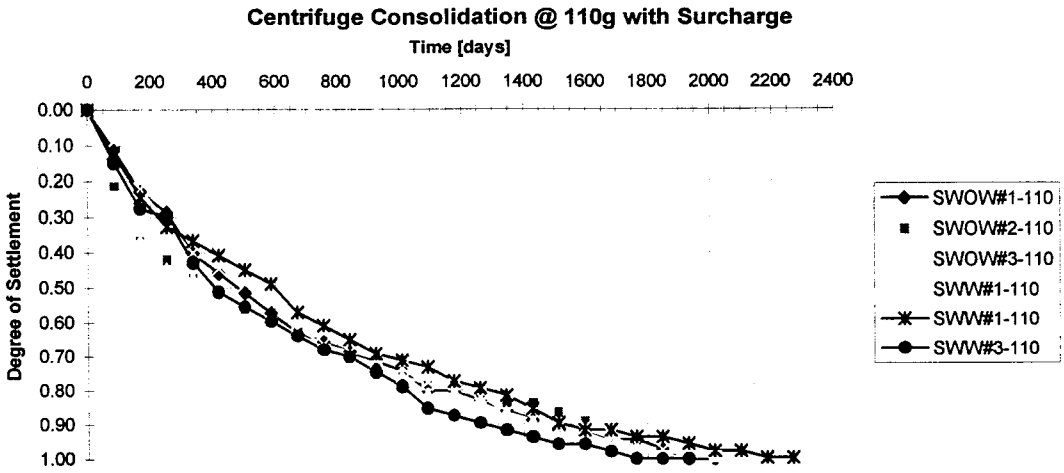

Figure 9.12 Normalized prototype results from 110 g tests

Different widths of wick drain: 10 cm (full size wick), 2.5 cm (1/4 size wick), and 1.25 cm (1/8 size wick) were tested at 110 g's in the centrifuge. These results are presented in Figure 9.13. The trend shows that the wider the wick drain, the more the settlements. This makes a logical conclusion.

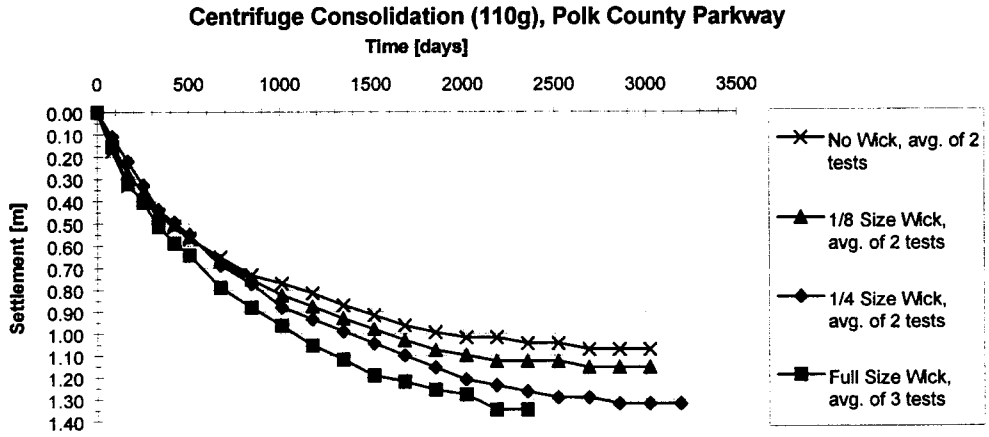

Figure 9.13 Prototype settlements with multiple size wick drains

CHAPTER 10
NUMERICAL EXAMPLES

This chapter presents numerical simulation examples of one and two-dimensional (plane strain) hyperelastic consolidation. Effects of large strain on consolidation settlement and excess pore pressure dissipation are compared with the same for the small strain formulation.

Time integration for all the numerical simulations in Chapters 10 and 11 was carried out by the one-step, first-order accurate, unconditionally stable backward difference scheme (see Section 4.4) obtained by setting $k = 1$, and $\beta_0 = \beta = \alpha_1 = 1$. The simulations, both the large strain and small strain formulations, were performed by a displacement-based finite element code PlasFEM.

10.1 Mixed Element

The type of elements used for consolidation simulation greatly affects the accuracy of the solution. It was found that only a few combinations of interpolation functions were capable of providing accurate solutions without incurring problems such as spurious pressure modes, mesh locking or poor convergence rate. The accepted test on the stability and convergence of a particular element is the Babuska-Brezzi [84, 85] condition. Hughes [86] has proposed an approximate method, based on the constraint ratio. He compares the number of equations provided by the displacement unknowns to

the number of incompressibility constraints. If the ratio is close to unity, the element has a tendency to lock and will perform poorly under incompressible conditions.

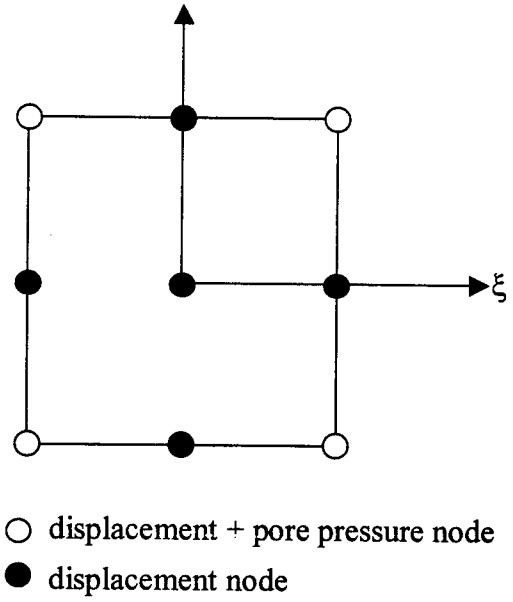

Figure 10.1 D9P4 mixed element

For the two-dimensional problems with mixed displacement/pressure, the D9P4 element (biquadratic 9-node displacement interpolation with a bilinear 4-node pore pressure interpolation) passes the Babuska-Brezzi condition and has a high constraint ratio. Consequently, D9P4 mixed elements, as shown in Figure 10.1, were employed for all finite element meshes used in Chapters 10 and 11.

10.2 One-dimensional Hyperelastic Consolidation

A stress-free hyperelastic porous solid skeleton is considered for one-dimensional consolidation example. The free energy function Ψ for linear elasticity is given in (5.38).

The assumed values of the material parameters are $\lambda = 57.7$ kPa, $\mu = 38.5$ kPa (equivalent to a Young's modulus $E = \mu(3\lambda + 2\mu) / (\lambda + \mu) = 100$ kPa and a Poison's ratio $\nu = 0.5\lambda / (\lambda + \mu) = 0.3$), and constrained modulus $D = \lambda + 2\mu = 134.7$ kPa.

The FE mesh, represented by a column of 10 D9P4 axisymmetric elements, is shown in Figure 10.2. The bottom base of the mesh is impervious and fixed with respect to vertical displacements. Free drainage (i.e., zero excess pore pressure) is allowed on top. The vertical permeability is assumed to have a value $k_v = 8.46\times10^{-4}$ m/day and the unit

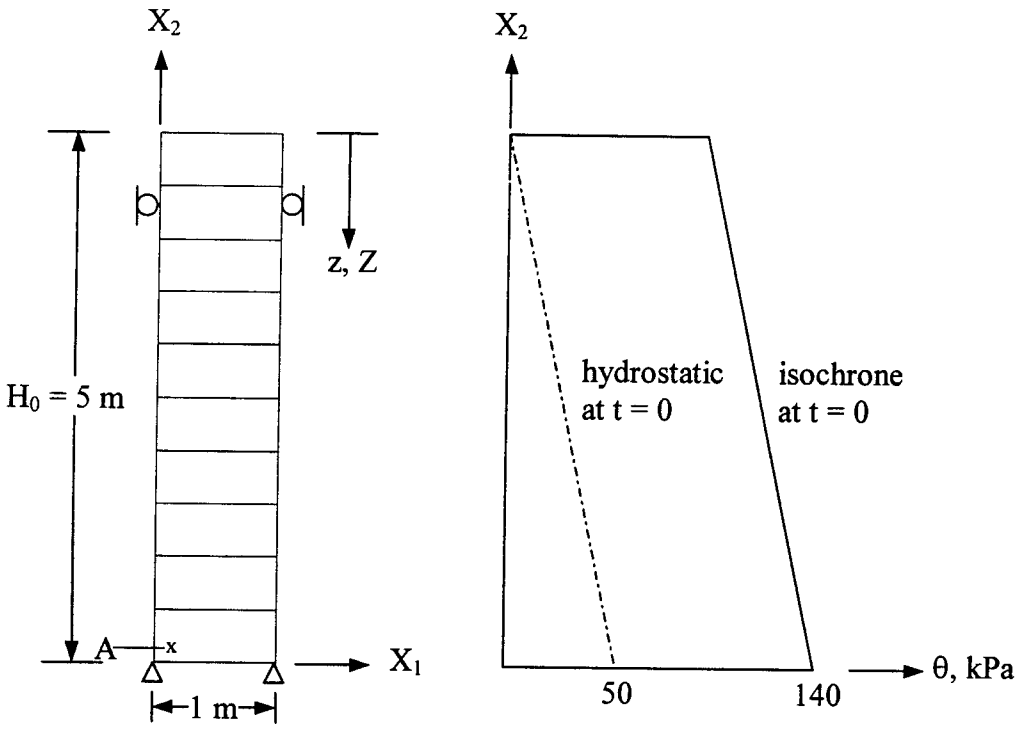

Figure 10.2 FE mesh and initial pore water pressures for one-dimensional consolidation problem

weight of water $\rho_w g = 10$ kN/m^3. The coefficient of consolidation can be calculated as $c_v = k_v D/(\rho_w g) = 1.14\times10^{-2}$ m^2/day. Normalized time factor is calculated as $T = c_v t / H_0^2$, where H_0 is the initial thickness of the soil column. During the consolidation stage, time steps are increased according to the equation $\Delta t_{n+1} = 1.5\ \Delta t_n$. This results in nearly equally spaced data points when the time history responses are plotted on a logarithmic time axis. Excess pore pressures are generated by applying a vertical downward Cauchy step load of $\Delta q^{(Cauchy)} = 90$ kPa at the top of the soil column.

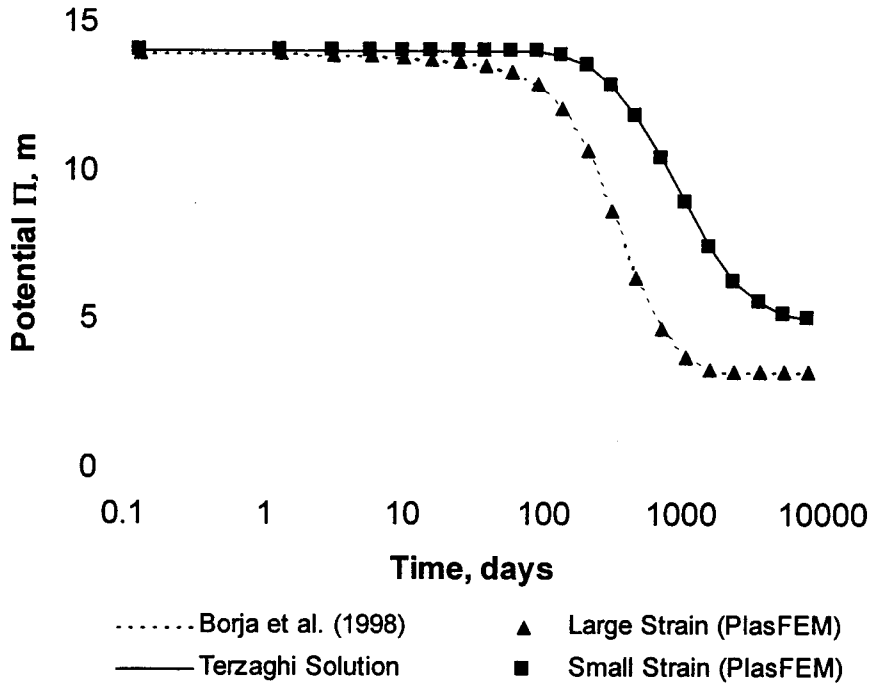

Figure 10.3 One-dimensional hyperelastic consolidation: variation of total potential with time

Figure 10.3 shows a comparison of the variations with respect to time of the fluid potential $\Pi = \Pi^\theta + \Pi^e = \theta / (J\rho_w g) + x_2$ at a Gauss Point A near the impervious base.

Point A is initially situated at a distance of the 4.894 m from the top of the undeformed soil column. Here the potential Π takes the physical meaning of being the total hydraulic head at this particular Gauss point. PlasFEM prediction of small strain formulation matched quite well with the analytical solution from the one-dimensional linear consolidation model of Terzaghi. Prior to consolidation, the fluid potentials for the small strain and the large strain models are the same and are 14 m, 9 m of which is the transient part produced by the 90 kPa imposed vertical load. Figure 10.3 shows that the fluid potential predicted by the Terzaghi solution decays to the initial steady state value of $\Pi^{(small)} = 5$ m since the height the soil column remains essentially the same at 5 m due to the small strain assumption. The large strain solution however approaches a steady-state value of $\Pi^{(large)} = 3.24$ m representing the final compressed height of the soil column. The large strain prediction is compared with the same reported in [89]; both the predictions are in exact match (see Figure 10.3).

The validity of the large strain solution can be checked by simple manual calculations (see Section A.24). The Jacobian J at the steady-state condition is calculated as 0.6484, which is the ratio of the final to initial column heights for the case of one-dimensional compression. Thus, $J = 0.6484 = 3.24/5$, and is constant throughout the height of the soil column. The final Kirchhoff effective vertical stress is equal to $\Delta q^{(Kirchhoff)} = J\Delta q^{(Cauchy)} = 58.35$ kPa, which is also distributed uniformly throughout the height of the soil column at steady-state condition.

Figure 10.4 shows the isochrones of Cauchy pore pressures plotted for different values of equivalent time factor T. Cauchy pore pressures were calculated as $\theta^{(Cauchy)} =$

$\theta^{(Kirchhoff)}/J$ at the Gauss points. Kirchhoff pore pressures at Gauss points were interpolated from the global solution of nodal values. Note that isochrones predicted by the large strain model move spatially as a result of the large deformation effect. For comparison purposes, the isochrones computed from the Terzaghi model are also plotted

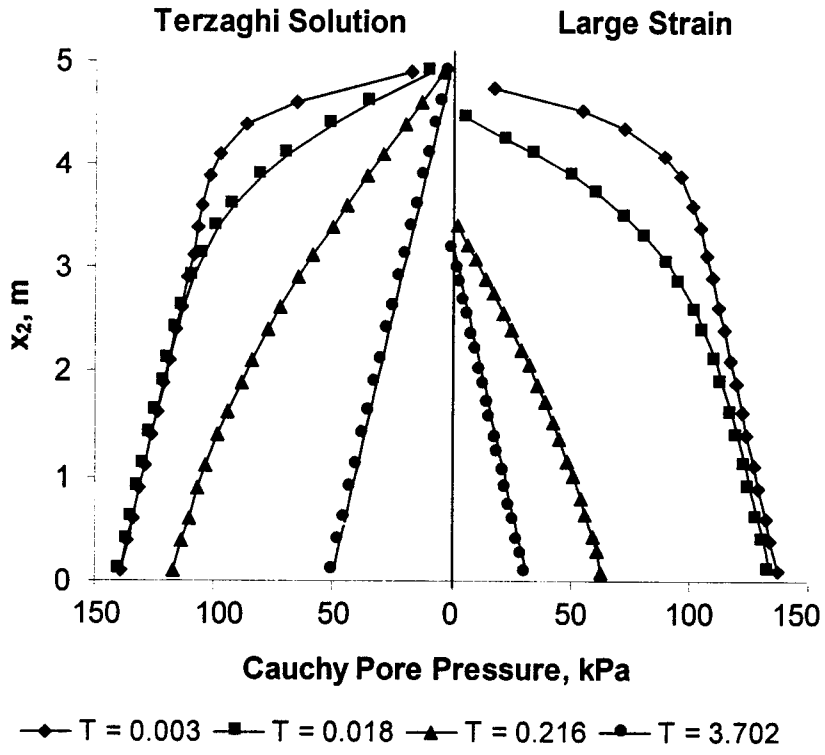

Figure 10.4 One-dimensional hyperelastic consolidation: isochrones of constant Cauchy pore pressure

in Figure 10.4 for the small strain formulation. The explicit expression of excess Cauchy pore pressure for one-dimensional small strain consolidation is given by [90]

$$\theta^{e(Cauchy)} = \sum_{m=0}^{m=\infty} \frac{2\theta_0^{e(Cauchy)}}{M} \sin(MZ)\exp\left(-M^2T\right); \qquad M = \frac{\pi}{2}(2m+1), \quad (10.1)$$

where $Z = z / H_0$ is normalized depth, $\theta_0^{e(Cauchy)}$ is initial excess pore pressure at t = 0. Z and z are measured from the top of the consolidating stratum (see Figure 10.2).

Finally, the variation of average degree of consolidation U with respect to time factor T is compared in Figure 10.5 for large and small strain formulations. The analytical expression for U for one-dimensional small strain consolidation, based on Terzaghi's linear consolidation model [30], is given by [90]

$$U = 1 - \sum_{m=0}^{m=\infty} \frac{2}{M^2} \exp\left(-M^2 T\right); \qquad M = \frac{\pi}{2}(2m+1). \tag{10.2}$$

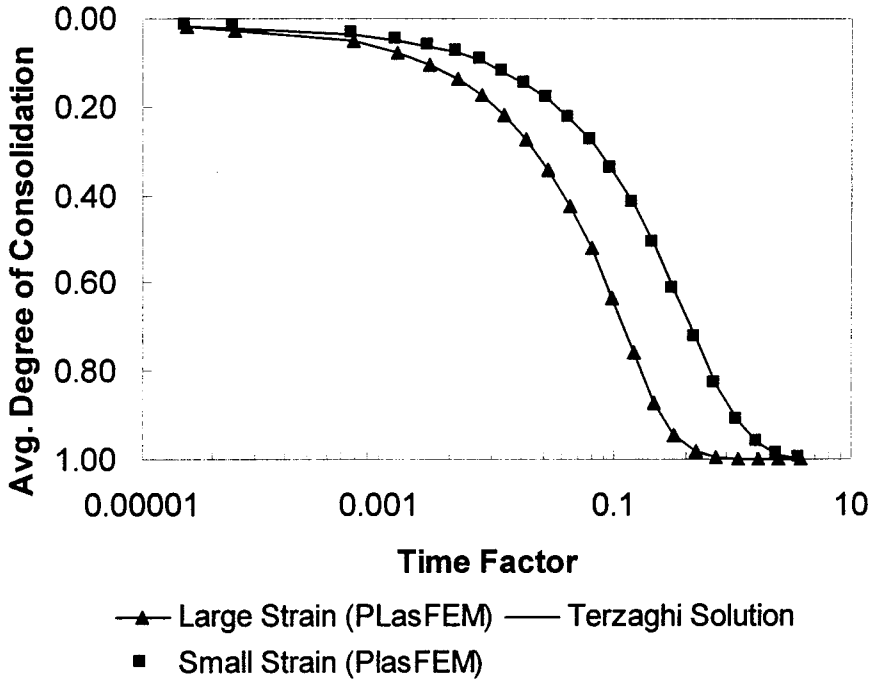

Figure 10.5 One-dimensional hyperelastic consolidation: variation of average degree of consolidation with time factor

U(T) for FEM solutions is plotted as the ratio of settlement at time T to the ultimate settlement at the end of consolidation. The small strain solution predicts a slower rate of consolidation than the large strain solution because the latter solution considers the reduction in length of the drainage path, which enhances the dissipation of excess pore pressure. Reduction of coefficient of permeability of the soil as it consolidates could have offset this effect, but this factor is not taken into account in this example.

10.3 Plane Strain Hyperelastic Consolidation

Closed-form solutions are available for the problem of plane strain, small deformation consolidation of an elastic half-space subjected to a uniform strip load. This problem may be simulated with a numerical algorithm for the case of small strain formulations and solutions compared. An attempt was made to replicate these solutions numerically and demonstrate the significance of the large strain effects on the response of a consolidating hyperelastic soil medium deforming in plane strain.

Figure 10.6 shows the finite element mesh used for the two-dimensional plane-strain problem. The problem consists of a strip load of half-width a = 5 m applied over a hyperelastic soil layer 20 m thick. The mesh is composed of 132 D9P4 elements with 575 displacement nodes and 156 pore pressure nodes. The bottom of the clay layer is assumed rigid against vertical displacement, perfectly draining, and subjected to a constant value of total potential equal to $\Pi = 20.0$ m. The material parameters are $\lambda = 0$ and $\mu = 250$ kPa (corresponding to a Young's modulus E = 500 kPa and a Poisson's ratio $\nu = 0$). A strip load of $\Delta q^{(Cauchy)} = 120$ kPa is applied nearly instantaneously ($\Delta t = 10$ days, which is negligible compared to the $t \cong 10000$ days required to reach complete consolidation) at

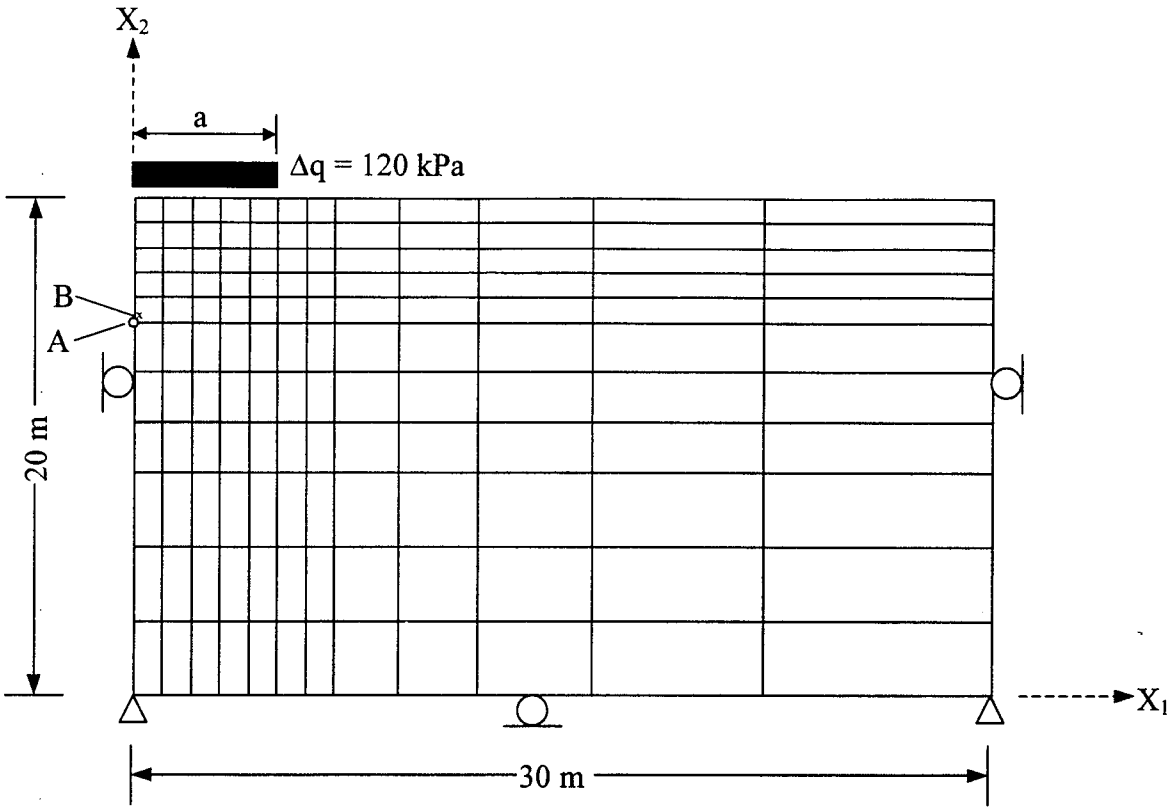

Figure 10.6 FE mesh for plane strain hyperelastic consolidation example

the ground surface, and is then held constant while the soil undergoes consolidation. Permeabilities are $k = k_{11} = k_{22} = 8.64\times10^{-4}$ m/day, and $k_{12} = k_{21} = 0$; fluid mass density is $\rho_w = 1.0$ Mg/m^3. The soil elements are assumed to be initially stress-free.

Figure 10.7 shows the closed-form solution for the time-variation of the centerline excess pore pressure at depth z = a beneath the strip load on a semi-infinite elastic half space [91]. Along with this solution are the predictions of the numerical model. For convenience, the excess pore pressures have been normalized with respect to the strip load intensity Δq according to the expression $(\theta - \theta_0) / \Delta q$, where θ_0 is the reference

hydrostatic Cauchy pore pressure. The point corresponding to z = a in the mesh of Figure 10.6 is node A, which is situated at a depth of 5 m from the base of the embankment. The small strain FE solution readily provides the time variation of the pore pressure at this point, since node A is a pore pressure node. However, the large strain model needs the values of the Jacobian to determine the Cauchy pore pressures, which are not readily

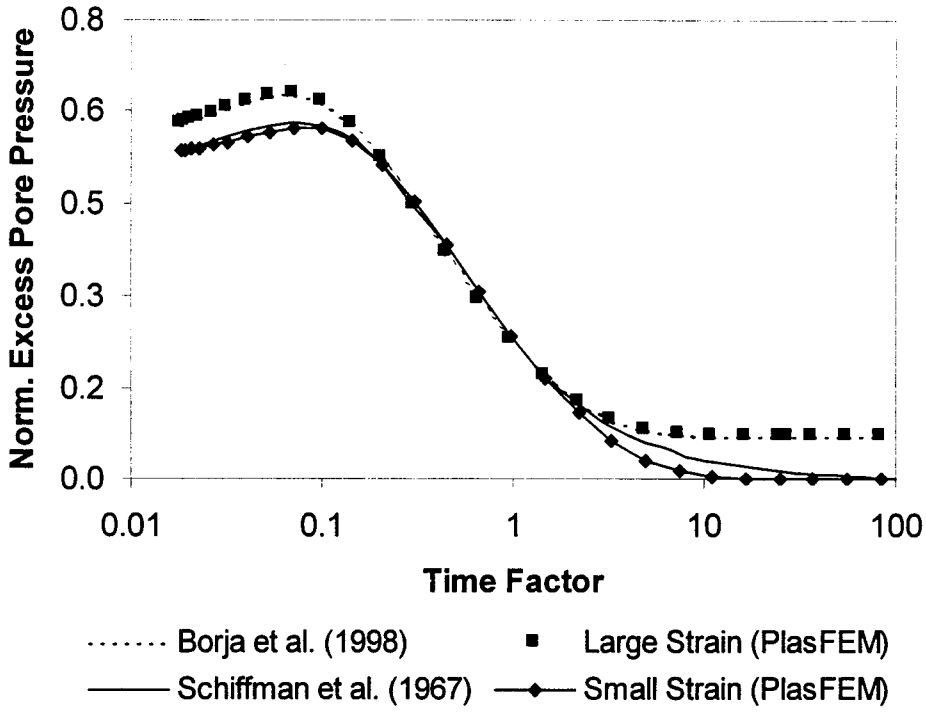

Figure 10.7 Plane strain hyperelastic consolidation: variation of centerline excess pore pressure at depth z = a with time

available at the nodal points. The nearest Gauss point to node A is chosen to assess the accuracy of the numerical model. For consistency in presentation, both the small strain and large strain FE solutions are evaluated at Gauss point B located at horizontal and vertical distances of 0.211m from node A, see Figure 10.6. A normalized time factor, T =

ct / a^2, where $c = 2\mu k / (\rho_w g)$ and t is elapsed time since the beginning of the consolidation, is used to describe the solutions in the time domain. Large strain prediction matched well with the results of [89].

A comparison of the curves shown in Figure 10.7 suggests that higher pore pressures are induced in the large strain case by the sudden application of the external load at the early stage of the consolidation process. Thereafter the dissipation occurs at almost the same rate up to a time factor $T \approx 5.0$, when the large strain solution stabilizes while the small strain solution is still decreasing. Note that the large strain solution asymptotically approaches a nonzero excess pore pressure since the final steady-state pore pressure is numerically different from the initially hydrostatic pore pressure due to variation in the geometric configuration of the problem. As expected, the small strain FE solution agrees better with the closed-form solution, but is not identical because of the limitation of the FE model in representing a half space and because of the use of a finite time increment to impose the strip load, among other factors. Both the closed-form and FE solutions exhibit the Mandel-Cryer effect, or the initial increase in excess pore pressure, which is a characteristic feature of the coupled solution [60].

Figure 10.8 shows the isochrones of constant Cauchy pore pressures predicted by the small and large strain models along the vertical line $X_1 = 0.211$ m beneath the strip load. This line is defined by the column of Gauss points closest to the axis of symmetry. Note that the large strain solution predicts a steady-state isochrone defined by a nearly straight line with an apparent slope equivalent to a fluid with mass density of about 1.23 Mg/m^3, which is greater than the assumed fluid density of 1.0 Mg/m^3. This is a result of local artesian condition characterized by steady-state upward seepage created by the

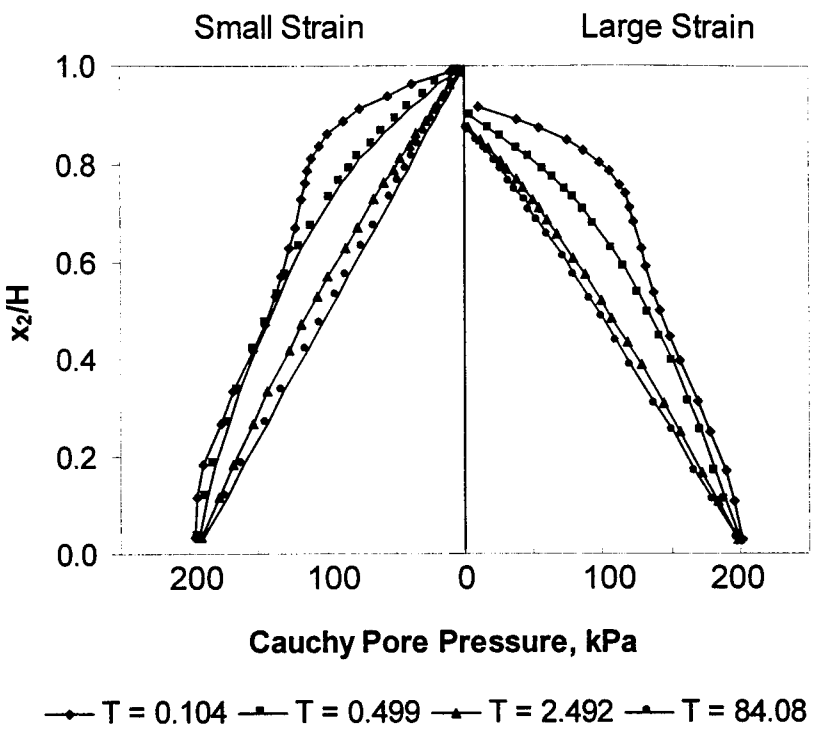

Figure 10.8 Plane strain hyperelastic consolidation: isochrones of constant Cauchy pore pressure

reduction in thickness of the consolidating layer, as the top and bottom drainage boundary conditions remain unchanged. The Cauchy pore pressure at the bottom boundary converges toward a steady-state value that is slightly higher than the initial value. This is a consequence of prescribing the essential boundary condition in the form of Kirchhoff pore pressure, which is amplified by the inverse of Jacobian that is less than unity due to volumetric compression of the soil.

CHAPTER 11
POLK COUNTY EXPRESSWAY

The Polk County Expressway is a multi-lane toll expressway constructed around Lakeland, Florida. The length of the expressway is about 39.4 km (24.5 miles). Major parts of the road construction crossed land areas that had retention ponds of phosphatic waste clay, deposited approximately 40 years ago as slurry from the phosphate beneficiation process. This chapter discusses the numerical predictions using finite element analysis of both primary (consolidation and swell) and secondary (creep) consolidation settlement of the phosphatic waste clay found in the construction site, in the presence of vertical wick drains and subject to surcharge loading, unloading and subsequent reloading (i.e., road construction).

Two different constitutive relations, hyperelastic-plastic MCC and hyperelastic-viscoplastic MCC models, are used for prediction of nonlinear responses of the soil skeleton of the phosphatic waste clay. The first addresses inviscid (time-independent) plasticity, i.e., for a given effective stress, deformation of the soil skeleton is constant over time. This is evident in Figures 11.18 to 11.20 where settlement reaches an equilibrium state once the excess pore pressure due to preloading has dissipated and the clay deposits have attained static effective stresses. The second model simulates the secondary compression response of the clay. Secondary compression (or creep settlement) continues even after the excess pore pressures have significantly dissipated (see Figures 11.23 to 11.25) since the stress-deformation response of the clay skeleton is

usually time-dependent, i.e., clay deposits under sustained effective stress undergo a slow rate of compression over a long period of time.

In the case of very thin specimens such as those used in laboratory consolidation tests, compression usually occurs in two distinct phases (see Figure C.1): an instantaneous primary consolidation and a delayed secondary compression. For specimens of finite thickness, e.g., retention ponds of phosphatic waste clay, the instantaneous and delayed effects are both present during the primary consolidation phase. Secondary compression becomes predominant after dissipation of most of the excess pore pressures.

11.1 Phosphatic Waste Clay

Phosphate, the primary source of phosphorous in inorganic fertilizers, is obtained from mining. The matrix of the excavated material is typically composed of 1/3 phosphate, 1/3 granular materials (sand), and 1/3 clays (montmorillonite, illite, and kaolinite) [84]. The beneficiation process converts the matrix to a dilute solution from which the phosphate is skimmed, and the granular material screened, leaving a dilute clay slurry for disposal.

Initially, the slurry (at the construction site of the Expressway) was introduced to mine cuts with a solid content of about 5%. Over the years the clay deposits underwent self-weight consolidation rendering higher solid content. At the time of the expressway construction the solid contents were in the range of 33% to 50% and the natural moisture contents were in the range of 100% to 200%.

Crucial to numerical simulations is the obtaining of representative material properties for use in the proposed constitutive models (Chapters 5 and 6). Studies of soil characteristics, both field and laboratory, performed by PSI (a geotechnical consulting firm), FDOT's Materials Office and the University of Florida's Geotechnical Centrifuge Laboratory were utilized for this purpose. A brief summary of soil characteristics data, obtained from different sources, is presented in the following.

Soil characterization conducted by PSI in 1995 classified the phosphatic waste clay as very soft with SPT blow counts typically ranging from 2 to 4. The average depths of the slime deposits were on the order of 7.6 m (25 feet) and were underlain by undisturbed soils. In some cases slime deposits were close to the existing ground surface, but in several cases they were overlain by 0.9 to 2.1 m (3 to 7 feet) of very loose to loose clayey sand spoils which were knocked over from spoil mounds during reclamation. Hard, indurated clay/silts were found at depth ranging from 9.1 to 13.7 m (30 to 45 feet). PSI concluded the following soil properties from both insitu and laboratory tests. The unit weight was in the order of 11.80 to 13.36 kN/m^3. The field vane shear strength in the area of interest varied from 12.3 to 22.3 kPa. The tri-axial undrained shear strength varied from 4.8 to 27.6 kPa. Wide variation was noticed in the field vane and tri-axial shear strengths depending on the site or location of the soil specimens. Series of laboratory consolidation tests were conducted by PSI at two different stages: initially at the reconnaissance stage and later after the placement of the surcharge loading. Summaries of these test results are presented in Tables 11.1 and 11.2 and corresponding SPT boring logs are shown in Figures 11.1 and 11.2, respectively.

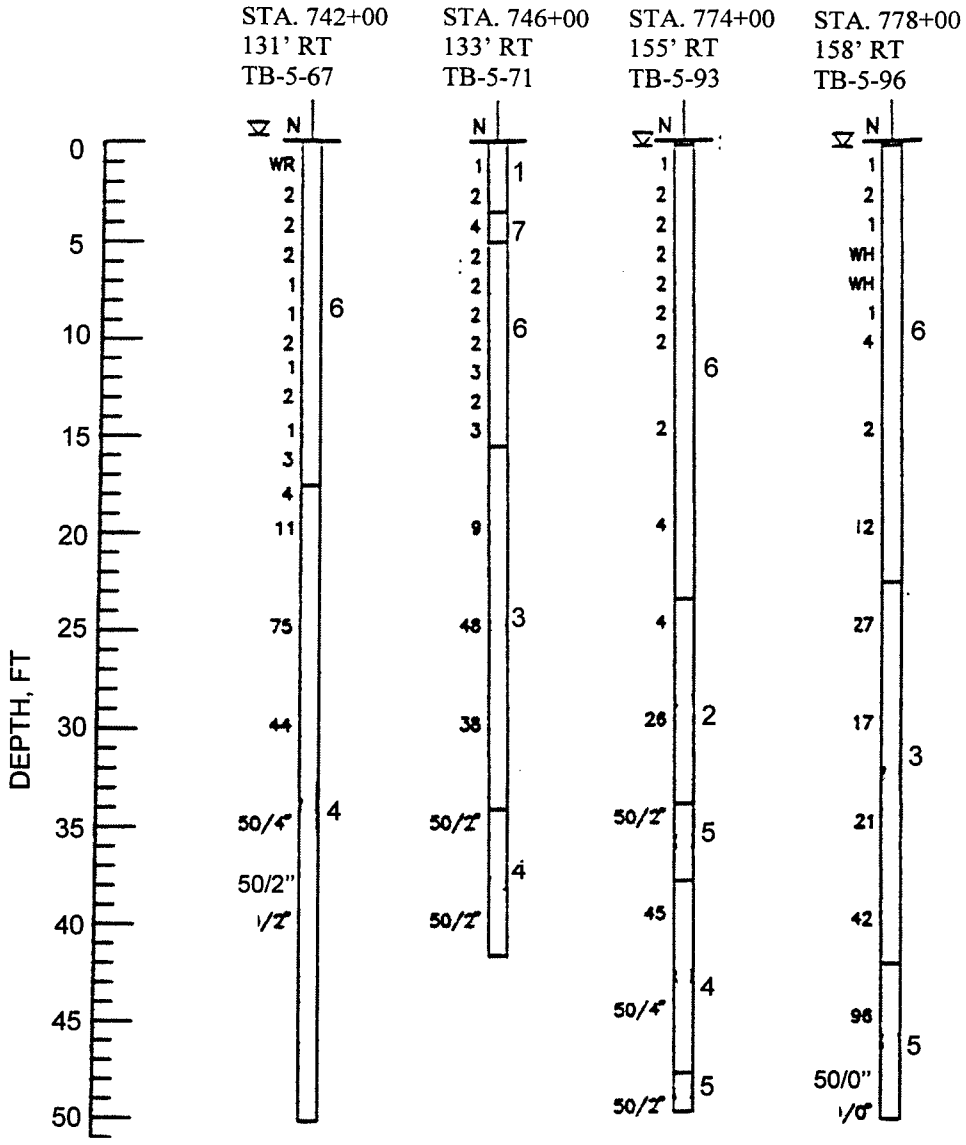

LEGEND

1 Mixed grayish-brown sand, trace silt and light gray clayey fine sand, (A-2-6)
2 Light brown to greenish-gray sand, some silt to silty fine sand, trace phosphates, limestone and cemented sands, (A-2-4)
3 Light greenish-gray to orangish-brown sandy silt to clayey silt, trace phosphates, (A-7-5)
4 Light gray to orangish-brown indurated clay/silt, trace phosphates, (A-4), (A-7-6)
5 Light gray limestone
6 Light greenish-gray to brown phosphatic clay slime, (A-7)
7 Brown to greenish-gray sandy clay, (A-6), (A-7-5), (A-7-6)

Figure 11.1 SPT boring logs for tests reported in Table 11.1 (Source: PSI)

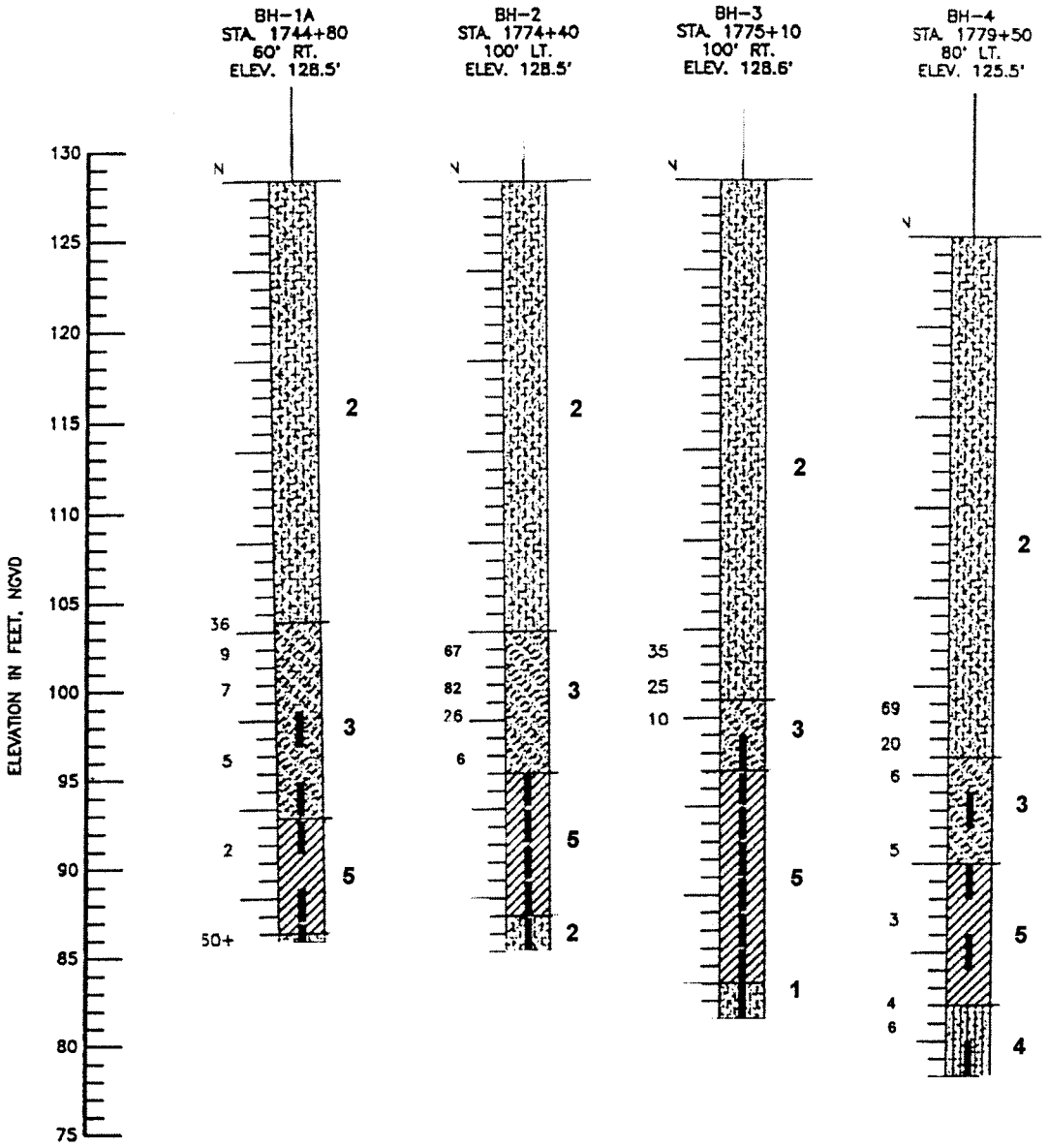

LEGEND

1 Grayish-brown sand, some silt to silty sand, (A-2-4)
2 Grayish-brown slightly silty fine sand to fine sand, (A-3), (A-2-4)
3 Light gray to greenish-gray, sand, some clay to clayey fine sand, trace phosphate grains and pebbles, (A-2-4), (A-2-6)
4 Dark greenish-gray silty to clayey sand to sandy clay, (A-2-7), (A-7)
5 Light greenish-gray to brown phosphatic clay slime, (A-7-5)

Figure 11.2 SPT boring logs for tests reported in Table 11.2 (Source: PSI)

Table 11.1 Summary of laboratory consolidation test results (initial exploration)

Test Date	Boring No.	Station No.	Offset	Depth of Shelby Tube	Initial Void Ratio	C_c	Cs	Precon. Pressure (tsf)
07/28/92	TB-5-67	742+00	131′ R	10′ – 12′	2.09	0.82	0.07	0.83
07/28/92	TB-5-71	746+00	133′ R	10′ – 12′	5.93	2.93	0.25	0.41
07/28/92	TB-5-93	774+00	155′ R	10′ – 12′	7.67	3.76	1.00	0.30
07/28/92	TB-5-96	778+00	158′ R	10′ – 12′	5.50	2.90	0.41	0.26

Table 11.2 Summary of laboratory consolidation test results (later exploration)

Test Date	Boring No.	Station No.	Offset	Depth of Sample	Initial Void Ratio	C_c	C_s	Precon. Pressure (tsf)
08/01/97	BH-1A	1744+80	60′ R	36′0″	2.38	0.95	0.215	1.48
08/25/97	BH-2	1774+40	100′ L	38′0″	3.40	1.51	0.36	1.47
07/31/97	BH-3	1775+10	100′ R	36′0″	2.97	1.33	0.37	1.68
08/14/97	BH-4(1)	1779+50	80′ L	36′0″	3.46	4.01	0.25	1.13
08/01/97	BH-4(2)	1779+50	80′ L	40′0″	3.41	1.55	0.462	1.05

The station numbers reported in Table 11.1 are survey baseline stations which were numbered differently from construction stations of Table 11.2. Survey baseline stations 742+00 to 778+00 are the same as construction centerline stations 1742+00 to 1778+00.

The centrifuge tests performed at the University of Florida revealed that the clays would not clog as a result of the consolidation process (i.e., sealing the drainage boundary). The following parameters were determined from centrifuge and laboratory tests [92] on recovered clay samples.

The Atterberg limits of the slime were as follows:

Liquid limit (LL): 215%
Plastic limit (PL): 67.15%

Plasticity index (PI): 148.85%

Water contents, determined before each individual test, were in the order of 190% to 205%. Solid contents for the recovered samples were consistently in the order of 33%. The specific gravity was estimated as 2.70. This is recognized as a reasonable value for phosphatic clays [93]. Void ratios, determined prior to each test, typically ranged from 4 to 5.5. A series of CRS (constant rate of strain) consolidation tests was performed to study correlations among void ratio, effective stress, coefficient of permeability, coefficient of consolidation, etc. Figure 11.3 and 11.4 present variations of coefficient of

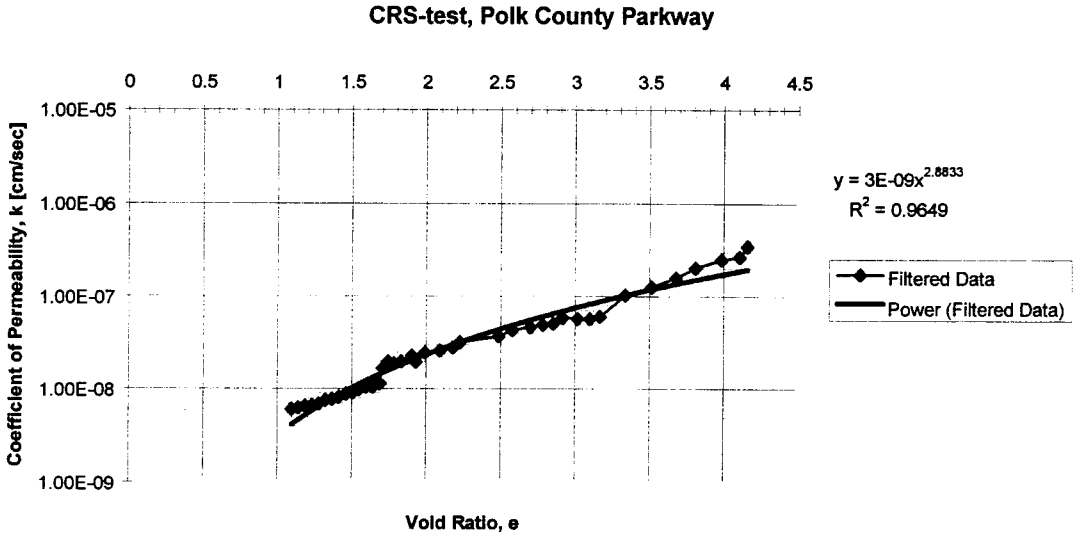

Figure 11.3 Permeability versus void ratio plot from CRS consolidation test

permeability and average effective stress with void ratio, respectively. See [92] for study of the other test results.

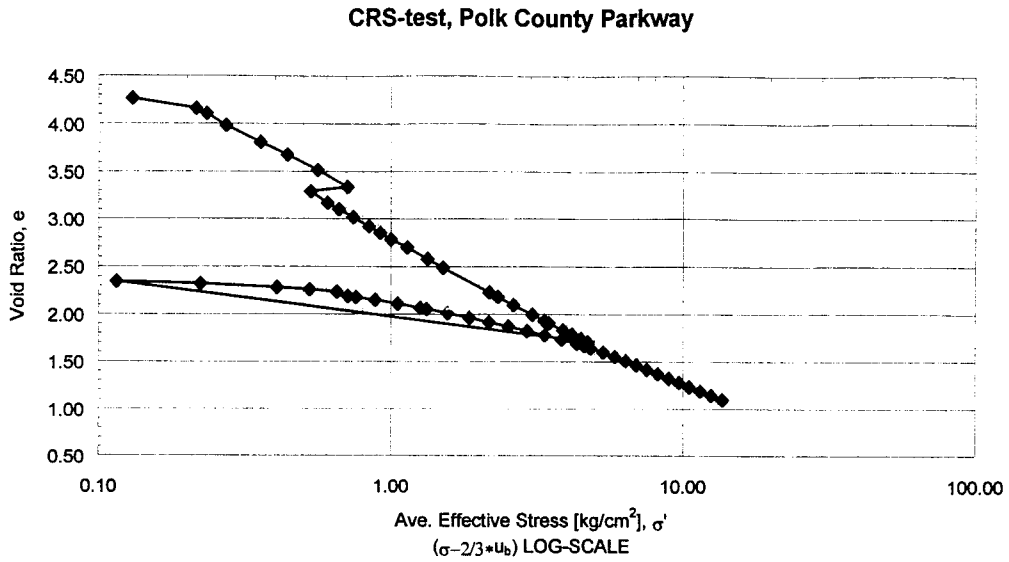

Figure 11.4 Void ratio versus effective stress plot from CRS consolidation test

11.2 Wick Drain and Instrumentation

To facilitate faster consolidation, an embankment acting as surcharge of 4.6 to 7.6 m (15 to 25 ft) of sand was placed on top of the existing ground surface of the slime deposit area. The surcharge load was aided by vertical wick drains, approximately 30,000 in number, installed in a triangular pattern with side lengths of 1.52 m. Figure 11.5 shows a plan of the wick drain installation. The wick drains, consisted of a polypropylene core of fluted configuration, designed for flexibility and maximum water flow. The permeability of the geotextile membrane surrounding the plastic core was 1.48×10^{-1} m/day. A schematic of the consolidation process through the wick drains is shown in Figure 11.6.

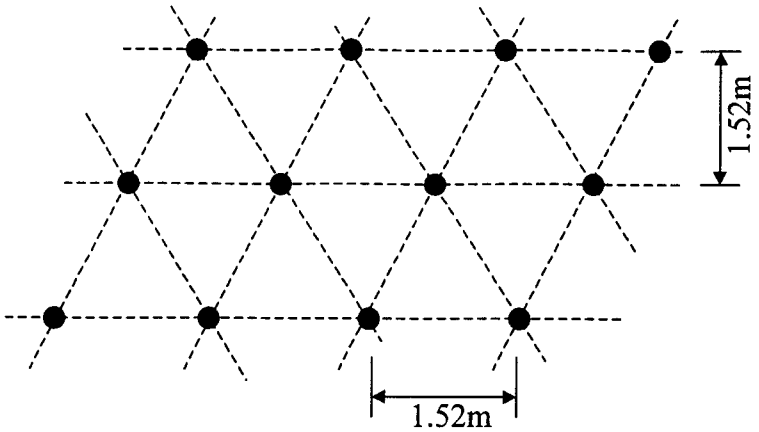

Figure 11.5 Plan of wick drain installation

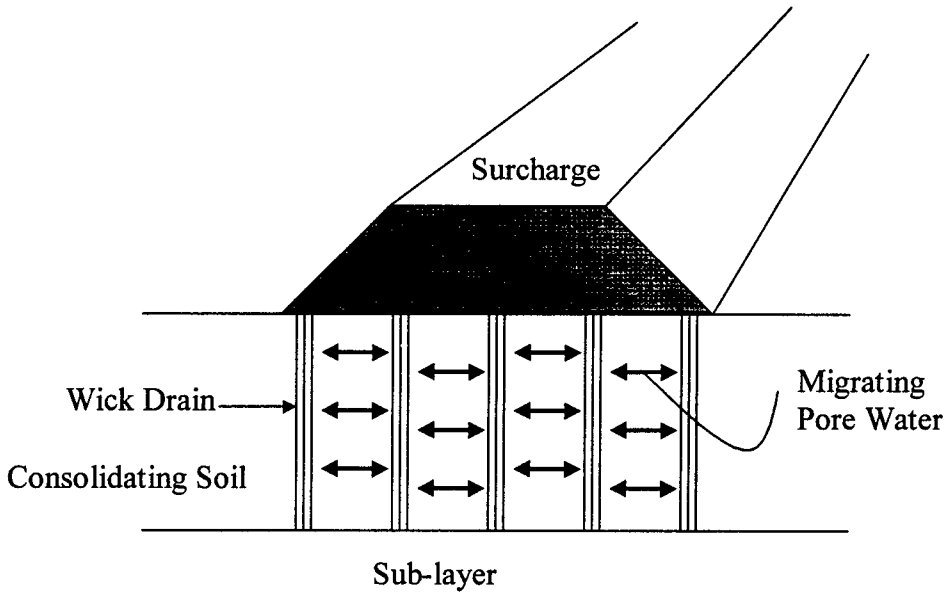

Figure 11.6 Principle of consolidation with wick drains

Surcharge Area No.1 (station 1727 to 1746) and Surcharge Area No. 2 (station 1768 to 1782) of the Polk County Expressway, Section 5, were instrumented by Atlanta

Testing & Engineering (a geotechnical consulting firm) for monitoring field settlements and pore pressures. Figures 11.7 and 11.8 show the instrumentation plans. Instrumentation included settlement plates, pneumatic settlement cells, piezometers, and vertical inclinometers. Monitoring was carried out over a period of approximately 700 days from the beginning of embankment placement. Field observation data were subsequently compared with numerical prediction as presented in the following.

11.3 Constitutive Model Parameters

Due to nonlinear elasticity, estimation of appropriate elastic moduli parameters such as μ_0, α, p_0, ε_{v0}^e is crucial for using the constitutive models discussed in Chapters 5 and 6. For this purpose, laboratory one-dimensional consolidation (oedometer) tests were simulated to obtain the constitutive model parameters for primary and secondary consolidation. The hyperelastic-plastic MCC model was used for the prediction of primary consolidation only while the hyperelastic-viscoplastic MCC model was used to predict both primary and secondary consolidation. A FE mesh for the oedometer cell (radius 3.18 cm, height 2.54 cm), composed of 2×2 D9P4 axisymmetric elements, is shown in Figure 11.11.

Figures 11.12 and 11.13 present the predictions and measurements of laboratory void ratio vs. log (applied pressure) response for large and small strain primary

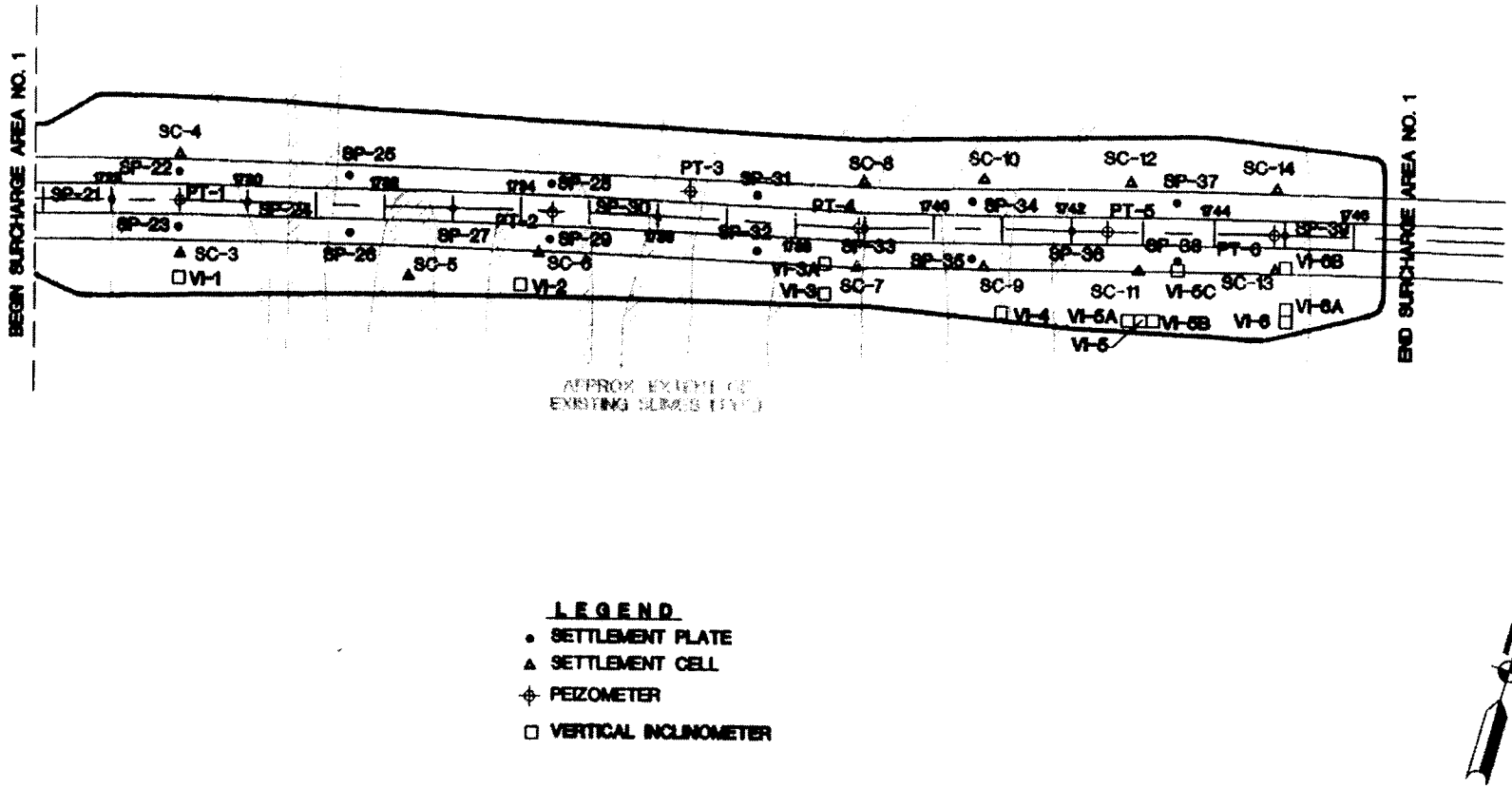

Figure 11.7 Instrumentation plan: surcharge area no. 1 of Polk County Expressway, Section 5
(Source: Atlanta Testing & Engineering)

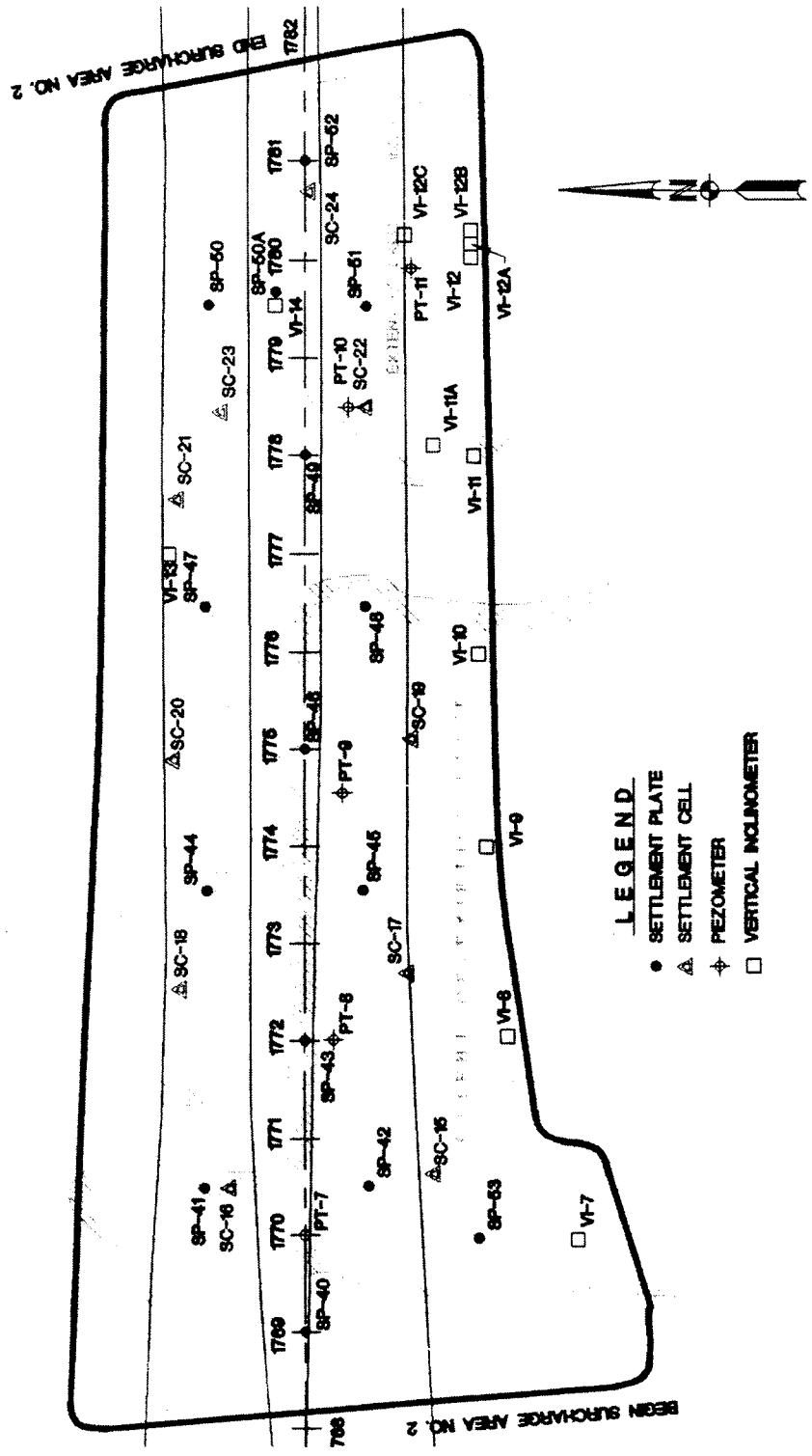

Figure 11.8 Instrumentation plan : surcharge area no. 2 of Polk County Expressway, Section 5
(Source: Atlanta Testing & Engineering)

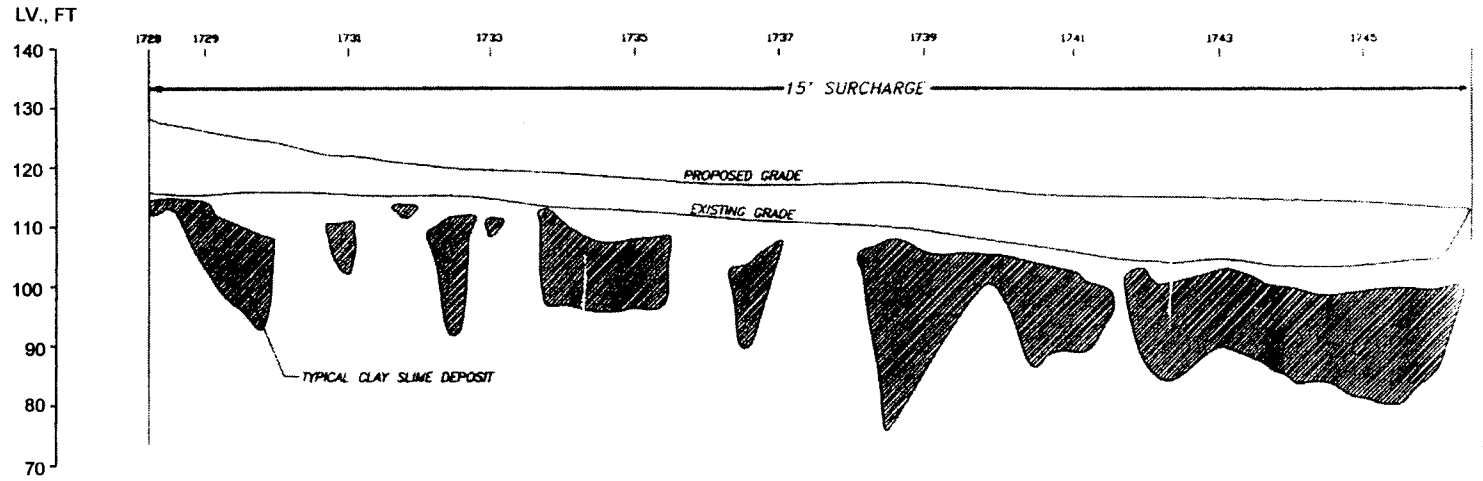

Figure 11.9 Cross-section of clay slime ponds in surcharge area no. 1
(Source: PSI)

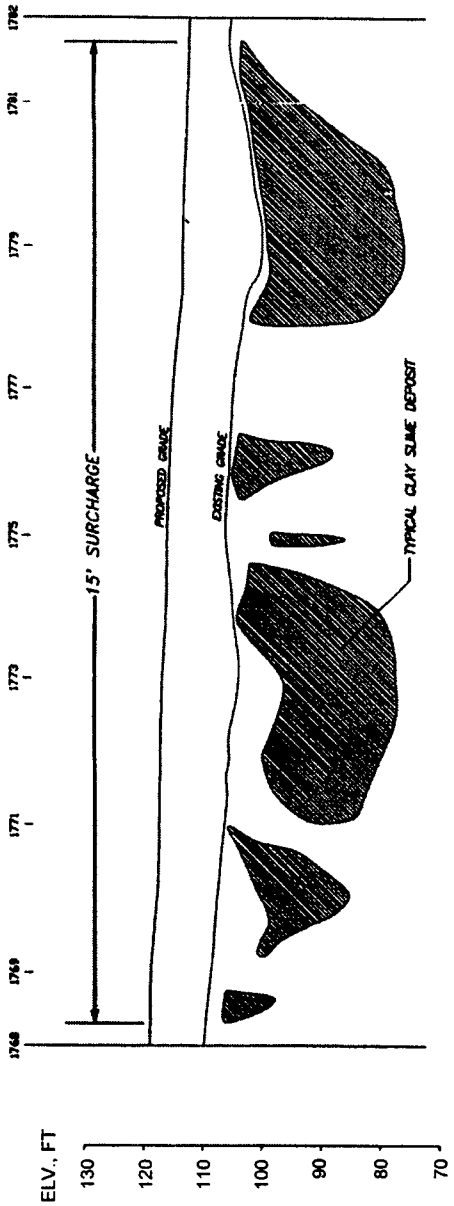

Figure 11.10 Cross-section of clay slime ponds in surcharge area no. 2
(Source: PSI)

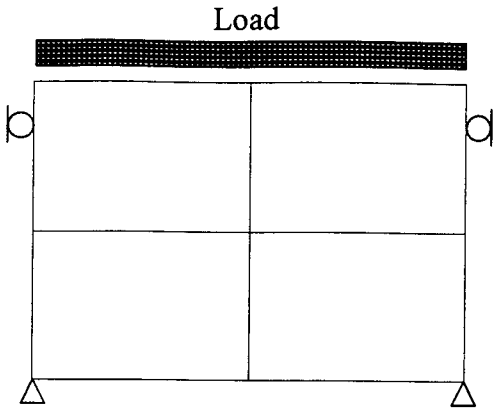

Figure 11.11 FE mesh for oedometer cell

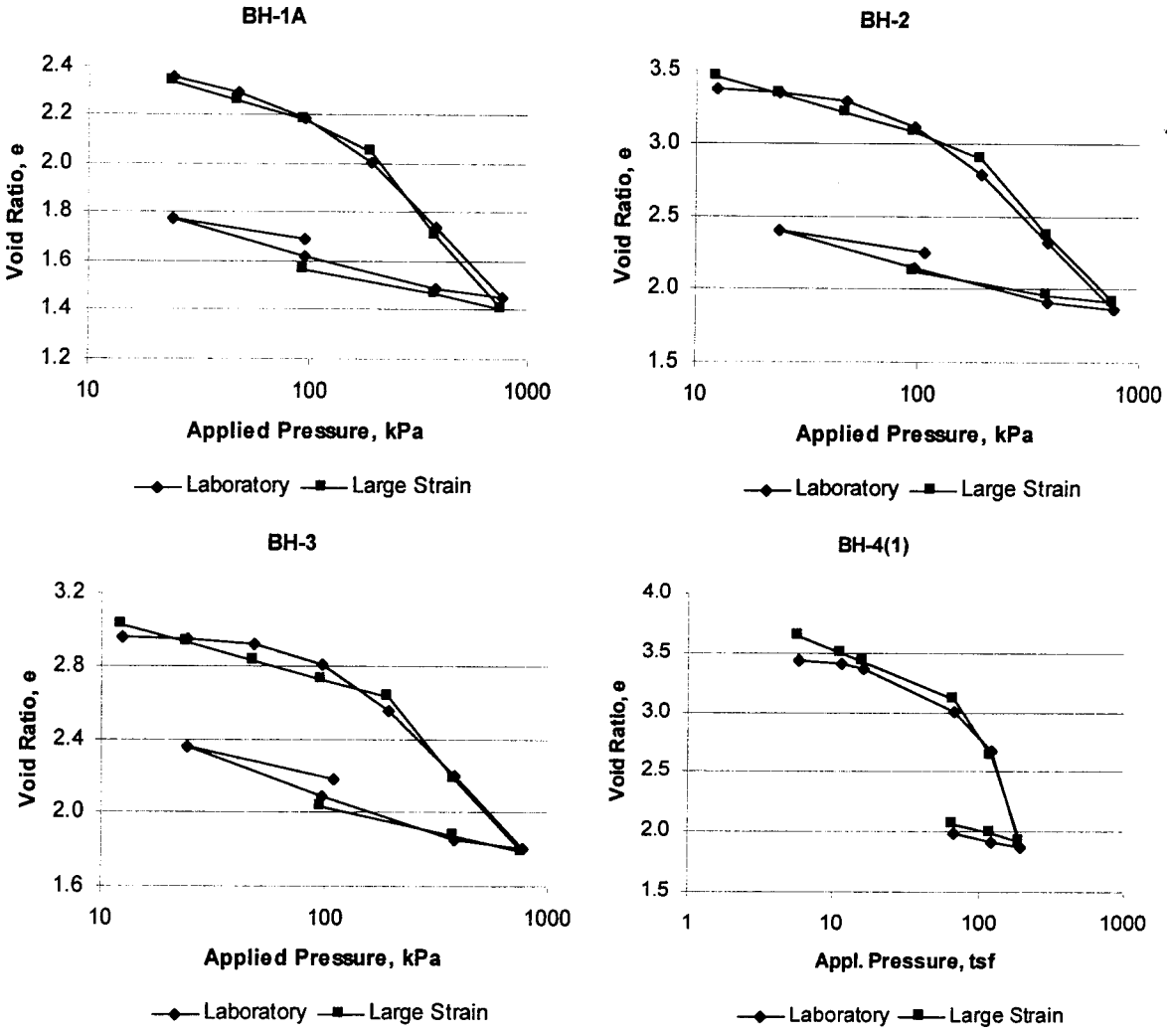

Figure 11.12 Large strain, hyperelastic-plastic simulation of laboratory consolidation tests

consolidation, respectively. Table 11.2 contains a summary of the laboratory consolidation test results. Constitutive model parameters, used for the simulation of laboratory results, are presented in Tables 11.3 and 11.4. For all the simulations it was

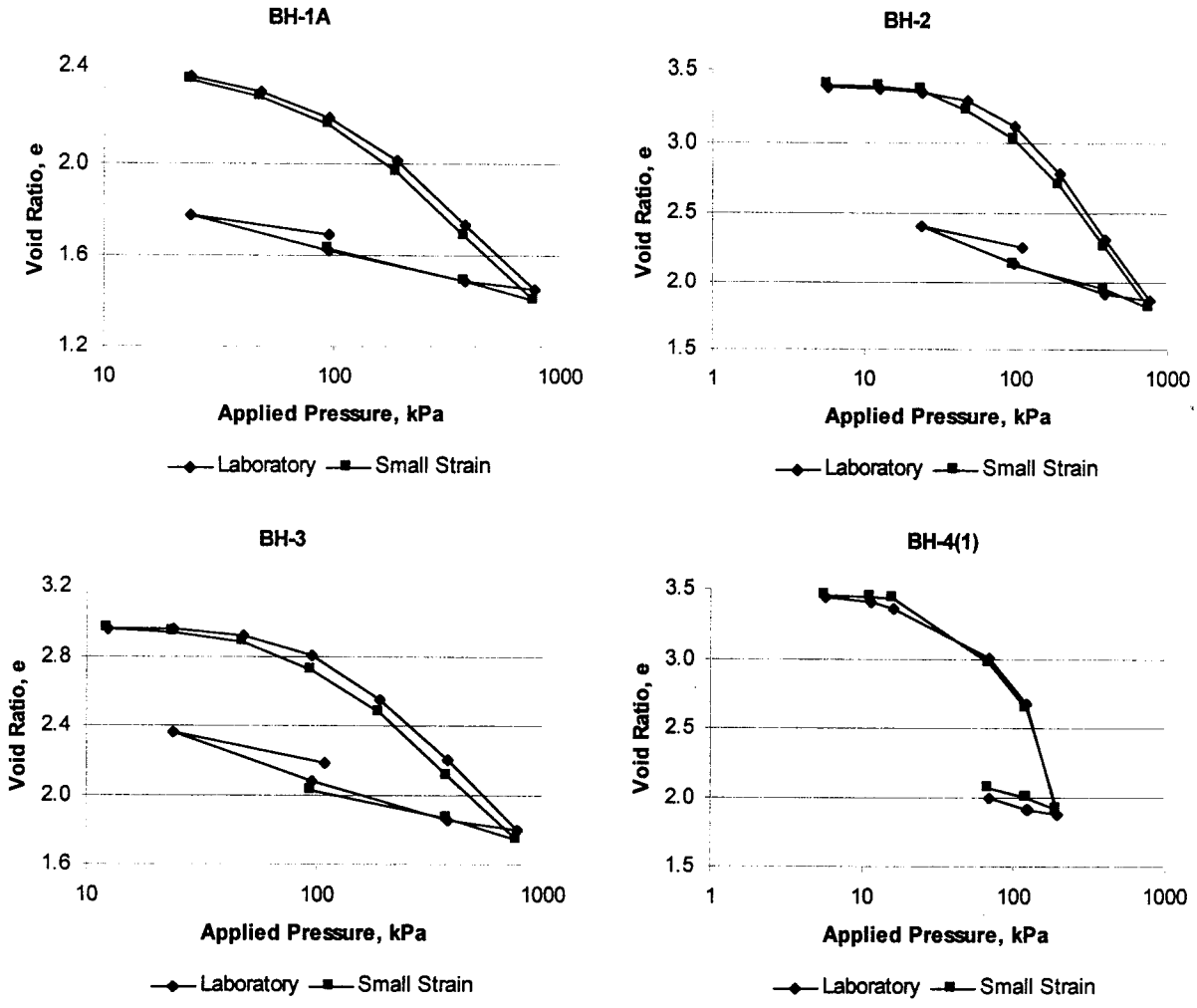

Figure 11.13 Small strain, hyperelastic-plastic simulation of laboratory consolidation tests

assumed that the critical state slope M =1.0, $\varepsilon^{e}_{v0} = 0.0$, saturated unit weight of clay γ_{sat} = 12.58 kN/m^3. The permeability coefficient k was assumed to have a constant value of 6.9×10^{-5} m/day. See Figure 11.3 for estimation of permeability coefficient.

Preconsolidation pressures p_{c0} (see Table 11.2) were obtained from the laboratory test plots using the Casagrande construction method.

Note that the MCC model's compressibility parameters λ and κ are different from the C_s and C_r (compression and swell indices, respectively) of the laboratory test data (see Tables 11.3 and 11.4) due to the different stress paths. λ and κ are defined for isotropic loading while C_s and C_r are obtained from the one-dimensional consolidation test (K_0 condition [64]). Also note in Tables 11.3 and 11.4 that the λ and κ for small strain were slightly different than those for large strain in order to produce similar stress-deformation responses. Since the large strain model updates geometry whereas the small doesn't, the stresses which are function of geometry, will be different unless the stiffness is adjusted.

Table 11.3 Hyperelastic-plastic MCC model parameters for large strain simulation of laboratory consolidation tests

Boring No.	μ_0 (kPa)	α	p_0 (kPa)	λ	κ	Laboratory Data	
						C_c	C_s
BH-1A	25.0	1.0	0.8	0.22	0.04	0.95	0.215
BH-2	25.0	1.0	0.6	0.28	0.05	1.51	0.36
BH-3	25.0	1.0	1.2	0.25	0.045	1.33	0.37
BH-4(1)	25.0	1.0	0.5	0.43	0.065	4.01	0.25

Table 11.4 Hyperelastic-plastic MCC model parameters for small strain simulation of laboratory consolidation tests

Boring No.	μ_0 (kPa)	α	p_0 (kPa)	λ	κ	Laboratory Data	
						C_c	C_s
BH-1A	25.0	1.0	0.8	0.12	0.036	0.95	0.215
BH-2	25.0	1.0	0.6	0.145	0.048	1.51	0.36
BH-3	25.0	1.0	1.2	0.135	0.045	1.33	0.37
BH-4(1)	25.0	1.0	0.5	0.40	0.065	4.01	0.25

Table 11.5 presents material parameters for the large and small strain simulations of the laboratory consolidation test that produce similar stress-deformation responses (Figure 11.14). The λ and κ values in Table 11.5 fall within the range of values presented

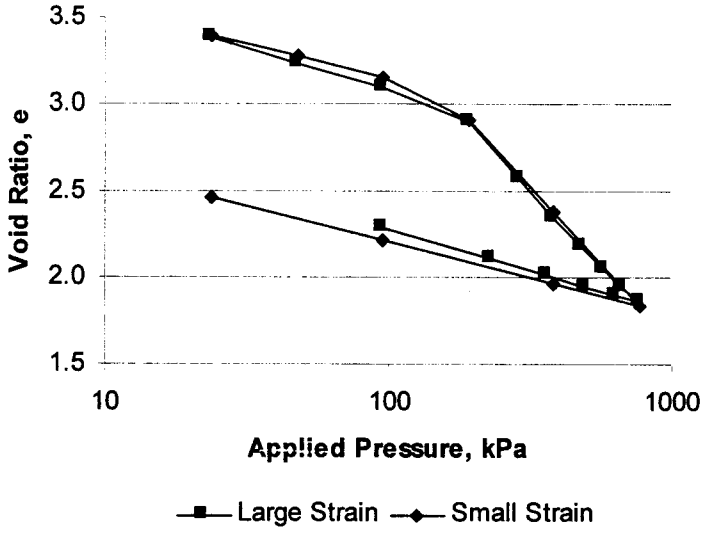

Figure 11.14 Hyperelastic-plastic simulation of laboratory consolidation test: large strain versus small strain

Table 11.5 Hyperelastic-plastic MCC model parameters for simulation of laboratory consolidation test

Parameter	Large Strain	Small Strain
μ_0 (kPa)	25.0	25.0
α	1.0	1.0
κ	0.06	0.05
λ	0.3	0.18
M	1.0	1.0
p_0 (kPa)	1.0	1.0
p_{c0} (kPa)	142.0	142.0
ε_{v0}^{e}	0.0	0.0
γ_{sat} (kN/m^3)	12.58	12.58

in Tables 11.3 and 11.4. As a result, this set of λ and κ values are used for subsequent predictions of field primary consolidation data for different pond depths.

Figure 11.15 presents predictions and measurements of laboratory axial strain rate data, primary and secondary consolidation combined, for the case of the large strain

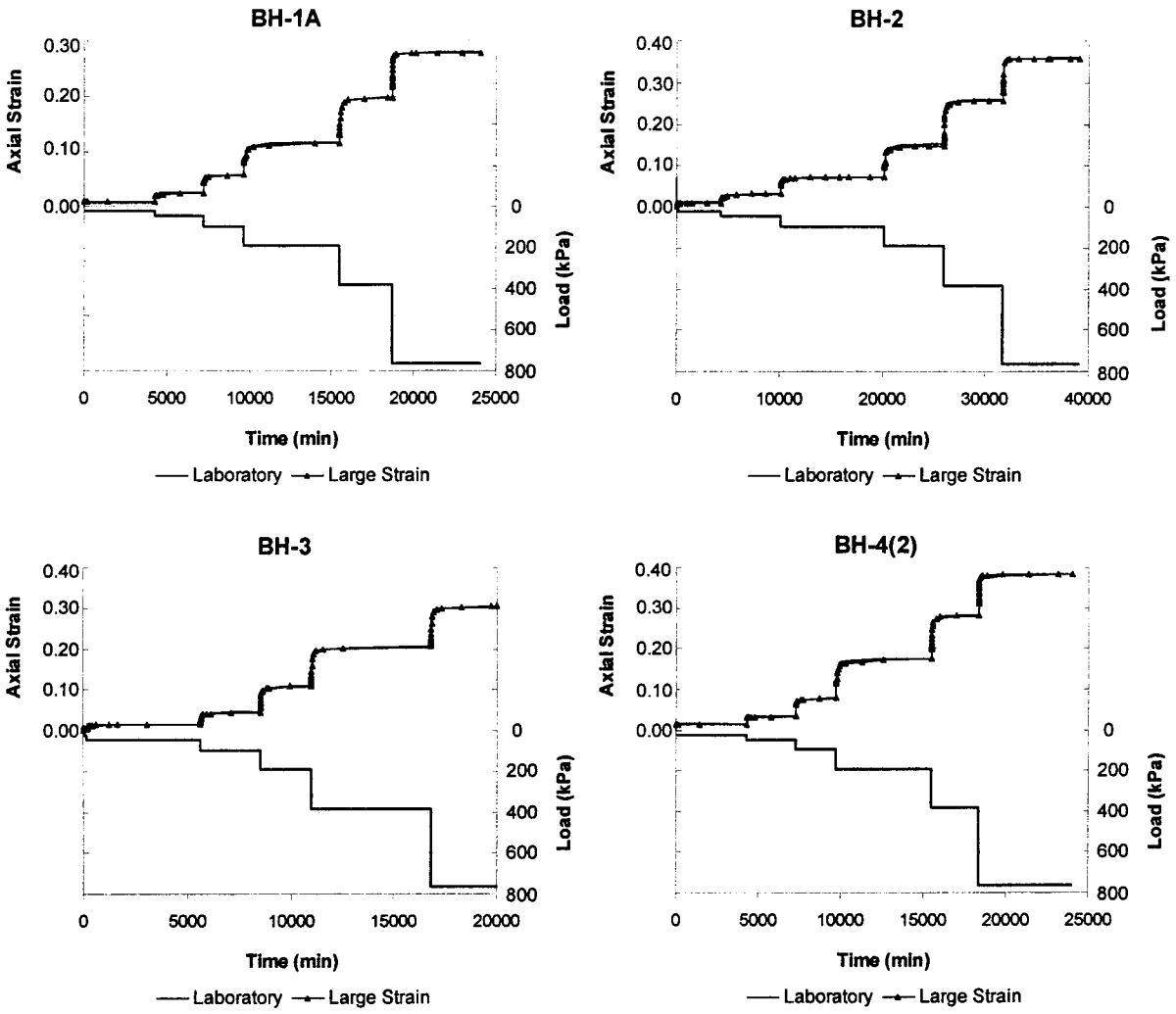

Figure 11.15 Large strain, hyperelastic-viscoplastic simulation of laboratory consolidation tests

Table 11.6 Hyperelastic-viscoplastic MCC model parameters for large strain simulation of laboratory consolidation tests

Boring No.	μ_0 (kPa)	α	P_0 (kPa)	γ	N	λ	κ	Laboratory Data	
								C_c	C_s
BH-1A	25.0	1.0	0.8	7.0×10^{-7}	1.5	0.12	0.036	0.95	0.215
BH-2	25.0	1.0	0.6	7.0×10^{-7}	1.8	0.145	0.048	1.51	0.36
BH-3	25.0	1.0	1.2	7.0×10^{-7}	1.5	0.135	0.045	1.33	0.37
BH-4(2)	25.0	1.0	0.5	7.0×10^{-7}	1.8	0.40	0.06	1.55	0.462

formulation. The viscoplastic constitutive model parameters used for the simulation are presented in Table 11.6. To be consistent with the elasto-plastic simulation, it was assumed that M =1.0, $\varepsilon_{V0}^{e} = 0.0$, $\gamma_{sat} = 12.58$ kN/m^3 and $k = 6.9\times10^{-5}$ m/day. Preconsolidation pressures p_{c0} were obtained from laboratory test results (see Table 11.2).

In the prediction of the laboratory consolidation test data and subsequently, the secondary (creep) settlement of the phosphatic waste clay, the viscous flow function $\varphi(f)$ (see (6.4a), (6.4b)) was normalized as follows

$$\varphi(f) = \left(\frac{f}{2p_{c,n}}\right)^{N}, \tag{11.1}$$

where $p_{c,n}$ is the converged preconsolidation pressure at the previous load step n. Use of a power function for $\varphi(f)$ did a better job matching the laboratory axial strain rate profile than an exponential function. Tables C.1 to C.4 show that the contribution of the secondary settlement to the total settlement for a sustained load increment in laboratory consolidation tests is significant (on average ranging from 8% to 15%). In order to ensure a higher contribution of viscoplastic strain ε^{vp}, the yield function f was normalized

adaptively with $p_{c,n}$ rather than a constant value so that product term $\gamma\varphi(f)$ of (6.2) remains small resulting in a yield condition.

Also notice that the compressibility parameters λ and κ for the viscoplastic model are slightly lower, thus resulting in a higher hardening modulus $\Theta = 1/(\lambda - \kappa)$ (see $(5.24)_2$), than in the elasto-plastic model, even though both formulations produced similar stress-deformation responses (compare between Tables 11.3 and 11.6). This phenomenon can be explained from analytical expressions of incremental strain in the plastic regime, since the hyperelasticity responses are identical for both the constitutive models. Incremental volumetric plastic strains are given by the following expressions for the viscoplastic and elasto-plastic MCC models, respectively (see (6.3) and $(5.29)_1$ for reference).

$$\Delta\varepsilon_v^{vp} = \Delta\gamma\varphi(f)\frac{\partial f}{\partial p} = \Delta\gamma\varphi(f)(2p - p_c). \tag{11.2a}$$

$$\Delta\varepsilon_v^{p} = \Delta\varphi\frac{\partial f}{\partial p} = \Delta\varphi(2p - p_c). \tag{11.2b}$$

For the same stress level, i.e., for a given value of p, $\Delta\gamma\varphi(f)$ of (11.2a) is consistently lower than $\Delta\varphi$ of (11.2b). Now, in order to produce similar value of incremental volumetric plastic strain, $(p_c)_{vicoplastic} < (p_c)_{elasto\text{-}plastic}$; $(\Delta p_c/p_c)_{vicoplastic} < (\Delta p_c/p_c)_{elasto\text{-}plastic}$. Consequently, $(\lambda - \kappa)_{viscoplastic} < (\lambda - \kappa)_{elasto\text{-}plastic}$ (see (5.24)).

11.4 FE Mesh

Due to the variability of the depths of the clay slime deposit (see Figures 11.9 and 11.10), three different pond depths: 2.44m, 4.57m, and 7.62m (8 ft, 15ft and 25 ft), were selected for FE meshes. Surcharge area no.2 had thicker slime deposit ponds then

surcharge area no.1 (compare Figures 11.9 and 11.10). Accordingly, a 7.62 m deep pond was selected for simulation of field data of the settlement cells located in surcharge area no.2. 2.44 m and 4.57 m deep ponds represented the slime deposits of surcharge area no.1. Tables 11.7 to 11.9 list the settlement cells and plates (see Figures 11.7 and 11.8 for their locations) that were represented by FE meshes of different pond depths.

Table 11.7 Settlement cells/plates represented by 2.44 m deep pond

Cell/Plate No.	Station No.	Offset	Max. Surcharge Height (m)
SC-5	1732+50	100' R	7.16
SP-23	1729+00	45' R	8.20
SP-33	1739+00	0	6.37
SP-37	1743+50	45' L	6.04

Table 11.8 Settlement cells/plates represented by 4.57 m deep pond

Cell/Plate No.	Station No.	Offset	Max. Surcharge Height (m)
SC-9	1740+50	50' R	6.58
SC-11	1743+00	70' R	6.52
SC-13	1745+00	80' R	6.55
SP-36	1742+00	0	6.40
SP-38	1743+50	45' R	6.52
SP-39	1745+00	0	6.55

Table 11.9 Settlement cells/plates represented by 7.62 m deep pond

Cell/Plate No.	Station No.	Offset	Max. Surcharge Height (m)
SC-17	1772+50	130'R	8.23
SC-18	1772+50	130'L	8.35
SC-20	1775+00	120'L	7.89
SC-21	1777+50	120'L	7.68
SC-23	1778+00	100'L	8.08

The meshes, comprised of axisymmetric D9P4 elements, are shown in Figure 11.17. Left vertical boundaries of the meshes are exposed to wick drains and so are subject to prescribed hydrostatic pore water pressures. The equivalent diameter of the cylinder of soil around each drain, shown in Figure 11.16, in the case of a triangular installation pattern (see Figure 11.5) is calculated as D = 1.06s = 1.61 m [94], where s is the spacing of the wick drain (= 1.52 m). The equivalent diameter of the wick drain, d_e is calculated as $d_e = 2(B + t)/\pi = 6.56$ cm [94], where B and t are the width and thickness of the wick drains, respectively. B = 10 cm, t = 0.3 cm for the wick drains used in the field. Accordingly, the radial distance of the left vertical boundaries of the meshes from the axis of symmetry is 3.28 cm (equivalent radius of wick drains). Bottom edges are assumed to be rigid, impervious while the top edges are subject to free drainage. Meshes are subdivided in four layers of materials to take into account the variability of material properties with depth, e.g., preconsolidation pressure, shear strength, etc. Layers of elements of any mesh are of equal height.

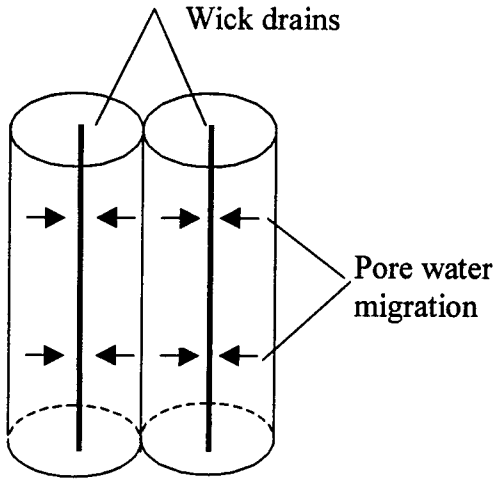

Figure 11.16 Schematic of contributive cylinder of soil surrounding wick drains

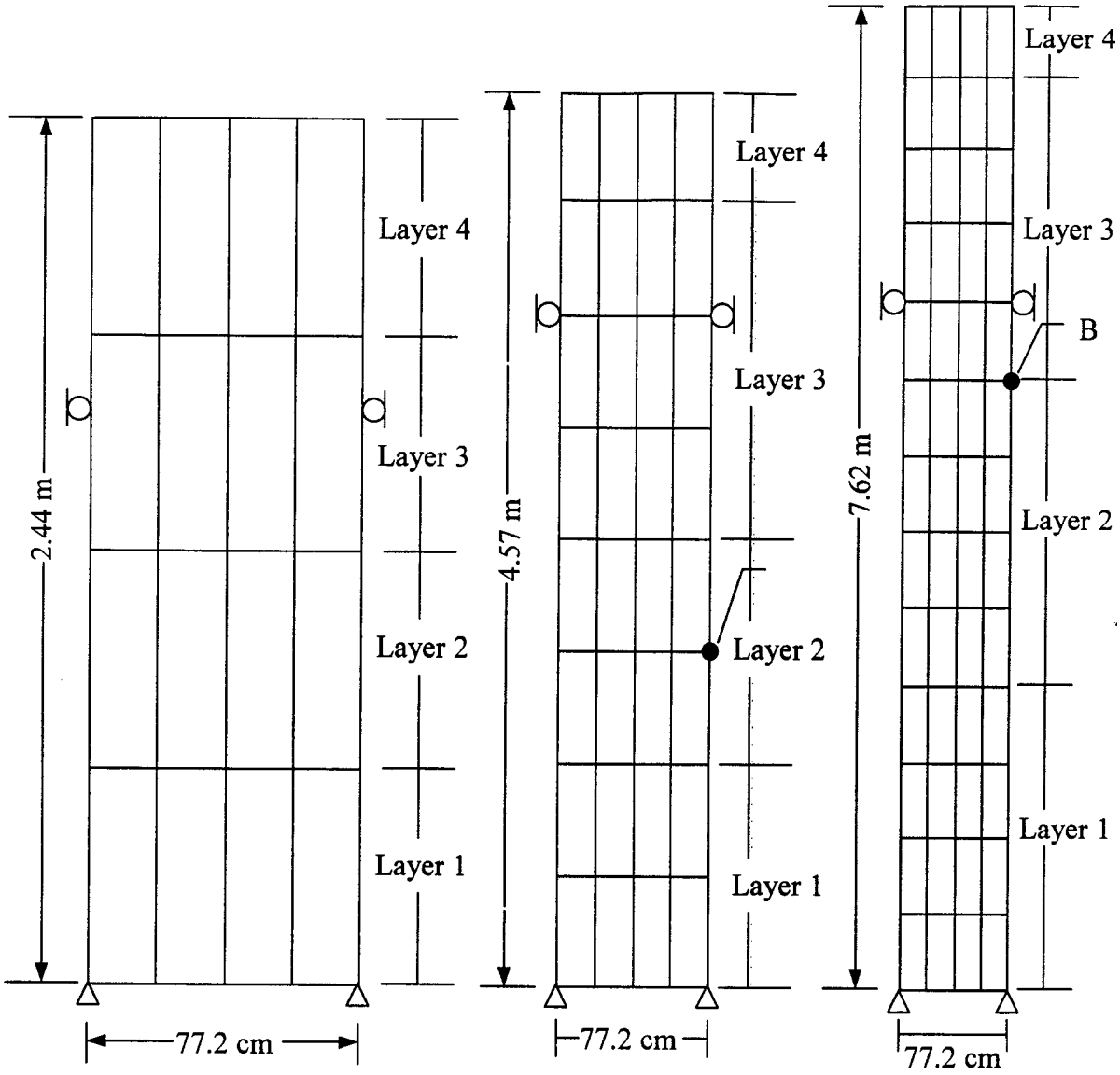

Figure 11.17 FE meshes for different pond depths

11.5 Prediction of Primary Consolidation

Material properties used for the prediction of primary consolidation are presented in Tables 11.10 to 11.12 for the different pond depths. Constitutive model parameters such as: μ_0, α, λ, κ, p_0 are obtained from Tables 11.3 to 11.5. The top layer of the meshes

(height ≈ 0.6 m) was assumed to be slightly overconsolidated due to dessication. As a result, μ_0 and p_{c0} have higher values for the top layers. Values of preconsolidation pressure, p_{c0} are estimated from Table 11.1. Notice that Table 11.1 shows lower p_{c0}, higher initial void ratio and higher C_c than those in Table 11.2. This is because the tests reported in Table 11.1 were performed before the slime deposits were subjected to increased overburden pressure either due to the placement of the surcharge load or fillings during the land reclamation process. Compare the boring logs in Figures 11.1 and 11.2. Consequently, p_{c0} values reported in Table 11.1 represent true estimates of the maximum past preconsolidation pressure of the slime deposits. For all the simulations, both large and small strain, it was assumed that $\varepsilon^e_{v0} = 0.0$ and the initial value (for large strain) of the saturated unit weight, $\gamma_{sat} = 12.58$ kN/m^3. Coefficients of permeability were assumed to be constant: $k_v = k_h = 6.9\times10^{-5}$ m/day.

Table 11.10 Material parameters for hyperelastic-plastic consolidation (pond depth 2.44 m)

Parameter	Layer 1	Layer 2	Layer 3	Layer 4
μ_0 (kPa)	25.0	25.0	25.0	35.0
α	1.0	1.0	1.0	1.0
λ (large strain)	0.3	0.3	0.3	0.3
κ (large strain)	0.06	0.06	0.06	0.06
λ (small strain)	0.18	0.18	0.18	0.18
κ (small strain)	0.05	0.05	0.05	0.05
M	1.0	1.0	1.0	1.0
p_0 (kPa)	1.2	0.8	0.8	0.8
p_{c0} (kPa)	40.0	37.5	35.0	40.0

Table 11.11 Material parameters for hyperelastic-plastic consolidation (pond depth 4.57 m)

Parameter	Layer 1	Layer 2	Layer 3	Layer 4
μ_0 (kPa)	25.0	25.0	25.0	35.0
α	1.0	1.0	1.0	1.0
λ (large strain)	0.3	0.3	0.3	0.3
κ (large strain)	0.06	0.06	0.06	0.06
λ (small strain)	0.18	0.18	0.18	0.18
κ (small strain)	0.05	0.05	0.05	0.05
M	1.0	1.0	1.0	1.0
p_0 (kPa)	1.5	1.0	1.0	1.0
p_{c0} (kPa)	50.0	42.5	37.5	40.0

Table 11.12 Material parameters for hyperelastic-plastic consolidation (pond height 7.62 m)

Parameter	Layer 1	Layer 2	Layer 3	Layer 4
μ_0 (kPa)	25.0	25.0	25.0	35.0
α	1.0	1.0	1.0	1.0
λ (large strain)	0.3	0.3	0.3	0.3
κ (large strain)	0.06	0.06	0.06	0.06
λ (small strain)	0.18	0.18	0.18	0.18
κ (small strain)	0.05	0.05	0.05	0.05
M	1.0	1.0	1.0	1.0
p_0 (kPa)	1.5	1.0	1.0	1.0
p_{c0} (kPa)	60.0	47.5	37.5	40.0

The surcharge load of sand was placed in steps over approximately 305 days and kept for about 180 days before unloading. Based on the existing surface elevation, surcharge height varied for locations of different settlement cells/plates. The maximum surcharge height (see Tables 11.7 to 11.9) varied within a range of 6.1 m to 8.23 m (20 ft to 27 ft); an average value of 7.32 m (24 ft) was selected for the numerical simulation.

Unloading of surcharge was done in a short period of time followed by reloading due to placement of the pavement. In the simulations, unloading was assumed completed within 48 days, kept for 32 days before the placement of pavement. The roadway construction period was estimated to be 48 days.

Figures 11.18 to 11.20 present the small strain and large strain primary consolidation predictions for the different pond depths. Note that the small strain formulation predicted higher settlement than the large strain formulation since the latter uses natural strain. The thicker the clay deposit, the higher was the ratio of small strain settlement to large strain settlement due to primary consolidation. Table 11.13 shows the comparison of settlements at the end of 485 days, immediately before unloading.

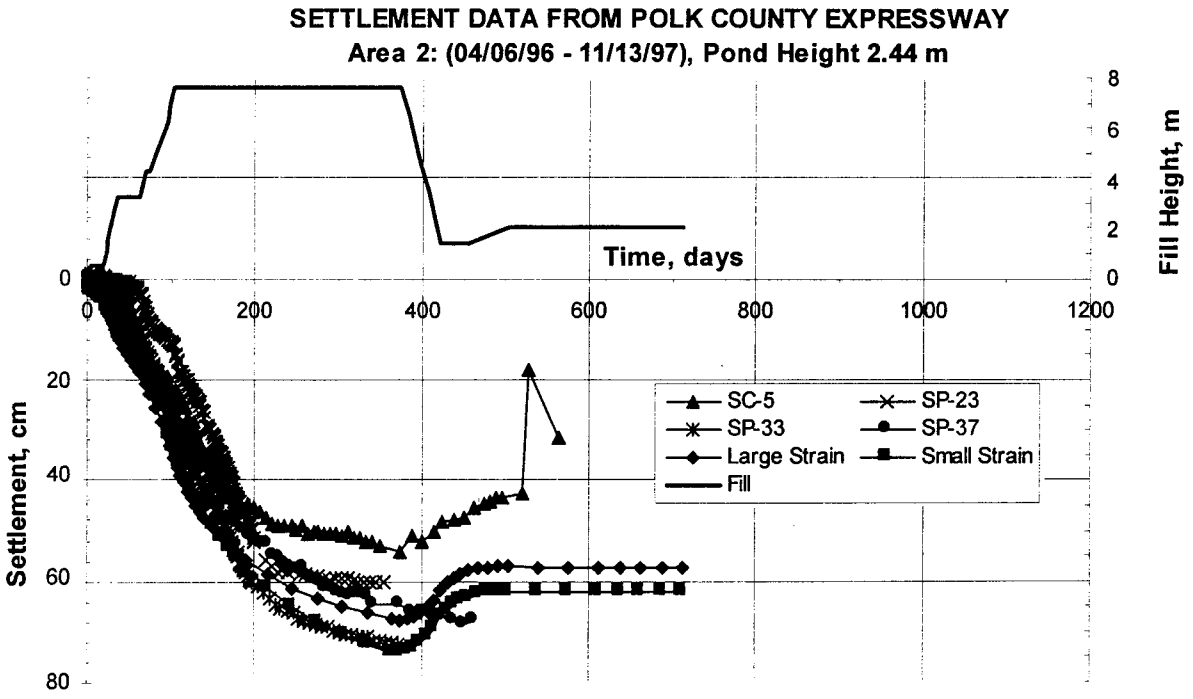

Figure 11.18 Hyperelastic-plastic consolidation settlement: pond depth 2.44 m

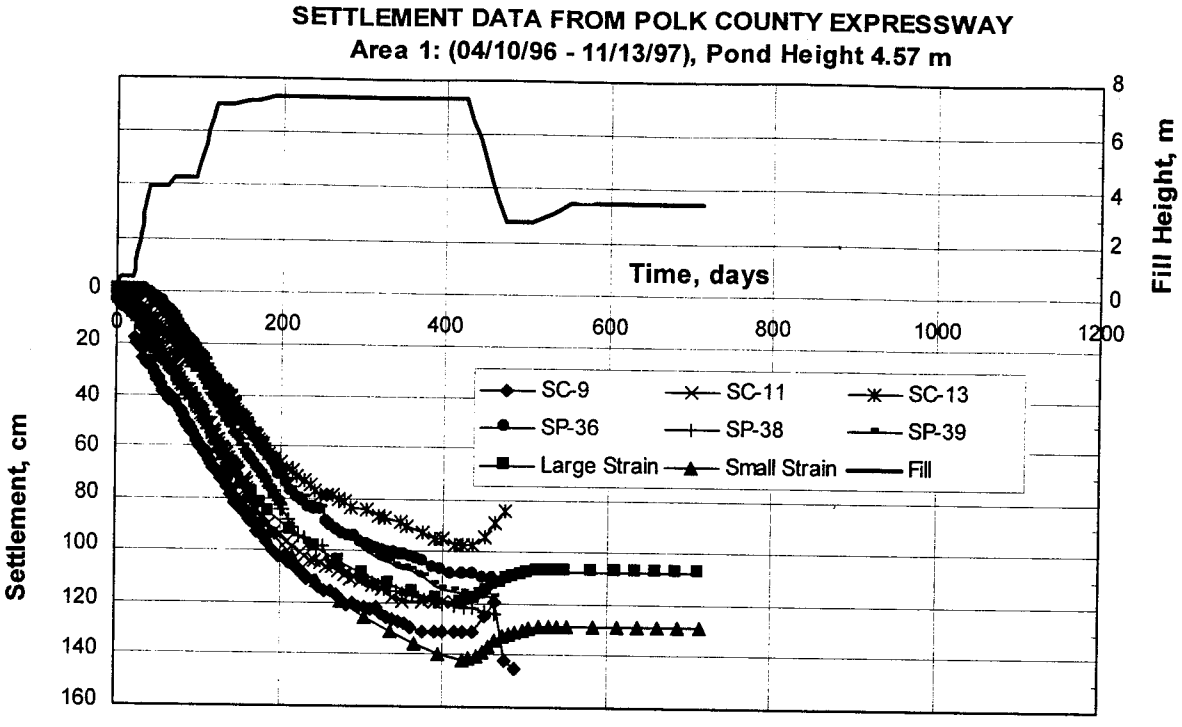

Figure 11.19 Hyperelastic-plastic consolidation settlement: pond depth 4.57 m

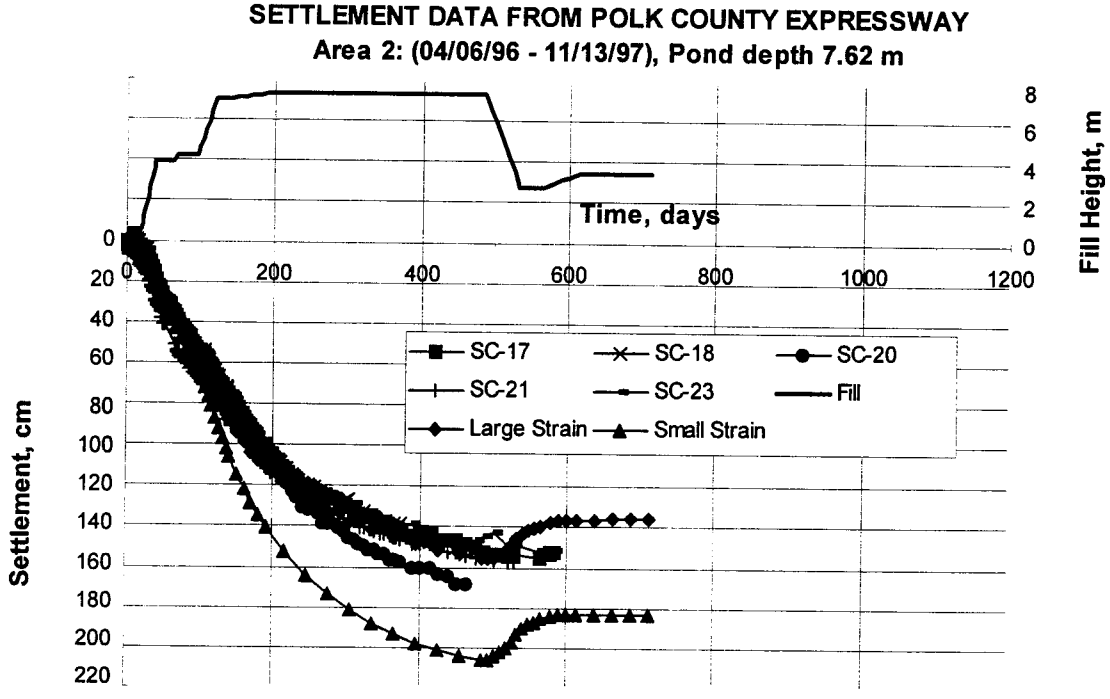

Figure 11.20 Hyperelastic-plastic consolidation settlement: pond depth 7.62 m

The small strain solution predicted a slower rate of consolidation than the large strain solution because the latter considered the reduction in length of the drainage path resulting in faster excess pore pressure dissipation. Consider the 4.57 m pond for a given time, e.g., 245 days (see Figure 11.19). Even though the small strain formulation shows 111.2 cm of settlement versus 99.2 cm for the large strain, the degree of consolidation (assuming 100% primary consolidation at 485 days) for the small strain is 75.7% (=111.2/146.9×100) versus 80% (=99.2/124.1×100) for the large strain. For all the ponds, primary consolidation reached a steady-state condition at around 700 days followed by elastic rebound during unloading. The large strain formulation did a good job predicting the primary consolidation field results for different pond depths.

Table 11.13 Comparison of primary consolidation settlements at 485 days: large strain versus small strain

Pond depth (m)	$\rho_{\text{small strain}}$ (cm)	$\rho_{\text{large strain}}$ (cm)	$\frac{\rho_{\text{small strain}}}{\rho_{\text{large strain}}}$
2.44	77.8	70.0	1.11
4.57	146.9	124.1	1.18
7.62	206.1	155.8	1.32

Field piezometer pore pressure data are compared with numerical predictions. For both the large and small strain simulations are conducted. Figure 11.21 shows the total Cauchy pore pressures at node point A (see Figure 11.17) of the 4.57 m deep pond. Piezometers PT-1 and PT-2 are represented by 4.57 m deep pond due to their location in surcharge area no. 1. See Table 11.14 for locations of piezometers. For the large strain

formulation, total Cauchy pore pressure, θ^{Cauchy} is computed as $\theta^{Kirchhoff}$ / J, J being the Jacobian at the Gauss integration point closest to node point A.

Table 11.14 Location of piezometers

Piezometer No.	Station No.	Offset
PT-1	1729+00	0'
PT-2	1734+50	0'
PT-7	1770+00	0'
PT-8	1772+00	30' R
PT-10	1778+50	60' R
PT-11	1780+00	104' R

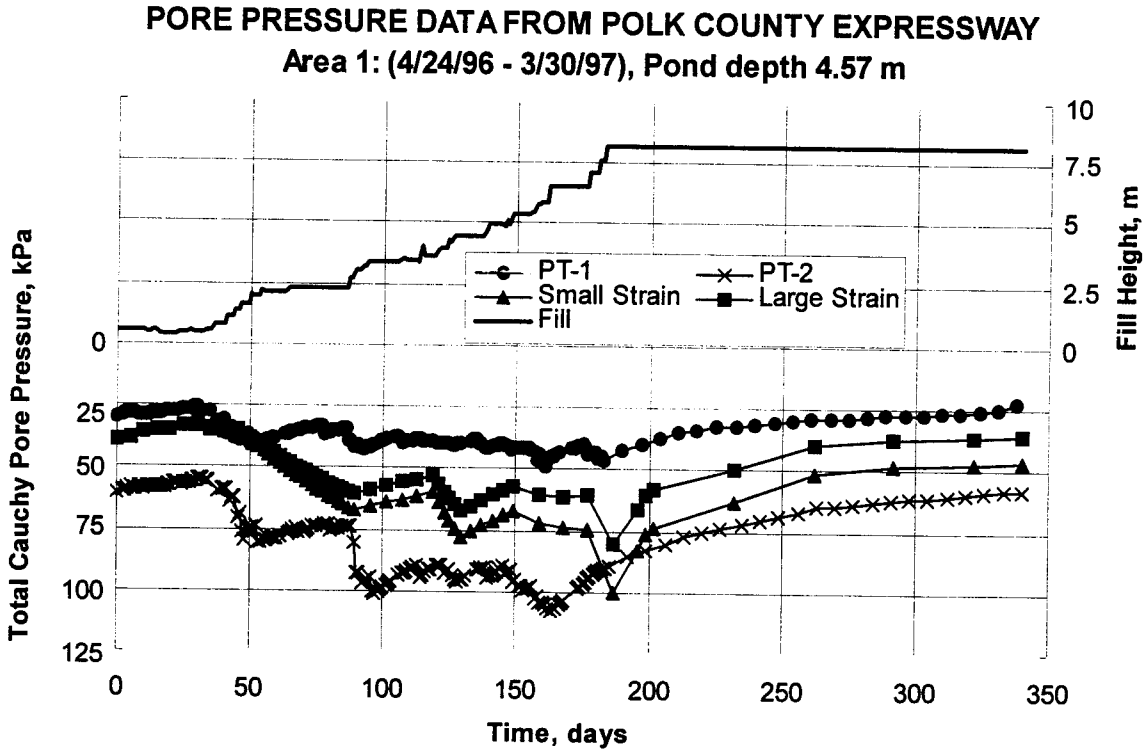

Figure 11.21 Piezometer data versus prediction of total Cauchy pore pressure: pond depth 4.57 m

Similarly, piezometer data from PT-7, PT-8, PT-10 and PT-11 are compared with predictions from the 7.62 m deep pond due to their locations at the site of deeper the retention ponds, i.e., surcharge area no. 2 (see Tables 11.14, 11.8 and Figure 11.10). Figure 11.22 presents the field data and numerical predictions. Total Cauchy pore pressures are evaluated at node point B of the 7.62 m deep pond (see Figure 11.17). θ^{Cauchy} is computed following the same technique as mentioned above.

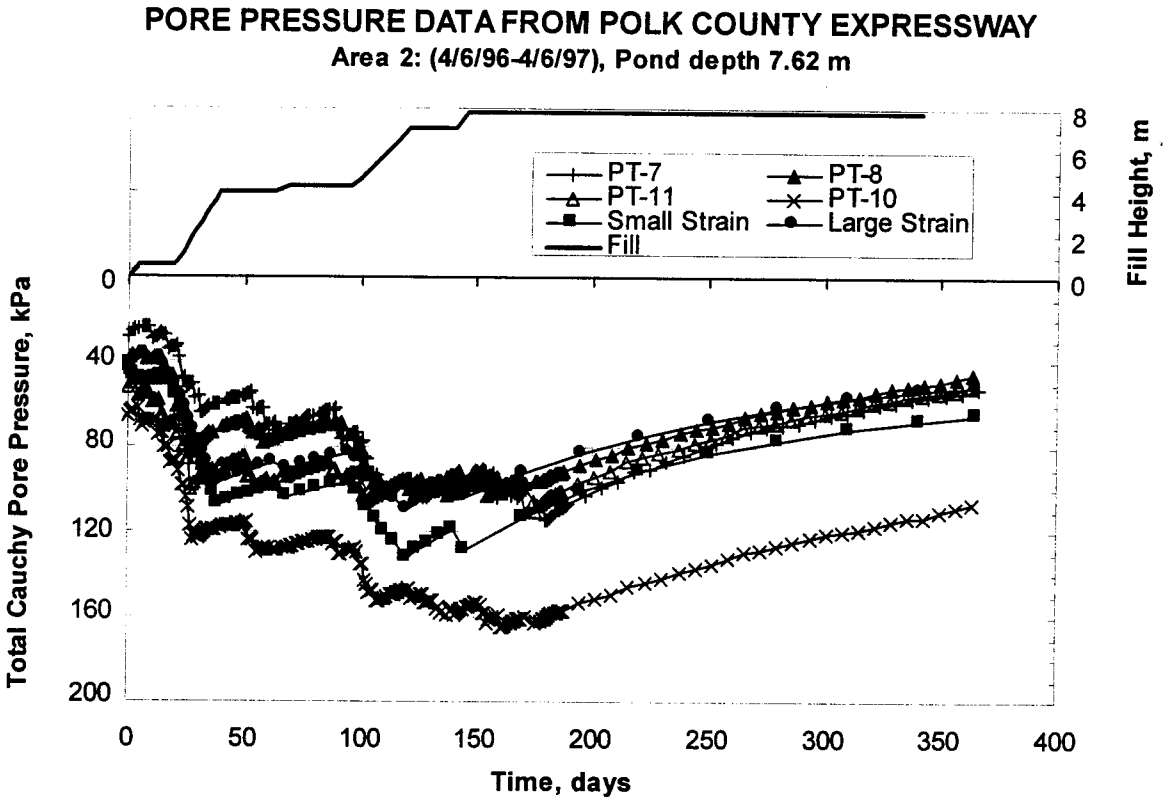

Figure 11.22 Piezometer data versus prediction of total Cauchy pore pressure: pond depth 7.62 m

θ^{Cauchy} from the small strain prediction are higher value than the large strain model; the ratio increases over time. This is due to the fact that the large strain formulation updates geometry. So, as the mesh undergoes settlement, the increasingly shorter drainage path results in a faster rate of excess pore pressure dissipation and lower values of θ^{Cauchy}. This phenomenon is demonstrated in Figure 9.5 in the case of the one-dimensional example.

11.6 Prediction of Secondary Consolidation

Secondary compression assists hydrodynamic lag from the beginning of the consolidation process but becomes dominant after the excess pore pressures have substantially dissipated. Actually there must be small excess pore pressures during secondary compression to cause water to flow from the soil. However, secondary compression proceeds very slowly and the velocity of flow is very small. Hence the associated excess pore pressures are immeasurably small. Secondary compression (or creep settlement) is a time-dependent phenomenon: the longer the clay remains under a constant effective stress, the denser it becomes.

Material parameters used for the prediction of viscoplastic consolidation (both primary and secondary) are presented in Tables 11.15 to 11.17. Hyperelasticity model parameters such as μ_0, α, p_0 and viscoplasticity parameters such as γ and N are obtained from Table 11.6. Higher values of μ_0 and p_{c0} are used for the top layer of elements (layer no.4 in Figure 11.17) assuming slight overconsolidation of the top layer. To be consistent, same variations of μ_0 and p_{c0} as in Tables 11.10 to 11.12 are used for the

prediction of secondary consolidation. For all the ponds, it was assumed that $\varepsilon_{v0}^{e} = 0.0$ and the initial value of $\gamma_{sat} = 12.58$ kN/m^3. Coefficients of permeability, k_v and k_h are assumed to have a constant value of 6.9×10^{-5} m/day (an average value taken from laboratory test result, see Figure 11.3). Figures 11.23 to 11.25 present the large strain predictions of hyperelastic-viscoplastic consolidation for the different pond depths.

Table 11.15 Material parameters for large strain, hyperelastic-viscoplastic consolidation (pond depth 2.44 m)

Parameter	Layer 1	Layer 2	Layer 3	Layer 4
μ_0 (kPa)	25.0	25.0	25.0	35.0
α	1.0	1.0	1.0	1.0
λ	0.3	0.3	0.3	0.3
κ	0.05	0.05	0.05	0.05
M	1.0	1.0	1.0	1.0
p_0 (kPa)	1.2	0.8	0.8	0.8
p_{c0} (kPa)	40.0	37.5	35.0	40.0
γ	7.0×10^{-7}	7.0×10^{-7}	7.0×10^{-7}	7.0×10^{-7}
N	1.5	1.5	1.5	1.5

Table 11.16 Material parameters for large strain, hyperelastic-viscoplastic consolidation (pond height 4.57 m)

Parameter	Layer 1	Layer 2	Layer 3	Layer 4
μ_0 (kPa)	25.0	25.0	25.0	35.0
α	1.0	1.0	1.0	1.0
λ	0.3	0.3	0.3	0.3
κ	0.05	0.05	0.05	0.05
M	1.0	1.0	1.0	1.0
p_0 (kPa)	1.5	1.0	1.0	1.0
p_{c0} (kPa)	50.0	42.5	37.5	40.0
γ	7.0×10^{-7}	7.0×10^{-7}	7.0×10^{-7}	7.0×10^{-7}
N	1.5	1.5	1.5	1.5

Table 11.17 Material parameters for large strain, hyperelastic-viscoplastic consolidation (pond height 7.62 m)

Parameter	Layer 1	Layer 2	Layer 3	Layer 4
μ_0 (kPa)	25.0	25.0	25.0	35.0
α	1.0	1.0	1.0	1.0
λ	0.3	0.3	0.3	0.3
κ	0.05	0.05	0.05	0.05
M	1.0	1.0	1.0	1.0
p_0 (kPa)	1.5	1.0	1.0	1.0
p_{c0} (kPa)	60.0	47.5	37.5	40.0
γ	7.0×10^{-7}	7.0×10^{-7}	7.0×10^{-7}	7.0×10^{-7}
N	1.5	1.5	1.5	1.5

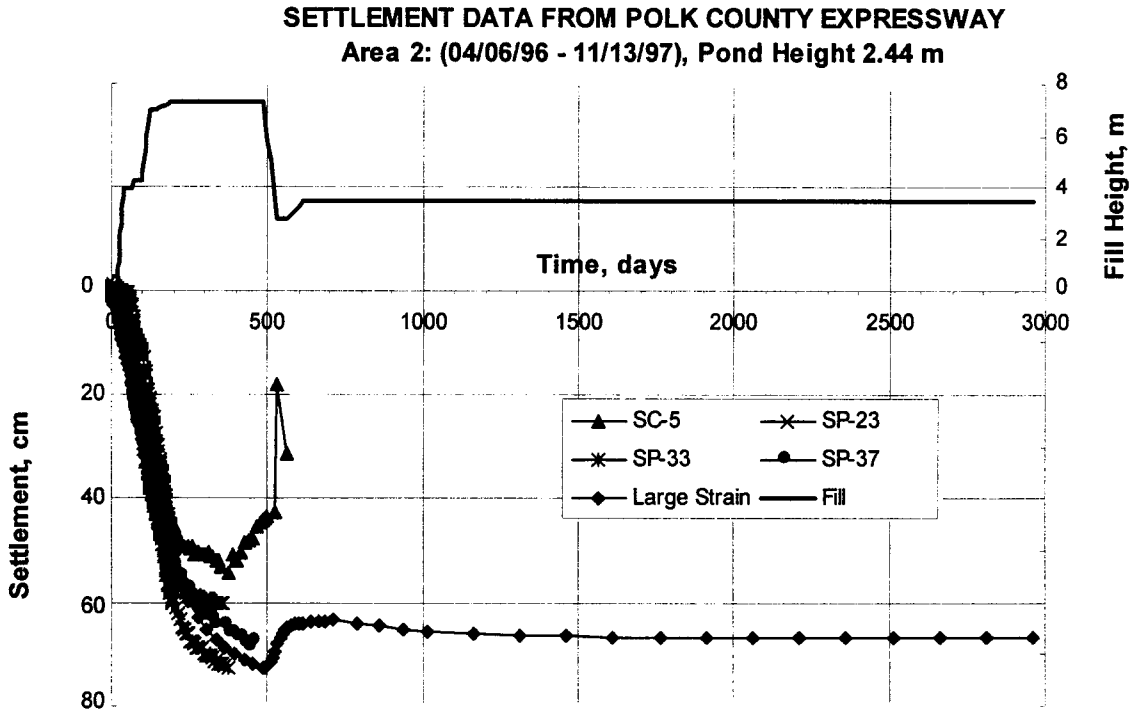

Figure 11.23 Hyperelastic-viscoplastic consolidation settlement: pond depth 2.44 m

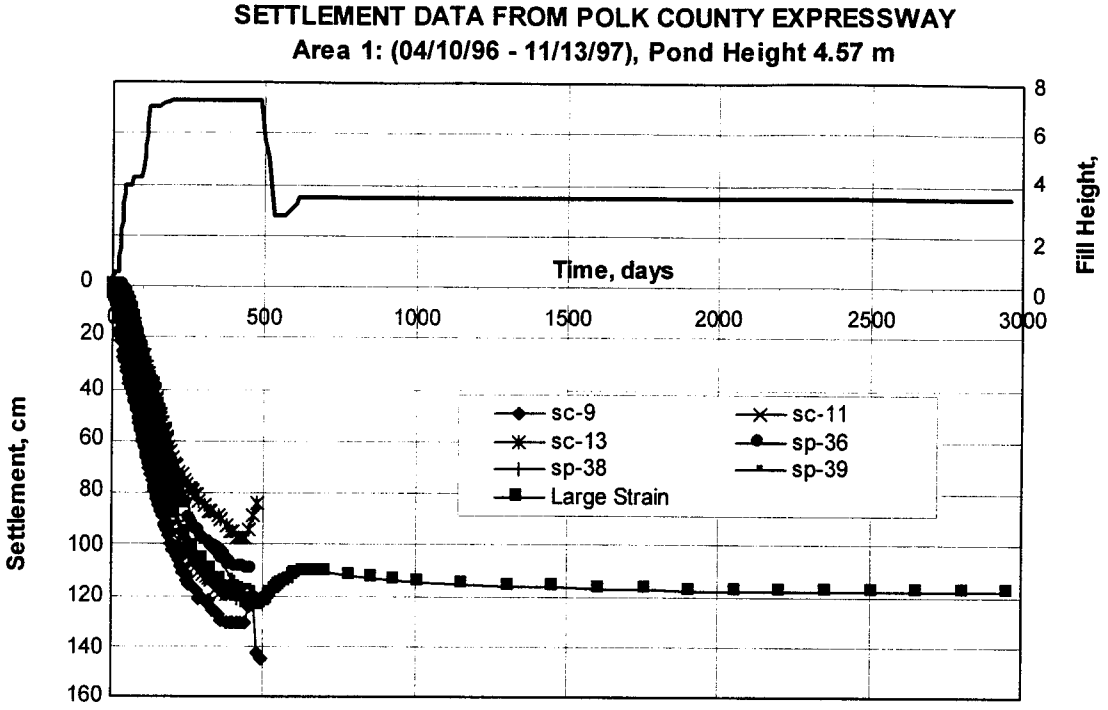

Figure 11.24 Hyperelastic-viscoplastic consolidation settlement: pond depth 4.57 m

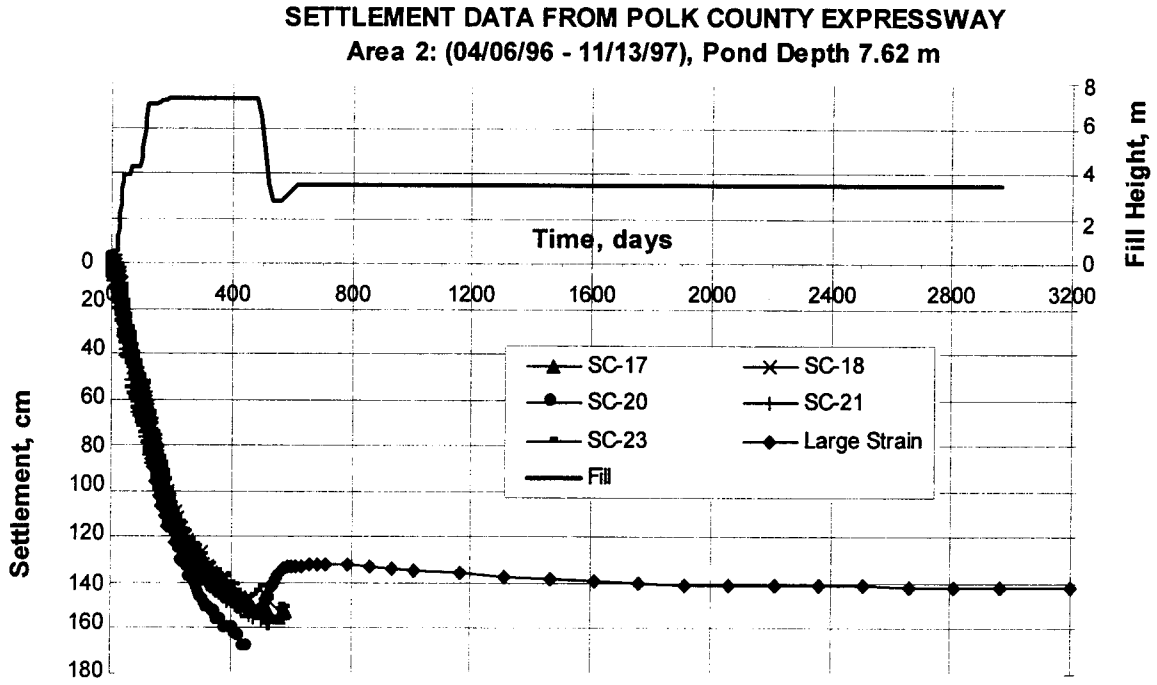

Figure 11.25 Hyperelastic-viscoplastic consolidation settlement: pond depth 7.62m

Monitoring of the field settlement was discontinued after approximately 700 days. Consequently, creep settlement over long periods of time could not be compared with numerical predictions. Figures 11.18 to 11.20 show that primary consolidation reaches equilibrium stage immediately after the pavement construction. So it is fair to assume that the settlement that occurs after road construction would be predominantly secondary compression under a constant effective stress. Table 11.18 compares the creep settlements that occurred over 3000 days for different pond depths. The deeper the clay deposit, the higher the creep settlement and the longer it took to reach an equilibrium stage. This phenomenon is self-explanatory. Column 3 of Table 11.18 presents time to reach a rate of settlement negligibly small, in this case < 2mm/year.

Table 11.18 Comparison of creep settlements for different ponds

Pond depth (m)	Creep settlement (cm)	Time to reach equilibrium (day)
2.44	3.6	1760
4.57	7.3	2200
7.62	10.0	3000

CHAPTER 12
SUMMARY

This study involved the prediction of primary (consolidation and swell) and secondary (creep) settlement of phosphatic waste clay, found at the construction site of Polk County Expressway. Centrifugal modeling and tests were performed to study the consolidation behavior of phosphatic waste clay. Central to this work was development and implementation of large strain based consolidation model in finite element code in order to predict both the laboratory and field data. Important findings from both centrifuge modeling and numerical predictions are summarized below.

12.1 Centrifugal Tests

A series of centrifuge tests were performed at the University of Florida's Geotechnical Centrifuge Laboratory. Centrifugal modeling (see Chapter) proved to be a valid tool for the study of the consolidation behavior of phosphatic waste clays.

The use of vertical wick drains in phospahtic waste clay recovered from the Polk County Parkway area has shown to have a successful effect on the rate and magnitude of the consolidation process which also has been verified by the field monitoring.

The tests performed with different fractions of the full size of the wick drain, resulted in decreasing magnitude of settlement with decreasing sizes of wick drains.

No clogging of the wick drains was observed during the centrifuge testing program.

12.2 Numerical Predictions

Laboratory consolidation test data were numerically simulated in order to obtain constitutive model parameters which were subsequently used for prediction of field data. Large strain model incorporates both material and geometrical nonlinearities. Material nonlinearities were represented by modified Cam-Clay (MCC) models with necessary modifications for large strain such as hyperelasticity and bilogarithmic compressibility law. In order to simulate secondary compression response or creep settlement, a hyperelastic-viscoplastic MCC model was developed based on Perzyna's overstress approach. Both large and small strain formulations were used for prediction. Large strain approach is observed to do better job simulating the field data compared to small strain solution. Following is the summary of important observations.

Stress-deformation response, i.e., void ratio versus log (applied pressure) curves from one-dimensional laboratory consolidation tests were predicted using both the large and small strain formulations. It is found that Cam-Clay model's compressibility parameters λ, κ are different from C_s, C_r (compression and swell indices, respectively) of the consolidation test data (see Tables 10.3 and 10.4). This is due to different stress paths; λ, κ are defined for isotropic or virgin compression loading while C_s, C_r are obtained from one-dimensional loading (stress path is K_0-condition). Also note in Tables 10.3 and 10.4 that the λ and κ for small strain are slightly different than those for large strain to produce similar stress-deformation responses. Since the large strain model updates geometry whereas small doesn't, the stresses which are F/area (i.e., function of geometry), will be different unless, the stiffness is adjusted.

Though small strain formulation performed well predicting laboratory consolidation test data its prediction of field settlement data was poor, whereas the large strain model did good job for both laboratory and field. Note that small strain formulation predicted higher settlement compared to large strain formulation since the latter uses natural strain. The thicker the clay deposit, the higher was the ratio of small strain settlement to large strain settlement due to primary consolidation.

Small strain solution predicted slower rates of consolidation than the large strain solution because the latter considered reduction in length of the drainage path resulting faster dissipation of excess pore pressure. Consider the 4.57 m pond for a given time, e.g., 245 days (see Figure 10.19). The degree of consolidation for the small strain is 75.7% (= 111.2/146.9×100) versus 80% (= 99.2/124.1×100) for the large strain.

Total Cauchy pore pressure, θ^{Cauchy} predicted from small strain model was higher than the same from large strain; the ratio increases over time. This is due to the fact that large strain formulation updates geometry. So, as the mesh undergoes settlement, increasingly less drainage path, i.e., faster rate of excess pore pressure dissipation occurs resulting lower value of θ^{Cauchy}.

The viscoplasticity model parameters γ and N were obtained from numerical simulation of laboratory consolidation test data. The proposed hyperelastic-viscoplastic MCC model did an excellent job predicting the rate of axial strain from laboratory consolidation tests which included both primary and secondary settlements.

Monitoring of the field settlement was discontinued at an early stage (around 700 days). Consequently, creep settlement over long period of time could not be compared with numerical prediction. Large strain simulations with viscoplastic MCC model were

run for a period of 3000 days in order to predict creep settlement. Table 10.18 compares creep settlements which occurred over 3000 days for different pond depths. The deeper the clay deposit, the larger the creep settlement and the longer it took to reach an equilibrium stage (rate of settlement is negligibly small, e.g., < 2mm/year).

For thick clay deposit large strain formulation did a much better prediction than small strain formulation due to geometry updating. As a result, large strain formulation is recommended for low solid content clay (void ratio > 2) where large displacement (>10% of initial thickness of deposit) is anticipated.

APPENDIX A
MATHEMATICAL DERIVATIONS

A.1 Gradient of the Jacobian, J

One can show from matrix algebra that if **a**(z) is a matrix of function z, then

$$\frac{d}{dz}(\det(\mathbf{a})) = \frac{da_{ij}}{dz} : \mathrm{COF}(a_{ij}), \tag{A.1}$$

where $\mathrm{COF}(a_{ij})$ is (i, j)th cofactor of the element a_{ij} of the matrix **a**. Therefore,

$$\frac{\partial J}{\partial x_i} = \left\{\frac{\partial}{\partial x_i}\left(\frac{\partial x_j}{\partial X_k}\right)\right\} : \mathrm{COF}(F_{jk}) = \left\{\frac{\partial}{\partial X_k}\left(\frac{\partial u_j}{\partial x_i}\right)\right\} : \mathrm{COF}(F_{jk}) = \mathbf{0}. \tag{A.2}$$

x and **X** represent spatial and material coordinates of a point X in undeformed configuration B, respectively.

Using the identity (A.2), one can obtain from (3.58) that grad $n^w = \mathbf{0}$. Since $n^s + n^w = 1$, grad $n^s = \mathbf{0}$. From (3.11), one can also derive that grad $\rho = \mathbf{0}$ knowing the fact that grad $\rho_\alpha = \mathbf{0}$ (α = s, w). Putting together, an important corollary emanates from the identity (A.2) as follows

$$\text{grad } J = \text{grad } \rho = \text{grad } n^s = \text{grad } n^w = \mathbf{0}. \tag{A.3a}$$

In reference configuration B, gradient of J takes the form

$$\text{GRAD } J = \frac{\partial J}{\partial X_i} = \frac{\partial J}{\partial x_j}\frac{\partial x_j}{\partial X_i} = \mathbf{0}. \tag{A.3b}$$

A.2 Balance of Energy of Saturated Soil

From (3.56), one can obtain the relation

$$\tau^w = n^w \theta \mathbf{1}, \tag{A.4}$$

where **1** is the second order identity tensor. Now, localized balance of energy of soil-water mixture in material form (3.61) can be rearranged as

$$J\rho\dot{\bar{E}} = \tau^s : \mathbf{d}^s + \tau^w : \mathbf{d}^w = \tau^s : \mathbf{d}^s + n^w\theta\mathbf{1} : \mathbf{d}^w = \tau^s : \mathbf{d}^s + n^w\theta \operatorname{div} \mathbf{v}^w. \tag{A.5}$$

Expanding the volume conservation equation (4.6) and using (A.3a), one can obtain

$$\operatorname{div} \mathbf{v}^w = \left(1 - \frac{1}{n^w}\right) \operatorname{div} \mathbf{v}. \tag{A.6}$$

Substituting (A.6) in (A.5), one can deduce

$$\begin{aligned} J\rho\dot{\bar{E}} &= \tau^s : \mathbf{d}^s + n^w\theta\left(1 - \frac{1}{n^w}\right)\operatorname{div} \mathbf{v}^s = \tau^s : \mathbf{d}^s + \left(1 - \frac{1}{n^w}\right) n^w\theta\mathbf{1} : \operatorname{grad} \mathbf{v}^s \\ &= \tau^s : \mathbf{d}^s + \left(1 - \frac{1}{n^w}\right)\tau^w : \mathbf{l}^s = \tau^s : \mathbf{d}^s + \left(1 - \frac{1}{n^w}\right)\tau^w : \mathbf{d}^s \\ &= \left[\tau^s + \left(1 - \frac{1}{n^w}\right)\tau^w\right] : \mathbf{d}^s = \tau : \mathbf{d}^s. \end{aligned} \tag{A.7}$$

A.3 Weak Form of $\operatorname{DIV} \tilde{\mathbf{P}} + \rho_0 \mathbf{g} = \mathbf{0}$

Weak or variational form of field equation of stress equilibrium (see (4.3)) can be written as

$$\begin{aligned} &\int_B \eta \cdot \left(\operatorname{DIV} \tilde{\mathbf{P}} + \rho_0 \mathbf{g}\right) dV = 0, \\ &\Rightarrow \int_B \left(\eta_i \frac{\partial \tilde{P}_{ij}}{\partial X_j} + \rho_0 \eta_i g_i\right) dV = 0. \\ &\Rightarrow \int_B \left(\frac{\partial}{\partial X_j}\left(\eta_i \tilde{P}_{ij}\right) - \frac{\partial \eta_i}{\partial X_j}\tilde{P}_{ij} + \rho_0 \eta_i g_i\right) dV = 0. \end{aligned} \tag{A.8}$$

η is vector of virtual displacement as defined in (4.11). Using Green's theorem, one can write

$$\int_B \left(\frac{\partial}{\partial X_j} \left(\eta_i \tilde{P}_{ij} \right) \right) dV = \int_{\partial B} \eta_i \tilde{P}_{ij} N_j \, dA = \int_{\partial B} \eta_i t_i \, dA, \tag{A.9}$$

where $\mathbf{N}$ is the unit outward normal to the surface ∂B in reference configuration.

$\mathbf{t} = \tilde{\mathbf{P}} \cdot \mathbf{N}$ is the traction vector prescribed on ∂B. Substituting (A.9) in (A.8) yields

$$\begin{aligned} &\int_{\partial B} \eta_i t_i \, dA - \int_B \left(\frac{\partial \eta_i}{\partial X_j} \tilde{P}_{ij} - \rho_0 \eta_i g_i \right) dV = 0, \\ &\Rightarrow \int_B \left(\text{GRAD}\, \eta : \tilde{\mathbf{P}} - \rho_0 \eta \cdot \mathbf{g} \right) dV - \int_{\partial B} \eta \cdot \mathbf{t} \, dA = 0. \end{aligned} \tag{A.10}$$

(A.10) presents the weak form described in (4.12).

A.4 Weak Form of $\text{div}\, \mathbf{v} + \text{div}\, \tilde{\mathbf{v}} = 0$

Weak form of the field equation of flow continuity (see (4.8)) can be written as

$$\begin{aligned} &\int_\Omega \psi \left(\text{div}\, \mathbf{v} + \text{div}\, \tilde{\mathbf{v}} \right) d\Omega = 0, \\ &\Rightarrow \int_\Omega \left(\psi \frac{\partial v_i}{\partial x_i} + \psi \frac{\partial \tilde{v}_i}{\partial x_i} \right) d\Omega = 0, \end{aligned} \tag{A.11}$$

where ψ represents an arbitrary virtual pore pressure filed as defined in (4.15). Using chain rule, one can write

$$\psi \frac{\partial \tilde{v}_i}{\partial x_i} = \frac{\partial}{\partial x_i} \left(\psi \tilde{v}_i \right) - \text{grad}\, \psi \cdot \tilde{\mathbf{v}}. \tag{A.12}$$

Substituting (A.12) in (A.11) yields

$$\begin{aligned} &\int_\Omega \psi \frac{\partial v_i}{\partial x_i} \, d\Omega + \int_\Omega \left\{ \frac{\partial}{\partial x_i} \left(\psi \tilde{v}_i \right) - \text{grad}\, \psi \cdot \tilde{\mathbf{v}} \right\} d\Omega = 0, \\ &\Rightarrow \int_\Omega \left(\psi \, \text{div}\, \mathbf{v} - \text{grad}\, \psi \cdot \tilde{\mathbf{v}} \right) d\Omega + \int_\Omega \frac{\partial}{\partial x_i} \left(\psi \tilde{v}_i \right) d\Omega = 0. \end{aligned} \tag{A.13}$$

Using Green's theorem, one may obtain

$$\int_{\Omega} \frac{\partial}{\partial x_i}(\psi \tilde{v}_i)\, d\Omega = \int_{\Gamma} \psi\, \tilde{\mathbf{v}} \cdot \mathbf{n}\, d\Gamma = -\int_{\Gamma} \psi\, q\, d\Gamma. \tag{A.14}$$

Here $q = -\tilde{\mathbf{v}} \cdot \mathbf{n}$ is the volumetric flow rate along the boundary $\Gamma^h = \phi_t(\partial B^h)$ (see (4.2b)); and q is positive when fluid is being supplied to the system. $\mathbf{n}$ is the outward unit normal to the deformed surface Γ. Substituting (A.14) in (A.13) yields

$$\int_{\Omega} (\psi\, \mathrm{div}\, \mathbf{v} - \mathrm{grad}\, \psi \cdot \tilde{\mathbf{v}})\, d\Omega - \int_{\Gamma} \psi\, q\, d\Gamma = 0. \tag{A.15}$$

(A.15) represents variational form $H(\phi, \Pi, \psi) = 0$ in spatial description (see (4.16)).

A.5 Area Transformation of Flow Rate

Push-forward of an infinitesimal area $d\Gamma \in \Gamma$ in spatial configuration to $dA \in \partial B$ in material configuration follows the relation [56]

$$\mathbf{n}\, d\Gamma = J\mathbf{N} \cdot \mathbf{F}^{-1} dA. \tag{A.16}$$

$\mathbf{N}$ and $\mathbf{n}$ are the outward normals to the undeformed surface ∂B and deformed surface $\Gamma = \phi_t(\partial B)$, respectively. $\mathbf{F}$ is the deformation gradient (see (3.44)). Multiplying both sides of (A.16) by $\tilde{\mathbf{v}}$ and exploiting the Piola identity $\tilde{\mathbf{V}} = J\mathbf{F}^{-1} \cdot \tilde{\mathbf{v}}$, one can deduce the following relation

$$\begin{aligned} -\tilde{v}_i n_i\, d\Gamma &= -\tilde{v}_i J N_j F^{-1}_{ji}\, dA \\ \Rightarrow q\, d\Gamma &= -\left(J\mathbf{F}^{-1} \cdot \tilde{\mathbf{v}}\right)_j N_j\, dA \\ \Rightarrow q\, d\Gamma &= -\tilde{\mathbf{V}} \cdot \mathbf{N}\, dA = Q\, dA, \end{aligned} \tag{A.17}$$

where Q and q are the volumetric flow rates along per unit area of the boundaries $\partial B^h \in \partial B$ and $\phi_t(\partial B^h)$, respectively. See Section 4.2 for definitions of $\tilde{\mathbf{v}}$, $\tilde{\mathbf{V}}$, Q and q.

A.6 Additive Decomposition of Principal Natural Strain

In the space of principal natural strain $\varepsilon \in R^3$, deformation gradient matrix $\mathbf{F}$ can be written as

$$\mathbf{F} = \begin{bmatrix} \lambda_1 & 0 & 0 \\ 0 & \lambda_2 & 0 \\ 0 & 0 & \lambda_3 \end{bmatrix} \tag{A.18}$$

λ_A's are the stretches in principal directions. In matrix form, product decomposition of $\mathbf{F}$ (see (4.27)) can be written as

$$\begin{bmatrix} \lambda_1 & 0 & 0 \\ 0 & \lambda_2 & 0 \\ 0 & 0 & \lambda_3 \end{bmatrix} = \begin{bmatrix} \lambda_1^e & 0 & 0 \\ 0 & \lambda_2^e & 0 \\ 0 & 0 & \lambda_3^e \end{bmatrix} \begin{bmatrix} \lambda_1^p & 0 & 0 \\ 0 & \lambda_2^p & 0 \\ 0 & 0 & \lambda_3^p \end{bmatrix} \Rightarrow \lambda_A = \lambda_A^e \lambda_A^p; \quad \forall\, A = 1,2,3. \tag{A.19}$$

Taking the natural logarithms of (A.19) yields

$$\ln(\lambda_A) = \ln\left(\lambda_A^e\right) + \ln\left(\lambda_A^p\right) \quad \Rightarrow \varepsilon_A = \varepsilon_A^e + \varepsilon_A^p. \tag{A.20}$$

Trial elastic left Cauchy-Green tensor $\mathbf{b}^{e,tr}$, defined in $(4.41)_1$, can be written in following product form:

$$\begin{aligned} \mathbf{b}^{e,tr} &= \mathbf{f}\,\mathbf{b}_n^e\,\mathbf{f}^t = \mathbf{f}\left(\mathbf{F}_n^e(\mathbf{F}_n^e)^t\right)\mathbf{f}^t \\ &= \left(\mathbf{f}\,\mathbf{F}_n^e\right)\left(\mathbf{f}\,\mathbf{F}_n^e\right)^t = \left\{\mathbf{f}\,\mathbf{F}_n\left(\mathbf{F}_n^p\right)^{-1}\right\}\left\{\mathbf{f}\,\mathbf{F}_n\left(\mathbf{F}_n^p\right)^{-1}\right\}^t \\ &= \left\{\mathbf{F}\left(\mathbf{F}_n^p\right)^{-1}\right\}\left\{\mathbf{F}\left(\mathbf{F}_n^p\right)^{-1}\right\}^t. \end{aligned} \tag{A.21}$$

In the space of principal strains, $\mathbf{b}^{e,tr}$ and $\mathbf{F}_n^p$ can be expressed in the following matrices:

$$\mathbf{b}^{e,tr} = \begin{bmatrix} \left(\lambda_1^{e,tr}\right)^2 & 0 & 0 \\ 0 & \left(\lambda_2^{e,tr}\right)^2 & 0 \\ 0 & 0 & \left(\lambda_3^{e,tr}\right)^2 \end{bmatrix}; \qquad \mathbf{F}_n^p = \begin{bmatrix} \lambda_{1,n}^p & 0 & 0 \\ 0 & \lambda_{2,n}^p & 0 \\ 0 & 0 & \lambda_{3,n}^p \end{bmatrix}. \quad (A.22)$$

Now, from (A.18) and $(A.22)_2$, one can write

$$\mathbf{F}\left(\mathbf{F}_n^p\right)^{-1} = \begin{bmatrix} \dfrac{\lambda_1}{\lambda_{1,n}^p} & 0 & 0 \\ 0 & \dfrac{\lambda_2}{\lambda_{2,n}^p} & 0 \\ 0 & 0 & \dfrac{\lambda_3}{\lambda_{3,n}^p} \end{bmatrix}. \quad (A.23)$$

Substituting (A.23) and (A.21) yields

$$\lambda_A^{e,tr} = \frac{\lambda_A}{\lambda_{A,n}^p} \quad \forall\ A = 1,2,3. \quad (A.24)$$

Taking natural logarithms of (A.24) produces

$$\ln\left(\lambda_A^{e,tr}\right) = \ln(\lambda_A) - \ln\left(\lambda_{A,n}^p\right) \quad \Rightarrow \varepsilon_A = \varepsilon_A^{e,tr} + \varepsilon_{A,n}^p. \quad (A.25)$$

A.7 Proof of Piola Identity: DIV **Y** = J div **y**

Piola transform of vector **y** is given by $\mathbf{Y} = J\mathbf{F}^{-1}\cdot\mathbf{y}$. Now DIV **Y** can be expanded using chain rule as follows:

$$\begin{aligned}
\mathrm{DIV}\,\mathbf{Y} &= \frac{\partial}{\partial X_i}(Y_i) = \frac{\partial}{\partial X_i}\left(JF^{-1}_{ij}y_j\right) = \frac{\partial}{\partial X_i}\left(J\frac{\partial X_i}{\partial x_j}y_j\right) \\
&= \frac{\partial J}{\partial X_i}\left(\frac{\partial X_i}{\partial x_j}y_j\right) + J\frac{\partial}{\partial X_i}\left(\frac{\partial X_i}{\partial x_j}\right)y_j + J\frac{\partial X_i}{\partial x_j}\frac{\partial y_j}{\partial X_i} \\
&= J\frac{\partial}{\partial x_j}\left(\frac{\partial X_i}{\partial X_i}\right)y_j + J\frac{\partial y_j}{\partial x_j} \\
&= J\,\mathrm{div}\,\mathbf{y},
\end{aligned} \tag{A.26}$$

since GRAD J = 0 (see (A.3b). **x** and **X** represent spatial and material coordinates of a point $X \in \mathsf{B}$, respectively. B is the undeformed, reference configuration.

A.8 Linearization of **F**, $\mathbf{F}^{-1}$

Linearization of **F** and $\mathbf{F}^{-1}$ is given by

$$L\mathbf{F} = \mathbf{F} + \delta\mathbf{F}; \qquad L\mathbf{F}^{-1} = \mathbf{F}^{-1} + \delta\mathbf{F}^{-1}. \tag{A.27}$$

Let $\delta\mathbf{u}$ be the variation of the displacement field **u**. One can express variation of **F** as

$$\delta\mathbf{F} = \left.\frac{\mathrm{d}}{\mathrm{d}\varepsilon}\right|_{\varepsilon=0} \frac{\partial(\mathbf{x}+\varepsilon\,\delta\mathbf{u})}{\partial\mathbf{X}} = \frac{\partial(\delta\mathbf{u})}{\partial\mathbf{X}} = \frac{\partial(\delta\mathbf{u})}{\partial\mathbf{x}}\cdot\frac{\partial\mathbf{x}}{\partial\mathbf{X}} = \mathrm{grad}\,\delta\mathbf{u}\cdot\mathbf{F} = \mathrm{GRAD}\,\delta\mathbf{u}. \tag{A.28a}$$

$\mathbf{F}\cdot\mathbf{F}^{-1} = \delta$; δ is the Kronecker delta. So, $\delta(\mathbf{F}\cdot\mathbf{F}^{-1}) = \mathbf{0}$; $\mathbf{F}\cdot\delta\mathbf{F}^{-1} = -\,\delta\mathbf{F}\cdot\mathbf{F}^{-1}$. One can write

$$\begin{aligned}
&\mathbf{F}\cdot\delta\mathbf{F}^{-1} = -(\mathrm{grad}\,\delta\mathbf{u}\cdot\mathbf{F})\cdot\mathbf{F}^{-1} = -\mathrm{grad}\,\delta\mathbf{u} \\
&\Rightarrow \delta\mathbf{F}^{-1} = -\mathbf{F}^{-1}\cdot\mathrm{grad}\,\delta\mathbf{u} = -\mathbf{F}^{-1}\cdot\mathrm{GRAD}\,\delta\mathbf{u}\cdot\mathbf{F}^{-1}.
\end{aligned} \tag{A.28b}$$

Substituting (A.28a) and (A.28b) in (A.27), one can deduce to (7.3a) and (7.3b).

A.9 Linearization of J, $\dot{J}$

Linearization of J, $\dot{J}$ is given by

$$\mathrm{L}J = J + \delta J; \qquad \mathrm{L}\dot{J} = \dot{J} + \delta\dot{J}. \tag{A.29}$$

In order to expand (A.29), one needs to obtain expressions for δJ, $\delta\dot{J}$. Variation of J, δJ can be written as

$$\begin{aligned}
\delta J &= \left.\frac{d}{d\varepsilon}\right|_{\varepsilon=0} \det \mathbf{F}(\mathbf{x}+\varepsilon\,\delta\mathbf{u}) = \left.\frac{d}{d\varepsilon}\right|_{\varepsilon=0} \det\left(\frac{\partial(\mathbf{x}+\varepsilon\,\delta\mathbf{u})}{\partial\mathbf{X}}\right) \\
&= \left[\left.\frac{d}{d\varepsilon}\right|_{\varepsilon=0} \frac{\partial(\mathbf{x}+\varepsilon\,\delta\mathbf{u})}{\partial\mathbf{X}}\right] : \mathrm{COF}(\mathbf{F}) = (\mathrm{grad}\,\delta\mathbf{u}\cdot\mathbf{F}) : \mathrm{COF}(\mathbf{F}) \\
&= (\mathrm{grad}\,\delta\mathbf{u})_{ik}\,\mathbf{F}_{kj}\,\mathrm{COF}(\mathbf{F}_{ij}) \\
&= (\mathrm{grad}\,\delta\mathbf{u})_{11}\,\mathbf{F}_{1j}\,\mathrm{COF}(\mathbf{F}_{1j}) + (\mathrm{grad}\,\delta\mathbf{u})_{22}\,\mathbf{F}_{2j}\,\mathrm{COF}(\mathbf{F}_{2j}) \\
&\quad + \cdots\cdots\cdots + (\mathrm{grad}\,\delta\mathbf{u})_{nn}\,\mathbf{F}_{nj}\,\mathrm{COF}(\mathbf{F}_{nj}) \\
&= J\{(\mathrm{grad}\,\delta\mathbf{u})_{11} + (\mathrm{grad}\,\delta\mathbf{u})_{22} + \cdots\cdots\cdots + (\mathrm{grad}\,\delta\mathbf{u})_{nn}\} \\
&= J\,\mathrm{div}\,\delta\mathbf{u}
\end{aligned} \tag{A.30}$$

Now $\dot{J} = \partial J/\partial t = J\ \mathrm{div}\ (\partial\mathbf{u}/\partial t) = J\ \mathrm{div}\ \mathbf{v}$. So, $\delta\dot{J} = \delta(J\ \mathrm{div}\ \mathbf{v}) = J\,\delta(\mathrm{div}\mathbf{v}) + \delta J\,\mathrm{div}\mathbf{v}$.

$$\begin{aligned}
\delta(\mathrm{div}\,\mathbf{v}) &= \delta\left(\mathrm{GRAD}\,\mathbf{V} : \mathbf{F}^{-t}\right) \\
&= \delta(\mathrm{GRAD}\,\mathbf{V}) : \mathbf{F}^{-t} + \mathrm{GRAD}\,\mathbf{V} : \delta\mathbf{F}^{-t} \\
&= \mathrm{GRAD}\,\delta\mathbf{V} : \mathbf{F}^{-t} - \mathrm{GRAD}\,\mathbf{V} : \left(\mathbf{F}^{-t}\cdot\mathrm{grad}\,\delta\mathbf{u}\right)^{t} \\
&= \mathrm{div}\,\delta\mathbf{v} - \mathrm{grad}\,\mathbf{v} : \mathrm{grad}^{t}\,\delta\mathbf{u}.
\end{aligned} \tag{A.31}$$

From (A.30) and (A.31), one can write expression for $\delta\dot{J}$ as

$$\delta\dot{J} = J\left[\mathrm{div}(\delta\mathbf{v}) - \mathrm{grad}\,\mathbf{v} : \mathrm{grad}^{t}(\delta\mathbf{u}) + \mathrm{div}(\delta\mathbf{u})\,\mathrm{div}\,\mathbf{v}\right]. \tag{A.32}$$

A.10 Linearization of ρ_0

$$\mathrm{L}\rho_0 = \rho_0 + \delta\rho_0 = \rho_0 + \delta(J\rho). \tag{A.33}$$

Using the relation (3.48), one can derive

$$\begin{aligned}
\delta(J\rho) &= \rho\,\delta J + J\,\delta\left\{\rho_s\left(1-n^w\right)+\rho_w n^w\right\} \\
&= \rho\,\delta J + J(\rho_w-\rho_s)\delta n^w \\
&= \rho\,\delta J + J(\rho_w-\rho_s)\delta\left\{1-\left(1-n_0^w\right)J^{-1}\right. \\
&= \rho\,\delta J + J(\rho_w-\rho_s)\left(1-n_0^w\right)J^{-2}\delta J \\
&= \rho_w\delta J \\
&= \rho_w J\,\mathrm{div}(\delta\mathbf{u}).
\end{aligned} \tag{A.34}$$

$\delta\rho_s = \delta\rho_w = 0$, since solid and fluid phases are assumed incompressible.

A.11 Relation between Tensors **A** and **D**

By definition (see Section 7.2.1),

$$\begin{aligned}
A_{ijkl} &= \frac{\partial P_{ij}}{\partial F_{kl}} = \frac{\partial}{\partial F_{kl}}\left(F_{im}S_{mj}\right) \\
&= F_{im}\frac{\partial S_{mj}}{\partial C_{ab}}\frac{\partial C_{ab}}{\partial F_{kl}} + S_{jl}\delta_{ik}.
\end{aligned} \tag{A.35}$$

$C_{ab} = F_{ca}F_{cb}$ (cf. (3.59)). Taking derivative of **C** yields,

$$\frac{\partial C_{ab}}{\partial F_{kl}} = \frac{\partial}{\partial F_{kl}}\left(F_{ca}F_{cb}\right) = F_{ka}\delta_{bl} + F_{kb}\delta_{al}. \tag{A.36}$$

Substitution of (A.36) in (A.35) results $A_{ijkl} = 2F_{im}F_{kn}D_{mjnl} + S_{jl}\delta_{ik}$, since $D_{mjnl} = D_{mjln}$.

A.12 Relation between Tensors **a** and **d**

Using (7.12), (7.15a), (7.15b) and the relation $\tau = \mathbf{F}\cdot\mathbf{S}\cdot\mathbf{F}^t$, expression of spatial tangential elasticity tensor **a** can be rearranged as follows:

$$\begin{aligned} a_{ijkl} &= F_{jm}F_{ln}A_{imkn} \\ &= F_{jm}F_{ln}\{2F_{ia}F_{kb}D_{ambn} + S_{mn}\delta_{ik}\} \\ &= 2F_{ia}F_{jm}F_{kb}F_{ln}D_{ambn} + (F_{jm}F_{ln}S_{mn})\delta_{ik} \\ &= d_{ijkl} + \tau_{jl}\delta_{ik}. \end{aligned} \tag{A.37}$$

So, $\mathbf{a} = \mathbf{d} + \tau \oplus \mathbf{1}$.

A.13 Spectrai Decomposition of **b**, **C**

Left and right Cauchy-Green tensors, **b** and **C**, respectively, are isotropic tensor functions since the transformations

$$\mathbf{Q}\cdot f(\mathbf{b})\cdot\mathbf{Q}^t = f\left(\mathbf{Q}\cdot\mathbf{b}\cdot\mathbf{Q}^t\right); \quad \mathbf{Q}\cdot f(\mathbf{C})\cdot\mathbf{Q}^t = f\left(\mathbf{Q}\cdot\mathbf{C}\cdot\mathbf{Q}^t\right) \tag{A.38}$$

holds for all orthogonal tensors **Q**. Let $f(\mathbf{b}) = \mathbf{b}^{m/2}$, m need not be restricted to integer values. Spectral decomposition of f(**b**) then takes the form

$$f(\mathbf{b}) = \mathbf{b}^{m/2} = \sum_{A=1}^{3} \lambda_A^m \mathbf{n}^{(A)} \otimes \mathbf{n}^{(A)}, \tag{A.39}$$

where λ_A and $\mathbf{n}^{(A)}$, respectively, are the eigenvalues and eigenvectors of the left stretch tensor $\mathbf{V} = \mathbf{b}^{1/2}$. Following the representation theorem [95], f(**b**) in a space $\in R^3$ may be expressed as a polynomial in **b** with scalar coefficients which are functions of the invariants of **b**:

$$f(\mathbf{b}) = \delta_0\mathbf{I} + \delta_1\mathbf{b} + \delta_2\mathbf{b}^2. \tag{A.40}$$

Here δ_0, δ_1, and δ_2 are functions of the principal invariants of **b** given by

$$I_1 = \mathrm{tr}(\mathbf{b}), \quad I_2 = \left[I_1^2 - \mathrm{tr}\left(\mathbf{b}^2\right)\right], \quad I_3 = \det(\mathbf{b}). \tag{A.41}$$

Consider **b** and hence f(**b**) as diagonalized, permitting the substitution of **b** and $\mathbf{b}^{m/2}$ with their corresponding principal values, λ_A^2 and λ_A^m, respectively, then (A.40) yields

$$\begin{aligned} f\left(\lambda_1^2\right) &= \delta_0 + \delta_1\lambda_1^2 + \delta_2\lambda_1^4 = \lambda_1^m, \\ f\left(\lambda_2^2\right) &= \delta_0 + \delta_1\lambda_2^2 + \delta_2\lambda_2^4 = \lambda_2^m, \\ f\left(\lambda_3^2\right) &= \delta_0 + \delta_1\lambda_3^2 + \delta_2\lambda_3^4 = \lambda_3^m. \end{aligned} \tag{A.41}$$

In case distinct eigenvalues, (A.41) has a unique solution for δ_0, δ_1, and δ_2 given as

$$\delta_0 = \sum_{A=1}^{3} \frac{f\left(\lambda_A^2\right) I_3 \lambda_A^{-2}}{D_A}; \quad \delta_1 = \sum_{A=1}^{3} \frac{f\left(\lambda_A^2\right)\left(\lambda_A^2 - I_1\right)}{D_A}; \quad \delta_2 = \sum_{A=1}^{3} \frac{f\left(\lambda_A^2\right)}{D_A}, \tag{A.42}$$

where $D_A = 2\lambda_A^4 - I_1\lambda_A^2 + I_3\lambda_A^{-2}$. Substituting (A.42) in (A.40), one can obtain the following expression

$$\mathbf{b}^{m/2} = \sum_{A=1}^{3} \lambda_A^m \left[\frac{\mathbf{b}^2 - \left(I_1 - \lambda_A^2\right)\mathbf{b} + I_3\lambda_A^{-2}\mathbf{1}}{2\lambda_A^4 - I_1\lambda_A^2 + I_3\lambda_A^{-2}}\right]. \tag{A.43}$$

The eigenvalues λ_A's are solutions of the characteristic polynomial

$$p(\lambda_A) = -\lambda_A^6 + I_1\lambda_A^4 - I_1\lambda_A^4 + I_1\lambda_A^4 = 0 \qquad \forall A = 1,2,3. \tag{A.44}$$

The equation has the solutions

$$\lambda_A = \frac{1}{\sqrt{3}}\left[I_1 + 2\left(I_1^2 - 3I_2\right)^{1/2}\cos\left(\frac{\theta + 2\pi\alpha}{3}\right)\right]^{1/2} \qquad \forall A = 1,2,3, \tag{A.45}$$

where

$$\theta = \cos^{-1}\left[\frac{2I_1^3 - 9I_1I_2 + 27I_3}{2\left(I_1^2 - 3I_2\right)^{3/2}}\right]. \tag{A.46}$$

Comparing (A.43) with spectral representation of (A.39), one can write

$$\mathbf{n}^{(A)} \otimes \mathbf{n}^{(A)} = \frac{\mathbf{b}^2 - \left(I_1 - \lambda_A^2\right)\mathbf{b} + I_3\lambda_A^{-2}\mathbf{1}}{2\lambda_A^4 - I_1\lambda_A^2 + I_3\lambda_A^{-2}} \quad \forall A = 1,2,3. \tag{A.47}$$

An analogous representation for $\mathbf{C}^{m/2}$ follows from the above procedure. For general case of distinct eigenvalues, spectral decomposition of $\mathbf{C}$ takes the form

$$C = \sum_{A=1}^{3} \lambda_A^2 \mathbf{N}^{(A)} \otimes \mathbf{N}^{(A)}, \qquad \left\|\mathbf{N}^{(A)}\right\| = 1; \tag{A.48}$$

since $\mathbf{C}$ is symmetric positive definite tensor i.e. $\mathbf{C} \in S_+^3$. $\mathbf{M}^{(A)}$ of (7.13) is defined as

$$\mathbf{M}^{(A)} = \lambda_A^{-2}\mathbf{N}^{(A)} \otimes \mathbf{N}^{(A)}. \tag{A.49}$$

where like (A.47), the product term $\mathbf{N}^{(A)} \otimes \mathbf{N}^{(A)}$ can be obtained as

$$\mathbf{N}^{(A)} \otimes \mathbf{N}^{(A)} = \lambda_A^2 \frac{\mathbf{C} - \left(I_1 - \lambda_A^2\right)\mathbf{1} + I_3\lambda_A^{-2}\mathbf{C}^{-1}}{2\lambda_A^4 - I_1\lambda_A^2 + I_3\lambda_A^{-2}} \quad \forall A = 1,2,3. \tag{A.50}$$

If $\lambda_1 = \lambda_2 \neq \lambda_3$, it can be easily deduced from (A.39) and (A.47) that

$$\mathbf{b}^{m/2} = \lambda_1^m + \left(\lambda_3^m - \lambda_1^m\right)\left[\frac{\mathbf{b}^2 - \left(I_1 - \lambda_3^2\right)\mathbf{b} + I_3\lambda_3^{-2}\mathbf{1}}{2\lambda_3^4 - I_1\lambda_3^2 + I_3\lambda_3^{-2}}\right]. \tag{A.51}$$

while

$$\mathbf{b}^{m/2} = \lambda_1^m \mathbf{1}. \tag{A.52}$$

if $\lambda_1 = \lambda_2 = \lambda_3$.

A.14 Derivation of $\partial\varepsilon_A/\partial\mathbf{C}$

Differentiation of $(A.48)_1$ gives

$$d\mathbf{C} = \sum_{A=1}^{3}\left[2\lambda_A d\lambda_A \mathbf{N}^{(A)}\otimes\mathbf{N}^{(A)} + \lambda_A^2\left(d\mathbf{N}^{(A)}\otimes\mathbf{N}^{(A)} + \mathbf{N}^{(A)}\otimes d\mathbf{N}^{(A)}\right)\right] \quad (A.53)$$

Contracting $d\mathbf{C}$ with $\mathbf{N}^{(A)}\otimes\mathbf{N}^{(A)}$ yields

$$\begin{aligned}\sum_{A=1}^{3} d\mathbf{C}:\left\{\mathbf{N}^{(A)}\otimes\mathbf{N}^{(A)}\right\} &= \sum_{A=1}^{3} dC_{ij}N_i^{(A)}N_j^{(A)}\\ &= \sum_{A=1}^{3}\left[2\lambda_A d\lambda_A\left(N_i^{(A)}N_i^{(A)}\right)\left(N_j^{(A)}N_j^{(A)}\right)\right.\\ &\quad \left.+\lambda_A^2\left\{\left(dN_i^{(A)}N_i^{(A)}\right)\left(N_j^{(A)}N_j^{(A)}\right)+\left(N_i^{(A)}N_i^{(A)}\right)\left(dN_j^{(A)}N_j^{(A)}\right)\right\}\right]\end{aligned} \quad (A.54)$$

From $(A.48)_2$ $N_i^{(A)}N_i^{(A)} = 1$. So, $d\left(N_i^{(A)}N_i^{(A)}\right) = 0$ or $N_i^{(A)}dN_i^{(A)} = 0$. Substituting these identities in (A.54) produces

$$\begin{aligned} &d\mathbf{C}:\left\{\mathbf{N}^{(A)}\otimes\mathbf{N}^{(A)}\right\} = 2\lambda_A d\lambda_A\\ &\Rightarrow d\mathbf{C}:\lambda_A^2\mathbf{M}^{(A)} = 2\lambda_A d\lambda_A\\ &\Rightarrow \frac{\partial\lambda_A}{\partial\mathbf{C}} = \frac{1}{2}\lambda_A\mathbf{M}^{(A)}\end{aligned} \quad (A.55)$$

Since $\varepsilon_A = \ln(\lambda_A)$, one can obtain

$$\frac{\partial\varepsilon_A}{\partial\mathbf{C}} = \frac{1}{2}\mathbf{M}^{(A)}. \quad (A.56)$$

A.15 Derivation of $\partial\mathbf{M}^{(A)}/\partial\mathbf{C}$

From (A.49) and (A.50), $\mathbf{M}^{(A)}$ can be written as

$$\mathbf{M}^{(A)} = \frac{\mathbf{C} - \left(I_1 - \lambda_A^2\right)\mathbf{1} + I_3\lambda_A^{-2}\mathbf{C}^{-1}}{D_A} \quad (A.57)$$

where $D_A = 2\lambda_A^4 - I_1\lambda_A^2 + \lambda_A^{-2} = \left(\lambda_A^2 - \lambda_B^2\right)\left(\lambda_A^2 - \lambda_C^2\right)$. {A,B,C} denotes an even permutation of the indices {1,2,3}. I_1 and I_3 are invariants of **C**, defines as

$$I_1 = \mathrm{tr}[\mathbf{C}] = \lambda_1^2 + \lambda_2^2 + \lambda_3^2; \quad I_1 = \det[\mathbf{C}] = \lambda_1^2\lambda_2^2\lambda_3^2. \tag{A.58}$$

Now,

$$\frac{\partial \mathbf{M}^{(A)}}{\partial \mathbf{C}} = \frac{1}{D_A}\left\{\frac{\partial u}{\partial \mathbf{C}} - \mathbf{M}^{(A)} \otimes \frac{\partial D_A}{\partial \mathbf{C}}\right\} \tag{A.59}$$

where $u = \mathbf{C} - \left(I_1 - \lambda_A^2\right)\mathbf{1} + I_3\lambda_A^{-2}\mathbf{C}^{-1}$. Consider (A.59) by parts. First, $\partial u/\partial \mathbf{C}$ can be expanded using the chain rule as

$$\begin{aligned}\frac{\partial u}{\partial \mathbf{C}} = \mathbf{I} - \mathbf{1} \otimes \frac{\partial I_1}{\partial \mathbf{C}} + 2\lambda_A \mathbf{1} \otimes \frac{\partial \lambda_A}{\partial \mathbf{C}} + \lambda_A^{-2}\mathbf{C}^{-1} \otimes \frac{\partial I_3}{\partial \mathbf{C}} \\ - 2\lambda_A^{-3}\mathbf{C}^{-1} \otimes \frac{\partial \lambda_A}{\partial \mathbf{C}} - I_3\lambda_A^{-2}\mathbf{I}_{C^{-1}}\end{aligned} \tag{A.60}$$

I is the fourth order identity tensor defined as $\mathbf{I}_{ijkl} = \frac{1}{2}\left[\delta_{ik}\delta_{jl} + \delta_{il}\delta_{jk}\right]$.

$\left(\mathbf{I}_{C^{-1}}\right)_{ijkl} = -\partial C_{ij}^{-1} / \partial C_{kl} = \frac{1}{2}\left[C_{ik}^{-1}C_{jl}^{-1} + C_{il}^{-1}C_{jk}^{-1}\right]$. In order to expand (A.60) to lowest order, one would need expressions for $\partial I_1/\partial \mathbf{C}$, $\partial I_3/\partial \mathbf{C}$ and $\partial \lambda_A/\partial \mathbf{C}$.

$$\frac{\partial I_1}{\partial \mathbf{C}} = \mathbf{1} \tag{A.61a}$$

$$\begin{aligned}\frac{\partial I_3}{\partial \mathbf{C}} = \frac{\partial}{\partial C_{kl}}\{\det(C_{mn})\} = \frac{\partial Cmn}{\partial C_{kl}}\mathrm{COF}(C_{mn}) \\ = I_3\frac{\mathrm{COF}(C_{mn})}{I_3} = I_3 C_{kl}^{-1} = I_3\mathbf{C}^{-1}.\end{aligned} \tag{A.61b}$$

See (A.55) for $\partial \lambda_A/\partial \mathbf{C}$. Substituting (A.55), (A.61a) and (A.61b), one can rewrite (A.60) as

$$\frac{\partial u}{\partial \mathbf{C}} = \mathbf{I} - \mathbf{1}\otimes\mathbf{1} + \lambda_A^2 \mathbf{1}\otimes\mathbf{M}^{(A)} + I_3\lambda_A^{-2}\mathbf{C}^{-1}\otimes\mathbf{C}^{-1} - I_3\lambda_A^{-2}\mathbf{C}^{-1}\otimes\mathbf{M}^{(A)} - I_3\lambda_A^{-2}\mathbf{I}_{C^{-1}} \tag{A.62}$$

Next, consider $\partial D_A/\partial \mathbf{C}$.

$$\frac{\partial D_A}{\partial \mathbf{C}} = D'_A \frac{\partial \lambda_A}{\partial \mathbf{C}} - \lambda_A^2 \frac{\partial I_1}{\partial \mathbf{C}} + \lambda_A^{-2}\frac{\partial I_3}{\partial \mathbf{C}}, \tag{A.63}$$

where $D'_A = 8\lambda_A^3 - 2I_1\lambda_A - 2I_3\lambda_A^{-3}$. Upon substitution of (A.55) and (A.61a), (A.61b) takes the form

$$\frac{\partial D_A}{\partial \mathbf{C}} = \frac{1}{2}D'_A\lambda_A\mathbf{M}^{(A)} - \lambda_A^2\mathbf{1} + I_3\lambda_A^{-2}\mathbf{C}^{-1}. \tag{A.64}$$

$$\begin{aligned}\frac{\partial \mathbf{M}^{(A)}}{\partial \mathbf{C}} &= \frac{1}{D_A}\left[\mathbf{I} - \mathbf{1}\otimes\mathbf{1} + I_3\lambda_A^{-2}\left(\mathbf{C}^{-1}\otimes\mathbf{C}^{-1} - \mathbf{I}_{C^{-1}}\right)\right] \\ &+ \frac{1}{D_A}\left[\lambda_A^2\left(\mathbf{1}\otimes\mathbf{M}^{(A)} + \mathbf{M}^{(A)}\otimes\mathbf{1}\right) - \frac{1}{2}D'_A\lambda_A\mathbf{M}^{(A)}\otimes\mathbf{M}^{(A)}\right] \\ &- \frac{1}{D_A}\left[I_3\lambda_A^{-2}\left(\mathbf{C}^{-1}\otimes\mathbf{M}^{(A)} + \mathbf{M}^{(A)}\otimes\mathbf{C}^{-1}\right)\right].\end{aligned} \tag{A.65}$$

A.16 Push Forward of $\partial \mathbf{M}^{(A)}/\partial \mathbf{C}$

Push forward of all the indices of $\partial \mathbf{M}^{(A)}/\partial \mathbf{C}$ yields $\mathbf{d}^{(A)}$ as given by (7.17). In tenor form $d^{(A)}_{ijkl} = F_{ia}F_{jb}F_{kc}F_{ld}\partial M^{(A)}_{ab}/\partial C_{cd}$. Consider push forward of each of the fourth order tensors on the right hand side of (A.65). Following expressions can be obtained.

$$\begin{aligned}F_{ia}F_{jb}F_{kc}F_{ld}I_{abcd} &= \frac{1}{2}\left[\left\{F_{ic}F^t_{ck}\right\}\left\{F_{jd}F^t_{dl}\right\} + \left\{F_{id}F^t_{dl}\right\}\left\{F_{jc}F^t_{ck}\right\}\right] \\ &= \frac{1}{2}\left(b_{ik}b_{jl} + b_{il}b_{jk}\right) = (I_b)_{ijkl}.\end{aligned} \tag{A.66a}$$

$$F_{ia}F_{jb}F_{kc}F_{ld}\delta_{ab}\delta_{cd} = \left\{F_{ib}F^{t}_{bj}\right\}\left\{F_{kd}F^{t}_{dl}\right\} = b_{ij}b_{kl}. \tag{A.66b}$$

$$\begin{aligned} F_{ia}F_{jb}F_{kc}F_{ld}C^{-1}_{ab}C^{-1}_{cd} &= \left\{F_{ia}C^{-1}_{ab}F^{t}_{bj}\right\}\left\{F_{kc}C^{-1}_{cd}F^{t}_{dl}\right\} \\ &= \left\{FC^{-1}F^{t}\right\}_{ij}\left\{FC^{-1}F^{t}\right\}_{kl} = \delta_{ij}\delta_{kl}. \end{aligned} \tag{A.66c}$$

$$\begin{aligned} F_{ia}F_{jb}F_{kc}F_{ld}\left(I_{C^{-1}}\right)_{abcd} &= \frac{1}{2}\left[\left\{F_{ia}C^{-1}_{ac}F^{t}_{ck}\right\}\left\{F_{jb}C^{-1}_{bd}F^{t}_{dl}\right.\right. \\ &\quad \left.\left. + \left\{F_{ia}C^{-1}_{ad}F^{t}_{dl}\right\}\left\{F_{jb}C^{-1}_{bc}F^{t}_{ck}\right\}\right] \\ &= \frac{1}{2}\left(\delta_{ik}\delta_{jl} + \delta_{il}\delta_{jk}\right) = I_{ijkl}. \end{aligned} \tag{A.66d}$$

$$F_{ia}F_{jb}F_{kc}F_{ld}\delta_{ab}M^{(A)}_{cd} = \left\{F_{ib}F^{t}_{bj}\right\}\left\{F_{kc}M^{(A)}_{cd}F^{t}_{dl}\right\} = b_{ij}m^{(A)}_{kl}. \tag{A.66e}$$

$$F_{ia}F_{jb}F_{kc}F_{ld}M^{(A)}_{ab}\delta_{cd} = m^{(A)}_{ij}b_{kl}. \tag{A.66f}$$

$$F_{ia}F_{jb}F_{kc}F_{ld}M^{(A)}_{ab}M^{(A)}_{cd} = \left\{F_{ia}M^{(A)}_{ab}F^{t}_{bj}\right\}\left\{F_{kc}M^{(A)}_{cd}F^{t}_{dl}\right\} = m^{(A)}_{ij}m^{(A)}_{kl}. \tag{A.66g}$$

$$F_{ia}F_{jb}F_{kc}F_{ld}C^{-1}_{ab}M^{(A)}_{cd} = \left\{F_{ia}C^{-1}_{ab}F^{t}_{bj}\right\}\left\{F_{kc}M^{(A)}_{cd}F^{t}_{dl}\right\} = \delta_{ij}m^{(A)}_{kl}. \tag{A.66h}$$

$$F_{ia}F_{jb}F_{kc}F_{ld}M^{(A)}_{ab}C^{-1}_{cd} = m^{(A)}_{ij}\delta_{kl}. \tag{A.66i}$$

Now, substituting (A.66a) to (A.66i) would yield push forward of $\partial\mathbf{M}^{(A)}/\partial\mathbf{C}$ in tensor form as follows

$$\begin{aligned} d^{(A)}_{ijkl} &= F_{ia}F_{jb}F_{kc}F_{ld}\frac{\partial M^{(A)}_{ab}}{\partial C_{cd}} \\ &= \frac{1}{D_A}\left[\left(I_b\right)_{ijkl} - b_{ij}b_{kl} + I_3\lambda_A^{-2}\left(\delta_{ij}\delta_{kl} - I_{ijkl}\right)\right] \\ &\quad + \frac{1}{D_A}\left[\lambda_A^2\left(b_{ij}m^{(A)}_{kl} + m^{(A)}_{ij}b_{kl}\right) - \frac{1}{2}D'_A\lambda_A m^{(A)}_{ij}m^{(A)}_{kl}\right] \\ &\quad - \frac{1}{D_A}\left[I_3\lambda_A^{-2}\left(\delta_{ij}m^{(A)}_{kl} + m^{(A)}_{ij}\delta_{kl}\right)\right]. \end{aligned} \tag{A.67}$$

A.17 Variation of k, K

Permeability tensor **k** varies with the void ratio e, or equivalently with the Jacobian J. Using chain rule variation of **k** can be expressed as

$$\delta\mathbf{k} = \frac{\partial \mathbf{k}}{\partial e}\frac{\partial e}{\partial J}\delta J = \frac{\partial \mathbf{k}}{\partial e}\frac{\partial e}{\partial J} J\,\mathrm{div}(\delta\mathbf{u}). \tag{A.68}$$

Expression of δJ is substituted from (7.4a). Assuming incompressibility of the solid phase, Jacobian J can be expressed as a function of void ratio given by

$$J = \frac{v}{V} = \frac{1+e}{1+e_0}, \tag{A.69}$$

where v and e are the volume and void ratio of soil-water mixture, respectively, in spatial configuration with corresponding values in reference configuration being V and e_0. Now, $\partial e/\partial J = 1 + e_0$. Substituting $\partial e/\partial J$ in (A.68) yields $\delta\mathbf{k} = (1+e_0)J\,\mathrm{div}\,(\delta\mathbf{u})\partial\mathbf{k}/\partial e$.

K is the pull-back permeability tensor defined as $\mathbf{K} = \mathbf{F}^{-1}\cdot\mathbf{k}\cdot\mathbf{F}^{-t}$. Variation of **K** takes the form $\delta\mathbf{K} = \delta\mathbf{F}^{-1}\cdot\mathbf{k}\cdot\mathbf{F}^{-t} + \mathbf{F}^{-1}\cdot\delta\mathbf{k}\cdot\mathbf{F}^{-t} + \mathbf{F}^{-1}\cdot\mathbf{k}\cdot\delta\mathbf{F}^{-t}$. Substituting $\delta\mathbf{F}^{-1}$ and $\delta\mathbf{k}$ from (7.3b) and (7.31), respectively, yields

$$\begin{aligned}
\delta\mathbf{K} &= -\mathbf{F}^{-1}\cdot\mathrm{GRAD}\,\delta\mathbf{u}\cdot\mathbf{F}^{-1}\cdot\mathbf{k}\cdot\mathbf{F}^{-t} + (1+e_0)J\,\mathrm{div}(\delta\mathbf{u})\mathbf{F}^{-1}\cdot\frac{\partial\mathbf{k}}{\partial e}\cdot\mathbf{F}^{-t} \\
&\quad -\mathbf{F}^{-1}\cdot\mathbf{k}\cdot\mathbf{F}^{-t}\cdot\mathrm{GRAD}^{t}\,\delta\mathbf{u}\cdot\mathbf{F}^{-t} \\
&= -2\mathbf{F}^{-1}\cdot\left\{\frac{1}{2}\left(\mathrm{GRAD}\,\delta\mathbf{u}\cdot\mathbf{K}\cdot\mathbf{F}^{t} + \mathbf{F}\cdot\mathbf{K}\cdot\mathrm{GRAD}^{t}\,\delta\mathbf{u}\right)\right\}\cdot\mathbf{F}^{-t} \\
&\quad + (1+e_0)J\,\mathrm{div}(\delta\mathbf{u})\mathbf{F}^{-1}\cdot\frac{\partial\mathbf{k}}{\partial e}\cdot\mathbf{F}^{-t} \\
&= -\mathbf{F}^{-1}\cdot\left\{2\,\mathrm{Sym}\left(\mathrm{GRAD}\,\delta\mathbf{u}\cdot\mathbf{K}\cdot\mathbf{F}^{t}\right) - (1+e_0)\,\mathrm{DIV}\left(J\mathbf{F}^{-1}\cdot\delta\mathbf{u}\right)\frac{\partial\mathbf{k}}{\partial e}\right\}\cdot\mathbf{F}^{-t}
\end{aligned} \tag{A.70}$$

K is symmetric since **k** is assumed symmetric for most practical purposes.

A.18 Variation of grad θ

$$\begin{aligned}\delta(\text{grad}\,\theta) &= \delta\left(\frac{\partial\theta}{\partial x_j}\right) = \delta\left(\frac{\partial\theta}{\partial X_i}\frac{\partial X_i}{\partial x_j}\right)\\ &= \frac{\partial(\delta\theta)}{\partial x_j} + \frac{\partial\theta}{\partial X_i}\delta F_{ij}^{-1}\end{aligned} \tag{A.71}$$

From (5.3b), $\delta\mathbf{F}^{-1}$ can be expressed in tensor form as $\delta F_{ij}^{-1} = -\dfrac{\partial X_i}{\partial x_k}\dfrac{\partial(\delta u_k)}{\partial x_j}$. (A.71) can then be rearranged as

$$\begin{aligned}\delta(\text{grad}\,\theta) &= \frac{\partial(\delta\theta)}{\partial x_j} - \frac{\partial\theta}{\partial x_k}\frac{\partial(\delta u_k)}{\partial x_j}\\ &= \text{grad}(\delta\theta) - \text{grad}\,\theta\cdot\text{grad}(\delta\mathbf{u}).\end{aligned} \tag{A.72}$$

A.19 Variation of $J\tilde{\mathbf{v}}$

Variation of $J\tilde{\mathbf{v}}$ is given by $\delta(J\tilde{\mathbf{v}}) = \delta J\,\tilde{\mathbf{v}} + J\,\delta\tilde{\mathbf{v}}$. Using the expressions of δJ and $\delta(\text{grad}\,\theta)$ from (A.30) and (A.72), respectively, one can expand $\delta(J\tilde{\mathbf{v}})$ as

$$\begin{aligned}\delta(J\tilde{\mathbf{v}}) &= \delta J\left\{-\mathbf{k}\cdot\left(\frac{\text{grad}\,\theta}{Jg\rho_w} + \frac{\mathbf{g}}{g}\right)\right\} + J\,\delta\left\{-\mathbf{k}\cdot\left(\frac{\text{grad}\,\theta}{Jg\rho_w} + \frac{\mathbf{g}}{g}\right)\right\}\\ &= -\mathbf{k}\cdot\left[\frac{\delta J\,\text{grad}\,\theta}{Jg\rho_w} + \delta J\frac{\mathbf{g}}{g}\right] - \frac{J\mathbf{k}}{g\rho_w}\cdot\left[\frac{J\,\delta(\text{grad}\,\theta) - \delta J\,\text{grad}\,\theta}{J^2}\right]\\ &\quad -\delta\mathbf{k}\cdot\left[\frac{\text{grad}\,\theta}{g\rho_w} + J\frac{\mathbf{g}}{g}\right]\end{aligned} \tag{A.73}$$

$$= -\delta J\,\mathbf{k}\cdot\frac{\mathbf{g}}{g}-\frac{\mathbf{k}}{g\rho_w}\cdot\delta(\operatorname{grad}\theta)-\delta\mathbf{k}\cdot\left[\frac{\operatorname{grad}\theta}{g\rho_w}+J\frac{\mathbf{g}}{g}\right]$$

$$= J\operatorname{div}(\delta\mathbf{u})\mathbf{k}\cdot\frac{\mathbf{g}}{g}-\frac{\mathbf{k}}{g\rho_w}\cdot\delta\{\operatorname{grad}(\delta\theta)-\operatorname{grad}\theta\cdot\operatorname{grad}(\delta\mathbf{u})\}-\delta\mathbf{k}\cdot\left[\frac{\operatorname{grad}\theta}{g\rho_w}+J\frac{\mathbf{g}}{g}\right]$$

$$= -\mathbf{k}\cdot\left[\frac{\operatorname{grad}(\delta\theta)-\operatorname{grad}\theta\cdot\operatorname{grad}(\delta\mathbf{u})}{g\rho_w}+J\operatorname{div}(\delta\mathbf{u})\frac{\mathbf{g}}{g}\right]$$

$$-(1+e_0)J\operatorname{div}(\delta\mathbf{u})\frac{\partial\mathbf{k}}{\partial e}\cdot\left[\frac{\operatorname{grad}\theta}{g\rho_w}+J\frac{\mathbf{g}}{g}\right].$$

A.20 Variation of grad η: τ

Variation of grad η: τ of takes the form

$$\begin{aligned}\delta(\operatorname{grad}\eta:\tau)&=\delta(\operatorname{GRADd}\eta:\mathbf{P})\\&=\operatorname{GRADd}\eta:\delta\mathbf{P}=\operatorname{GRADd}\eta:\delta(\mathbf{F}\cdot\mathbf{S})\\&=\operatorname{GRADd}\eta:(\delta\mathbf{F}\cdot\mathbf{S}+\mathbf{F}\cdot\delta\mathbf{S}).\end{aligned}\tag{A.74}$$

Since η is vector of arbitrary virtual displacement, $\delta\eta = \mathbf{0}$. See Section 3.5.3 for relations among **P**, τ and **S**.

First, consider expansion of $\mathbf{F}\cdot\delta\mathbf{S}$. From the expression of **D** (see (7.14)), one can write $\delta\mathbf{S} = \mathbf{D}\,\delta\mathbf{C}$, or in tensor form $\delta S_{ij} = D_{ijkl}\delta C_{kl}$. Using (3.59) and (7.3a), δ**C** can be expanded as follows

$$\begin{aligned}\delta C_{ij}&=\delta\left(F_{ki}F_{kj}\right)=\delta F_{ki}F_{kj}+F_{ki}\delta F_{kj}\\&=(\operatorname{grad}\delta u)_{kl}F_{li}F_{kj}+F_{ki}(\operatorname{grad}\delta u)_{km}F_{mj}\\&=2F_{li}F_{kj}(\operatorname{grad}\delta u)_{kl}.\end{aligned}\tag{A.75}$$

Collecting the expressions for δ**S** and δ**C**, one may obtain following expansion for $\mathbf{F}\cdot\delta\mathbf{S}$

$$(F\cdot\delta S)_{ij}=F_{ik}\delta S_{kj}=F_{ik}D_{kjmn}\{2F_{am}F_{bn}(\operatorname{grad}\delta u)_{ab}\tag{A.76}$$

Substituting (A.76) and (7.15b), it can be derived as

$$
\begin{aligned}
\mathrm{GRAD}\,\boldsymbol{\eta} : \delta(\mathbf{F}\cdot\delta\mathbf{S}) &= (\mathrm{GRAD}\,\eta)_{ij}(F\cdot\delta S)_{ij} \\
&= (\mathrm{grad}\,\eta)_{ic}\,F_{cj}F_{ik}\,D_{kjmn}\{2F_{am}F_{bn}(\mathrm{grad}\,\delta u)_{ab}\} \\
&= (\mathrm{grad}\,\eta)_{ic}\{2F_{ik}F_{cj}F_{am}F_{bn}D_{kjmn}\}(\mathrm{grad}\,\delta u)_{ab} \\
&= (\mathrm{grad}\,\eta)_{ic}\,d_{icab}(\mathrm{grad}\,\delta u)_{ab} \\
&= \mathrm{grad}\,\boldsymbol{\eta} : \mathbf{d} : \mathrm{grad}\,\delta\mathbf{u}.
\end{aligned}
\tag{A.77}
$$

Next, consider expansion of $\delta\mathbf{F}\cdot\mathbf{S}$. Substituting (7.3a) and (3.57), one may obtain following tensor expansion:

$$
\begin{aligned}
(\delta F\cdot S)_{ij} &= \delta F_{ik}S_{kj} \\
&= (\mathrm{grad}\,\delta u)_{il}F_{lk}\{F^{-1}_{km}\tau_{mn}F^{-t}_{nj} \\
&= (\mathrm{grad}\,\delta u)_{il}\delta_{lm}\tau_{mn}F^{-1}_{jn}.
\end{aligned}
\tag{A.78}
$$

Then, using (A.78) following contraction with GRAD η is possible.

$$
\begin{aligned}
\mathrm{GRAD}\,\eta : (\delta\mathbf{F}\cdot\mathbf{S}) &= (\mathrm{GRAD}\,\eta)_{ij}(\delta F\cdot S)_{ij} \\
&= (\mathrm{grad}\,\eta)_{ik}F_{kj}(\mathrm{grad}\,\delta u)_{il}\delta_{lm}\tau_{mn}F^{-1}_{jn} \\
&= (\mathrm{grad}\,\eta)_{ik}\{F_{kj}F^{-1}_{jn}\}(\mathrm{grad}\,\delta u)_{il}\delta_{lm}\tau_{mn} \\
&= \{(\mathrm{grad}\,\eta)_{ik}\delta_{kn}\}\{(\mathrm{grad}\,\delta u)_{il}\delta_{lm}\}\tau_{mn} \\
&= \{(\mathrm{grad}\,\eta)_{ik}\delta_{kn}\}\{(\mathrm{grad}\,\delta u)_{il}\delta_{lm}\}\tau_{mn} \\
&= (\mathrm{grad}\,\eta)_{in}\tau_{mn}(\mathrm{grad}\,\delta u)_{il} \\
&= (\mathrm{grad}\,\eta)_{ij}\{\tau_{lj}\delta_{ki}\}(\mathrm{grad}\,\delta u)_{kl} \\
&= \mathrm{grad}\,\eta : (\tau\oplus\mathbf{1}) : \mathrm{grad}\,\delta\mathbf{u}
\end{aligned}
\tag{A.79}
$$

Substituting (A.77) and (A.79) in (A.74), one can write variation of grad η: τ as

$$
\delta(\mathrm{grad}\,\eta : \tau) = \mathrm{grad}\,\eta : (\mathbf{d} + \tau\oplus\mathbf{1}) : \mathrm{grad}\,\delta\mathbf{u}. \tag{A.80}
$$

A.21 Variation of GRAD η: **P**

Following (A.74), variation of GRAD η: **P** of can be written as

$$\delta(\mathrm{GRADd}\,\eta : \mathbf{P}) = \mathrm{GRADd}\,\eta : (\delta\mathbf{F}\cdot\mathbf{S} + \mathbf{F}\cdot\delta\mathbf{S}). \tag{A.81}$$

First, consider expansion of $\mathbf{F}\cdot\delta\mathbf{S}$. From the expression of **D** (see (7.14)), one can write $\mathbf{F}\cdot\delta\mathbf{S} = \mathbf{F}\cdot(\mathbf{D}\,\delta\mathbf{C})$, or in tensor form $(F\cdot\delta S)_{ij} = F_{ik}D_{kjmn}\delta C_{mn}$. Using (3.59) and (7.3a), $\delta\mathbf{C}$ can be expanded as follows

$$\begin{aligned}\delta C_{mn} &= \delta(F_{am}F_{an}) = \delta F_{am}F_{an} + F_{am}\delta F_{an}\\ &= (\mathrm{GRAD}\,\delta u)_{am}F_{an} + F_{am}(\mathrm{GRAD}\,\delta u)_{an}.\end{aligned} \tag{A.82}$$

Substituting (A.82), one can further expand $\mathbf{F}\cdot\delta\mathbf{S}$ as

$$\begin{aligned}(F\cdot\delta S)_{ij} &= F_{ik}D_{kjmn}\{(\mathrm{GRAD}\,\delta u)_{am}F_{an} + F_{am}(\mathrm{GRAD}\,\delta u)_{an}\}\\ &= F_{ik}\{D_{kjmn} + D_{kjnm}\}(\mathrm{GRAD}\,\delta u)_{am}F_{an}\\ &= 2F_{ik}D_{kjmn}(\mathrm{GRAD}\,\delta u)_{am}F_{an}\\ &= \{2F_{ia}D_{ajbl}F_{kb}\}(\mathrm{GRAD}\,\delta u)_{kl},\end{aligned} \tag{A.83}$$

since $D_{kjmn} = D_{kjmn}$. Next, consider the following expansion of $\delta\mathbf{F}\cdot\mathbf{S}$.

$$\begin{aligned}(\delta F\cdot S)_{ij} &= \delta F_{ik}S_{kj}\\ &= (\mathrm{GRAD}\,\delta u)_{ik}S_{kj}\\ &= (\mathrm{GRAD}\,\delta u)_{kl}S_{lj}\delta_{ki}.\end{aligned} \tag{A.84}$$

Now substituting (A.83), (A.84) and $(7.12)_2$ in (A.81), one can obtain

$$\begin{aligned}\delta(\mathrm{GRADd}\,\eta : \mathbf{P}) &= (\mathrm{GRAD}\,\eta)_{ij}(\delta F\cdot S + F\cdot\delta S)_{ij}\\ &= (\mathrm{GRAD}\,\eta)_{ij}\{2F_{ia}D_{ajbl}F_{kb} + S_{lj}\delta_{ki}\}(\mathrm{GRAD}\,\delta u)_{kl}\\ &= (\mathrm{GRAD}\,\eta)_{ij}A_{ijkl}(\mathrm{GRAD}\,\delta u)_{kl}\\ &= \mathrm{GRAD}\,\eta : \mathbf{A} : \mathrm{GRAD}\,\delta\mathbf{u}.\end{aligned} \tag{A.85}$$

(A.80) and (A.85) are equivalent expressions since both are obtain from variation of same quantity i.e. GRAD η: **P**. Following push forward of (A.85) would prove that.

$$
\begin{aligned}
\delta(\mathrm{GRADd}\,\eta:\mathbf{P}) &= (\mathrm{GRAD}\,\eta)_{ij}\{2F_{ia}D_{ajbl}F_{kb}+S_{lj}\delta_{ki}\}(\mathrm{GRAD}\,\delta u)_{kl}\\
&= (\mathrm{grad}\,\eta)_{ic}F_{cj}\{2F_{ia}D_{ajbl}F_{kb}+S_{lj}\delta_{ki}\}(\mathrm{grad}\,\delta u)_{kd}F_{dl}\\
&= (\mathrm{grad}\,\eta)_{ic}\{2F_{ia}F_{cj}F_{kb}F_{dl}D_{ajbl}+F_{cj}S_{lj}\delta_{ki}F_{dl}\}(\mathrm{grad}\,\delta u)_{kd}\\
&= (\mathrm{grad}\,\eta)_{ic}\left\{2F_{ia}F_{cj}F_{kb}F_{dl}D_{ajbl}+\underbrace{F_{cj}S_{jl}F^{t}_{ld}}_{\tau_{cd}}\delta_{ik}\right\}(\mathrm{grad}\,\delta u)_{kd}\\
&= (\mathrm{grad}\,\eta)_{ic}\{d_{ickd}+\tau_{cd}\delta_{ik}\}(\mathrm{grad}\,\delta u)_{kd}\\
&= \mathrm{grad}\,\eta:(\mathbf{d}+\tau\oplus\mathbf{1}):\mathrm{grad}\,\delta\mathbf{u}.
\end{aligned}
\tag{A.86}
$$

See (7.15b) for push forward of **D** to **d**. (A.80), (A.85) and (A.86) can be combined to following equivalent expressions

$$
\begin{aligned}
\delta(\mathrm{grad}\,\eta:\tau) &= \delta(\mathrm{GRAD}\,\eta:\mathbf{P})\\
&= \mathrm{grad}\,\eta:(\mathbf{d}+\tau\oplus\mathbf{1}):\mathrm{grad}\,\delta\mathbf{u} = \mathrm{GRAD}\,\eta:\mathbf{A}:\mathrm{GRAD}\,\delta\mathbf{u}.
\end{aligned}
\tag{A.87}
$$

A.22 Variation of $\mathrm{grad}\,\psi\cdot J\tilde{\mathbf{v}}$

Expansion of $\delta(\mathrm{grad}\,\psi\cdot J\tilde{\mathbf{v}})$ takes the form

$$
\delta(\mathrm{grad}\,\psi\cdot J\tilde{\mathbf{v}}) = \delta(\mathrm{grad}\,\psi)\cdot J\tilde{\mathbf{v}} + \mathrm{grad}\,\psi\cdot\delta(J\tilde{\mathbf{v}}). \tag{A.88}
$$

Following the same derivation of $\delta(\mathrm{grad}\,\theta)$ (see Section A.18), one may obtain

$$
\delta(\mathrm{grad}\,\psi) = -\mathrm{grad}\,\psi\cdot\mathrm{grad}(\delta\mathbf{u}), \tag{A.89}
$$

since $\delta\psi = 0$.

Substituting $\delta(\mathrm{grad}\,\psi)$, $J\tilde{\mathbf{v}}$ and $\delta(J\tilde{\mathbf{v}})$ from (A.89), (7.37b) and (7.37c), respectively, one can expand (A.88) as

$$
\begin{aligned}
&\delta\left\{(\mathrm{grad}\,\psi)_i (J\tilde{v})_i\right\} \\
&= \left\{-(\mathrm{grad}\,\psi)_k (\mathrm{grad}\,\delta u)_{ki}\right\}\left\{-k_{ij}\left(\frac{(\mathrm{grad}\,\theta)_j}{\rho_w g}+\frac{J}{g}g_j\right)\right\} \\
&-(\mathrm{grad}\,\psi)_i k_{im}\left\{\frac{(\mathrm{grad}\,\delta\theta)_m-(\mathrm{grad}\,\theta)_l(\mathrm{grad}\,\delta u)_{lm}}{\rho_w g}+\frac{J}{g}\mathrm{div}(\delta\mathbf{u})g_m\right\} \\
&-(1+e_0)J\,\mathrm{div}(\delta\mathbf{u})(\mathrm{grad}\,\psi)_i\frac{\partial k_{ij}}{\partial e}\left\{\frac{(\mathrm{grad}\,\theta)_j}{\rho_w g}+J\frac{g_j}{g}\right\} \\
&= -(\mathrm{grad}\,\psi)_i\frac{k_{im}}{\rho_w g}(\mathrm{grad}\,\delta\theta)_m+\left\{(\mathrm{grad}\,\psi)_i\frac{k_{im}}{\rho_w g}(\mathrm{grad}\,\theta)_l(\mathrm{grad}\,\delta u)_{lm}\right. \\
&\left.+(\mathrm{grad}\,\psi)_k\frac{k_{ij}}{\rho_w g}(\mathrm{grad}\,\theta)_j(\mathrm{grad}\,\delta u)_{ki}\right\}+\left\{(\mathrm{grad}\,\psi)_k(\mathrm{grad}\,\delta u)_{ki}k_{ij}g_j\frac{J}{g}\right. \\
&\left.-(\mathrm{grad}\,\psi)_k\underbrace{\delta_{ia}k_{am}}_{k_{im}}g_m\frac{J}{g}\mathrm{div}(\delta\mathbf{u})\right\} \qquad \text{(A.90)} \\
&-(1+e_0)(\mathrm{grad}\,\psi)_i J\,\mathrm{div}(\delta\mathbf{u})\delta_{im}\frac{\partial k_{mj}}{\partial e}\left\{\frac{(\mathrm{grad}\,\theta)_j}{\rho_w g}+J\frac{g_j}{g}\right\} \\
&= -\mathrm{grad}\,\psi\cdot\frac{\mathbf{k}}{\rho_w g}\cdot\mathrm{grad}\,\delta\theta \\
&+2\left\{(\mathrm{grad}\,\psi)_i\frac{1}{2}\left(\left(\frac{k}{\rho_w g}\cdot\mathrm{grad}^t\delta u\right)_{ij}+\left(\mathrm{grad}\,\delta u\cdot\frac{k^t}{\rho_w g}\right)_{ij}\right)(\mathrm{grad}\,\theta)_j\right\} \\
&+\left\{\mathrm{grad}\,\psi\cdot[\mathrm{grad}\,\delta\mathbf{u}-(\mathrm{div}\,\delta\mathbf{u})\mathbf{1}]\cdot\mathbf{k}\cdot\frac{\mathbf{g}}{g}J\right\} \\
&-(1+e_0)\mathrm{grad}\,\psi\cdot(J\,\mathrm{div}(\delta\mathbf{u})\mathbf{1})\cdot\frac{\partial\mathbf{k}}{\partial e}\cdot\left\{\frac{\mathrm{grad}\,\theta}{\rho_w g}+J\frac{\mathbf{g}}{g}\right\} \\
&= -\mathrm{grad}\,\psi\cdot\frac{\mathbf{k}}{\rho_w g}\cdot\mathrm{grad}\,\delta\theta+2\left\{\mathrm{grad}\,\psi\cdot\mathrm{Sym}\left(\frac{\mathbf{k}}{\rho_w g}\cdot\mathrm{grad}^t\delta\mathbf{u}\right)\cdot\mathrm{grad}\,\theta\right\} \\
&+\left\{\mathrm{grad}\,\psi\cdot[\mathrm{grad}\,\delta\mathbf{u}-(\mathrm{div}\,\delta\mathbf{u})\mathbf{1}]\cdot\mathbf{k}\cdot\frac{\mathbf{g}}{g}J\right\} \\
&-(1+e_0)\mathrm{grad}\,\psi\cdot(J\,\mathrm{div}(\delta\mathbf{u})\mathbf{1})\cdot\frac{\partial\mathbf{k}}{\partial e}\cdot\left\{\frac{\mathrm{grad}\,\theta}{\rho_w g}+J\frac{\mathbf{g}}{g}\right\}.
\end{aligned}
$$

A.23 Variation of $\mathrm{GRAD}\psi \cdot \tilde{\mathbf{V}}$

$\delta\left(\mathrm{GRAD}\psi \cdot \tilde{\mathbf{V}}\right) = \mathrm{GRAD}\psi \cdot \delta\tilde{\mathbf{V}}$ since $\delta\psi = 0$. Substituting (7.27) and (7.28),

$\mathrm{GRAD}\psi \cdot \delta\tilde{\mathbf{V}}$ can be expanded as

$$\begin{aligned}\mathrm{GRAD}\,\psi \cdot \delta\tilde{\mathbf{V}} = &-\mathrm{GRAD}\,\psi \cdot \delta\mathbf{K} \cdot \left(\frac{\mathrm{GRAD}\theta}{g\rho_w} + J\mathbf{F}^t \cdot \frac{\mathbf{g}}{g}\right) \\ &-\mathrm{GRAD}\,\psi \cdot \mathbf{K} \cdot \left(\frac{\mathrm{GRAD}\delta\theta}{g\rho_w} + \left(\mathrm{DIV}\left(J\mathbf{F}^{-1} \cdot \delta\mathbf{u}\right)\mathbf{F}^t + J\,\mathrm{GRAD}^t\delta\mathbf{u}\right) \cdot \frac{\mathbf{g}}{g}\right).\end{aligned} \tag{A.91}$$

Substituting expression of $\delta\mathbf{K}$ from (7.30), one may obtain

$$\begin{aligned}&\mathrm{GRAD}\,\psi \cdot \delta\mathbf{K} \cdot \left(\frac{\mathrm{GRAD}\theta}{g\rho_w} + J\mathbf{F}^t \cdot \frac{\mathbf{g}}{g}\right) \\ &= -2\,\mathrm{GRAD}\psi \cdot \mathbf{F}^{-1} \cdot \mathrm{Sym}\left(\mathrm{GRAD}\delta\mathbf{u} \cdot \frac{\mathbf{K}}{g\rho_w} \cdot \mathbf{F}^t\right) \cdot \mathbf{F}^{-t} \cdot \mathrm{GRAD}\theta \\ &-2\,\mathrm{GRAD}\psi \cdot \mathbf{F}^{-1} \cdot \mathrm{Sym}\left(\mathrm{GRAD}\delta\mathbf{u} \cdot \mathbf{K} \cdot \mathbf{F}^t\right) \cdot J\frac{\mathbf{g}}{g} \\ &+(1+e_0)\mathrm{GRAD}\,\psi \cdot \mathbf{F}^{-1} \cdot \mathrm{DIV}\left(J\mathbf{F}^{-1} \cdot \delta\mathbf{u}\right)\frac{\partial\mathbf{k}}{\partial e} \cdot \mathbf{F}^{-t} \cdot \left(\frac{\mathrm{GRAD}\theta}{g\rho_w} + J\mathbf{F}^t \cdot \frac{\mathbf{g}}{g}\right).\end{aligned} \tag{A.92}$$

Second term of (A.92) can be further expanded as

$$\begin{aligned}&2\,\mathrm{GRAD}\psi \cdot \mathbf{F}^{-1} \cdot \mathrm{Sym}\left(\mathrm{GRAD}\delta\mathbf{u} \cdot \mathbf{K} \cdot \mathbf{F}^t\right) \cdot J\frac{\mathbf{g}}{g} \\ &= \mathrm{GRAD}\psi \cdot \mathbf{F}^{-1} \cdot \left(\mathrm{GRAD}\delta\mathbf{u} \cdot \mathbf{K} \cdot \mathbf{F}^t + \mathbf{F} \cdot \mathbf{K} \cdot \mathrm{GRAD}^t\,\delta\mathbf{u}\right) \cdot J\frac{\mathbf{g}}{g} \\ &= \mathrm{GRAD}\psi \cdot \mathbf{F}^{-1} \cdot \mathrm{GRAD}\delta\mathbf{u} \cdot \mathbf{K} \cdot \mathbf{F}^t \cdot J\frac{\mathbf{g}}{g} + \mathrm{GRAD}\psi \cdot \mathbf{K} \cdot \mathrm{GRAD}^t\,\delta\mathbf{u} \cdot J\frac{\mathbf{g}}{g}\end{aligned} \tag{A.93}$$

Substituting (A.92) and (A.93) in (A.91) yields

$$
\begin{aligned}
\mathrm{GRAD}\psi\cdot\delta\tilde{\mathbf{V}} &= -\mathrm{GRAD}\psi\cdot\frac{\mathbf{K}}{g\rho_w}\cdot\mathrm{GRAD}\delta\theta \\
&+ 2\,\mathrm{GRAD}\psi\cdot\mathbf{F}^{-1}\cdot\mathrm{Sym}\left(\mathrm{GRAD}\delta\mathbf{u}\cdot\frac{\mathbf{K}}{g\rho_w}\cdot\mathbf{F}^{t}\right)\cdot\mathbf{F}^{-t}\cdot\mathrm{GRAD}\theta \\
&+ \mathrm{GRAD}\psi\cdot\mathbf{F}^{-1}\cdot\mathrm{GRAD}\delta\mathbf{u}\cdot\mathbf{K}\cdot\mathbf{F}^{t}\cdot J\frac{\mathbf{g}}{g} \\
&- \mathrm{GRAD}\psi\cdot\mathbf{K}\cdot\mathrm{DIV}\left(J\mathbf{F}^{-1}\cdot\delta\mathbf{u}\right)\mathbf{F}^{t}\cdot\frac{\mathbf{g}}{g} \\
&- (1+e_0)\,\mathrm{GRAD}\psi\cdot\mathbf{F}^{-1}\cdot\mathrm{DIV}\left(J\mathbf{F}^{-1}\cdot\delta\mathbf{u}\right)\frac{\partial\mathbf{k}}{\partial e}\cdot\mathbf{F}^{-t}\cdot\left\{\frac{\mathrm{GRAD}\theta}{\rho_w g}+J\mathbf{F}^{t}\cdot\frac{\mathbf{g}}{g}\right\}
\end{aligned}
\tag{A.94}
$$

A.24 Hand Calculation of One-dimensional Large Strain, Hyperelastic Consolidation

For the large strain example of one-dimensional hyperelastic (axisymmetric) consolidation (see Section 9.2)

$$
\varepsilon=\begin{bmatrix}0\\ \varepsilon_2\\ 0\end{bmatrix},\qquad \beta=\begin{bmatrix}\beta_1\\ \beta_2\\ \beta_1\end{bmatrix}. \tag{A.95}
$$

ε and β are the vectors of principal natural strains and principal effective Kirchhoff stresses, respectively. Subscript 1 represents radial and circumferential directions while subscript 2 represents the vertical direction. Using (5.3) one can obtain

$$
\varepsilon_v=\varepsilon_2,\quad \varepsilon_s=\frac{2}{3}\varepsilon_2. \tag{A.96}
$$

From (5.6), Kirchhoff stresses can be expressed in terms of stress invariants as

$$
\beta_1=p-\frac{q}{3},\quad \beta_2=p+\frac{2q}{3}. \tag{A.97}
$$

Stress invariants p and q can be obtained from the derivative of free energy function Ψ given by

$$p = \frac{\partial \Psi}{\partial \varepsilon_V} = K\varepsilon_V = K\varepsilon_2, \quad q = \frac{\partial \Psi}{\partial \varepsilon_S} = 3\mu\varepsilon_S = 2\mu\varepsilon_2 . \tag{A.98}$$

See (5.38) for the expression of Ψ in case of isotropic, linear elasticity. Substituting (A.98) in (A.97), β_2 can also be written as

$$\beta_2 = \left(K + \frac{4\mu}{3}\right)\varepsilon_2 = D\varepsilon_2 . \tag{A.99}$$

D is the constrained modulus. At steady-state condition Jacobian J is constant throughout the height of the soil column, so is β_2 since $\beta_2 = J\Delta q^{(Cauchy)}$. For one-dimensional constrained compression $J = \lambda_2$; λ_2 being the principal stretch in vertical direction i.e. the ratio of the final to initial column height. Equivalent expressions for β_2 yield $\beta_2 = D\varepsilon_2 = D \ln(\lambda_2) = \Delta q^{(Cauchy)}\lambda_2$. Unknown quantity λ_2 can now easily be obtained from the following equation

$$f(\lambda_2) = \Delta q^{(Cauchy)}\lambda_2 - D\ln(\lambda_2) = 0. \tag{A.100}$$

For this example, D = 134.7 kPa, $\Delta q^{(Cauchy)}$ = -90 kPa. Plugging these values in (A.100), one can obtain $\lambda_2 = 0.6484$.

APPENDIX B
FINITE ELEMENT MATRICES

Matrices for D9P4 axisymmetric elements, discussed in Chapter 8, are given in the following.

(a) Interpolation matrices:

$$\mathbf{N}^{\phi} = \begin{bmatrix} N_1^{\phi} & 0 & N_2^{\phi} & 0 & \cdots\cdots & N_9^{\phi} & 0 \\ 0 & N_1^{\phi} & 0 & N_2^{\phi} & \cdots\cdots & 0 & N_9^{\phi} \end{bmatrix}. \tag{B.1}$$

$$\mathbf{N}^{\theta} = \begin{bmatrix} N_1^{\theta} & 0 & N_2^{\theta} & 0 & N_3^{\theta} & 0 & N_4^{\theta} & 0 \\ 0 & N_1^{\theta} & 0 & N_2^{\theta} & 0 & N_3^{\theta} & 0 & N_4^{\theta} \end{bmatrix}. \tag{B.2}$$

$\mathbf{N}^{\phi} \in R^{2\times 18}$, $\mathbf{N}^{\theta} \in R^{2\times 8}$. N_i^{ϕ}'s (i = 1,2,...,9) and N_j^{θ}'s (j = 1,2,3,4) are biquadratic displacement interpolation functions and bilinear pore pressure interpolation functions, respectively. See any reference book of finite element for the interpolation function in natural coordinates $\xi, \eta \in [-1,1]$ (see Figure 9.1).

(b) Strain-displacement transformation matrix:

$$\mathbf{B} = [\mathbf{B}_1 \;\; \mathbf{B}_2 \;\; \mathbf{B}_3 \cdots\cdots \mathbf{B}_9] \in R^{5\times 18} \tag{B.3}$$

where

$$\mathbf{B}_i = \begin{bmatrix} \dfrac{\partial N_i^{\phi}}{\partial x} & 0 \\ 0 & \dfrac{\partial N_i^{\phi}}{\partial y} \\ \dfrac{N_i^{\phi}}{r} & 0 \\ \dfrac{\partial N_i^{\phi}}{\partial y} & 0 \\ 0 & \dfrac{\partial N_i^{\phi}}{\partial x} \end{bmatrix}. \tag{B.4}$$

x, y are spatial coordinates in R^2 space. Radius r in (B.4) is interpolated as $r = \sum_{i=1}^{9} N_i^{\phi} x_i$.

Volumetric counterpart of **B** matrix is defined as

$$\mathbf{b} = \{\mathbf{1}\}^t \mathbf{B}, \quad \{\mathbf{1}\} = \{1 \quad 1 \quad 1 \quad 0 \quad 0\}^t; \tag{B.5}$$

$$\mathbf{b} = [\mathbf{b}_1 \quad \mathbf{b}_2 \quad \mathbf{b}_3 \cdots\cdots \mathbf{b}_9] \in R^{1\times 18}. \tag{B.6}$$

Here

$$\mathbf{b}_i = \begin{bmatrix} \dfrac{\partial N_i^{\phi}}{\partial x} + \dfrac{N_i^{\phi}}{r} & \dfrac{\partial N_i^{\phi}}{\partial y} \end{bmatrix}. \tag{B.7}$$

(c) Gradient-pressure transformation matrix:

$$\mathbf{E} = \begin{bmatrix} \dfrac{\partial N_1^{\theta}}{\partial x} & 0 & \dfrac{\partial N_2^{\theta}}{\partial x} & 0 & \cdots\cdots & \dfrac{\partial N_4^{\theta}}{\partial x} & 0 \\ 0 & \dfrac{\partial N_1^{\theta}}{\partial y} & 0 & \dfrac{\partial N_2^{\theta}}{\partial y} & \cdots\cdots & 0 & \dfrac{\partial N_4^{\theta}}{\partial y} \end{bmatrix} \tag{B.8}$$

(d) Material stiffness matrix:

$$\tilde{\mathbf{D}} = \begin{bmatrix} d_{1111} & d_{1122} & d_{1133} & d_{1112} & d_{1121} \\ d_{2211} & d_{2222} & d_{2233} & d_{2212} & d_{2221} \\ d_{3311} & d_{3322} & d_{3333} & d_{3312} & d_{3321} \\ d_{1211} & d_{1222} & d_{1233} & d_{1212} & d_{1221} \\ d_{2111} & d_{2122} & d_{2133} & d_{2112} & d_{2121} \end{bmatrix} \tag{B.9}$$

Components of $\tilde{\mathbf{D}}$ are obtained directly from fourth-order tensor **d** of (7.16).

(e) Initial stress matrix:

$$\mathbf{T} = \begin{bmatrix} \tau_{11} & 0 & 0 & \tau_{12} & 0 \\ 0 & \tau_{22} & 0 & 0 & \tau_{12} \\ 0 & 0 & \tau_{33} & 0 & 0 \\ \tau_{12} & 0 & 0 & \tau_{22} & 0 \\ 0 & \tau_{12} & 0 & 0 & \tau_{11} \end{bmatrix} \tag{B.10}$$

(f) Pore pressure matrix:

$$\mathbf{I}_\theta = \theta^h \begin{bmatrix} 1 & 0 & 0 & 0 & 0 \\ 0 & 1 & 0 & 0 & 0 \\ 0 & 0 & 1 & 0 & 0 \\ 0 & 0 & 0 & 0 & 1 \\ 0 & 0 & 0 & 1 & 0 \end{bmatrix} \tag{B.11}$$

APPENDIX C
LABORATORY CONSOLIDATION TEST DATA

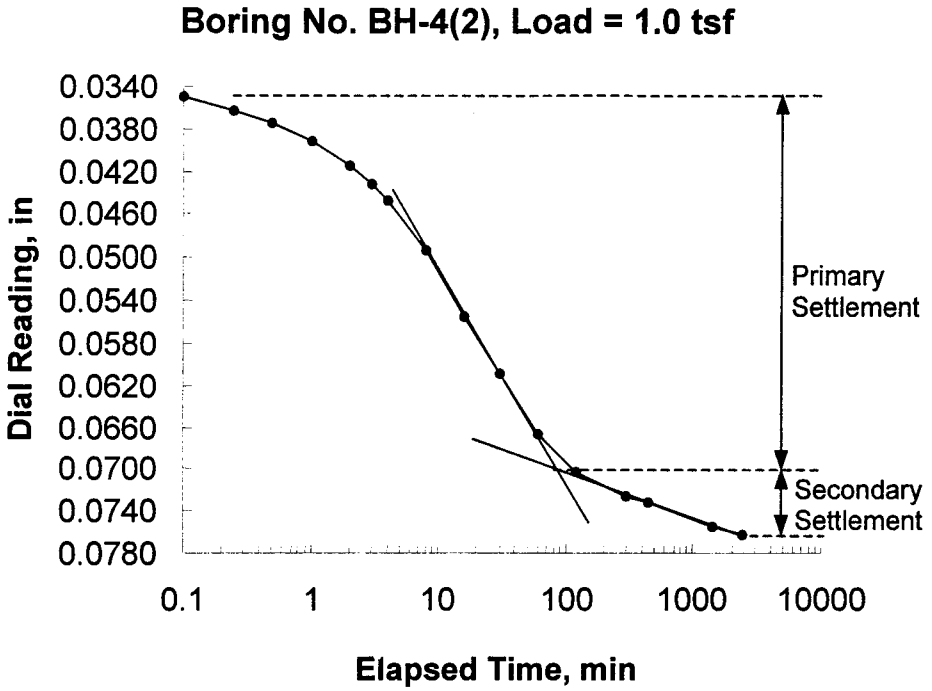

Figure C.1 Primary and secondary settlement from laboratory consolidation data

Table C.1 Settlement Data from Consolidation Test Results (Boring No. BH-1A)

Load (tsf)	Total Settlement (in)	Primary Settlement (in)	Secondary Settlement (in)	Primary Settlement (%)	Secondary Settlement (%)
0.5	0.0202	0.018	0.0022	89.11	10.89
1.0	0.0292	0.0289	0.0003	98.97	1.03
2.0	0.0613	0.053	0.0083	86.46	13.54
4.0	0.0801	0.0744	0.0057	92.88	7.12
8.0	0.084	0.0753	0.0087	89.64	10.36

Table C.2 Settlement Data from Consolidation Test Results (Boring No. BH-2)

Load (tsf)	Total Settlement (in)	Primary Settlement (in)	Secondary Settlement (in)	Primary Settlement (%)	Secondary Settlement (%)
0.25	0.00736	0.00648	0.00088	88.04	11.96
0.5	0.01814	0.01324	0.0049	72.99	27.01
1.0	0.0408	0.0341	0.0067	83.58	16.42
2.0	0.0809	0.0683	0.0126	84.43	15.57
4.0	0.1077	0.0937	0.014	87.00	13.00
8.0	0.0989	0.0897	0.0092	90.70	9.30

Table C.3 Settlement Data from Consolidation Test Results (Boring No. BH-3)

Load (tsf)	Total Settlement (in)	Primary Settlement (in)	Secondary Settlement (in)	Primary Settlement (%)	Secondary Settlement (%)
0.5	0.0098	0.0089	0.0009	90.82	9.18
1.0	0.0294	0.026	0.0034	88.44	11.56
2.0	0.0669	0.0606	0.0063	90.58	9.42
4.0	0.096	0.083	0.013	86.46	13.54
8.0	0.0982	0.0877	0.0105	89.31	10.69

Table C.4 Settlement Data from Consolidation Test Results (Boring No. BH-4(2))

Load (tsf)	Total Settlement (in)	Primary Settlement (in)	Secondary Settlement (in)	Primary Settlement (%)	Secondary Settlement (%)
0.5	0.0195	0.0175	0.002	89.74	10.26
1.0	0.0433	0.0366	0.0067	84.53	15.47
2.0	0.0972	0.0869	0.0103	89.40	10.60
4.0	0.105	0.0978	0.0072	93.14	6.86
8.0	0.1033	0.0935	0.0098	90.51	9.49

REFERENCES

1. M. A. Biot, General theory of three-dimensional consolidation, J. Appl. Phys. 12 (1941) 155-164.

2. M. A. Biot, Theory of elasticity and consolidation for a porous anisotropic solid, J. Appl. Phys. 26 (1955) 182-185.

3. R. I. Borja, Finite element formulation for transient pore pressure dissipation: a variational approach, Int. J. Solids Struct. 22 (11) (1986) 1201-1211.

4. R. I. Borja, Linearization of elasto-plastic consolidation equations, Engrg. Comput. 6(12) (1989) 163-168.

5. R. I. Borja, One-step and linear multistep methods for nonlinear consolidation, Comput. Methods Appl. Mech. Engrg. 85 (1991) 239-272.

6. R. I. Borja, Composite Newton-PCG and quasi-Newton iterations for nonlinear consolidation, Comput. Methods Appl. Mech. Engrg. 88 (1991) 27-60.

7. J. T. Christian, Two- and three dimensional consolidation in, in: C.S. Desai and J.T. Christian, eds., Numerical Methods in Geotechnical Engineering (McGraw-Hill, San Fransisco, CA 1977) 399-426.

8. J. H. Prevost, Mechanics of continuous porous media, Int. J. Engrg. Sci. 18 (1980) 787-800.

9. J. H. Prevost, Implicit-explicit schemes for nonlinear consolidation, Comput Methods Appl. Mech. Engrg. 39 (1983) 225-239.

10. H. J. Siriwarden and C. S. Desai, Two numerical schemes for nonlinear consolidation, Int. J. Numer. Methods Engrg. 17 (1981) 405-426.

11. J. C. Small, J. R. Booker and E. H. Davis, Elasto-plastic consolidation of soils, Int. J. Solids Struct. 12 (1976) 431-488.

12. J. P. Carter, J. R. Booker and J. C. Small, The analysis of finite elasto-plastic consolidation, Int. J. Numer. Anal. Methods Geomech. 3 (1979) 107-129.

13. M. Chopra and G. F. Dargush, Finite-element analysis of time-dependent large-deformation problems, Int. J. Numer. Anal. Methods Geomech. 16 (1992) 101-130.

14. H. D. Hibbit, P. V. Marcal and J. R. Rice, A finite element formulation for problems of large strain and large displacement, Int. J. Solids Struct. 6 (1970) 1069-1086.

15. J. Mandel, Thermodynamics and plasticity, in: J. J. Delagado Domingers, N. R. Nina and J. H. Whitelaw, eds., Foundations of Continuum Thermodynamics (Macmillan, London, 1974) 283-304.

16. J. C. Simo and T. J. R. Hughes, Elastoplasticity and viscoplasticity – Computational aspects, Springer Ser. Appl. Math. (Springer-Verlag, Berlin, 1989).

17. R. Hill, The Mathematical Theory of Plasticity (Clarendon, Oxford, 1950).

18. A. E. Green and P. M. Naghdi, A general theory of elasto-plastic continuum, Arch. Rat. Mech. Anal. 18 (1965) 251-281.

19. J. C. Simo and R. L. Taylor, Quasi-incompressible finite elasticity in principal stretches, Continuum basis and numerical algorithms, Comput. Methods Appl. Mech. Engrg. 85 (1991) 273-310.

20. J. C. Simo, Algorithms for static and dynamic multiplicative plasticity that preserve the classical return mapping schemes of the infinitesimal theory, Comput. Methods Appl. Mech. Engrg. 99 (1992) 61-112.

21. R. J. Atkin and R. E. Craine, Continuum theories of mixtures: basic theory and historical development, Quat. J. Mech. Appl. Math. 29 (1976) 209-224.

22. R. M. Bowen, Theory of mixtures, in: A. C. Eringen, ed., Continuum Physics 3 (Academic Press, New York, 1976) 1-27.

23. A. C. Eringen and J. D. Ingram, A continuum theory of critically reacting media – I, Int. J. Engrg. Sci. 3 (1965) 197-212.

24. J. D. Ingram and A. C. Eringen, A continuum theory of critically reacting media – II: Constitutive equations of reacting fluid mixtures, Int. J. Engrg. Sci. 5 (1967) 289-322.

25. A. E. Green and P. M. Naghdi, A dynamic theory of interacting continua, Int. J. Engrg. Sci. 3 (1965) 231-241.

26. C. Truesdell and R. Toupin, The Classical Field Theories, in: S. Flügge, ed., Handbuck der Physik III(1) (Springer-Verlag, Berlin, 1960).

27. P. S. Huyakorn and G. Pinder, Computational Methods of subsurface Flow (Academic Press, New York, 1983).

28. K. H. Roscoe and J. B. Burland, On the generalized stress-strain behavior of 'wet' clay, in: J. Heyman and F. K. Leckie, eds., Engineering Plasticity (Cambridge University Press, Cambridge, 1968) 535-609.

29. A. Schofield and P. Wroth, Critical State Soil Mechanics (McGraw-Hill, New York, 1968).

30. K. von Terzaghi, Theoretical Soil Mechnaics (John Wiley & Sons, New York, 1943).

31. M. A. Biot, Theory of deformation of a porous viscoelastic anisotropic solid, J. of Appl. Physics 27(5) (1956) 459-467.

32. M. A. Biot, Mechanics of Incremental Deformations (John Wiley & Sons, New York, London, Sydney, 1965 p.504).

33. J. Ghaboussi and S. U. Dikmen, Liquefaction analysis of horizontally layered sands, J. of Geotechnical Engineering Division, ASCE 104(GT3) (1974) 341-356.

34. R. S. Shandu and E. L. Wilson, Finite element analysis of seepage in elastic media, J. of Engrg. Mech. Division, ASCE 95(EM3) (1969) 641-652.

35. J. H. Prevost, Consolidation of anelastic porous media, J. of Engrg. Mech. Divisions, 107(EM1) (1981) 169-186.

36. J. H. Prevost, Non-linear transient phenomenon in saturated porous media, Comput. Methods Appl. Mech. Engrg. 30 (1982) 3-18.

37. O. C. Zienkiewicz and T. Shiomi, Dyanamic behavior of saturated porous media, the generalized Biot formulation and its numerical solution, Int. J. Numer. Anal. Methods Geomech. 8 (1984) 71-96.

38. P. D. Kiousis and G. Z. Voyiadjis, Lagrangian continuum theory for saturated porous media, J. of Engrg. Mechanics, ASCE 111(10) (1985) 1277-1288.

39. R. I. Borja and E. Alarcón, A mathematical framework for finite strain elastoplastic consolidation, Part 1: Balance laws, formulation and linearization, Comput. Methods Appl. Mech. Engrg. 122 (1995) 145-171.

40. A. Needleman and V. Tvergraad, Finite element analysis of localization plasticity, in: J. T. Oden and G. F. Carey, eds., Finite Elements, Vol. V: Special Problems in Solid Mechanics (Prentice-Hall, Englewood Cliffs, NJ, 1984).

41. J. H. Argyris and J. St. Doltsins, On the large strain inelastic analysis in natural formulation – Part I: Quasistatic problems, Comput. Methods Appl. Mech. Engrg. 20 (1979) 213-252.

42. J. H. Argyris, J. St. Doltsins, P. M. Pimenta and H. Wüstenberg, Theromechanical response of solids at high strains – natural approach, Comput. Methods Appl. Mech. Engrg. 32 (1982) 3-57.

43. J. C. Simo and M. Ortiz, A unified approach to finite deformation elastoplastic analysis based on the use of hyperelastic constitutive equations, Comput. Methods Appl. Mech. Engrg. 49 (1985) 221-245.

44. J. C. Simo, On the computational significance of the intermediate configuration and hyperelastic stress relations in finite deformation elastoplasticity, Mech. Mater. 4 (1985) 439-451.

45. J. C. Nagtegaal, D. M. Paeks and J. R. Rice, On numerically accurate finite element solutions in the fully plastic range, Comput. Methods Appl. Mech. Engrg. 4 (1974) 153-177.

46. J. C. Simo, R. L. Taylor and K. S. Pister, Variational and projection methods for the volume constraint in finite deformation elastoplasticity, Comput. Methods Appl. Mech. Engrg. 51 (1985) 177-208.

47. J. C. Simo, A framework for finite strain elastoplasticity based on maximum plastic dissipation and multiplicative decomposition: Part I. Continuum formulation; Part II. Computational aspects, Comput. Methods Appl. Mech. Engrg. 66 (1988) 199-219, 68 (1988) 177-208.

48. G. Weber and L. Anand, Finite deformation constitutive equations and a time integration procedure for isotropic, hyperelastic-viscoelastic solids, Comput. Methods Appl. Mech. Engrg. 79 (1990) 173-202.

49. A. L. Eterovich and K. J. Bathe, A hyperelastic-based large strain elasto-plastic constitutive formulation with combined isotropic-kinematic hardening using logarithmic stresses and strain measures, Int. J. Numer. Methods Engrg. 30 (1990) 1099-1115.

50. Dj. Peric, D. R. J. Owen and M. E. Honnor, A model for finite strain elastoplasticity, in: R. Owen, E. Hinton and E. Onate, eds., Proc. 2nd Int. Conf. On Computational Plasticity (Pineridge, Swansea, 1989) 111-126.

51. B. Moran, M. Ortiz and F. Shi, Formulation of implicit finite element methods for multiplicative plasticity, Int. J. Numer. Methods Engrg. 29 (1990) 483-514.

52. S. J. Kim and J. T. Oden, Finite element analysis of a class of problems in finite strain elstoplasticity based on the thermodynamical theory of materials of type N, Comput. Methods Appl. Mech. Engrg. 53 (1985) 277-302.

53. E. H. Lee, Elastic-plastic deformation at finite strains, J. Appl. Mech. (1969) 1-6.

54. R. I. Borja, C. Tamagnini and A. Amorosi, Coupling plasticity and energy-conserving elasticity models for clays, J. of Geotech. and Geoenv. Engrg., ASCE 123(10) (1997) 948-957.

55. R. I. Borja and C. Tamagnini, Cam-Clay plasticity Part III: Extension of infintesimal model to include finite strains, Comput. Methods Appl. Mech. Engrg. 155 (1998) 73-95.

56. L. Malvern, Introduction to the Mechanics of a Continuous Medium (Prentice-Hall, Englewood Cliffs, NJ, 1969).

57. R. L. Schiffman, Stress components of a porous medium, J. of Geophysical Research, 75 (1970) 4035-4038.

58. C. W. Gear, Simultaneous numerical solution of differential/algebraic equations, IEEE Trans. Circuit theory, CT-18 (1971) 89-95.

59. C. W. Gear, Numerical Initial Value Problems in Ordinary Differential Equations (Prentice-Hall, Englewood Cliffs, NJ, 1971).

60. C. W. Gear and K. W. Tu, The effect of variable mesh size on the stability of multistep methods, SIAM J. Numer. Anal. 11 (5) (1974) 1025-1043.

61. C. W. Gear, B. Leimkuhler and G. K. Gupta, Automatic integration of Euler-Lagrange equations with constraints, J. Comput. Appl. Math. 12/13 (1985) 77-90.

62. T. Kato, On the Trotter-Lie Product Formula, Proc. Japan Acad. 50 (1974) 694-698.

63. M. Ortiz and E. P. Popov, Accuracy and Stability of Integration Algorithms for Elastoplastic Constitutive Relations, Int. J. Numer. Methods Engrg. 21 (1985) 1561-1576.

64. T. W. Lambe and R. V. Whitman, Soil Mechanics (John Wiley & Sons, NY, 1969).

65. M. Zyntynski, M. K. Randolph, R. Nova, and C. P. Wroth, On modeling the unloading-reloading behavior of soils, Int. J. Numer. Anal. Methods Geomech., 2 (1978), 87-93.

66. A. Gens and D. M. Potts, Critical state models in computational geomechanics, Engrg. Comput., 5 (1988) 178-197.

67. J. C. Simo and G. Meschke, A new class algorithms for classical plasticity extended to finite strains. Application to geomaterials, Comput. Mech. 11 (1993) 253-278.

68. G. T. Houlsby, The use of variable shear modulus in elastic-plastic model for clays, Comput. Geotech. 1 (1985) 3-13.

69. K. Hashiguchi and M. Ueno, Elasto-plastic constitutive laws for granular materials, in: S. Murayama and A. N. Schofield, eds., Consitutive Equations of Soils, Proc. 9th Int. Conf. Soil Mech. Found. Engrg., Specialty Session 9 (Tokyo, 1977) 73-82.

70. R. Butterfield, A natural compression law for soils, Géotechnique 29 (1979) 469-480.

71. K. Hashiguchi, On the linear relations of V-ln p and ln υ-ln p for isotropic consolidation of soils, Int. J. Numer. Analyt. Methods Geomech. 19 (1995) 367-376.

72. P. Perzyna, The constitutive equations for workhardening and rate sensitive plastic materials, Proc. of Vibrational Problems, Warsaw, 4(1963), No. 3, 281-290.

73. O.C. Zienkiewicz, C. Humpheson, and R. W. Lewis, Associated and non-associated viscoplasticity and plasticity in soil mechanics, Geotechnique, 25(1975) 671-689.

74. T. Adachi and F. Oka, Constitutive equations of normally consolidated clay based on elasto-viscoplasticity, Soils and Foundations, 22 (1982), No. 4, 57-70.

75. Y. Dafalias, Bounding surface elastoplasticity-viscoplasticity for particulate cohesive media, Proc. IUTAM Symp. on Deformation and Failure of Granular Materials, (1982) 97-107.

76. M. G. Katona, Evaluation of viscoplastic cap model, J. Geotech. Engrg., ASCE, 110 (1984), 1106-1125.

77. G. Y. Baladi and B. Rohani, Development of an elasto-viscoplastic constitutive relationship for earth materials, Mechanics of Engineering Materials, eds., C. S. Deasi and R. H. Gallagher (John Wiley & Wiley Ltd., London, 1984) 23-43.

78. W. Olszak and P. Perzyna., The constitutive equations of the flow theory for a non-stationary yield condition, Proc. 11th Int. Congress of Applied Mechanics, (1966), 545-553.

79. H. Sekiguchi, Rheological characteristics of clays, Proc. 9th ICSMFE, 1 (1977), 289-292.

80. A. Dragon and Z. Mroz, A model for plastic creep of rock-like materials accounting for the kinetics of fracture, Int. Journal Rock Mech. Min. Sci. Geomech., Abstr., 16 (1979), 253-259.

81. R. Nova, A viscoplastic constitutive model for normally consolidated clay, Proc. IUTAM Symp. on Deformation and Failure of Granular Materials, (1982) 287-295.

82. T. Matsui and N. Abe, Elasto/viscoplastic constitutive equation of normally consolidated clays based on flow surface theory, Proc. 5th ICONMG, 1(1985), 407-413.

83. J. E. Marsden and T. J. R. Hughes, Mathematical Foundation of Elasticity (Prentice-Hall, Englewood Cliffs, NJ, 1983).

84. D. Bloomquist, Centrifuge modeling of Large Scale Consolidation Phenomena in Phosphatic Clay Retention Ponds, Ph.D. dissertation, University of Florida, 1982.

85. F. C. Townsend and D. L. Israel, Centrifugal Model Evaluation of Consolidation Characteristics of Waste Phosphatic Clay, Final Report, University of Florida, 1983.

86. I. Babuska, The finite element method with Lagrangian multipliers, Numerische Matmatik, 20 (1973), 179-192.

87. F. Brezzi, On the existence, uniqueness and approximation of saddle-point problems arising from Lagrangian multipliers, Reveu Française d' Automatique Informatique Reserche Opertionelle, Analyse Numérique, 8 (1974), 129-151.

88. T. J. Hughes, The Finite Element Method – Linear Static and Dynamic Finite Element Analysis (Prentice-Hall, Englewood Cliffs, NJ, 1987).

89. R. I. Borja, C. Tamagnini and E. Alarcón, Elastoplastic consolidation at finite strain Part 2: Finite element implementation and numerical examples, Comput. Methods Appl. Mech. Engrg. 159 (1998) 103-122.

90. R. F. Scott, Principles of Soil Mechanics (Addison-Wesley, Reading, MA, 1963).

91. R. L. Schiffman, A. Chen and J. C. Jordan, The Consolidation of a Half Plane, MATE Report 67-3 (U. Illinois, Chicago Circle, 1967).

92. P. E. Andersen, Centrifugal and Numerical Modeling of the Consolidation Behavior of Phosphatic Waste Clay, Master's Thesis, University of Florida, 1997.

93. M. C. McVay, F. C. Townsend and D. Bloomquist, Quiescent consolidation of phosphatic waste clays, Journal of Geotechnical Engineering Division, ASCE, 112-11 (1986), 1033-1049.

94. M. R. Hausmann, Engineering Principles of Ground Modification (McGraw-Hill, New York, 1990).

95. J. Serrin, Mathematical Principles of Classical Fluid Mechanics, Encyclopedia of Physics, Vol. VIII/1, S. Flugge, ed. (Springer-Verlag, Berlin, 1959)